UNIVERSITY OF BIRMINGHAM

THE EFFECTS OF ULTRASOUND ON ENDOTHELIAL CELL BEHAVIOUR AND ANGIOGENESIS

By

LISA SHRIANE

A thesis submitted to the University of Birmingham for the degree of

DOCTOR OF PHILOSOPHY

School of Dentistry

College of Medical and Dental Sciences

University of Birmingham

July 2025

ABSTRACT

Ultrasonic surgical devices working at kHz frequencies are used to cut hard and soft tissues. Such precision instruments facilitate access and visualisation during surgery and the ultrasound may also promote healing. The biological effects of ultrasound exposure have been reported *in vitro* and *in vivo* and represents a developing field of research. However, the effects of low frequency kHz ultrasound on cells remains under-researched. The aim of the present work was to study the effects of low frequency ultrasound on angiogenesis which is essential for initial wound healing and subsequently post-surgical healing.

Human umbilical vein endothelial cells (HUVECs) were exposed to 45 kHz ultrasound for 5 min using a DuoSon commercial device. The angiogenic response was analysed via F-actin staining, cell counting, a tube formation assay and qPCR techniques at multiple time points. The HUVEC cytoskeleton was observed to be largely unaffected after DuoSon exposure. Significant increases in viable cell number were measured 72 h after 25 mW/cm^2 (27 %, $p < 0.001$) and 75 mW/cm^2 (25 %, $p < 0.001$) exposure compared with untreated cells. This stimulatory effect was not observed in the tube formation ability of HUVECs, however a time-dependent effect was apparent. Ultrasound-treated HUVECs retained tube formation ability for longer during the *in vitro* assay compared with untreated cells when analysed 72 h after exposure. Exposure to 75 mW/cm^2 also resulted in significantly reduced *eNOS* expression ($p < 0.05$) compared with untreated cells 6 h after exposure. The expression levels were comparable with untreated cells by 72 h. This indicated an early effect on gene expression that returned to control levels by 72 h in contrast to the viable cell numbers.

The DuoSon exposure system provided initial observations of a cellular response to 45 kHz ultrasound. However the exposure set up did not allow measurement of the ultrasound delivered to cell monolayers. Furthermore, the levels of ultrasound would be increased by reflections at multiple interface boundaries in the set up used. To overcome such difficulties, a standardised *in vitro* acoustic absorbing tank exposure system was designed. An acoustically transparent CLINIcell® cassette was placed in a degassed water-filled tank lined with ultrasound absorbing tiles. This demonstrated a reduction of ultrasound reflections within the acoustic field during pressure field scanning. The exposure system also allowed thermal control of the water. HUVECs exposed to 45 kHz appeared with non-uniform morphology in certain instances 72 h after exposure. Cell viability was unaffected, though no significantly damaging effect in viable cell number was observed as seen with the DuoSon analysis. Interestingly, qPCR revealed a significant downregulation ($p < 0.05$) in *eNOS* 72 h after exposure compared with downregulation observed 6 h after DuoSon delivery.

In conclusion, this work demonstrated an effect of 45 kHz ultrasound on HUVEC behaviour. HUVEC viability was not significantly damaged, rather an increase in viable cell number was measured. An apparent ability to retain tube formation ability was also observed. Significant intracellular effects were observed, specifically a downregulation in *eNOS* expression. A visible effect of ultrasound was observed in some instances of altered cell shape which may provide reasoning for the cellular responses measured. The acoustic absorbing tank developed in this study provides researchers with a standardised exposure method for delivery of ultrasound *in vitro*. This will allow improved understanding of the biological effects of ultrasound which in turn will assist in the future development of ultrasonic surgical instruments and other medical devices.

ACKNOWLEDGMENTS

The amount of people I could thank for their contributions throughout this PhD would be enough for Thesis Part II.

Firstly, to my supervisors Professor Damien Walmsley, Dr Ben Scheven and Dr Richard Shelton. Thank you for hiring me as a research technician in the first instance and then to encourage me to put forward a PhD proposal. It was a big step I could not have taken without your constant advice and guidance. Gratitude must also be given to Professor Gabriel Landini who was so generous with sharing his image analysis expertise and his time, always more than willing to listen to any problems be it academic or otherwise. To the wider 'Ultrasurge' team I could not have asked for a more welcoming community of scientists from all fields of research. Every meeting and conference was so friendly, thought-provoking and helpful to my work – the international trips weren't too shabby either.

Within Dentistry I have been incredibly lucky to have support both as part of the technical team and as a student. To my fellow technicians (the backbone of Dentistry research!): Gay, Michelle, Helen, Jianguo, Jonathan, Silke and Sim thank you for the countless chats, teas, sweets and for always being available to take over duties and understanding if I had to dash off to labs or go slog away at my thesis.

To my fellow students in the PGR office, thank you for letting me join the PGR WhatsApp chats even if I was a technician spy and may have used them as reminders of lab rules – sorry! I am so grateful to have made so many friends throughout our PhD eras: Dario (my PCA guru and the Jack to my Karen), Ben (my PCR guru), Olga, Maria, Rachel, Sandeep, Lea, Peter,

Lauter, Lu, Alex, Jiwon and Veksina. Never at work have I laughed so much, drank so many espressos, completed so many crosswords or taken so many limerick requests!

To my ‘outside of science’ friends thank you for being such a fun escape from what can be an all-consuming PhD bubble. To Amy and Sean, pushing some 20+ years now and still can’t get rid of each other; always available for chats, drinks, short city breaks or across the world adventures. To Ffyona, Casey, Clodagh, Alex, Indie and Dan our countless bottomless brunches, games nights and story-filled holidays have been the perfect timeouts and resets in my PhD years. All your constant support and willingness to help in whatever way you could even in a subject that is so alien was truly appreciated.

To my family in the Shriane, Doyle and Walsh clans thank you for always asking about my research it genuinely helped me understand what I was doing even the “sums and that” parts. Lastly special thanks to Mom, Dad and Dan, whether it be listening to me practice presentations for the umpteenth time, dealing with my stress of a broken laptop, taking me to the Blues or having the most amazement at my conference posters I have ever seen; your support and genuine interest in my work was a source of constant encouragement throughout my PhD.

TABLE OF CONTENTS

LIST OF ABBREVIATIONS

ANOVA – analysis of variance

AMD - age-related macular degeneration

B2M - beta-2-microtubulin

BAECs - bovine aortic endothelial cells

CABG - coronary artery bypass grafting

CAD - coronary artery disease

CCK-8 – cell counting kit - 8

CD31 – cluster of differentiation 31

cDNA – complementary deoxyribonucleic acid

cEGM – complete endothelial growth medium

CNRQ – calibrated normalised relative quantity

Cp - crossing point

Cq – quantification cycle

DAPI - 4′,6-diamidino-2-phenylindole

DIPG - diffuse intrinsic pontine glioma

DNA – deoxyribonucleic acid

dNTPs – deoxynucleoside triphosphates

DPBS – Dulbecco's phosphate buffered saline

dsDNA – double stranded DNA

eNOS – endothelial nitric oxide synthase

ERK - extracellular signal-regulated kinase 1/2

FDA - food and drug administration

FEM – finite element modelling

GAPDH - glyceraldehyde 3 phosphate dehydrogenase

HEPES BSS - HEPES buffered saline solution

HIFU – high intensity focused ultrasound

HMECs - human microvascular endothelial cells

HSD - honestly significant difference

HUVEC – human umbilical vein endothelial cell

Hz - hertz

ISPTA - spatial peak temporal average intensity

kHz - kilohertz

LIPUS – low intensity pulsed ultrasound

MAPK - mitogen-activated protein kinase

MHz - megahertz

MIQE - minimum information for publication of quantitative real-time PCR experiments

MPa - megapascals

mRNA – messenger ribonucleic acid

ms - microseconds

mW - milliwatt

NAT - nucleic acid testing

NHS – national health service

NO – nitric oxide

O.D. - optical density

p38 MAPK - p38 mitogen activated protein kinase

PBS – phosphate buffered saline

PCA - principal component analysis

PCI - percutaneous coronary intervention

PECAM-1 - platelet endothelial cell adhesion molecule

PFA - paraformaldehyde

PI3 - phosphoinositide-3-kinase

PKB/AKTB – protein kinase B (also known as AKTB)

PlGF - placental growth factor

qPCR – real time quantitative polymerase chain reaction

RNA – ribonucleic acid

RPL27 - ribosomal protein L27

RT buffer – reverse transcription buffer

RT – room temperature

SDT - sonodynamic therapy

SEM – scanning electron microscopy

sqRT-PCR – semi quantitative reverse transcription and polymerase chain reaction

TNS - trypsin neutralising solution

VEGF – vascular endothelial growth factor

VEGF-R – vascular endothelial growth factor receptor

VWD - von Willebrand disease

VWF - von Willebrand factor

WPBs - Weibel-Palade bodies

YWHAZ - tyrosine 3-monooxygenase

LIST OF EQUATIONS

LIST OF FIGURES

LIST OF TABLES

Chapter 1.

INTRODUCTION

1.1 General introduction

Ultrasound refers to all sound that is above the human auditory range. The first published medical application was in diagnostic imaging in 1942 (Dussik, 1942). Since this pioneering development, the use of ultrasonic devices in different branches of medicine such as diagnostics, therapeutics and dentistry has become common practice. There has been a growing interest in the development of new ultrasonic surgical devices. Such devices have been available for clinical use since the 1970s (Vercellotti et al., 2001). However, the advancement of technology over recent years, such as that within the use of partial or fully automated robotics in surgical theatres (Ng & Tam, 2014), allows for further expansion within this field of medical ultrasound.

One of the main advantages of using surgical ultrasonic devices is the combination of a precise, tissue-selective cutting tool that may potentially contribute to accelerated healing processes through the many biological influences ultrasound has been shown to possess. A biological process that is crucial to all healing activity is angiogenesis – the development of new blood vessels from existing vasculature (Folkman & Shing, 1992). Research into the effects of ultrasound on angiogenesis is not a novel field. There have been multiple *in vivo* and *in vitro* studies investigating the potential enhancing and inhibiting effects. However, the direct effect of ultrasound in the kilohertz (kHz) frequency range of ultrasonic surgical devices is underreported in literature, with only few studies reporting effects on endothelial morphology and increased release of coagulation factors after exposure to 23.5 kHz (Karsch et al., 2002) as well as increased production of nitric oxide (NO) a key regulator in angiogenesis following 27 kHz ultrasound exposure to endothelial cells (Altland et al., 2004).

1.2 Introduction to angiogenesis

Vascular growth is one of the first events during embryonic development and organogenesis that eventually creates the largest network in the human body. The maintenance and remodelling of the vascular network is critical to sustaining life from embryo to adulthood. There are three main forms of vascular growth: vasculogenesis, angiogenesis and arteriogenesis. The primitive capillary plexus is formed via vasculogenesis involving differentiation of mesodermal cells to endothelial precursor cells (angioblasts) which further differentiate into blood islands and the subsequent *de novo* formation of a blood vessel network (Risau & Flame, 1995). Once the primary vascular network is established, continued growth of the vasculature occurs via the angiogenesis process (Risau, 1997). Arteriogenesis is a distinct form of vascular remodelling referring to the rapid expansion and remodelling of collateral arteries following an occlusion to a main artery to increase blood supply to the ischemic region (Buschmann & Schaper, 1999).

As the main process of continued blood vessel growth, angiogenesis is vital during embryogenesis to ensure delivery of oxygen and nutrients to the maturing embryo, as well as during the female menstrual cycle (Gordon et al., 1995), wound healing (Folkman & Shing, 1992) and bone repair (Carano & Filvaroff, 2003). Two types of angiogenesis have been described: sprouting and intussusceptive (non-sprouting) angiogenesis.

1.2.1 Sprouting angiogenesis

Sprouting angiogenesis is characterised by the formation of branches/sprouts of endothelial cells from a single blood vessel, which migrate towards an angiogenic stimulus to form a new blood vessel (Fig 1.1). Various molecules can act as angiogenic stimuli such as cytokines, chemokines, growth factors including fibroblast growth factor (*FGF*) and the most-studied pro-angiogenic growth factor: vascular endothelial growth factor (*VEGF*) (Duran et al., 2017). These numerous molecules are secreted by parenchymal cells as a response to environmental factors such as inflammation (Granger & Senchenkova, 2010) and most commonly hypoxia (Krock et al., 2011). However, the release of *VEGF* and the subsequent signalling cascade is regarded as the main mediator of angiogenesis.

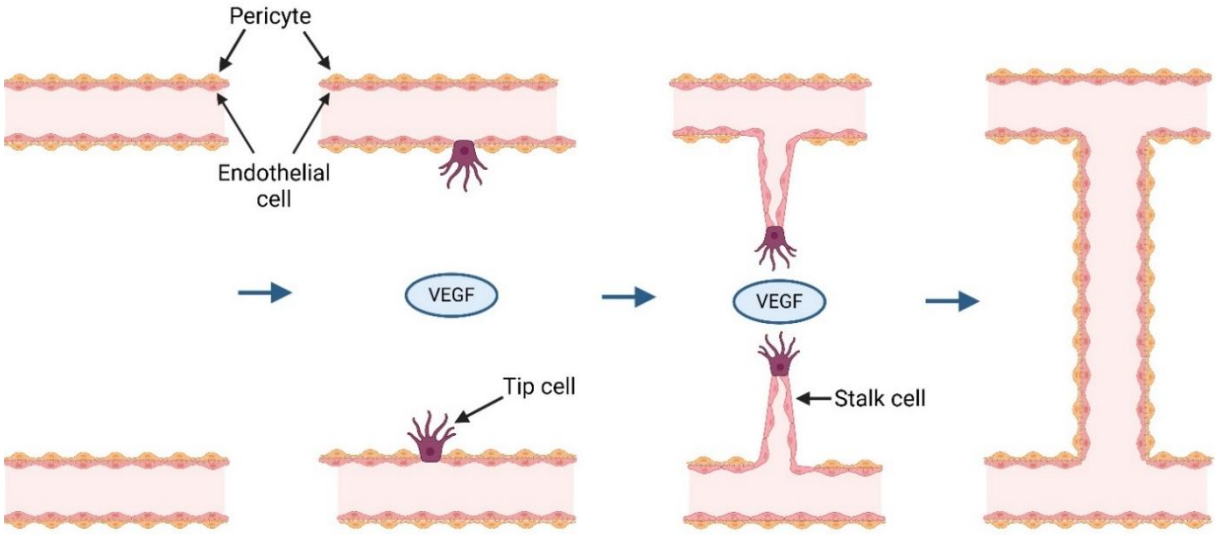

Figure 1.1 Diagram of the sprouting angiogenesis process.
Endothelial cells form a monolayer in the inner lining of a blood vessel wall, pericytes envelope the endothelial cell monolayer. The endothelial cells within the area of highest *VEGF* concentration activates to form a tip cell (shown in purple). The tip cell navigates towards the *VEGF* signal via numerous *VEGF* receptor-containing filopodia. Stalk cells proliferate behind extending the sprout. The tip cells of two opposing sprouts fuse to form a lumen which creates an interconnecting network of blood vessels. Image created in Biorender.com

The migration of a blood vessel to the angiogenic stimulus as a sprout, rather than as a sheet of endothelial cells, proves not all endothelial cells respond to an angiogenic stimulus (Karamysheva, 2008). Instead, one cell is selected to lead the sprout of endothelial cells towards the signal, this cell is known as the tip cell. Tip cells are characterised by numerous motile filopodia that sense and guide the sprout towards gradients of *VEGF-A* with little or no proliferation occurring, only migration (Carmeliet & Jain, 2011; Siemerink et al., 2013). The endothelial cells that follow the tip cell creating the sprout are known as stalk cells. Stalk cells, unlike tip cells, do proliferate elongating the sprout until opposing tip cells meet, to form and reestablish endothelial cell junctions which fuse to form a lumen (De Smet et al., 2009). The selection of endothelial cells to either become tip cells or stalk cells is a dynamic process mediated by *VEGF-A* and *Notch* signalling pathways. Tip cell formation and sprouting are identified in areas with a high level of *VEGF-A*, a low gradient of *VEGF-A* results in reduced tip cell migration (Gerhardt et al., 2003). Interference of *Notch* signalling via pharmacological administration of known *Notch* pathway inhibitors or genetic alteration to *Notch* ligand *delta-like ligand 4* (*Dll4*) has been demonstrated to increase the number of tip cells and sprouting activity (Hellström et al., 2007). Tip cells express increased levels of (*Dll4*) compared with stalk cells as a result of *VEGF-VEGFR-Dll4-Notch-VEGFR* negative feedback loop. *VEGF-VEGFR2* binding leads to increased expression of *Dll4* in tip cells, this in turn activates the *Notch* signalling pathway on adjacent cells reducing *VEGFR2* expression, suppressing tip cell formation and migratory ability inducing stalk cell phenotype. Stalk cells in turn express another *Notch* ligand, *Jagged 1*, which suppresses *Notch* signalling in the adjacent tip cell increasing *VEGFR2* expression and therefore the ability to bind to *VEGF* and continue the *VEGF/Notch* crosstalk (Blanco & Gerhardt, 2013).

As the sprout migrates towards the angiogenic stimuli, such as *VEGF-A*, led by the tip cell and elongated by proliferating stalk cells, a lumen develops within the stalk cell sprout. Though exact mechanisms are unknown, models have been suggested to explain lumen formation within stalk cells reviewed by Tung et al., (2012). Briefly, one such model proposes tubulogenesis to occur via intracellular vesicular fusion within stalk cells effectively "hollowing" the cell. The lumen is then opened on either end through vacuolar fusion with adjacent hollowed cells forming an intercellular lumen across multiple adjacent stalk cells (Davis & Camarillo, 1996; Kamei et al., 2006). Once tip cells from opposing sprouts fuse, a continuous lumen is formed. After blood flow is established through the newly formed lumen, *VEGF-A* signalling is decreased and the newly formed vessel matures into a stabilized capillary via pericyte recruitment and attachment (Adair & Montani, 2010).

1.2.2 Intussusceptive (non-sprouting) angiogenesis

Sprouting angiogenesis was originally believed to be the only form of angiogenesis, until an alternative mechanism of angiogenesis was proposed in 1986 following examination of postnatal rat lung blood vessel structure using scanning electron microscopy (SEM) (Caduff et al., 1986). These SEM observations showed that during the capillary growth phase small holes, rather than sprouts, formed within the alveolar microvasculature resembling a "pillar" within the blood vessel lumen. This form of growth was subsequently termed intussusceptive (in-itself) or splitting angiogenesis, due to extension of the vessel wall into a lumen, effectively splitting a singular vessel into two (Fig 1.2). The formation of a pillar is the trademark characteristic of intussusceptive angiogenesis, differing from endothelial cell proliferation characteristic of sprouting angiogenesis. Intussusceptive angiogenesis leads to a faster growth of existing vasculature compared with sprouting angiogenesis as there is no

endothelial cell proliferation only endothelial cell protrusion and fusion (Ribatti & Djonov, 2012). The molecular mechanisms of intussusceptive angiogenesis are not as clearly defined as the sprouting mechanism; yet it is known that four phases of pillar formation occur. Phase I involves the extension of opposite capillary walls into the lumen forming an inter-endothelial transluminal bridge. Phase II begins with the perforation of the endothelial bilayer to create an interstitial pillar core which is invaded by myofibroblasts and pericytes in phase III. Growth of the transcapillary pillar results in the splitting into two blood vessels in the final phase IV (Burri & Tarek, 1990; Kurz et al., 2003).

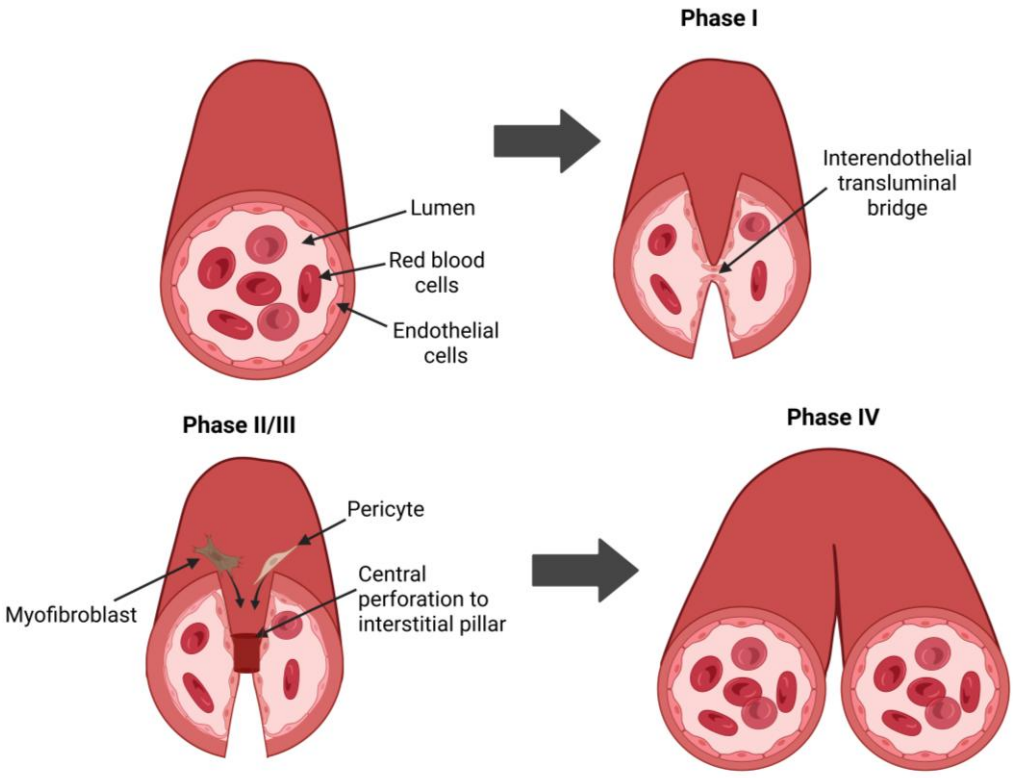

Figure 1.2 Diagram of the intussusceptive angiogenesis process.
During the 'splitting' process, the blood vessel wall of a single vessel extends into the lumen from opposing sides forming a transcapillary inter-endothelial bridge. The bridge connection is then perforated centrally to form a transcapillary pillar which grows following endothelial cell retraction and fibroblast and pericyte invasion. The pillar growth eventually splits the vessel into two separate vessels. Image created in Biorender.com

1.2.3 Intracellular regulators of angiogenesis

Both sprouting and intussusceptive angiogenesis are dynamic processes involving numerous molecular signalling pathways that regulate many cellular mechanisms. Some of the main mediators of angiogenesis and associated roles are described below.

1.2.3.1 Vascular endothelial growth factor (*VEGF*)

There are several members of the *VEGF* family including *VEGF-A*, *VEGF-B – D*, and placental growth factor (*PlGF*) all present in the human genome. These secreted proteins are characterised by the presence of a cystine-knot three-dimensional structure important for cell-cell signalling and receptor binding (Holmes & Zachary, 2005; Vitt et al., 2001). The most researched and described growth factor regarding angiogenesis is *VEGF-A* (Ferrara & Davis-Smyth, 1997). The biological effects of *VEGF-A* and other members of the *VEGF* family occur via the binding to vascular endothelial growth factor receptors (*VEGFR*s) found on endothelial cell membranes as shown in Fig 1.3. Three receptors have been identified in mammalian genomes: *VEGFR1*, *VEGFR2* and *VEGFR*3. These are tyrosine kinase receptors that are auto-phosphorylated upon ligand binding, activating downstream signalling cascades involved in multiple cellular processes (Patel et al., 2023). The binding of ligands to *VEGFR*3 promotes lymphangiogenesis and the growth of vessels in the lymphatic system (Takahashi & Shibuya, 2005). The binding of *VEGFR1* and *VEGFR2* with the respective *VEGF* ligands (including the shared compatibility with *VEGF-A*) result in activation of pathways associated with vasculogenesis and angiogenesis. *VEGFR1* has a tenfold higher affinity for *VEGF-A* (Shibuya & Claesson-Welsh, 2006) although the most direct angiogenic effect of *VEGF-A* is exhibited through interaction with *VEGFR2*. *VEGF-A*/*VEGFR2* binding promotes endothelial cell proliferation through the extracellular signal-regulated kinase/mitogen-activated protein

kinase (*ERK/MAPK*) pathway (Ferrara, 2004), endothelial cell survival through the phosphoinositide 3-kinase (*PI3K*)/protein kinase B (*PKB*)/*AKT* pathway (Ferrara, 2004; Koch et al., 2011) and endothelial cell migration through the p38 mitogen-activated protein kinase (*p38-MAPK*) pathway, (Cébe -Suarez et al., 2006). The activation of the *PKB/AKT* signalling pathway also leads to an increase in endothelial nitric oxide synthase (*eNOS*) production increasing vascular permeability, one of the earliest markers of angiogenesis (Bates & Harper, 2002).

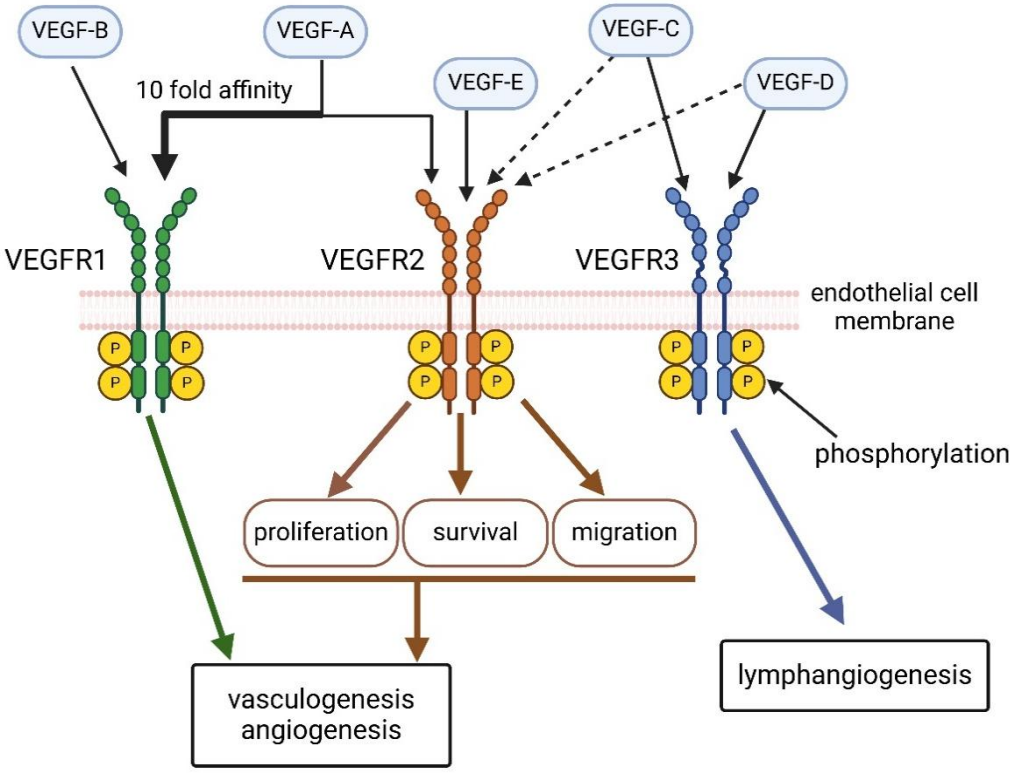

Figure 1.3 Schematic outline of the angiogenic effect of VEGF ligands and the respective receptors.

Three tyrosine kinase receptors *VEGFR1*, 2 and 3 bind to specific *VEGF* ligands. *VEGFR2* shares ligand affinity with *VEGFR*3, however only processed *VEGF-C* and *D* (dashed arrow) can bind to *VEGFR2*. *VEGF-A*, the main mediator of angiogenesis, binds to both *VEGFR1* and *2* with a higher affinity for *VEGFR1* indicating antagonistic effects of *VEGFR1*. Although much weaker than *VEGFR2* signalling, *VEGF-A*/*R1* binding does promote vasculogenesis and angiogenesis. The most direct angiogenic effect is through *VEGF-A*/*R2* binding. Activating downstream signalling pathways promoting endothelial cell proliferation, survival and migration.

1.2.3.2 Endothelial nitric oxide synthase (*eNOS*)

eNOS is a constitutively expressed enzyme with key roles in the regulation of cellular function. As the name suggests, *eNOS* when activated, causes the production of nitric oxide (NO) through the conversion of L-arginine and oxygen to L-citrulline and NO (Tran et al., 2022). NO is important in a variety of cellular physiological functions as a regulator of cell metabolism (Tenopoulou & Doulias, 2020), as a neurotransmitter (Bredt & Snyder, 1992) and, importantly for the present study, as a mediator for vascular homeostasis and angiogenesis (Ziche & Morbidelli, 2000). NO production induces angiogenesis via increased endothelial cell proliferation, migration (Lu et al., 2015) and survival (Dimmeler & Zeiher, 1999). The expression of *eNOS* and subsequent production of NO is regulated by numerous transcription factors that bind to the *eNOS* promoter described in a review by Fleming and Busse (2003). Posttranscriptional regulation occurs through multiple RNA-protein interactions affecting *eNOS* mRNA stability before it is translated into the *eNOS* protein. Transforming growth factor-β1 (Saura et al., 2002) and hydrogen peroxide (Thomas et al., 2002) increase *eNOS* expression, whereas tumour necrosis factor-α has an inhibitory effect on *eNOS* mRNA stability (Yoshizumi et al., 1993). Posttranscriptional regulation also occurs via the actin cytoskeleton described in 1.2.3.3. Phosphorylation of *eNOS* is the most studied posttranslational process regulating activity with eight phosphorylation sites identified. Another level of complexity to this regulation is associated with the phosphorylation site; some result in activation of *eNOS* whereas others result in inhibition of *eNOS* (Heiss & Dirsch, 2014). In summary, *eNOS* regulation is a complex process involving multiple factors that affect the production of NO and subsequent angiogenesis processes.

1.2.3.3 Actin cytoskeleton

The cytoskeleton of a cell is essential in maintaining cellular shape, internal organisation and essential functions including cell division and motility. There are three main elements that make up the cytoskeleton: microfilaments (actin filaments), microtubules and intermediate filaments (Fletcher & Mullins, 2010). Actin, along with actin related proteins (ARPs) is one of the most abundant, highly conserved proteins in seemingly all eukaryotic cells (Goodson & Hawse, 2002; Pollard, 2016). Actin is present in cells as a monomer, G-actin, or as a filament, F-actin, the product of G-actin polymerisation. The monomeric G-actin forms a ribonucleoprotein with *eNOS* increasing *eNOS* activity and inducing *eNOS* phosphorylation and activation (Mi et al., 2011; Searles at al., 2004). The total amount of actin within a cell never changes, rather the ratio of monomer to polymer is continuously regulated through remodelling (Osborn et al., 2006). This remodelling of the actin cytoskeleton is crucial to the maintenance and growth in a variety of cell types such as plant cells (Wasteneys & Galway, 2003), immune cells (Dupré & Prunier, 2023) and endothelial cells (Nair et al., 2022). It has been shown that blocking the formation and organisation of actin filaments causes defects in cell motility, migration and membrane protrusion – hallmarks of angiogenesis (Chau et al., 2022; Laviña et al., 2018; Monkley et al., 2011). The elongation of endothelial cells, during sprouting angiogenesis is also driven by remodelling of F-actin filaments (Sauteur et al., 2014).

1.2.3.4 Platelet cell adhesion molecule (*PECAM-1*)

The characteristics of angiogenesis are the formation of inter-endothelial cell junctions and the adhesive ability of endothelial cells. A cell adhesion molecule highly expressed at these junctions is platelet cell adhesion molecule (*PECAM-1*/*CD31*). *PECAM-1* is a glycoprotein

also recognised as an endothelial cell marker due to its ubiquitous and abundant expression on endothelial cell membranes (Müller et al., 2002). Evidence for *PECAM-1* involvement in angiogenesis was identified in an *in vivo* animal model where angiogenesis was inhibited after blocking *PECAM-1* function using anti*PECAM-1* antibodies (DeLisser et al., 1997; Matsumura et al., 1997; Zhou et al., 1999) and *in vitro* (Cao et al., 2002; Matsumura et al., 1997). The presence and functionality of *PECAM-1* is critical to endothelial cell adhesion and junction formation due to its homophilic binding properties (Lertkiatmongkol et al., 2016). As the most abundant component of endothelial cell junctions, the ability to form *PECAM-1/PECAM-1* interactions strongly influence the endothelial junction integrity which is essential for the overall integrity of the vascular network (Privratsky et al., 2011).

1.2.3.5 von Willebrand factor (*VWF*)

Another endothelial cell marker that plays a role in angiogenesis is the glycoprotein von Willebrand factor (*VWF*) that is synthesised by endothelial cells and megakaryocytes (Mannucci, 1995). *VWF* is stored in Weibel-Palade bodies (WPBs) within endothelial cells, the formation of such bodies *VWF* also initiates (Sporn et al., 1986; Wagner et al., 1991). *VWF* has been shown to regulate angiogenesis in an inhibitory manner. *In vitro* experimentation showed knockdown of the *VWF* gene resulted in increased HUVEC angiogenic behaviour (Starke et al., 2011). *In vivo* experimentation showed increased vascular density in *VWF* deficient mice (Starke et al., 2011; Xu et al., 2017) and clinically dysfunction of *VWF* causes abnormalities in the vasculature of patients with von Willebrand disease - VWD (Sadler et al., 2006).

1.3 Angiogenic therapy

1.3.1 Treatment approach for disease

Defective vasculature can result in severe diseases as shown in cases of VWD due to the limited or absent delivery of oxygen and nutrients. Medical management of ischaemic tissue disease, via the use of clinically approved drugs such as statins, beta blockers and aspirin (Fraker et al., 2007), aims to alleviate symptoms of stable coronary artery disease (CAD). For patients with severe CAD the promotion of blood vessel growth through more invasive techniques increases blood flow and restores function to ischaemic tissue. The two accepted treatment approaches are coronary artery bypass grafting (CABG) introduced in 1968 (Favaloro, 1998) and percutaneous coronary intervention (PCI) introduced in 1977 (Gruntzig, 1978). CABG involves the use of harvested arteries or veins (grafts/conduits) to redirect blood flow bypassing blocked sections of the artery. PCI is less invasive requiring the placement of a stent to dilate narrowed or blocked areas of the coronary artery. Over the past 20 years there has been an ongoing debate into the compared effectiveness of the two treatments described in various review articles (Habib et al., 2015; Lisko et al., 2019; Simoons & Windecker, 2010; Spadaccio & Benedetto, 2018). The consensus from trials studied is that CABG is the most optimal treatment for patients with more severe and multivessel coronary disease. However, there are patients remaining that do not qualify for surgical intervention. End-stage CAD patients and patients with compounding conditions pose a high surgical risk. A potential treatment option for such patients is therapeutic angiogenesis - the influence on the angiogenesis process and its many molecular regulators (Khan et al., 2002; Sellke et al., 1998). Proposed methods of inducing angiogenesis involve protein (growth factor), gene and cell delivery to the ischemic tissue region, as well as using small microparticles (exosomes) as a drug delivery system (Johnson et al., 2019).

It is not only an insufficient vascular system that can lead to diseases. Uncontrolled blood vessel growth, known as excessive angiogenesis, can also lead to the development of several conditions. Abnormal growth of blood vessels, development of disorganised and dysfunctional vessels and abnormal remodelling of blood vessels is found in a variety of diseases such as cancer (Carmeliet & Jain, 2000), arthritis (Walsh, 1999), and blindness (Sapieha et al., 2010). The treatment of such diseases via angiogenesis intervention is known as antiangiogenic therapy and is mostly associated with cancer treatment. The most common way of controlling angiogenesis is the delivery of process inhibitors. In cancer treatment anti-angiogenic drugs are used to target specific pathways in the angiogenesis process – notably the *VEGF*/*VEGFR2* signalling pathway as in the case of the drug Bevacizumab (Kazazi-Hyseni et al., 2010). Bevacizumab was the first approved anti-angiogenic drug proven to slow down tumour growth rate and extend patient lives. There are now more than a dozen FDA-approved angiogenesis inhibitors used for cancer treatment (Yoo & Kwon, 2013). However, there are issues with the use of antiangiogenic drugs in cancer treatment. Inhibitors do not target the cancerous cells directly; rather a means of preventing tumour growth therefore extending patient's lifespan but not treating the tumours themselves (Mukherji, 2010). There is also a drawback with development of tumour resistance to inhibitor drugs (Shojaei, 2012). Nonetheless anti-angiogenic therapy is a promising field of research for cancer therapy and other diseases associated with uncontrolled angiogenesis.

1.3.2 Angiogenesis and surgery

The process of wound healing and tissue repair is an essential part of the surgical procedure. Disruption to the surgical wound healing process may happen through infection, delayed healing or hypergranulation. This is one of the largest causes of post-surgery morbidity in

Europe (Pearse et al., 2012). Wound management places a large burden on NHS finances; as reported in a 2017/2018 cohort study the annual NHS cost was measured at £8.3 billion, of which £5.6 billion was attributed to managing unhealed wounds (Guest et al., 2020). Specifically, the mean annual cost per patient with an unhealed surgical wound was £2024.49, compared with £884.11 to care for healed surgical wounds. The large disparity in cost attributed to healed versus unhealed surgical wounds highlights the importance correct wound healing has economically as well as morally for patients' standard of living. These figures represent a 48 % increase in patient management cost compared to a 2012/2013 cohort study (Guest et al., 2017). Therefore, with the increase of population, the number of surgeries and the cost of supplies since 2017/2018, it can be hypothesised these numbers will continue to rise. The need for solutions and improvements to surgical wound healing should not be ignored.

Angiogenesis plays a crucial role in wound healing – in fact 60 % of new granulation tissue consists of blood vessels (Pettet et al., 1996). A state of hypoxia at the wound site initiates the angiogenesis process (Section 1.2). Pro-angiogenic factors stored by platelets and inflammatory cells are released stimulating endothelial cell proliferation, migration and sprouting (Yoshida et al., 2003). The formation of new blood vessels allows delivery of oxygen and nutrients to the site of damage, removal of waste products and deposition of new connective tissue. Once oxygen delivery is restored, inflammation at the site is decreased and consequently a decline in proangiogenic factors is noted. Newly formed vessels are stabilised and ultimately angiogenesis is suppressed (Kumar et al., 2009).

The necessity for adequate blood supply in tissue repair can be seen in cases of bone fracture healing. Bone tissue has the capability to regenerate itself through the generation of new bone in a process termed osteogenesis (Ferguson et al., 1999). However fracture healing is not always successful with 10 % of fractures resulting in delayed healing or non-union of broken bones (Stegen et al., 2015). An inadequate vascular network is associated with improper fracture healing evidenced in several research studies analysing the association of angiogenesis with proper bone healing ability. Hausman et al., (2001), used *in vivo* administration of an angiogenesis inhibitor TNP-470 in rat models. There was an absence of bone healing capability with a significant decrease in bone strength and stiffness, traits that are consistent with clinical atrophic non-union cases. Similar failures of osteogenesis were found in other rat models following TNP-470 administration (Fang et al., 2005). Osteogenesis is dependent on the vascular network and followed by the correct regulation of the angiogenesis process.

As these studies have demonstrated a dependency of correct wound and bone healing on angiogenesis, therapeutic angiogenesis may be implicated in the enhancement of wound healing and tissue repair post-surgery. Finding a non-invasive method to stimulate angiogenesis with the aim of accelerating the healing process, with minimum distress to the patient, has been of clinical interest for many years. The use of ultrasound is an approach that may be adopted to assist in the angiogenesis process. Such a method may be applied during the surgical procedure itself, rather than aftercare, in the use of ultrasonic surgical devices and the subsequent biological effects of ultrasound.

1.4 Introduction to ultrasound

The human auditory range can detect sound waves with frequencies between 20 Hz and 20 kilohertz (kHz) (Fig 1.4). Sound waves that have frequencies above this limit are classified as ultrasound waves whilst those with frequencies lower than this range are known as infrasound waves.

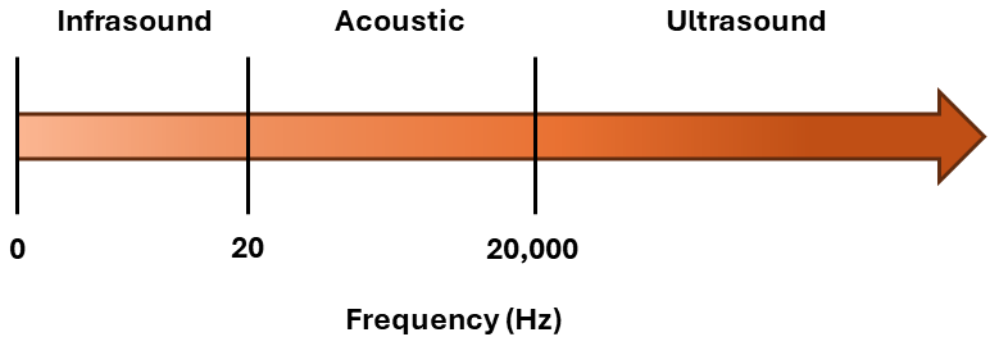

Figure 1.4 Classification of sound wave frequencies.
Sound waves above frequencies of 20 kHz are known as ultrasound waves. Sound below the acoustic lower frequency limit of 20 Hz is known as infrasound.

1.4.1 A brief history of ultrasound

The discovery of sound waves inaudible to the human ear is credited to Italian biologist, Lazzaro Spallanzani during studies of echolocation in bats in 1794. It was realised blinded bats could avoid obstacles just as well as unblinded bats, however if the bat's ears were plugged with wax, there were consistent collisions with the obstacles, indicating sound was a more important sense than sight for navigation (Kaproth-Joslin et al., 2015). The next breakthrough in ultrasonics would arrive nearly a century later, in 1880, when the Curie brothers published the discovery of piezoelectricity. When pressure is applied to quartz crystals an electrical charge proportional to the force applied is produced. This discovery was

a fundamental step in the development of ultrasonic technology (Mould, 2007). A student of Pierre Curie, Paul Langevin, furthered this initial discovery in 1915 during his work with the French Navy where they were developing an underwater detection system to locate German U-boats using echolocation (Zimmerman, 2002). By 1917 Langevin had exploited the dual nature of piezoelectric quartz crystals as both a transmitter and receiver of sound waves and thus began the modern ultrasonics era. The device was made of thin quartz crystals held together by glue between two metal plates. Application of an alternating current resulted in the emission of high frequency megahertz (MHz) sound. When employed underwater this device could emit and detect the returning echo sound wave. This allowed navy intelligence to map and locate submarines which was crucial for underwater enemy detection during the First World War (Katzir, 2012). An attempt to develop an underwater detection system, more aptly known as collision avoidance system, was made by Canadian electrical engineer Reginald Fessenden after the catastrophic sinking of the Titanic in 1912. The device tested the ability of using a Morse code generator as an echo sounder to produce high frequency sound waves. The device was able to detect icebergs up to 2 miles away, however the use of continuous waves rather than intermittent pulses created interference which unfortunately limited the commercial application of this device (Zimmerman, 2002). Langevin, rather than Fessenden, is therefore credited with the invention of **So**und **Na**vigation and **R**anging "SONAR". While SONAR is still used in underwater imaging, mapping and communications, the principle of using sound waves to detect objects in a surrounding area has also been applied to the medical diagnostics field in ultrasonography.

1.4.2 The principle of sound

Sound is a mechanical vibration that propagates as a wave through or along a medium (solid, liquid or gas). As the wave travels, the particles within the medium oscillate around the resting position. Particles are not permanently displaced during wave propagation; there is no mass movement but a transfer of energy via a sequence of compression where particles move closer together, and rarefaction where particles separate (O'Brien, 2007). These periods of compression and rarefaction can be represented as periodic oscillations of peaks and troughs over time (Fig 1.5). These peak and troughs of the waves correspond with the maximum displacement of particles from the resting positions which is termed amplitude. It is measured as the maximum pressure above or below the line of equilibrium (top of a peak or bottom of a trough) (Patey & Corcoran, 2021).

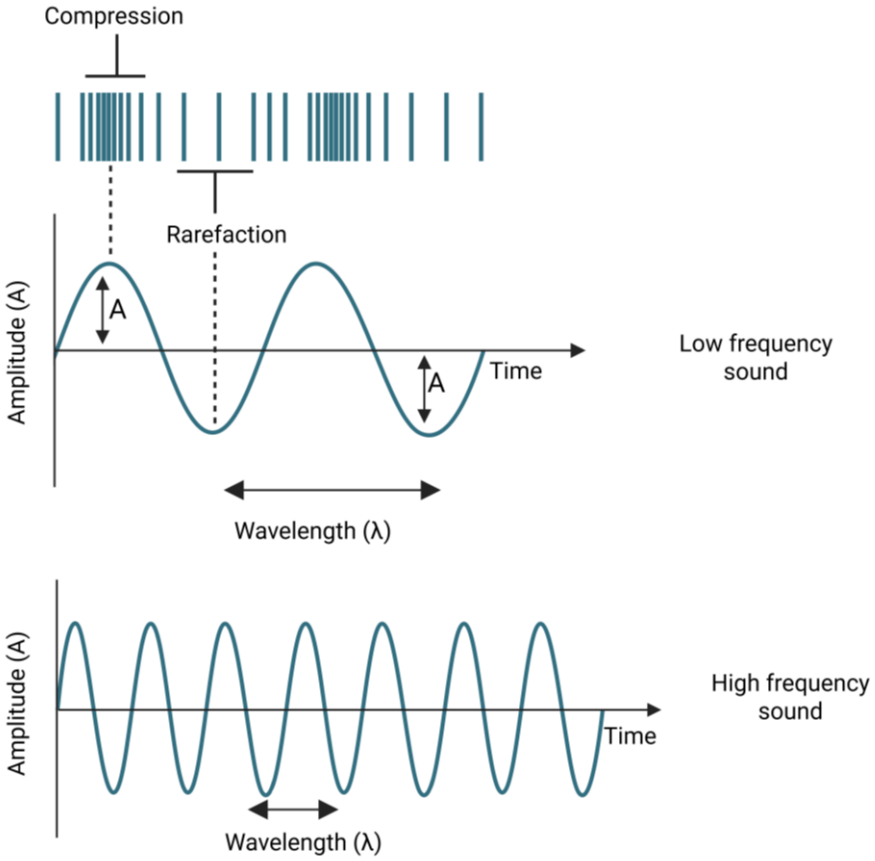

Figure 1.5 Diagram of longitudinal wave propagation.
Longitudinal waves consist of particles oscillating back and forth parallel to the direction of the wave. This creates areas of compression where particles are closer together and rarefaction where particles are spaced further apart. The areas of compression and rarefaction correspond with peaks and troughs of amplitude (A) seen in the sound wave. Amplitude (A) is shown as the peak displacement from rest. Wavelength (λ) is the distance between one peak to the next adjacent peak or trough to the next trough. Low frequency sound waves have a longer wavelength compared with higher frequency sound waves.

The distance of one complete oscillation or cycle – one peak to the next or trough to the next, is known as wavelength universally represented by λ. The time it takes for one cycle to complete is known as the wave period (*T*). Sound frequency (*f*) is defined as the number of oscillations per second measured in Hertz (Hz). The frequency of a sound wave is determined by the speed of the wave within a medium, known as the speed of propagation or velocity (*v*). When the velocity of a wave is constant, frequency is inversely proportional to wavelength;

the higher the frequency, the shorter the wavelength (Fig 1.5). The relationship between the properties of sound can be demonstrated by the following equations.

Equation 1.1. The relationship between wave velocity (*v*), period (*T*) frequency (*f*) and wavelength (*λ*).

$$f = \frac{1}{T}$$

$$T = \frac{1}{f}$$

$$v = f\,\lambda$$

$$v = \frac{\lambda}{T}$$

1.4.2.1 Acoustic impedance and attenuation

As a sound wave propagates through medium, it encounters resistance and opposition to the propagation by the medium which is known as acoustic impedance (*Z*). Specific acoustic impedance of a material is recognised as the product of the material density (*p*) and the speed of the sound wave passing through the medium (*c*) (Patey & Corcoran, 2021) (Equation 1.2).

Equation 1.2 Definition of an acoustic material's impedance value.

$$\mathrm{Z} = p\,c$$

The loss of a wave's energy and decrease of amplitude as it propagates through a medium is known as the attenuation of a wave. There are three main forms of wave attenuation: reflection, refraction and scattering (Fig 1.6).

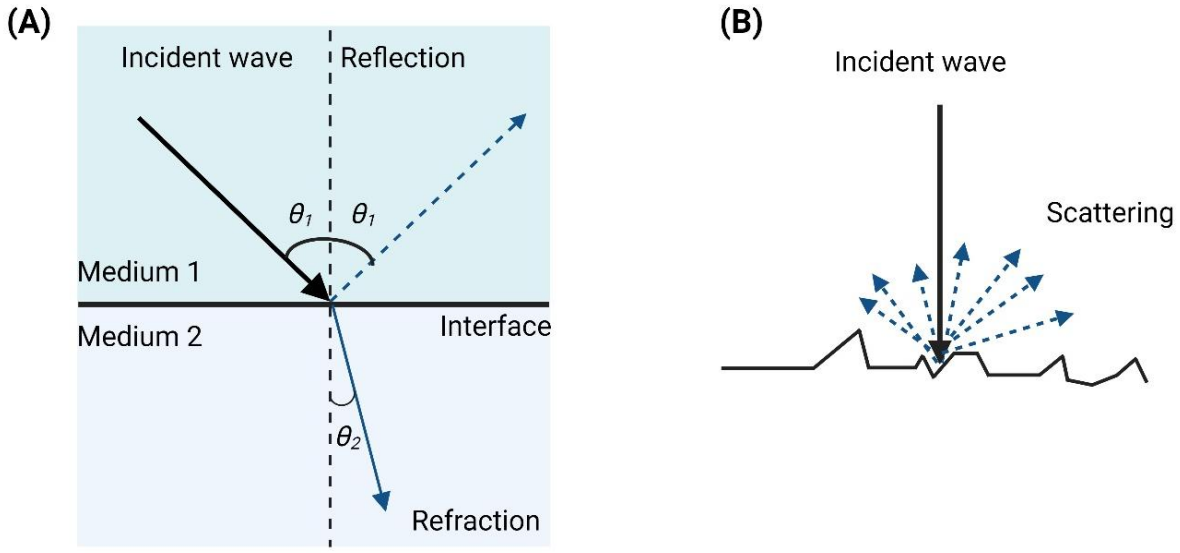

Figure 1.6 Transmission of an acoustic wave through a medium interface.
(A) An acoustic wave passes through a medium. As it encounters an interface between this medium and a different medium part of the wave will be reflected at the same angle as the incident wave (Θ_1). Part of the wave will pass into the different medium at a different refracted angle (Θ_2). (B) At an interface with an irregular surface or where the impedance value is smaller than the incident wave wavelength, the wave is reflected in many directions and is scattered.

Reflection occurs when there is a change in acoustic impedance during wave propagation, for example at a boundary of two different mediums. The greater the difference in impedance values the more energy reflected at the boundary interface than transmitted through the medium. A phenomenon that can occur due to wave reflection is the creation of standing waves. Standing waves are created when an incident wave is reflected to the source at a boundary such that the reflected wave superimposes on the incident wave. The superimposition of waves creates areas of maximum displacement amplitude (antinodes) and areas of minimum displacement (nodes) (Snehota et al, 2020). Large acoustic impedance mismatches occur at the boundaries of air, water, and solids. In the human body the different densities of the tissue will lead to a range of acoustic impedance mismatches. The largest mismatch will occur between hard and soft tissues. Not all of the wave is reflected; the

remainder of the wave energy will pass across the boundary into the other medium at a refracted angle. If the acoustic wave meets a boundary with an irregular surface, the wave will be reflected in multiple directions, termed scattering. If the boundary or scattering object is significantly smaller than the wavelength of the acoustic wave (λ) the scattering effect is specifically termed Rayleigh scattering. For example, Rayleigh scattering occurs within the body when an ultrasound wave encounters red blood cells moving within blood vessels (Meola et al., 2021).

1.5 Biological effects of ultrasound

The use of ultrasonic surgical devices in a variety of clinical settings today is thanks to early experiments from the 1920s. Paul Langevin, the credited inventor of the hydrophone, was the first observer of detrimental effects on living tissue by an ultrasound beam. When high intensity ultrasound was applied within a small tank, fish within the beam of energy were killed immediately (Langevin, 1920). A later experiment also observed high intensity ultrasound killing small animals such as fish, frogs and rupture of protists *Spirogyra* and *Paramecium* (Wood & Loomis, 1927). The specific ultrasound conditions for both studies were unreported and the mechanisms behind such detrimental effects were unclear. Nevertheless, such effects have generated continued research interest since first being observed as researchers look to identify the mechanisms involved in the biological effects of ultrasound. The biological effects of ultrasound may be separated into two categories: thermal and non-thermal effects.

1.5.1 Thermal effects

The amplitude of an ultrasound wave decreases during propagation through medium as the energy transferred within the wave is either absorbed or dispersed in a process termed attenuation. The most common form of attenuation in the human body is the absorption of wave energy and conversion to thermal energy increasing the temperature of the surrounding tissue (Patey & Corcoran, 2021). The amount of energy absorbed is directly related to the frequency and intensity of the wave. Higher frequencies and intensities of the ultrasound will lead to a larger thermal effect. The size of the area within an ultrasound beam will also alter the amount of heat absorbed as intensity is defined per unit area. A focused beam will result in greater thermal effect compared with an unfocused acoustic field (Quarato et al., 2023). The intensity of an ultrasound beam and thus the thermal effect is also influenced by the temporal aspect of the ultrasound delivery. Ultrasound can be delivered in a pulsed manner of intermittent short bursts with periodic on/off cycles, or in a continuous manner involving constant steady delivery of ultrasound energy with no on/off cycles. Pulsed wave emission results in temporal variations in intensity with peak intensity during the pulse "on" period and zero intensity during the "off" period between pulses. The temporal average intensity, measured over the complete pulse period, is therefore lower than the peak intensity. The temporal average intensity is the more relevant parameter to assess thermal effect of pulsed ultrasound as heating is cumulative and proportional to energy absorption over time. The lower the temporal average intensity, the longer the "off" periods of ultrasound resulting in a lower overall energy delivered and subsequently lower thermal effect. Contrastingly, during continuous wave emission, intensity is constant over time, resulting in a higher cumulative heating effect due to the absence of "cooling off" periods (Quarato et al., 2023).

The amount of heat energy absorption by a tissue is related to various properties of the tissue itself. Hence, each tissue has a different attenuation coefficient and this will lead to a range of thermal effects as ultrasonic energy passes through the tissues (Table 1.1). One such example of a property affecting the heat energy absorption is the amount of protein present; as the amount of protein increases, absorption of the wave energy increases (Stewart & Stratmeyer, 1982). Protein makes up ~ 50% of bone therefore bone has a high attenuation coefficient compared with blood. However lung tissue contains a smaller protein content than bone yet has a higher attenuation coefficient. In the case of lung tissue, the high attenuation coefficient can be attributed to the internal lung structure of many branching bronchioles giving rise to several alveolar ducts, which in turn contain numerous gaseous alveolar sacs (Dunn & Fry, 1961). The presence of these multiple air and tissue interfaces results in the reflection and scattering of the acoustic wave as it travels through the lung tissue leading to a high attenuation coefficient.

Table 1.1 Attenuation coefficients of different tissues.
Tissues within the human body demonstrate different attenuation coefficients due to their varying compositions. Table adapted from (Quarato et al., 2023; Shankar & Pagel, 2011).

Tissue	**Attenuation Coefficient (Decibels/cm/MHz)**
Blood	0.15
Skin	0.35
Fat	0.63
Soft Tissue	0.75
Bone	15.00
Lung	40.00

Heat transfer through living tissue depends on thermal conduction, perfusion (blood flow) and the metabolism of the tissue. These factors have been used to create a mathematical bioheat transfer model for heat propagation in living tissue (Pennes, 1998). The thermal effect of ultrasound on tissue can thus be determined and controlled by altering ultrasound exposure parameters. Therapeutic applications of ultrasound take advantage of such thermal effects to increase blood flow, increase the elasticity of collagenous structures leading to improvements of mobility, decreasing joint stiffness and reduction of pain (ter Haar, 1999). The increase of blood supply to the area results in better oxygen and nutrient supply improving angiogenic therapy approaches to treatment (Section 1.3). Enzymatic activity in cells, which is a temperature dependent process, will also be improved. The temperature coefficient rule for enzymes (Q_{10}) states that enzymatic activity increases by a factor of 3 with each 10 °C increase in temperature (O'Brien, 2007). However, exposure to temperatures ≥ 45 °C will be detrimental and cause protein denaturation, disruption and ultimate cessation of enzymatic activity leading to cell death (Lepock, 2005). Exposure to temperatures below the critical limit of 45°C have been shown *in vitro* to have lethal effects if exposed for lengthy time periods. HeLa cells exposed to temperatures of 41 – 45 °C resulted in cell death exponentially proportional to the length of exposure time (Gerner et al., 1976)

1.5.2 Non-thermal effects

Thermal effects may be reduced where the ultrasound is emitted at low frequency, intensity and peak-negative acoustic pressure. Pulsed ultrasound rather than a continuous wave emission will also reduce any heating. As biological effects from the ultrasound are still observed this suggests that there may also be non-thermal effects occurring in the tissues

caused (Dyson, 1982). Non-thermal effects of ultrasound, also known as mechanical effects, include cavitation, acoustic streaming, and radiation forces.

1.5.2.1 Cavitation

As a sound wave propagates through a liquid it causes areas of high acoustic pressure (compression) and low acoustic pressure (rarefaction). Once the liquid cannot support the negative pressure a microscopic bubble is formed. The growth, expansion and rapid collapse of these bubbles is known as cavitation. The acoustic pressure of a sound wave can result in either non-inertial (stable) (Fig 1.7 A) or inertial (transient) (Fig 1.7 B) cavitation.

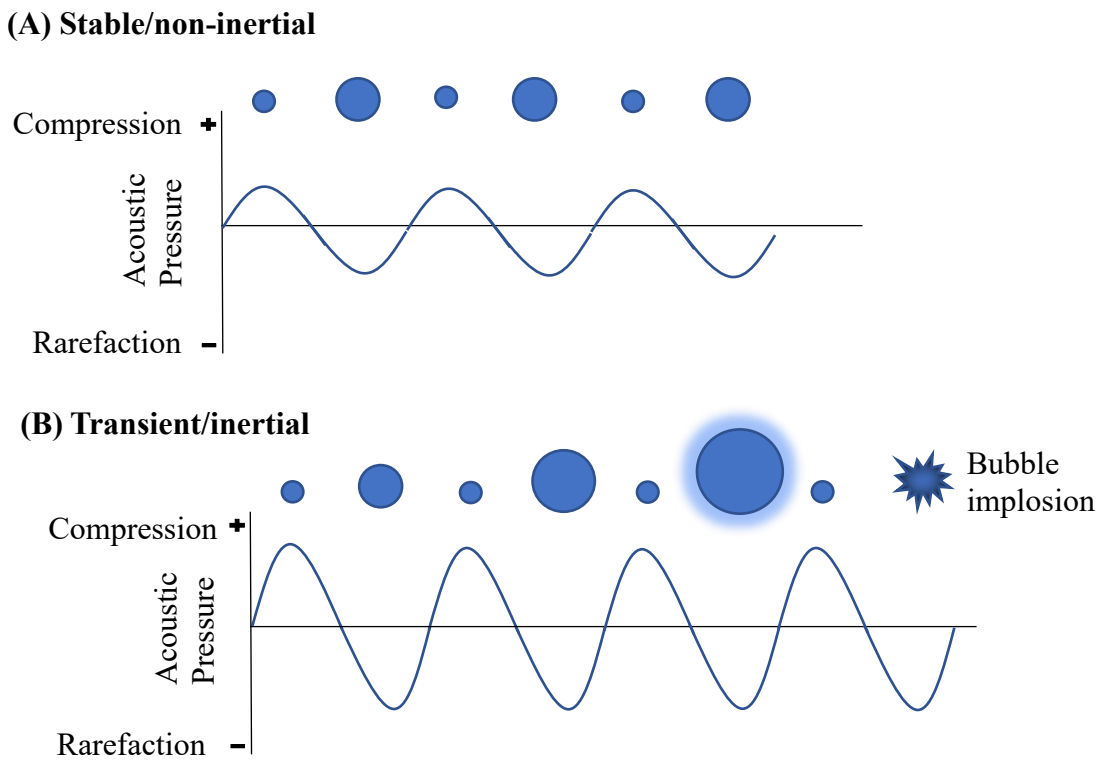

Figure 1.7 Diagramatic depiction of the cavitation process.
(A) At low to moderate peak-negative acoustic pressure microscopic gas bubbles oscillate slightly increasing and decreasing in size. This is known as stable or non-inertial cavitation. (B) When the peak-negative acoustic pressure exceeds that which the medium can withstand gas bubbles expand and collapse rapidly to a much smaller size. This implosion creates localised temperature and pressure hotspots and release of large amounts of mechanical energy. This is known as transient or inertial cavitation.

Inertial cavitation involves high acoustic pressure that exceeds a threshold based on specific sound field and bubble parameters (Leighton, 1998) resulting in expansion of gas bubbles to at least double the diameter after which implosion occurs (Wu & Nyborg, 2008). The implosion creates localised increases of temperature and pressure that can lead to the formation of free radicals known to be involved in various biochemical reactions (Suslick, 1990). The large amount of energy released has also been exploited in surgical applications such as in lithotripsy treatment, where gallstones are broken down (Vakil & Everbach, 1993) and ultrasonic tooth cleaning in dentistry (Lea et al., 2005).

During non-inertial cavitation, sustained oscillation of gas bubbles occurs around a resting equilibrium. The oscillations may be small and symmetrical under low amplitude ultrasound, or larger and asymmetric in exposure to high amplitude ultrasound (Karthikesh & Yang, 2021). The sustained oscillations create a stream of fluid flow around the gas bubble size known as acoustic microstreaming which can create shear forces around the bubble. The forces associated with the acoustic microstreaming can lead to effects in the tissue and cells in the vicinity (Schafer & Cleary, 2023). Such cellular effects include alterations to cell permeability (Deng et al., 2012; Ward et al., 2000), cell proliferation (Liu et al., 2018; Mizrahi et al., 2007) and influence on gene expression regulation (Karthikesh & Yang, 2021). Non-inertial cavitation can also produce heat on the surface of the bubble but to a lesser extent than inertial cavitation (Karthikesh & Yang, 2021). All effects of stable cavitation are dependent on the bubble size.

Cancer treatment research has explored the combination of the biological effects of ultrasound cavitation with chemical therapy in an area known as sonodynamic therapy (SDT). The

advancement on this area since its first recognition by Yumita et al in 1989 and has resulted in SDT becoming a promising treatment proposal for malignant tumours specifically brain tumours, with ongoing clinical trials for glioblastoma (ClinicalTrials.gov Identifier: NCT04845919; NCT05362409; NCT05370508; NCT06039709; Sanai et al., 2022) and diffuse intrinsic pontine glioma - DIPG (Kilburn et al., 2024).

1.5.2.2 Acoustic Streaming

Acoustic streaming is a phenomenon which occurs when a high-pressure acoustic wave propagates through a fluid medium and induces a nonlinear acoustic effect of fluid motion (Lighthill, 1978). This fluid motion of particles within an acoustic wave was first described by Lord Rayleigh in 1884 (Strutt, 1884) and is a phenomenon still utilised today in different fields such as in medical applications for tumour diagnostics (Nightingale et al., 1995), fluid mixing in engineering applications (Chen et al., 2022) and cleaning in ultrasonic (low frequency < 100 kHz) and megasonic (high frequency; ≥ 1000 kHz) scales (Boluriaan & Morris 2003).

During stable/non-inertial cavitation, oscillating bubbles produce a small-scale streaming flow of fluid in the direction of sound propagation known as acoustic microstreaming as described previously. The effects of acoustic microstreaming are used in several medical applications including ultrasonic scaling instruments in dentistry (Khambay & Walmsley, 1999) and in sonothrombolysis for the treatment of stroke patients (Molina et al., 2006). Microstreaming creates shear stress on the membrane of surrounding cells altering membrane permeability (Williams, 1973) allowing the entry of macromolecules such as DNA and drug molecules

making this mechanism of ‘sonoporation’ a potential drug or gene-delivery therapy (Wu, 2018).

1.5.2.3 Acoustic radiation forces

As a sound wave travels through a medium and encounters an object within the sound field absorption, scattering and reflection may occur. Energy and momentum are transferred from the propagating wave to the medium. The change in energy density and wave momentum generates an acoustic radiation force (Sarvazyan et al., 2010). Radiation forces may be either primary or secondary (Doinikov, 2003). Primary forces effect single particles causing movement within the field, where secondary forces result in particle-particle interactions such as attraction or repulsion. Acoustic radiation forces have been used for tissue elasticity imaging (Doherty et al., 2013), monitoring tissue lesions during ultrasonic therapy (Lizzi et al., 2003) and assisting drug and gene delivery systems (Dayton et al., 1999).
Radiation pressure forces may also be responsible for some of the cellular effects of ultrasound such as sonophoresis in which the skin barrier is disrupted increasing permeability and subsequently enhancing the uptake of drugs through the skin (Polat et al., 2011).

1.6 Medical applications of ultrasound

The non-invasive nature of ultrasound is ideal for medical applications. Ultrasound is applied at different frequencies and intensities depending on the area of the body where it is to be used and the purpose of application. Frequencies between 3 and 5 MHz and at low intensity (1 to 50 mW/cm^2) are used in diagnostic applications. Therapeutic ultrasound usually uses frequencies between 1 and 3 MHz at a range of intensities from 0.1 to 2 W/cm^2 (Doan et al., 1999). Ultrasound frequencies in the kHz range (20 to 60) at high intensities are used in

dentistry for the removal of soft and hard calcified deposits from teeth which is termed scaling (Walmsley, 1988). The discovery of ultrasound and venture into medical applications of ultrasound in the mid twentieth century has allowed vast expansion of ultrasonics in both diagnostic and therapeutic medicine (Fig 1.8).

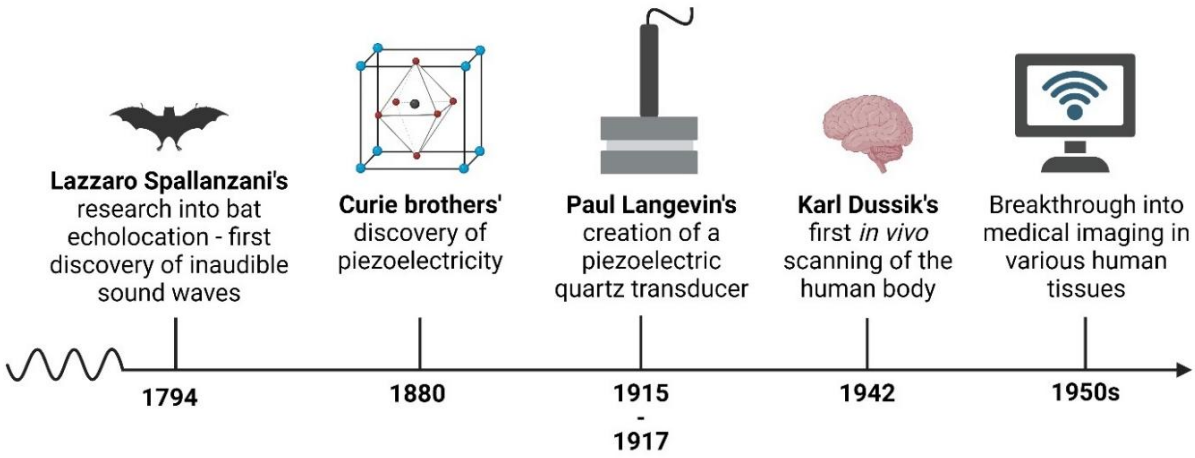

Figure 1.8 Timeline of the major discoveries in the history of ultrasound.
The history of ultrasound began in the 18th century. Since then, multiple discoveries have contributed to the modern ultrasonics of today. From discoveries of piezoelectricity leading to the creation of transducers. These transducers started the modern ultrasonics era. Now ultrasonics is a common practice in medical science since the first ultrasonic imaging in the 1950s.

1.6.1 Diagnostic ultrasound

The first application of ultrasound in medical diagnostics was by neurologist Karl Dussik who measured the transmission of ultrasound waves through a patient's partially submerged skull to identify intracranial tumours using the "through-transmission" technique (Dussik, 1942). Two transducers were placed either side of the skull and the changes in sound power passing between the transducers was recorded on heat-sensitive paper creating 'ventriculograms' or images of the brain's ventricles. This represented the first attempt at *in vivo* scanning of a human organ. However, this method was found to have limitations as the ventriculograms

obtained contained artefacts generated by reflections and attenuation of the structure of the skull. This approach was replaced with the pulse-echo method. Research into the use of pulse-echo ultrasonics in diagnostic medicine continued with American physician George D. Ludwig analysing the physical properties of various human tissue and ultimately the ability to locate gallstones and foreign bodies in various animal and human tissue (Ludwig, 1949). A few years later the detection and 2-D imaging of breast tumours was realised (Wild & Neal, 1951) which led to the development of a handheld transducer that could detect colonic and ovarian abnormalities (Wild & Reid, 1954). Another breakthrough in ultrasonic medical imaging was the first sonograms of a foetus in the womb (Donald et al., 1958).

Ultrasonic imaging is usually applied between frequencies of 2 to 15 MHz depending on the tissue being imaged and its depth within the human body. The penetration depth of ultrasound is related to attenuation (absorption) of transmitted energy into the surrounding tissues during wave propagation. High frequencies with shorter wavelengths are attenuated by tissue more readily than waves with low frequency and longer wavelengths (ter Haar, 1999). Higher frequencies allow for enhanced resolution of images due to a shorter wavelength providing the ability to distinguish between two points in close proximity to each other (Vernon & Lewin, 2018). Therefore higher frequencies are employed to image more superficial structures compared with deeper tissues where lower frequency ultrasound is used.

1.6.2 Therapeutic ultrasound

Ultrasonic therapy was already in clinical use in the 1950s whilst research into diagnostics was still in early development. Low intensity (1 MHz) unfocused beams of ultrasound were first used to treat tendonitis and bursitis by heating the affected tissue to increase blood flow

and alleviate symptoms (Lehmann, 1953). Since these first trials, therapeutic ultrasound has now become an accepted therapy for musculoskeletal conditions (Wong et al., 2007) such as plantar fasciitis (Heigh et al., 2019), lower back and neck pain (Saber & Saber, 2017) and osteoarthritis (Zeng et al., 2014; Zhang et al., 2016a). The effectiveness of ultrasound has also been explored in other conditions such as Ménière's disease (James et al., 1960), kidney stones (Chaussy et al., 1980), bone fractures (Heckman et al., 1994) and certain cancers (Tempany et al., 2011).

Ultrasonic therapy can be used to treat a multitude of medical conditions depending on the parameters applied to the emission. Two forms of ultrasonic therapy with differing intensities are high-intensity focused ultrasound (HIFU) and low-intensity pulsed ultrasound (LIPUS). HIFU applies a high intensity ultrasound beam (5 W/cm^2 to 10,000 W/cm^2) to a focused area inducing critical thermal damage to the targeted tissue which results in coagulated necrosis and cell death. Such thermoablation devices have been used clinically since 1997 (Wu et al., 2004) for treating several types of cancers (Shehata, 2012). Such high frequency ultrasound may also enhance targeted drug/gene delivery through microbubble disruption (Etame et al., 2012).

LIPUS is the pulsed emission of a low intensity ultrasound beam (< 3 W/cm^2) more commonly associated with physical therapy such as soft tissue regeneration (Ikai et al., 2008) and fracture healing (Claes & Willie, 2007). LIPUS is an FDA approved method for treating recent fractures (Poolman et al., 2017) with devices commercially available to aid bone healing acceleration such as the Osteotron IV (ITO Ultrashort Wave Co. Ltd., Tokyo, Japan) and the Exogen (Bioventus LLC, Durham, N.C.).

1.6.2.1 Low frequency therapeutic ultrasound

Low frequency kHz ultrasound is routinely used in dental care (Walmsley, 1988; 2015) and in surgical procedures involving tissue cutting and removal (Miller et al., 2012). Additionally low frequency ultrasound in the range of 40 – 50 kHz, has been used in therapeutic applications, termed longwave therapy. Several longwave medical devices are commercially available and used in physical therapy applications such as the Phys-Assist (Orthosonics Ltd, UK) and the DuoSon (SRA Developments, UK)

The rationale behind the use of longwave therapy relates to the penetration depth in the human body. Attenuation is related to frequency; lower frequencies are less readily attenuated by tissues and therefore can achieve a greater penetration depth within the body. The ability to penetrate the body to a larger depth than achieved by traditional MHz devices, led to the development of a 45 kHz device originally for treatment of ankle sprains (Bradnock et al, 1996). This was also shown to stimulate osteoblast collagen production *in vitro* (Reher et al., 1999). The molecular mechanisms that related to the apparent enhancement in bone regeneration after longwave therapy identified an upregulation in early and late bone markers in osteoblast-like cells (Maddi et al., 2006). Man et al., (2012a) also found an increase in osteoblast proliferation and migration following 45 kHz exposure suggesting a potential therapeutic effect on the bone healing process. Longwave therapy has also been studied for its effects in dental repair processes. Stimulatory effects on the dentine-pulp complex have been proposed due to observations of enhanced proliferation (Ghorayeb et al., 2013), differentiation and mineralisation in dental pulp stem cells (Man et al., 2012b).

Angiogenesis is critical to both bone and dental repair; kHz ultrasound has demonstrated increased *VEGF* expression in osteoblasts and odontoblasts (Reher et al., 1999; Scheven et al, 2009) and gene expression in odontoblast-like cells (Man et al., 2012b). Therefore it can be suggested a longwave effect on the angiogenesis process may be a contributing factor to ultrasound enhancement on bone and dental healing. Though this hypothesis seems an interesting research field, effects of kHz ultrasound on angiogenesis and the cells primarily involved, such as endothelial cells, is noticeably lacking in literature.

1.6.3 Ultrasonic surgical devices

The use of ultrasonic surgical devices began in dentistry in the 1950s with the development of an ultrasonic drills and most successfully descalers. The Dentsply-Cavitron combined the ultrasonic vibration of a descaler tool tip with flow of water to remove dental calculus (Balamuth, 1963). Balamuth's vision of "additional applications of ultrasonics to dentistry in the future" has been upheld as various updated versions of the Cavitron system are still available and in practice today. The mechanics of this system was also successfully adapted into the field of ophthalmology with a vibrating ultrasound tip with irrigation flow used to perform cataract surgery (Fledelius, 1997). Surgical ultrasonics was then introduced into tissue surgeries in soft tissue removal in the 1970s and became commercially available for osteotomies in the 2000s (Vercellotti et al., 2001).

A range of ultrasonic surgical devices are commercially available each with different designs, frequency capabilities and modes of action depending on the intended use. Typically, surgical devices range between 20 – 100 kHz (Lucas et al., 2009). Schafer & Cleary (2023) review a variety of ultrasonic surgical devices used in medical therapy and highlight the differences in mechanisms dependent on the device. Briefly, ultrasonic surgical tools are now available for

use in aspiration surgeries for rapid tissue removal utilised in neurosurgery and gynaecology, phacoemulsification in cataract surgeries and bone cutting surgeries.

1.6.3.1 Advantages of ultrasonic surgery

Ultrasonic surgical devices allow for more control and precision compared with manual tissue cutting devices. The improvements in precision, size of incisions needed and consequently reduction in surrounding soft tissue damage has been reported in literature since the 1970s and 1980s (Aro et al., 1980; Horton et al., 1981; Volkov & Shepeleva, 1974). The nature of precise cutting and the amount of unintended damage that will occur to the surrounding tissue can be determined by the tissue selectivity of ultrasonic devices. Ultrasonic device settings can be altered to target specific areas. For example, the Dentsply-Cavitron descaler working at a lower amplitude removed calculus without destroying tooth enamel. No cutting of the soft tissue occurred (Balamuth, 1963). Ultrasound working at kHz frequencies is useful in blood clot dissolving applications. Insertion of an oscillating ultrasound wire device disrupts clots but does not damage the surrounding vessel walls (Ariani et al., 1991). The tissue selective nature of ultrasonic devices has garnered support for use in maxillofacial, craniofacial and neurocranial procedures (Ramieri et al., 2015).

A further benefit to the use of ultrasonic surgical devices is observed where ultrasonic cutting devices are used clinically to both cut and coagulate tissues simultaneously. The sealing of blood vessels during surgery can be controlled by altering the amplitude settings of the device. The sealing takes place via the heat produced by the vibrating tip, the pressure of clamping the vessels together and the time taken (Houser & Noschang, 2018; Lucas et al., 2023). Although a recent comparative review of ultrasonic devices and traditional clamping

methods in hepatectomy surgeries revealed traditional methods resulted in shorter operating times, ultrasonic devices resulted in overall less complications including bile leakage and blood loss (Yu et al., 2024). Less effort is also needed from the operator using ultrasonic bone cutting devices as less force is needed to be applied to create a tissue incision resulting in lower operator fatigue during surgery. The reduction in force needed during device application will also lead to a reduction in the risk of unnecessary damage to the tissue being cut.

1.6.3.2 Limitations to ultrasonic surgical devices

Although the benefits of using ultrasonic surgical devices have been reported for some time, there are still limitations to its use. Occurrences of overheating of devices is one of the disadvantages that was identified by Aro and Horton in the 1980s. Since then, efforts have been made to reduce this risk by using piezoelectric transducers that do not need additional cooling systems (Lucas et al., 2023). Although the risk of the device overheating has been reduced, it can still occur. A trial comparing a Sonopet® ultrasonic knife with conventional powered devices in deep maxilla and mandible surgery (Kato et al., 2021) identified high temperatures at the tip of the device due to an insufficient internal cooling system. The nature of the maxilla and mandible osteotomy required partial removal of the cooling irrigation sheath to expose more of the Sonopet® blade. This meant that the injection of saline through the sheath to the blade tip was decreased and insufficient for cooling. Such observations highlight the importance of monitoring ultrasonic devices during surgical operations and altering operational protocols depending on the procedure being performed. There is also a risk of high temperature at the cutting site causing necrosis and thermal damage to the surrounding tissue. High temperatures are caused by friction of the ultrasonic blade and the

tissue, absorption of ultrasonic energy by the tissue and burning of any debris present at the incision area (Lucas et al., 2023).

Though operational times can be reduced in certain procedures such as vessel sealing, it has been reported that in certain cases of bone cutting surgeries the cutting speed of the devices have been significantly lower (Kato et al., 2021; Khambay & Walmsley 2000; Spinelli et al., 2014) or unaffected (Landes et al., 2008). However it was acknowledged by Kato et al (2021), that the significantly longer bone-cutting time using the Sonopet® device compared with powered devices (11 % longer) could be decreased once the surgeon has gained familiarity with using the device. Therefore in some instances it is not due to the effectiveness of the device, rather its operation. Other disadvantages relate to cost benefit considerations arising in particular from sterilisation of devices. The manufacturing and replacement of ultrasonic tips and sterilisation in pressurised autoclaves can damage the piezoelectric materials which may prove costly in the long term (Schafer & Cleary, 2023).

1.6.3.3 Future of surgery enabled by ultrasonics

A recent advancement in surgical procedures is the incorporation of robots in various surgical specialties such as head and neck surgery, gynaecology and general surgery. The use of a da Vinci Surgical System robot in in prostate surgery led to an increase in the popularity and use of robot-assisted surgery (Ng & Tam, 2014). As of 2020 more than 7 million surgeries had been performed using the da Vinci robot in various surgeries (D'Ettorre et al., 2021). The use of robotics allows for precise incisions with seven degrees of freedom and in small spaces. The da Vinci robot has also been successfully integrated with laparoscopic ultrasonic

surgeries aiding in soft tissue cutting and vessels sealing with ultrasonic shears (Schafer & Cleary, 2023).

As technology has advanced, so has the ingenuity in ultrasonic surgical device design. Li et al (2021) identified the requirement for miniaturisation of ultrasonic devices to allow further integration with surgical robotic designs. Miniaturised surgical devices open more possibilities for minimally invasive surgeries, and the incorporation of these with robotics allowing controlled precise manoeuvring in hard-to-reach areas (Li et al., 2021). The use of 3D printing materials to manufacture miniaturised transducers with complex geometry has also been investigated to enhance the development of miniaturised ultrasonic surgical devices (Cleary et al., 2021; Lu et al., 2023).

1.7 Ultrasound effect on angiogenesis

As the technology and design for ultrasonic surgical devices expands, understanding the biological effect these devices may exert during operation will assist in their clinical use. One such process that may be affected by ultrasonic devices is angiogenesis. Multiple *in vivo* and *in vitro* studies have been performed in this research field, however the studies described in the following sections emitted ultrasound in a variety of exposure configurations and at different acoustic parameters, the definitions of which are shown in Table 1.2.

Table 1.2 Definitions of acoustic parameters described in literature

Acoustic Parameter	Description	Units
Frequency	Number of oscillations per second	Hertz (Hz)
Duration	Total time that ultrasound is applied	seconds (s) or min
Cycle	One complete repetition of the wave pattern: one maximum compression and maximum rarefaction	Number of cycles (*n*)
Pulse Frequency	Number of pulses per second	Hertz (Hz)
Pulse Duration	Time taken for a single pulse: "on" time for a pulse cycle	microseconds (μs) or milliseconds (ms)
Duty cycle	Ratio of the "on" time versus the total pulse period	%
Intensity	The amount of acoustic energy passing through a unit area per unit of time	mW/cm²
Spatial-peak temporal-average intensity (ISPTA)	The maximum intensity measured within the sound field averaged over time	mW/cm²
Peak Negative Acoustic Pressure	Maximum negative (rarefactional) pressure measured in an acoustic wave	megapascals (MPa)

1.7.1 *In vivo* animal studies

Studies investigating the effect of therapeutic ultrasound on angiogenesis have used animal models with ischaemic tissue conditions (Hanawa et al., 2014; Huang et al., 2014; Shindo et al., 2016). A summary of select *in vivo* studies is outlined in Table 1.3.

One symptom of peripheral artery disease (PAD) is the lack of blood flow to the feet. Mice with hindlimb ischaemia have been used as an *in vivo* model to assess the use of ultrasound as a minimally invasive therapeutic approach for such PAD cases. Mice were treated with

continuous 1 MHz, 0.3 mW/cm^2 ultrasound for 3, 6 or 9 min. After 14 days, a significant increase in wound healing and blood perfusion, detected by thermal imaging of the ischaemic area, was seen in mice treated for 9 min compared with the control. Western blot techniques also showed a significant increase in angiogenesis-protein levels after 9 min treatment (Huang et al., 2014).

The therapeutic effect of LIPUS has also been investigated in porcine and mice models of myocardial ischaemia (Hanawa et al., 2014; Shindo et al., 2016). In both studies animals were treated with LIPUS for 20 min at 1.875 MHz using a diagnostic ProSound α10 device (HITACHI Aloka Medical, Ltd., Mitaka, Japan). Porcine models were treated with LIPUS 3 times in one week. The treated pigs exhibited improved myocardial function after 4 weeks identified through echocardiography of the left ventricle identifying a significant increase in wall thickness compared with control groups. Increased capillary number and improved blood flow in ischaemic regions compared with non-ischaemic tissue after LIPUS therapy was also found 4 weeks post treatment (Hanawa et al., 2014). Similar positive results were seen in the mice models at different time points post treatment. Improved mortality was observed in LIPUS-treated mice in the 2 months study period following treatment. As well as ventricular remodelling in mice with myocardial infarction after 8 weeks. Earlier angiogenic responses were identified in the expression of angiogenic regulators (*VEGF* and *eNOS*). Upregulation of these genes was observed 6 days after treatment in the infarcted region (Shindo et al., 2016). However, in this set up mice were placed under an agar phantom gel mimicking the attenuation coefficient of living tissues. Therefore, it is unknown what ultrasound power levels the infarcted regions were experiencing, as the wave would be attenuated by the phantom agar but then additionally by the mice tissue itself. The pulse frequency and ISPTA

also differed from Hanawa's 2014 study meaning the maximum amount of ultrasound energy applied to the mice was not comparable between the two studies, though there was still similar results in a proangiogenic response.

Researchers in the same group also assessed LIPUS therapy in mice with pressure overloaded hearts with the same reported acoustic parameters as Shindo's 2016 study allowing more reliable response comparisons. LIPUS-treated mice demonstrated increased capillary density in the overloaded left ventricle and activation of angiogenesis signalling pathways 8 weeks after ultrasound exposure (Ogata et al., 2017). This study provides more confidence in the proangiogenic response to LIPUS in addition to the Shindo study due to the similarities in ultrasound exposure reported.

LIPUS has also been used to assess the effect of angiogenesis in wound healing (Fantinati et al., 2016). Diabetic Wistar rat models were subjected to third degree thermal injury and immediately treated with 3 MHz LIPUS pulsed at 100 kHz for 3 min on the injury site. In the early phase of wound healing (days 7 to 14), ultrasound was beneficial, significantly increasing levels of granulation tissue deposition and wound contraction, whilst decreasing levels of necrotic tissue. However it was acknowledged that the increase in angiogenesis and inflammation continued into the remodelling phase of wound healing (day 21) which can be detrimental to the healing process causing scar formation and contributes to the onset of chronic wounds. A review article by DiPietro in 2016 highlighted the importance of regulated angiogenesis in wound healing processes. Therefore the application of LIPUS may not be beneficial in the long-term healing of burn injuries in diabetic patients.

Table 1.3 Summary of findings from *in vivo* studies investigating the effect of ultrasound in ischaemic animal models.

Literature on the effects of ultrasound to angiogenesis *in vivo* shows the many different ultrasound exposure settings between research groups. Statistically significant results are noted * (P<0.05), **(P<0.01), *** (P<0.001), NS (non-significant)

Paper	*In Vivo* Model	Ultrasound Settings	Results
Hanawa et al., 2014	Porcine with chronic myocardial ischaemia	Frequency: 1.875 MHz Pulse Frequency: 7.1 kHz No. Cycles: 1, 16, 32, 48, 64 Spatial-peak temporal-average intensity (ISPTA): 151∼193 mW/cm^2 Duration: 20 min	↑ ventricle wall thickness * ↑ capillary density * ↑ blood flow *
Huang et al., 2014	Mice with hindlimb ischaemia	Frequency: 1 MHz Intensity: 0.3 W/cm^2 Duration: 3, 6, 9 min	Exposure time dependent response: 9-min exposure: ↑ capillary density ** ↑ blood perfusion ** ↑ angiogenic factor protein expression ** 3 & 6 min exposure: NS
Shindo et al., 2016	Mice with myocardial infarction	Frequency: 1.875 MHz Pulse Frequency: 4.9 kHz No. Cycles: 32 Intensity: 0.25 W/cm^2 ISPTA: 117–174 mW/cm^2 Duration: 20 min	↓ mortality * ↑ expression of angiogenic growth factors * ↑ capillary density *
Ogata et al., 2017	Mice with pressure overloaded heart	Frequency: 1.875 MHz Pulse Frequency: 4.9 kHz, No. Cycles: 32 Intensity: 0.25 W/cm^2 ISPTA: 117–162 mW/cm^2 Duration: 20 min	↑ capillary density * ↓ myocardial ischaemia * ↑ expression of angiogenic growth factors * Activation of angiogenesis signalling pathways
Fantinati et al., 2016	Rat – diabetic with 3rd degree burns	Frequency: 3 MHz Pulsed Frequency: 100 Hz Intensity: 0.5 W/cm^2 Duration: 3 min	↑ angiogenesis * ↑ wound contraction * ↑ inflammation * ↓ necrotic tissue *

The overall finding of these studies were similar although the acoustic parameters regarding ultrasound emission differed; therapeutic ultrasound and LIPUS exposure produced apparent stimulatory effects on angiogenesis and subsequent ischaemic tissue healing. LIPUS and MHz appears to be a promising therapeutic approach to cardiovascular diseases and wound healing via animal model studies. Nevertheless, LIPUS and MHz frequency ultrasound has been utilised in commercially available therapeutic devices, whereas the therapeutic effect of kHz ultrasound is still largely unknown *in vivo*.

1.7.2 *In vitro* studies on therapeutic ultrasound and angiogenesis

In vitro studies of angiogenesis utilise the culture and growth of endothelial cells, which is the primary cell type involved in the angiogenesis process. Several *in vitro* studies have measured the effect of therapeutic ultrasound on angiogenesis in different cell types and these are summarised in Table 1.4. A pro-angiogenic response to LIPUS was found in bovine aortic endothelial cells (BAECs) (Mizrahi et al., 2007). Cells were exposed to 1 MHz ultrasound pulsed at 40 kHz for either 15 min or 30 min exposure time and analysed for angiogenic responses. A significant increase in cell proliferation was found 12 hours after 15 min ultrasound exposure, however, data following the 30 min exposure were not published in this paper. In addition there was increased endothelial sprouting activity and migration 3 days after 15 min exposure. The cell sprouts started to decrease after this time which is indicative of the latter phase of the angiogenesis process with a decrease in angiogenic activity during vessel pruning where selected unnecessary vessels regress to refine the newly formed vasculature (DiPietro, 2016). However the data for the 30 min exposure effect on cell sprouting activity is not presented. In contrast to the increased cell proliferation and sprouting activity, a decrease in *VEGFR2* protein expression was identified immediately after both

15 min and 30 min treatment which became a significant decrease 12 h after exposure; though this may not mean a disagreement in a pro-angiogenic response reported in this study. Various studies prior to Mizrahi et al., 2007 also identified conflicting levels of *VEGFR2* expression in response to angiogenic stimuli. *VEGF* stimulation in BAECs resulted in an immediate downregulation of the *VEGFR2* receptor (Duval et al., 2003), whilst another study found a 2 - fold increase of *VEGFR2* expression following *VEGF* stimulation in BAECs (Herve et al., 2005) although the treatment times of these two studies varied. Duval et al., (2003) followed a protocol of 15, 30 and 60 min *VEGF* treatment, whereas Herve et al., (2005) stimulated BAECs with 72 h *VEGF* treatment. The confounding results highlight the complexity of receptor responses to angiogenic stimuli and the temporal changes in gene and protein expression during the angiogenesis process.

An array of endothelial cells are available for *in vitro* use though the most commonly used are human umbilical vein endothelial cells HUVECs (Jaffe et al., 1973). Multiple *in vitro* studies investigating the effect of LIPUS on HUVECs have identified a pro-angiogenic response. Significant upregulation of *VEGF* mRNA expression has been identified 3 h after 20 min LIPUS exposure (Hanawa et al., 2014), whereas a later study within the same research group found a significant increase in *VEGF* expression at a later time point 6 h after treatment (Shindo et al., 2016). This further shows the dynamic expression of angiogenic molecular mediators following treatment *in vitro*. This also highlights the influence *in vitro* exposure methods have on cellular response. The upregulation of *VEGF* expression observed at different time points may be due to the experimental design differences between the studies as the LIPUS settings varied slightly between the groups, as well as the exposure methods. The method of exposure by Hanawa et al., 2014 is not described in the publication. Shindo et al,

2016 exposed cells to ultrasound using a tissue-mimicking phantom agar between the transducer and the cell layer. This difference may result in varied ultrasonic energy being transmitted to the cells as the wave attenuation will differ between the phantom agar medium and the coupling medium Hanawa et al., 2014 may have used.

Another study (Huang et al., 2015) investigated the effect of 1 MHz, 0.3 W/cm^2 continuous wave ultrasound on HUVEC tube formation, migration and gene expression. A time-dependent response was also seen in this study. The longest exposure length of 9 min showed significant responses compared with insignificant effects after 3 and 6 min exposure. Tube formation by HUVECs was significantly increased 6 h after treatment as identified by Matrigel^{TM} tube formation assay. This assay allows visualisation of 'tube-like' structures in the 3-D basement membrane Matrigel^{TM} matrix representing capillary formation *in vitro*. Cell motility was also significantly increased, as well as *eNOS* protein expression which indicated an increased angiogenic response. The same group (Huang et al., 2017) also found an inhibiting effect of 9 min exposure on HUVEC apoptosis. A 'rescuing' of cells induced to undergo apoptosis was observed with a significant enhancement of cell viability and attenuation of apoptosis via the cell survival phosphoinositide-3-kinase-serine/threonine protein kinase (*PI3K/AKT*) pathway. These studies demonstrated the potential of 1 MHz continuous ultrasound as a therapeutic angiogenesis stimulator.

However, Su et al (2019) also demonstrated the anti-angiogenic effect of LIPUS. HUVECs were exposed to 0.5 MHz ultrasound for 1 min at various settings ranging from 1000 – 4000 cycles of 70 – 280 mW/cm^2 intensity respectively. A dose-dependent response was seen in this case as the highest intensity significantly inhibited cell proliferation and migration

whereas lower intensities of 70 – 210 mW/cm^2 did not have a significant effect compared with controls. LIPUS also inhibited tube formation *in vitro* however it is unclear what ultrasound settings were used in this assay. The main aim of that study was to understand how LIPUS may have anti-angiogenic effects. It was suggested that LIPUS induced cell death via the p38 MAPK stress signalling pathway to induce apoptosis. The effect was attributed to non-thermal mechanisms as the temperature in the cell culture dish did not rise above 35 °C. This is an important consideration that *in vitro* studies should measure temperature effect as well as cellular responses.

Although i*n vitro* studies are fundamental to the understanding of a range of research questions in cellular and molecular biology, there are drawbacks and challenges especially in these cases of ultrasound exposure. For example, consideration must be given to the fact that the exposure methods in this collection of studies varied which can have an impact on the amount of ultrasonic energy the cells experienced. The variety in the terminology used to describe acoustic outputs also leads to difficulties in making critical assessments of literature regarding ultrasound bioeffects. As shown in Table 1.2 there are many ways to describe acoustic parameters, each describing a different aspect of the ultrasound beam. It is largely accepted to report the power of an ultrasound beam as intensity (mW/cm^2). However the power of ultrasound is more commonly associated with thermal bioeffects (Section 1.5.1); if mechanical bioeffects such as cavitation are considered then it is arguably more apt to describe ultrasound as peak-negative acoustic pressure values which is currently underreported in literature. Therefore standardised reporting of acoustic output could also be as important an advance in the research field of *in vitro* ultrasonics. Further challenges of *in vitro* exposure are described in the following section.

Table 1.4 Summary of findings from *in vitro* studies investigating the effect of ultrasound on angiogenesis.
As evident from the different ultrasound settings in each study, there is no standardised ultrasound exposure system which makes comparisons between studies difficult. Statistically significant results are noted * ($p < 0.05$), **($p < 0.01$), *** ($p < 0.001$), NS (non-significant).

Paper	Cell Type	Ultrasound Settings	Experimental Configuration	Main Results
Mizrahi et al., 2007	Bovine Aortic Endothelial Cells (BAECs)	Frequency: 1 MHz Intensity: 2.2 W/cm^2 Pulsed frequency: 40 Hz Pulsed duration: 5 ms Duration: 15, 30 min	Transducer placed 22 cm below petri dish. Perspex tube connected the transducer and petri dish Caster oil as coupling medium	↑ cell proliferation * ↑ cell migration * ↑ cell sprouting * ↓ *VEGFR2* expression *VEGFR2* redistribution
Hanawa et al., 2014	HUVECs	Frequency: 1.875 MHz Pulse frequency: 7.1 kHz No. cycles: 1, 16, 32, 48, 64 ISPTA: 151~193mW/cm^2 Duration: 20 min	Not described in literature	↑ *VEGF* expression *
Huang et al., 2015	HUVECs	Frequency: 1 MHz Intensity: 0.3 W/cm^2 Duration: 3, 6, 9 min	6 well and 96 well culture plates Transducer placed below with gel coupling pad.	Exposure time dependent. 9-min exposure: ↑ angiogenic factor expression ** ↑ tube formation and length ** ↑ cell migration and motility * 3 & 6 min exposure: NS

Huang et al., 2017	HUVECs	Frequency: 1 MHz Intensity: 0.3 W/cm^2 Duration: 9 min	6 well and 96 well culture plates Transducer placed below with gel coupling pad.	↑ cell viability to control * ↑ cell viability to apoptosis-induced cells ** ↓ apoptosis **
Shindo et al., 2016	HUVECs	Frequency: 1.875 MHz Pulse frequency: 4.9 kHz No. cycles: 32 Intensity: 0.25 W/cm^2 ISPTA: 117–174 mW/cm^2 Duration: 20 min	Transducer placed above an agar phantom surrounding cell culture. Cell culture dish placed in a Teflon plate	↑ cell proliferation * ↑ *VEGF* expression *
Su et al., 2019	HUVECs, HMECs (human microvascular endothelial cells)	Frequency: 0.5 MHz Intensity: 210 mW/cm^2 No. cycles: 1000-4000 Duration: 1 min	Transducer beneath 6 cm culture dish with degassed water coupler	↓ tube formation ** ↓ cell viability *** ↓ cell proliferation and migration (NS) ↓ expression of apoptosis inhibitor ** ↑ apoptosis rate and cell death ***

1.7.2.1 Challenges of *in vitro* ultrasound exposure

Currently there is no singular, standardised method to analyse the *in vitro* cellular effect of ultrasound. Throughout literature, multiple experimental designs have been used in the investigation of ultrasonic effects in a variety of cell types.

One configuration involves positioning an ultrasonic transducer underneath a culture vessel. Multi-well plates have been employed in this configuration in HUVEC ultrasonic studies as mentioned previously by Huang et al., (2015), but also in studies of mesenchymal stem cell (Gao et al., 2016), odontoblast-like cell (Patel et al., 2015) and neuronal cell studies (Al-Maswary et al., 2024). In the methodology of Huang et al., (2015) cells positioned in wells farthest away from the transducer were referred to as 'control' wells. However investigations by Gupta et al., (2022) and Patel et al., (2015) showed these wells also experience ultrasonic interference due to wave propagation through the plate. Patel et al., (2015) found an increase in odontoblast cell number in wells not directly exposed to ultrasound but positioned at a distant corner of a 6-well plate. Gupta et al., (2022) investigated wave propagation in multi-well plates further and demonstrated the vibration of the entire 6-well plate during ultrasound exposure resulting in different wells experiencing different intensities and peak pressure amplitudes. Referring to 'control' wells that are present in a multi-well plate during ultrasound exposure cannot be considered as untreated controls and responses may not be indicative of truly untreated cells.

The use of a singular polystyrene culture dish placed above a transducer has been used in HUVEC studies mentioned previously. Either placed directly above separated by only coupling gel as adopted by Huang et al., (2015; 2017) and Su et al., (2019) or at a further

distance as Mizrahi et al., (2007) employed. While the use of singular culture dishes circumvents unwanted wave propagation to adjacent cells, there still lies an issue of standing wave phenomenon. Standing waves were likely to occur between the transducer and coupling agent at the bottom of the culture dish and at the culture medium and air boundary as these different media present acoustic impedance mismatch boundaries (Secomski et al., 2017). In fact, Mizrahi et al measured higher than expected acoustic pressures within the petri dish and concluded these were due to significant standing waves and reflections from the dish walls as well as the air/water interface.

Producing standing wave-free conditions is hard to achieve, if achievable at all. Though there are ways to reduce standing wave formation such as transmitting ultrasound waves from above and/or introducing an ultrasound absorbing material into the acoustic environment. Transmission from above a cell culture vessel (Fig 1.9 B) reduces standing wave formation in that it removes the artefact of unwanted wave propagation through the culture vessel material (Fig 1.9 A). However standing waves may still form from reflections within the culture vessel leading to higher-than-expected levels of ultrasound transmission (Gupta et al., 2022). Introduction of absorbing material into the experimental set-up is a possible way to reduce standing wave formation. The methodology implemented by Shindo et al., (2016) applied ultrasound above the cell culture dish passing through a tissue-mimicking agar phantom. The agar phantom had the same attenuation coefficient as tissue to more closely mimic *in vivo* conditions. Additionally, the culture dish was surrounded by an ultrasound absorbing Teflon plate to reduce the occurrence of standing waves. Silicone moulds have also been used to encase cell culture dishes during ultrasound exposure (Man et al., 2012a; Man et al., 2012b; Patel et al., 2015; Scheven et al., 2009).

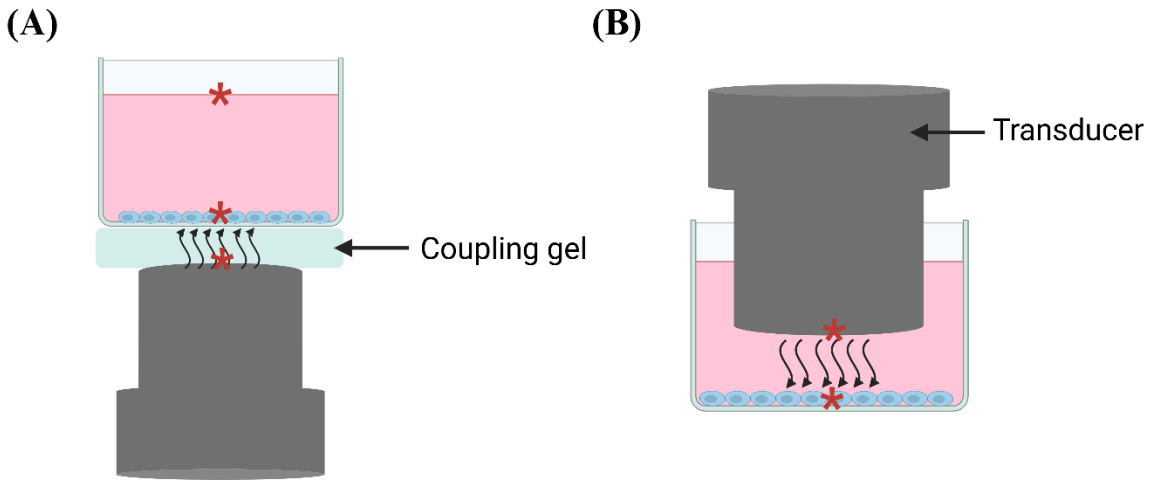

Figure 1.9 Schematic diagrams of experimental methods used to expose cells to ultrasound *in vitro*.

(A) One method used in literature involves emitting ultrasound from the bottom of a cell culture dish via a coupling gel. (B) Another method involves immersion of the transducer head into the cell culture dish. Ultrasound is emitted directly onto the cell culture from above. However standing waves are likely to form at boundaries between materials of different acoustic impedances as drawn by * on the diagram. Images created in BioRender.com.

1.7.2.2 Alternative *in vitro* exposure method: acoustic absorbing tank

One of the major drawbacks of *in vitro* ultrasound exposure is the uncertainty of the precise dose of ultrasound that the cells are experiencing. The cells should not receive unwanted interferences from reflections, standing waves or cavitation effects amongst other interferences. A configuration that aims to minimise this problem is the submergence of the entire ultrasonic exposure set up in degassed water (Fig 1.10 B). Positioning a transducer and cell culture vessel longitudinally underwater reduces the interference of the water/air boundary. Addition of an ultrasonic absorber to the configuration further reduces the influence of standing waves in the propagation path (Snehota et al., 2020). One challenge in this method is the selection of a culture vessel that maintains sterility underwater whilst facilitating cell attachment and growth. The CLINIcell® cassette (Mabio, France) is a device

that has been used in fully immersed ultrasonic studies in the characterisation of microbubbles (Nio et al., 2017; Shekhar et al., 2019). The CLINIcell® is a polycarbonate cassette with two 50 µm thick, polycarbonate films in the centre (Fig 1.10 A). The films allow gaseous exchange thereby facilitating cell culture. The Luer lock system on either side of the cassette ensures sterile conditions during the culture period, as well as a watertight system during immersion within the tank. However, acoustic characterisation of the cassette is needed before deployment in the tank configuration. Such an arrangement does overcome many of the problems associated with unwanted ultrasonic interferences. However further work is required to assess the suitability of such an exposure system in identifying the biological effects of ultrasound.

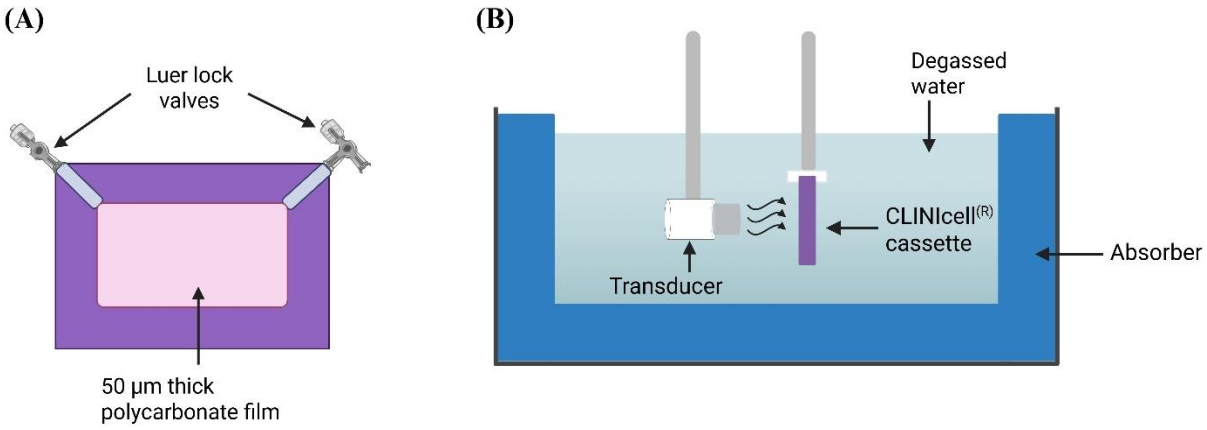

Figure 1.10 Illustrations of a CLINIcell® cassette and the deployment in an acoustic absorbing tank for ultrasound exposure.
(A) The CLINIcell® cassette is a polycarbonate frame with 2 gas permeable polycarbonate films in the centre. Luer lock valves allow insertion of cell culture into the polycarbonate film area. (B) The cassette can be used as a cell culture vessel for underwater tank *in vitro* ultrasound exposure. Acoustic absorbers present in the configuration act to minimise reflections from the tank walls. Placing the transducer and cells longitudinal in the tank minimises the influence of the water/air boundary.

1.8 Research aims and objectives

The overall aim of this study was to assess the effect of 45 kHz ultrasound on endothelial cell behaviour *in vitro*. This includes the effect on the ability to form new blood vessels i.e., angiogenesis. The hypothesis of the study is that low frequency ultrasound exhibits a pro-angiogenic effect on endothelial cells, based on the findings of previous studies (Section 1.7.2). To test this hypothesis the following objectives will be set:

Objective 1: To investigate the effect of kHz ultrasound with multiple exposure conditions on HUVEC number, viability and morphology using a commercial therapeutic device.

Objective 2: To investigate the effect of kHz ultrasound generated by a commercial therapeutic device on the angiogenic responses of HUVECs using gene expression and tube formation analysis.

Objective 3: To develop an *in vitro* exposure system that allows acoustic field characterisation with the ability to distinguish between thermal and non-thermal biological effects.

Objective 4: To assess the effect of kHz ultrasound on HUVEC behaviour in the characterised acoustic field.

Chapter 2.

MATERIALS AND METHODS

2.1 Human umbilical vein endothelial cell (HUVEC) culture

Pooled donor HUVECs (500,000 cells/vial), accompanying endothelial growth medium (EGM) and supplement mix were purchased from PromoCell (Heidelberg, Germany). These cells were used to assess the effect of ultrasound on endothelial cell behaviour and the associated angiogenesis process. Upon arrival, the 1 ml cryovial of 500,000 cells were immediately transferred to -196 °C in liquid nitrogen (LN_2) storage until further use. The addition of supplement mix and 1 % penicillin/streptomycin (P/S), Sigma-Aldrich, UK) produced complete endothelial growth media (cEGM) used for HUVEC culture. The final supplement concentration of cEGM is shown in Table 2.1.

For use, HUVECs were removed from LN2 storage and thawed at 37 °C for 1 min. The cells were then seeded onto two 0.1 % gelatin-coated T25 flasks (Fisher, UK) containing 5 ml cEGM following the manufacturers recommendation of 10,000 cells/cm^2 plating density. Cell cultures were maintained at 37 °C in a humidified atmosphere of 5 % CO_2 using a HeraCell 150i incubator (Thermo Scientific, UK). Culture medium was replenished every 2-3 days until cells reached 70-80 % confluency determined visually using a Motic AE21 brightfield microscope (China) and subsequently passaged at a 1:3 split ratio or used for experiments, or cryopreservation. Cells were cryopreserved in cryo-serum-free freezing medium (PromoCell, Germany) at a concentration of $1x10^6$ cells/ml in 2 ml cryovials (Fisher, UK) and stored in LN_2 from passage 2 for subsequent experiments. Cells were only used between passage 2 and 5 in all experiments. Cell stocks were routinely screened for mycoplasma contamination using the EZ-PCR detection kit (Sartorius, UK). This kit involved the nucleic acid testing (NAT) method which amplifies mycoplasma-specific DNA and allows detection within samples through agarose gel electrophoresis.

Table 2.1. cEGM composition.
Final supplement volumes added to 500 ml endothelial growth medium.

Foetal Calf Serum	10 ml
Endothelial Cell Growth Supplement	2 ml
Epidermal Growth Factor (recombinant human)	50 ng
Basic Fibroblast Growth Factor (recombinant human)	0.5 µg
Heparin	45 mg
Hydrocortisone	0.5 mg

2.1.1 0.1 % gelatin coating

All culture flasks, well plates and cassettes used in HUVEC culture work were coated with 0.1 % (w/v) gelatin (Sigma-Aldrich, UK). 0.2 g of gelatin was added to 200 ml sterile phosphate buffered saline (PBS). The prepared mixture was autoclaved at 121 °C for 15 min and stored at 4-8 °C for a maximum of 2 months. 1 ml/10 cm^2 of gelatin solution was used to coat culture flasks prior to cell seeding. The coated flasks and plates were placed in a 37°C incubator (HeraCell 150i incubator, Thermo Scientific, UK) for 20 min to allow gelatin adsorption after which any excess solution was removed by pipetting prior to cell addition.

CLINIcell® cassettes were coated with 10 ml 0.1 % gelatin. The gelatin was added via syringe to the membrane chamber ensuring the entire membrane surface was coated and then placed in a 37°C incubator for 20 min for adsorption. Excess gelatin was removed via syringe prior to cell addition.

2.2 *In vitro* ultrasound configurations

Two configurations of *in vitro* ultrasound exposure were used in this research project. One used a DuoSon therapeutic device; the other used a custom-designed transducer constructed by Dr Xuan Li in University of Glasgow. Ultrasound was emitted at 45 kHz in continuous wave mode in all exposure set-ups.

2.2.1 DuoSon therapeutic device

Ultrasound was applied at a continuous wave of 45 kHz using a commercial therapeutic DuoSon device (SRA Developments, Ashburton, UK). The DuoSon is a dual frequency ultrasound therapy unit that emits ultrasound at 1 MHz, 45 kHz or both simultaneously. There are 8 possible modes of delivery; in this project three low frequency modes were used (modes 3, 4 & 6) which were designed and requested by Dr Ben Scheven, University of Birmingham School of Dentistry. The device had been calibrated and serviced using force balance reading testing on a number of occasions prior to this study by the supplier. The DuoSon device had also been calibrated previously by a fellow PhD student Jill Savva at University of Glasgow (Savva, PhD thesis, 2023) and characterised by a previous University of Birmingham researcher (Patel et al., 2015). Each mode emitted ultrasound at 45 kHz frequency in a continuous wave but with different acoustic power and intensity, as shown in Table 2.2.

Table 2.2 DuoSon low frequency 45 kHz modes.
Three low frequency (LF) modes were used in this project. All modes were designed and calibrated by the supplier to emit a continuous wave at the stated intensity settings.

Mode		Total Acoustic Power (mW)	LF Acoustic Intensity (mW/cm^2)
3	LF1	159	10
4	LF2	406	25
6	LF3	1217	75

All experiments using the DuoSon transducer for ultrasound exposure were undertaken in a class II safety cabinet (ScanLaf Mars 1500, LaboGene, Denmark). A custom-designed clamp stand manufactured by research colleagues in the **S**cience and **T**echnologies **O**f **R**obotics in **M**edicine (STORM) lab at University of Leeds was used to immerse the DuoSon transducer head into a 35 mm culture dish at a fixed position and determined distance from the bottom of the culture dish (Fig 2.1 A). The stand comprised a stage (LJ750/M, Thorlabs) that aligned a 35 mm culture dish with the transducer head position. This stage could be raised to a precise distance from the tip of the transducer head to the culture surface of the dish. In this study the distance between the transducer and surface of the culture dish was set at 5 mm (Fig 2.1 B). The stage was cleaned with 10 % chemgene detergent (Fisher, UK) and 70 % ethanol (Merck, UK) before placing in the class II safety cabinet. The DuoSon transducer was cleaned with 10 % chemgene and 70% ethanol prior to placement in the class II cabinet. The DuoSon transducer face was also submerged into 70 % ethanol followed by warmed cEGM before any cell culture experiments and in between each culture dish treatment.

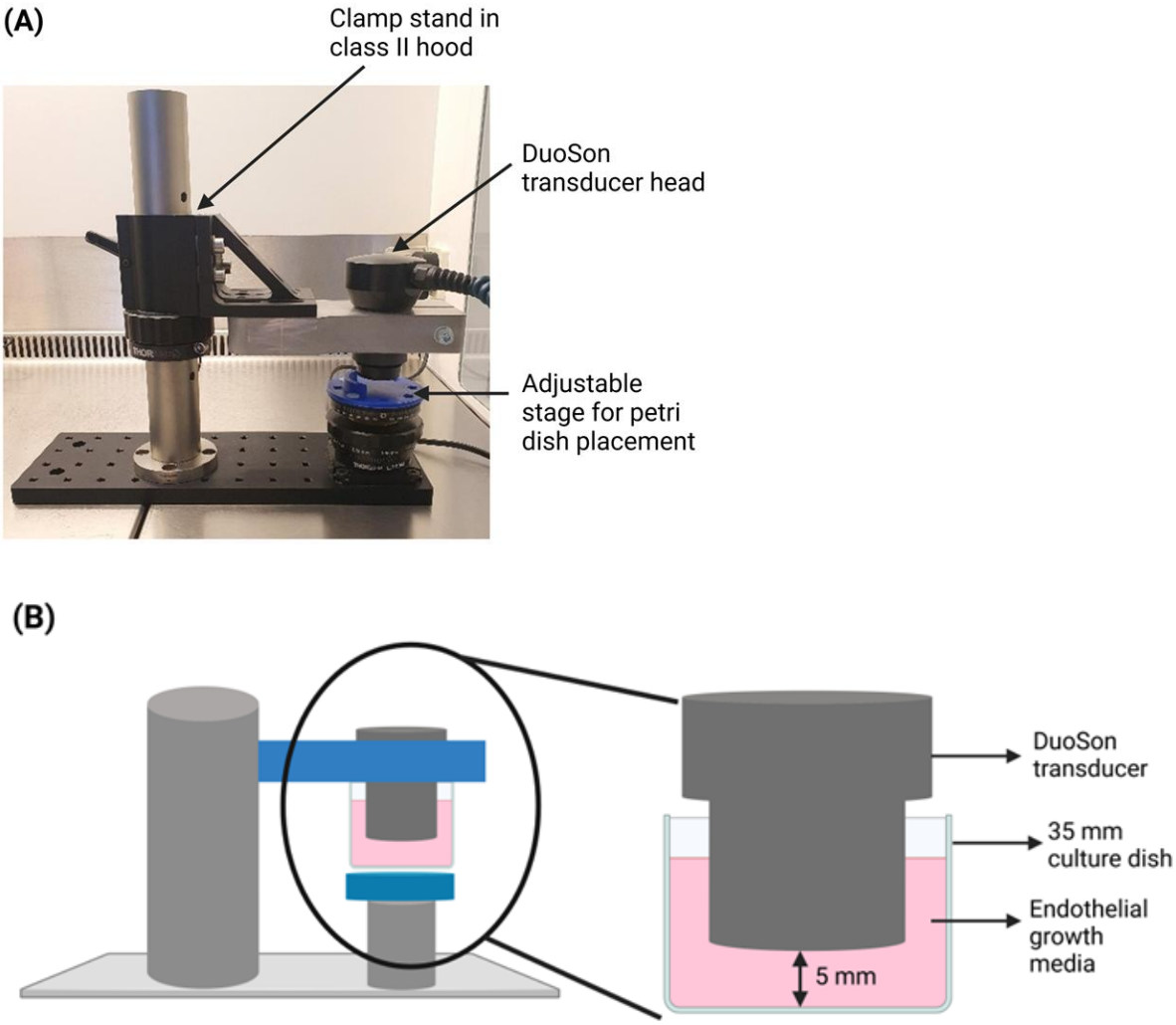

Figure 2.1 Diagrams of the experimental set up using a DuoSon transducer.
(A) The custom-built clamp stand Leeds included an adjustable stage to position a 35 mm petri dish a set distance from the transducer face. (B) Schematic diagram of the *in vitro* set up. The transducer was positioned 5 mm away from the base of the cell culture dish and immersed in 5 ml warmed cEGM. Image created in BioRender.com.

2.2.2 Acoustic absorbing tank

A second exposure system was developed to minimise standing wave formation and to provide a more controlled exposure environment for the delivery of ultrasound. The exposure method consisted of a glass tank filled with deionised degassed water, lined with ultrasonic absorbing tiles (Apltile SF5048, Precision Acoustics, Dorchester, UK). A custom-made 45 kHz transducer transmitted ultrasound to cells within a watertight polycarbonate

CLINIcell® cassette. A rig was constructed to hold the transducer and cassettes in a reproducible position 5 mm apart as in the DuoSon experimental method (Fig 2.2). The centre of the cassette was aligned to the centre of the transducer face using a laser spirit level (Laser Level Pro 4, Victorian Systems, UK). Once aligned the positioning was marked onto the aluminium poles to ensure repeated alignment in multiple experiments.

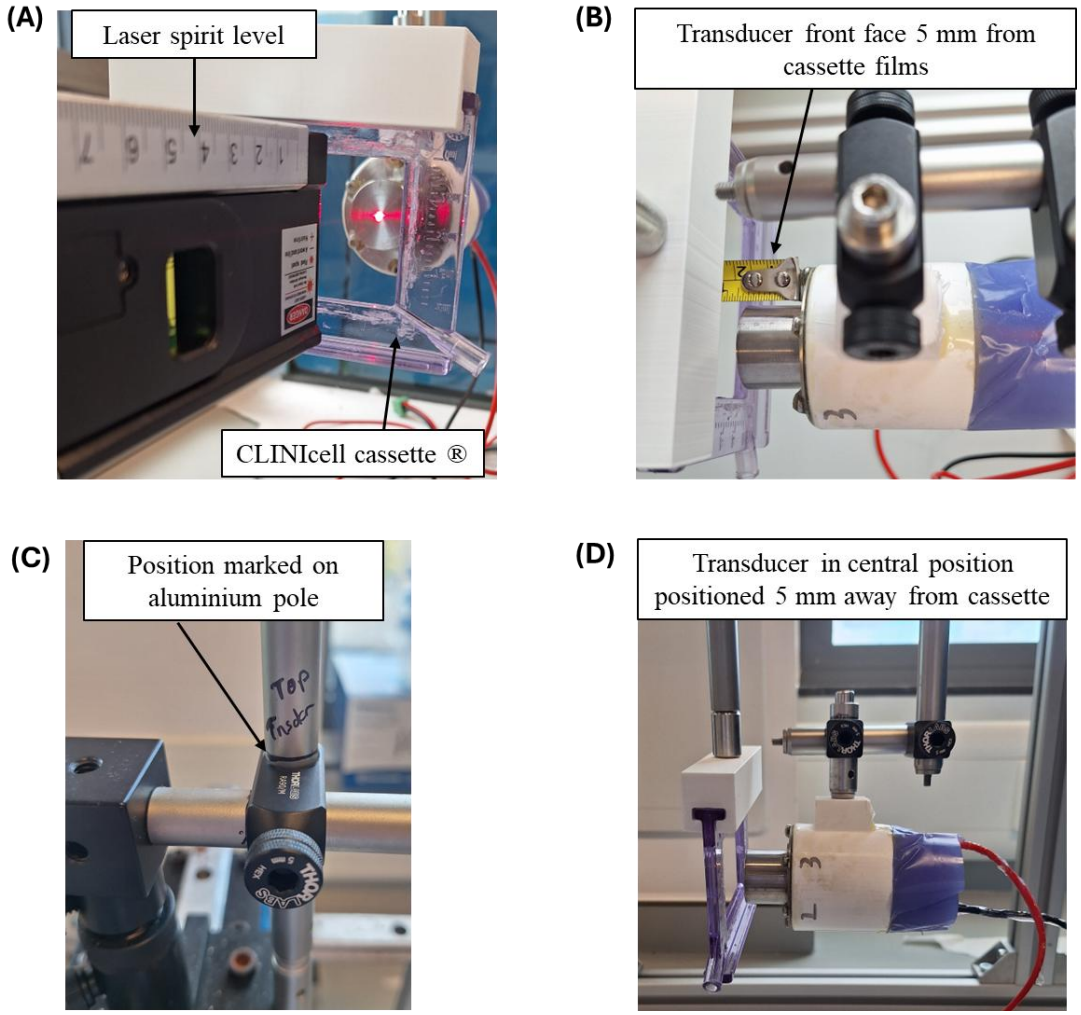

Figure 2.2 Positioning of 45 kHz transducer and CLINIcell® cassette.
(A) The centre of the transducer face was aligned with the centre of the cassette using a laser spirit level. (B) The transducer front face was positioned 5 mm from the cassette. (C) Once aligned the positions were marked for repeated experiments. (D) Final positioning of transducer and cassette for all cellular tank experiments.

2.2.2.1 Tank design

A 60 cm x 30 cm x 30 cm (length x height x width) glass tank (Diversa, Poland) was lined with 50 mm thick low frequency absorbing polyurethane structured tiles (Apltile SF5048, Precision Acoustics, Dorchester, UK) as demonstrated in Fig 2.3 A. The tiles were cut to ensure all the tank glass was covered and there were no 'acoustic' gaps. The tank was filled with 22 L deionised degassed water. Deionised water was degassed by boiling for 1 h using a 30 L urn (Igenix, UK), left on a rolling boil for 10 min and then sealed in airtight 5 L Duran bottles overnight. Once filled, the transducer and cassette could be submerged in the tank due to pre-determined markings on the aluminium rig as described previously (Section 2.2.2) (Fig 2.3 B).

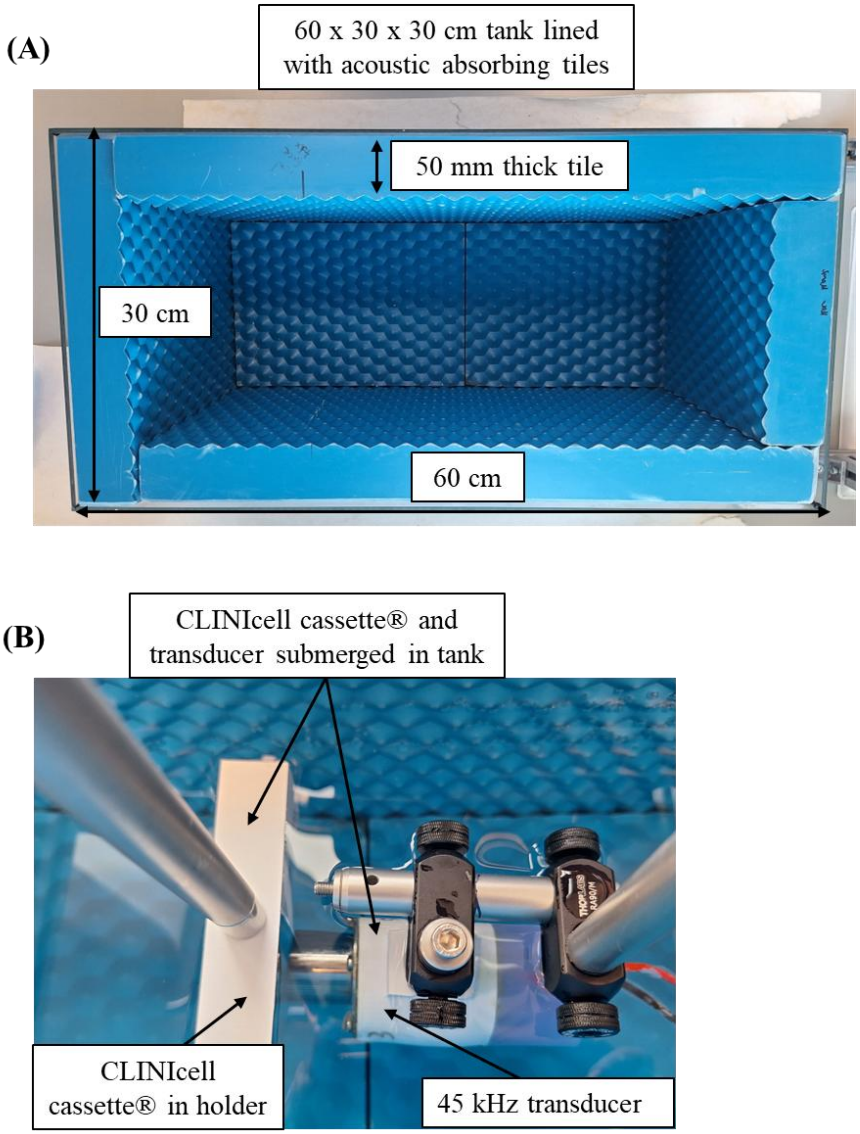

Figure 2.3 Photographs of tank configuration.
(A) All sides of the 60 cm x 30 cm x 30 tank were lined with acoustic absorbing tiles. (B) The 45 kHz transducer and CLINIcell® cassette were fully submerged in the tank, held at fixed positions during ultrasound exposure.

2.2.2.2 CLINIcell® cassette

CLINIcell® cassettes (Laboratoires MABIO International, Tourcoing Cedex, France) with a culture surface area of 25 cm^2 were used for cell culture experiments in the tank exposure configuration. The cassettes consisted of two 50 µm thick polycarbonate films within a polycarbonate frame. HUVECs were added to the cassette using a 20 ml syringe (Fisher, UK)

via the inlet valve, seeded at the same density as DuoSon experiments (10,000 cells/cm^2). The outlet valve was opened during any syringe application to allow gas to escape. This ensured no bubbles were visibly left in the culture after addition. Cassettes were placed in a 3D printed cassette holder (Fig 2.4) and aligned to positions marked on the aluminium tank rig.

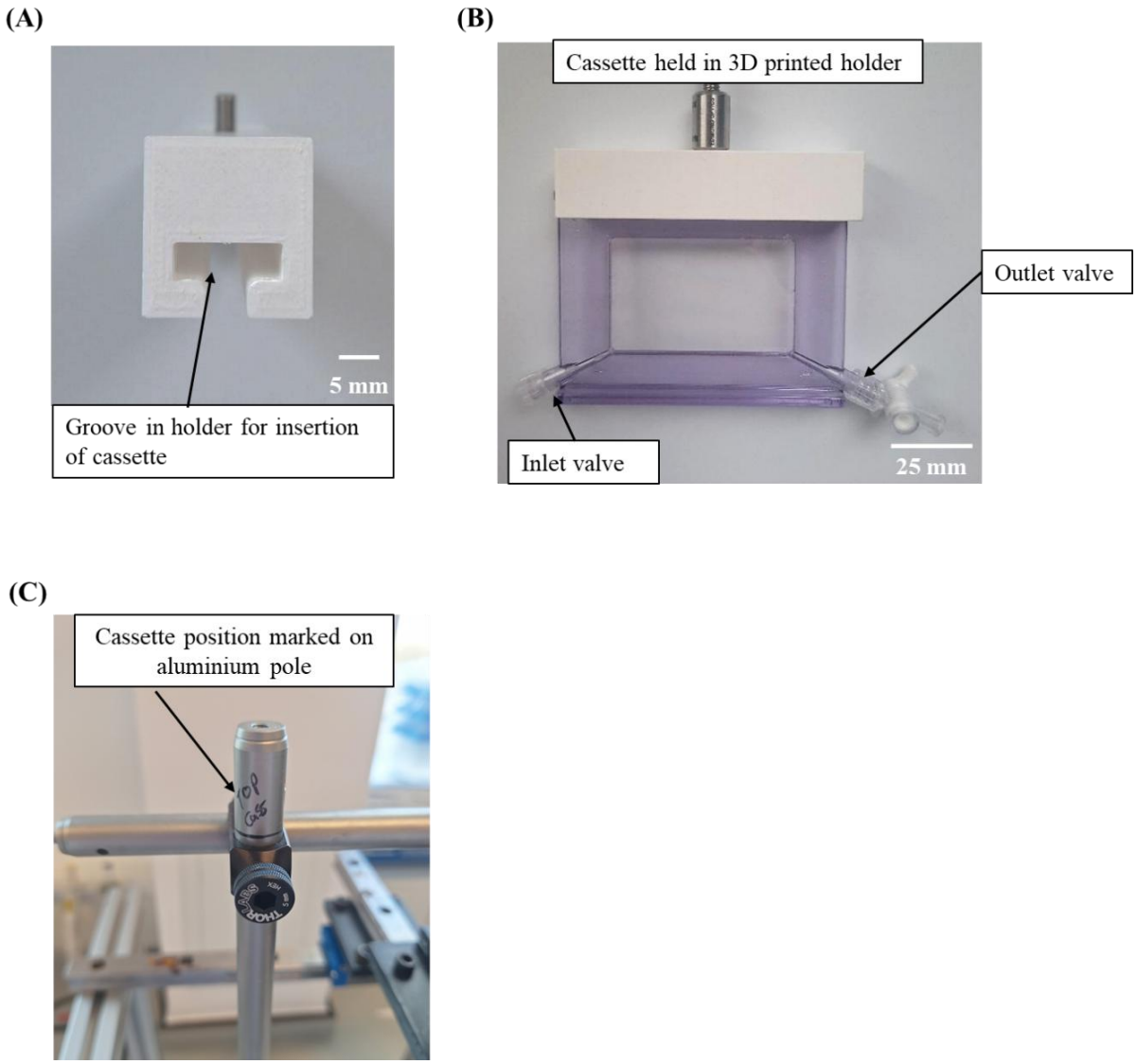

Figure 2.4 Photographs of a 3-D printed CLINIcell® cassette holder.
(A) A fixture was 3-D printed to allow holding of a CLINIcell® cassette in a fixed position during ultrasound exposure in the tank. (B) Cassette is fixed in position within the holder. (C) Final positions are marked on the aluminium poles for repeated experiments.

2.2.2.3 45 kHz ultrasound transducer

A 45 kHz transducer was designed and fabricated in collaboration with colleague Dr Xuan Li at the Department of Engineering, the University of Glasgow. A silicone mould was made by surrounding the rear of the transducer in 1:1 mixture of duplicating silicone (Centri^{TM} Duplika 12 A : Centri^{TM} Duplika 12 B, WHW Plastics, England, UK) and left to set for 1 h. Once set, the mould surrounded the wires found at the rear of the transducer that connects to the PiexoDrive FLEX driver. The mould prevented any splitting and exposure of wires during immersion in the tank and during ultrasound treatment (Fig 2.5).

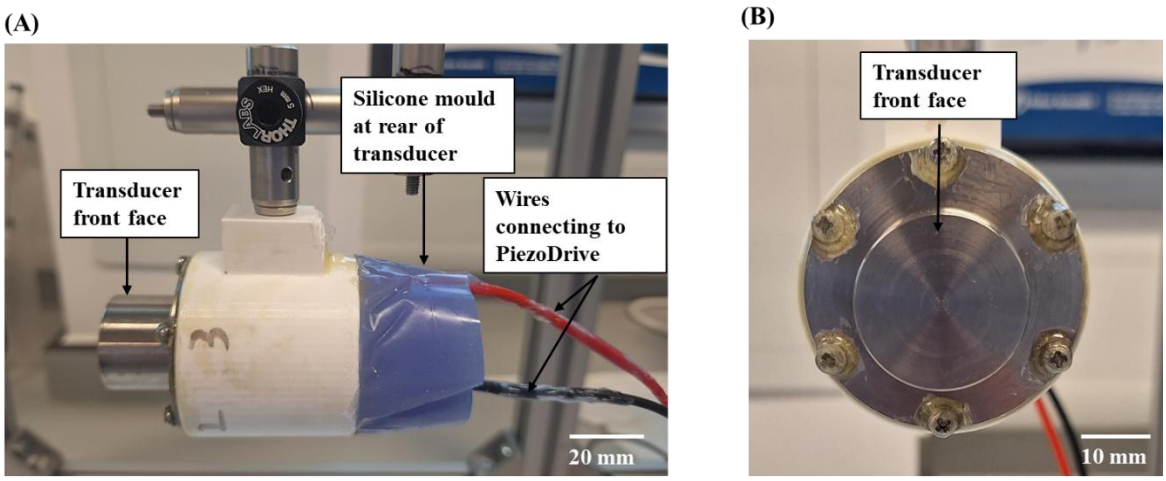

Figure 2.5 Photographs of custom-designed 45 kHz transducer.
(A) A silicone mould encased exposed wiring to the back of the transducer. (B) The 45 kHz transducer face was designed with the same dimensions as the DuoSon transducer head, 25 mm x 25 mm.

The transducer was driven by a PDUS210-FLEX ultrasonic driver (Piezodrive, New South Wales, Australia) using Piezodrive software (version 500014) to transmit an acoustic signal. An external 800 Ohm, 18.2 turn transformer (TX210-800) supplied an internal driving voltage to convert the acoustic signal from the transducer into acoustic energy.

Prior to any experiments an impedance sweep of the transducer was performed to check the driving frequency of the transducer was 45 kHz. The transducer was fully immersed in the tank. The centre of the transducer face was positioned 11 cm from the surface water and tiles lining the bottom of the tank. The impedance sweep settings are described in Table 2.3.

Table 2.3 Impedance sweep settings.
Settings applied to the Piezodrive software for a 45 kHz impedance sweep.

Voltage (V peak – peak)	1
Max Load Power (W)	210
Start Frequency (Hz)	42000
End Frequency (Hz)	48000
Step (Hz)	100
Min Delay (ms)	10

2.3 Characterisation of ultrasound exposure systems

2.3.1 DuoSon thermal measurements in 35 mm culture dish

The temperature of culture medium (cEGM) within a 35 mm culture dish was recorded during 30 min of ultrasound exposure. 5 ml cEGM was added to a 35 mm culture dish and placed in a 37 °C incubator for 24 h. The dish was then removed and vertically aligned with the transducer tip using the clamp configuration. The transducer was immersed in the cEGM 5 mm from the surface of the culture dish. Ultrasound was applied at 45 kHz using the 3 low frequency modes of 10, 25 and 75 mW/cm^2. The control consisted of immersing the transducer in the dish with the same configuration although the transducer was not activated. The temperature of the cEGM was measured using two K-type thermocouples connected to a

USB data logger (Pico Technology, UK) and recorded at 1-second intervals using PicoLog data logging software (Fig 2.6).

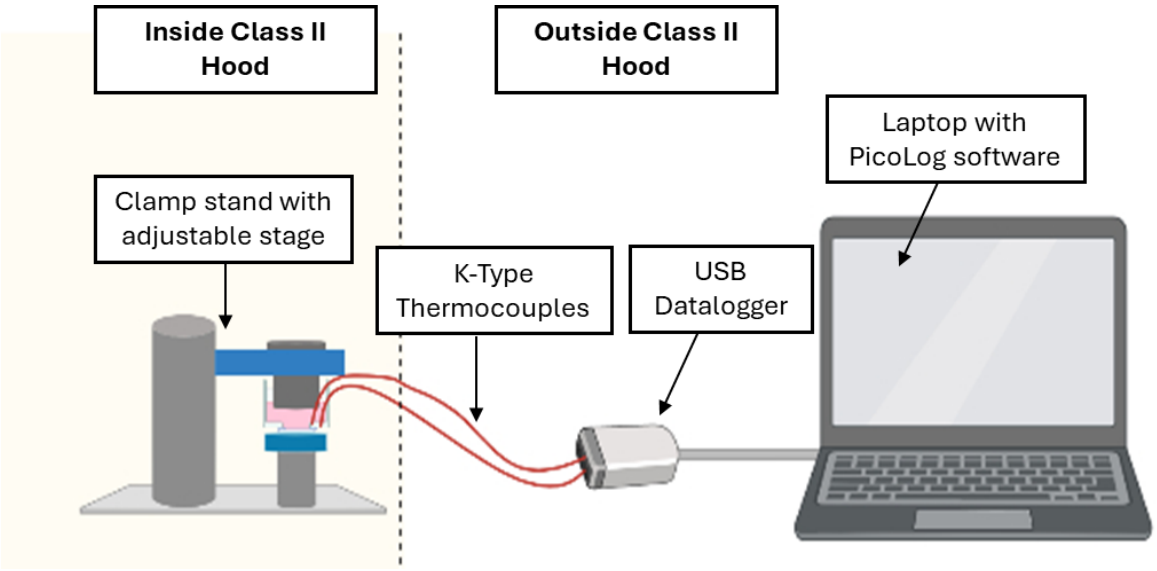

Figure 2.6 Diagram of DuoSon thermal reading experimental setup.
Two K-Type thermocouples were submerged in 5 ml cEGM in a 35 mm dish. The transducer was maintained 5 mm away from the dish surface in a clamp stand. PicoLog software was used to record the temperature every second for 30 min. Image created in BioRender.com.

2.3.2 Acoustic absorbing tank temperature measurements

Potential thermal effects of ultrasound exposure in the acoustic absorbing tank were investigated using the same temperature recording process as described for petri dish temperature monitoring. The tank water was heated to 37 °C using a water immersion heater. The heater was removed prior to any ultrasound emission to remove any interference in the ultrasonic field. Temperature was monitored during ultrasound exposure by submerging the thermocouples in the tank water, positioned near the transducer face. The temperature of culture medium within the CLINIcell® cassette was measured by placing a thermocouple

within the media inlet valve. A single temperature reading was taken immediately before and after 5 min ultrasound exposure driven using currents of 0.02, 0.04 and 0.06 A.

2.3.3 Pressure field mapping of acoustic absorbing tank

The acoustic field of the tank during 45 kHz continuous wave emission was measured using a low frequency scanning system at the University of Glasgow, designed for measuring frequencies of 500 kHz or less. The collaboration with University of Glasgow was arranged via the joint EPSRC 'Surgery Enabled by Ultrasonics' project. The aim of this study was to expose cells to ultrasound with minimal wave interference.

The 60 cm x 30 cm x 30 cm tank, lined with acoustic absorbing tiles, was filled with degassed deionised water prior to scanning. The transducer was driven at 45 kHz, 0.04 A as described in section 2.2.2.3. Cells were not present during scanning measurements. LabVIEW-based control software, designed by University of Glasgow researchers for previous research, was linked to a motorised stage to control the position and movement of a mounted 4 mm needle hydrophone (Precision Acoustics, Dorchester, UK) in the X Y Z planes (Fig 2.7). The 4 mm needle hydrophone was calibrated at additional low frequencies from 20 – 45 kHz by Precision Acoustics (Appendix Table 7.1). The hydrophone was connected to a preamplifier which in turn was connected to a DC coupler. The hydrophone output was recorded by a Picoscope which was 'triggered' to take hydrophone measurements at certain time points by a DAC card amplifier. The DAC card amplified the trigger sent to the Picoscope ensuring the hydrophone measurements were saved in a MATLAB file format. These measurements were then imported to a MATLAB script written by Hilde Metzger (PhD student, University of Glasgow) to produce a 2D pressure map of the scanned field in MPa (Appendix 7.4.2).

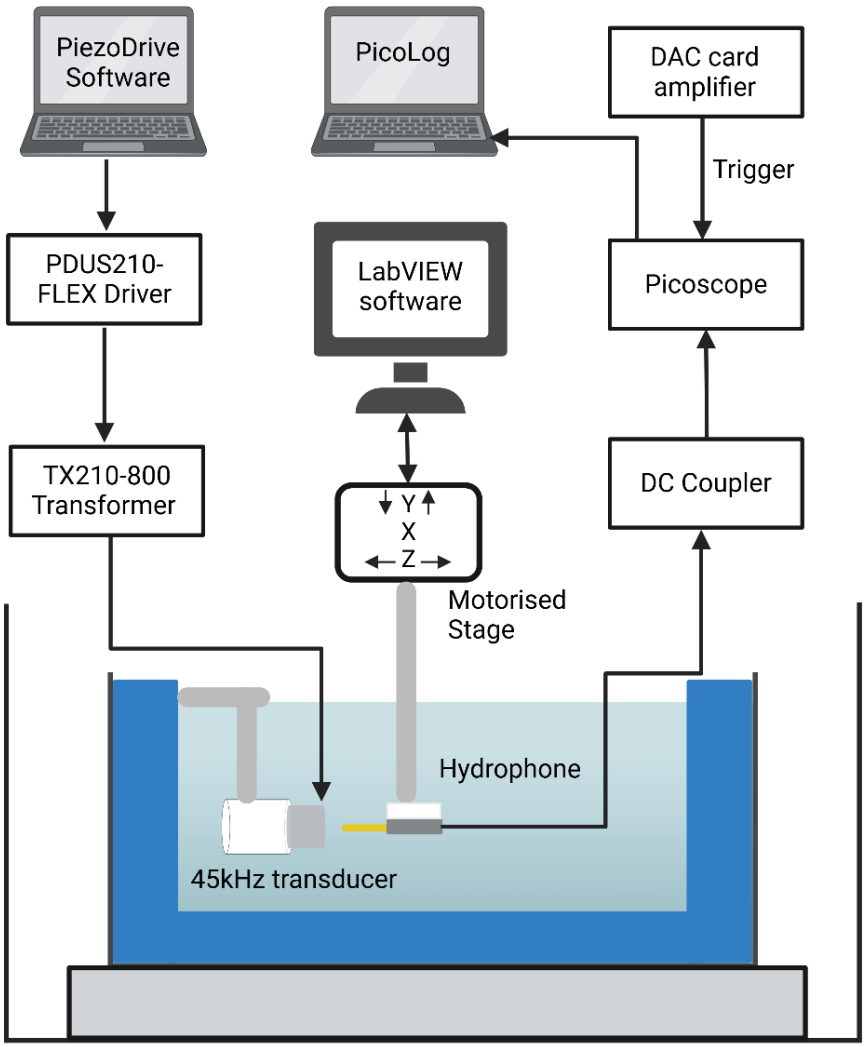

Figure 2.7 Diagram of acoustic pressure mapping methodology.
The acoustic field of 45 kHz transducer was measured using a 4 mm needle hydrophone. A scanning tank setup present at University of Glasgow was utilised to control the movement of the hydrophone to create pressure maps in transverse and longitudinal directions. Hydrophone output was recorded using PicoLog software and recorded as a MatLab file through a DAC card trigger to the Picoscope.

The 4 mm diameter needle hydrophone was submerged in the centre of the tank, 11 cm from the water surface and 11 cm from the bottom tiles through ruler measurement. The hydrophone was positioned perpendicular to the centre of the transducer front face aligned manually and by adjusting the XY position using an alignment programme in LabVIEW.

Once centralised the hydrophone was moved in the Z plane to the desired starting position of 5 mm or 25 mm from the transducer face through the alignment programme. Once aligned, the position was set to zero in the programme.

A wetting time of at least 20 min followed, meaning the hydrophone was submerged in the water but not switched on, to ensure no air was trapped inside or on the surface of the hydrophone before scanning commenced and for the temperature of the hydrophone to equalise with the water (Robinson & Green, 1997). The movement of the hydrophone during ultrasound exposure was programmed using a scan submergent step programme in LabVIEW. The mapped areas of interest were transverse scans across the transducer face 5 mm and 25 mm away and a longitudinal scan starting 5 mm away from the transducer face and moving in the Z plane to 25 mm distance. All scans had the XY dimensions of 105 mm x 85 mm corresponding with the dimensions of the CLINIcell® cassette.

The transverse scan 5 mm from the transducer front face, provided knowledge of the beam profile that would be interacting with the cells placed within the cassette during ultrasound exposure (Fig 2.8 A, transverse scan 1). The hydrophone was positioned 5 mm away, perpendicular to the centre of the transducer front face. Once in the correct starting position, coordinates of the scan were entered into the LabVIEW stepped scan programme (Table 2.4).

Table 2.4 Submergent scan settings for transverse scans.
The settings inputted into the submergent scan programme controlled the robotic motor to move the hydrophone 2.5 mm at 2 mm/s over an area of 105 mm x 85 mm. The settings were the same for all transverse scans: 5 mm, 25 mm no cassette and 25 mm with cassette.

	X plane	**Y plane**	**Z plane**
Dimension (mm)	105	85	0
Step (mm)	2.5	2.5	0
Speed (mm/s)	2	2	0

After every movement of 2.5 mm the hydrophone stopped and was 'triggered' to take a measurement and save the Picoscope reading as a MATLAB file.

Further scans were made 25 mm from the transducer front face, one without a CLINIcell® cassette present (Fig 2.8 A, transverse scan 2) and another with a cassette present (Fig 2.8 B, transverse scan 3). The CLINIcell® cassette was filled with deionised water and placed 5 mm away from the transducer in between the transducer and hydrophone. These scans were made to analyse any wave attenuation caused by the polycarbonate cassette.

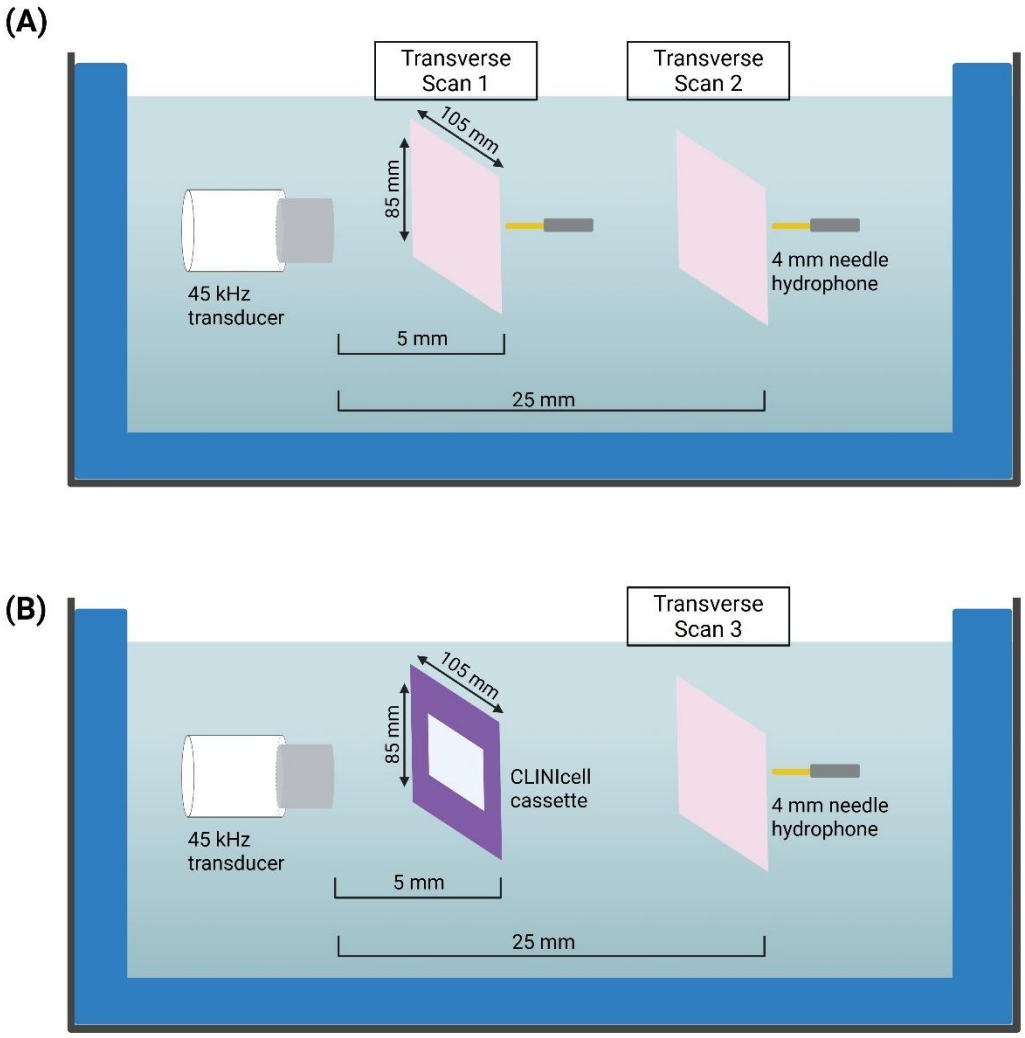

Figure 2.8 Schematic representing transverse pressure field scans of acoustic field in absorbing tank.

(A) Transverse scan 1 represents a scan taken 5 mm away from the transducer face 105 mm x 85 mm (X Y plane). Transverse scan 2 was taken 25 mm away from the transducer face with the same scan dimensions without a CLINIcell® cassette present. (B) A transverse scan with the same dimensions was conducted 25 mm away from the transducer face, with a CLINIcell® cassette present 5 mm away from the transducer face. Drawing not to scale.

A longitudinal scan in the YZ plane was conducted to analyse the acoustic field in relation to distance from the front face of the transducer (Fig 2.9). The hydrophone was positioned 5 mm away from the transducer front face following the alignment programme protocol described. The submergent step programme was used to move the transducer further away from the transducer in the YZ plane 85 mm x 25 mm using the settings in Table 2.5.

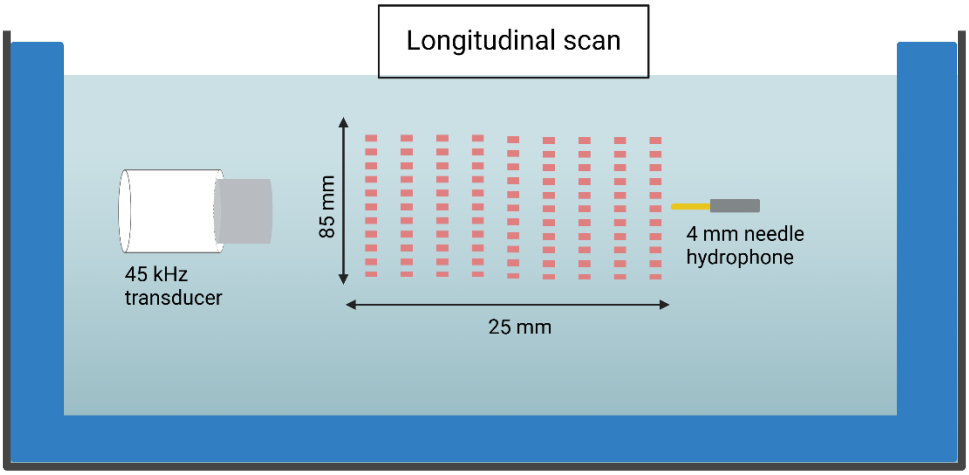

Figure 2.9 Schematic representing a longitudinal pressure field scan of acoustic field in absorbing tank.

A longitudinal scan was taken during 45 kHz exposure in an acoustic absorbing tank. A 4 mm needle hydrophone took measurements in a scan field of 85 mm x 25 mm (Y Z plane). Drawing not to scale.

Table 2.5 Submergent scan settings for the longitudinal scan.

The settings inputted into the submergent scan programme controlled the robotic motor to move the hydrophone 2.5 mm at 2 mm/s over an area of 85 mm x 25 mm in YZ direction.

	X plane	**Y plane**	**Z plane**
Dimension (mm)	0	85	25
Step (mm)	0	2.5	2.5
Speed (mm/s)	0	2	2

Multiple point scan measurements were taken 5 mm, 25 mm and 25 mm with a CLINIcell® cassette present from the transducer face to assess the pressure output in relation to increasing current levels (A) applied to the transducer. The current settings used for measurements ranged from 0.001 A to 0.075 A. The data was saved as a MATLab file using the Picoscope trigger and converted to linear relationship graphs using a MatLab script written by University of Glasgow PhD student Jack Stevenson (Appendix 7.4.2).

2.4 Exposure of ultrasound to HUVECs

Two different methods of ultrasound exposure were utilised in this project. The DuoSon device was used in a class II safety cabinet and cells were exposed to the transducer separated by 5 mm in a 35 mm culture dish. A degassed water tank method was subsequently used in a characterised acoustic field with increased control over temperature and reducing reflection and standing wave formation due to the presence of acoustic absorbing tiles.

2.4.1 Ultrasonic exposure in 35 mm culture dish

Once HUVECs had grown to ~80 % confluency in a T75 flask, cEGM was removed and cells washed with 3 ml HEPES buffered saline solution (HEPES BSS, Promocell, Heidelberg, Germany). To detach the cells, 2.5 ml 0.04 %/0.03 % trypsin/EDTA solution (Promocell, Heidelberg, Germany) was added. Once cells were observed as detached using brightfield microscopy visualisation (Motic AE21, China), the reaction was stopped through the addition of 2.5 ml trypsin neutralising solution (TNS; 0.05 % Trypsin Inhibitor/0.1 % Bovine Serum Albumin; Promocell, Heidelberg, Germany). The dissociated cell suspension was collected into a Falcon tube (Appleton Woods, UK) and centrifuged at 220 x g for 3 min (5804R,

Eppendorf, UK). The supernatant was discarded and the pellet resuspended in 2 ml cEGM to determine cell number using an improved Neubauer haemocytometer (Hawksley, UK).

HUVECs were seeded into 0.1 % gelatin-coated 35 mm culture dishes (CytoOne®, StarLab, UK) at a density of 9.6 x10^4 cells/well in 2 ml cEGM. The culture dishes were then incubated at 37 °C overnight prior to ultrasonic treatment. Before ultrasonic treatment 3 ml cEGM was added to ensure the DuoSon transducer face was immersed. The transducer face was cleaned with 70 % ethanol and washed in 37 °C warmed sterile cEGM prior to each cell treatment. Cells were treated with 45 kHz ultrasound for 5 min at either 10, 25 or 75 mW/cm^2 (Section 2.2.1) and compared with an untreated control where the transducer face was submerged, but no ultrasound applied.

2.4.2 Ultrasonic exposure in CLINIcell® cassette

HUVECs were seeded in a CLINIcell® cassette at the same seeding density of 10,000 cells/cm^2 as in the DuoSon experiments. Cells were suspended in 10 ml warmed sterile cEGM and added through the inlet valve of the cassette using a 20 ml Luer Lock syringe (Fisherbrand, Fisher, UK). The valve on the opposite side of the cassette was also opened during cell addition to facilitate the escape of bubbles and reduce the pressure applied to the cassette membrane. Once added, the valves were closed, tightened and the cassettes were kept at 37 °C, 5 % CO_2 overnight to allow cell attachment to the polycarbonate membrane.

Following overnight culture, the tank was filled with 22 L of degassed water, previously described (Section 2.2.2.1), by careful pouring of 5 L Duran bottles to minimise the

possibility of regassing. The water was heated to 37 °C using an immersion heater (Schimer, UK) prior to cassette addition. Before cassettes were placed in the tank an impedance sweep was carried out for the 45 kHz transducer (Section 2.2.2.3). The CLINIcell® cassette was placed in the 3D printed cassette holder and mounted to the marked positions in the rig for full immersion 5 mm from the transducer face.

Once transducer and cassette were positioned and water was at 37 °C, the immersion heater was removed from the tank before ultrasound exposure. Continuous wave ultrasound exposure was initiated at 45 kHz, 0.04 A as programmed with the PiezoDrive software (version 500014). After 5 min exposure the cassette was removed from the tank and placed in the 37 °C incubator until further analysis.

2.5 Viable cell number analysis

HUVEC number and viability were analysed following exposure to ultrasound as proliferation is one of the key indicators of angiogenic potential. The two methods employed in this study were manual cell counting and a cell counting kit 8 (CCK-8) assay.

2.5.1 Trypan blue exclusion assay

Viable cell number was quantified using a trypan blue viability assay protocol following ultrasound exposure. Trypan blue is a dye that penetrates damaged cell membranes. Viable cells with an intact cell membrane appear clear and unstained using light microscopy (Strober, 2001). Nonviable cells have a permeable cell membrane allowing trypan blue to pass into the cell cytoplasm and appear blue-stained using light microscopy.

For DuoSon experiments, cEGM was removed and cells were washed with 1 ml PBS to remove any remaining cell debris. Cells were then trypsinised with 1 ml 0.04 % / 0.03 % Tryspin/EDTA solution until all cells were detached as observed using brightfield microscope visualisation (Motic AE21, China). Once detached, 1 ml TNS was added to the cells, transferred to a Falcon tube and centrifuged at 220 x g for 3 min to obtain a cell pellet.

For CLINIcell® cassette experiments, cEGM was removed via syringe and cells washed with 5 ml PBS and manual inversion of the cassette to ensure all the membrane surface was covered. PBS was removed and 5 ml trypsin/EDTA added. Cassettes were placed on an orbital mixer (DLAB, GeneBio Systems, Canada) for 5 min. Once cells were observed as detached using brightfield microscope visualisation, 5 ml TNS was added to the cassette and thoroughly mixed. The 10 ml mixture was then added to a Falcon tube and centrifuged at 220 x g for 3 min.

The following methods were used for both DuoSon and CLINIcell® cassette trypan blue analysis.

The cell pellet was resuspended in warmed cEGM. 20 µL of the cell suspension was added to an equal volume of 0.4 % trypan blue solution (Sigma-Aldrich, UK). 10 µL of this suspension was added to the chambers of an Improved Neubauer haemocytometer (Hawksley, UK). A Motic AE21 light microscope was used to count live (unstained) and dead (stained) cells within the 4 outer corner grids of each chamber. Cell number was calculated by multiplying the average number of cells by 10^4, the dilution factor (2) and the volume of suspension. Cell viability was calculated using the following equation:

Equation 2.1. Cell viability equation after trypan blue exclusion assay.

$$\%\ Cell\ Viability\ = \frac{Number\ of\ Live\ Cells}{Number\ of\ Total\ Cells} \times 100$$

2.5.2 Cell counting kit 8 (CCK-8) proliferation assay

The CCK-8 cell counting kit involves the reduction of water-soluble tetrazolium salt 8 (WST-8) to formazan by cellular dehydrogenases. Formazan is soluble in cell culture medium producing an orange-coloured dye which can be measured using absorbance microplate readers at 450 nm. The amount of formazan produced in the culture medium is proportional to the dehydrogenase activity and subsequently the number of viable cells. Optical density (O.D) readings obtained can then be used to calculate the number of viable cells using calibration curve data. Calibration curves were prepared following two-fold serial dilutions of a known starting cell concentration to plot known cell numbers against O.D absorbance readings. Negative control wells were also present in all experiments containing cEGM and 10 % CCK-8 reagent.

CCK-8 readings were taken 24 h and 72 h after ultrasound exposure. cEGM was removed from the cell culture dish and cells were washed twice with 37 °C warmed PBS. Fresh 37 °C cEGM was added to the cell culture dishes along with 200 µL CCK-8 reagent and mixed by pipetting. The dishes were then placed in the 37 °C incubator for 180 min. After the incubation period, 100 µL was removed from each well and added to a 96 well microplate (Fisher, UK). The plate was then placed in a microplate reader (ELX800, Biotek, USA) and O.D readings were obtained at 450 nm using the Gen5 software (Agilent Biotek, USA). Standard curve readings were also taken after 180 min incubation.

2.6 Gene expression analysis

2.6.1 Isolation of RNA

Total RNA was isolated from untreated and treated cells 6 h, 24 h and 72 h after ultrasound treatment using a RNeasy plus mini kit (QIAGEN, UK) following the manufacturer's protocols. Cells were removed from the culture dish and cassette following the trypsinisation protocols (Section 2.5). Once a cell pellet was obtained, the pellet was then suspended in 200 µL PBS and centrifuged at 220 x g for 3 min to wash the cells. The PBS wash was repeated a second time. PBS was removed and 350 µL RLT buffer (QIAGEN, UK) was added to the cell pellet. The pellet was resuspended in the RLT buffer with repeated pipetting and vortexing (Vortex-Genie 2, Scientific Industries, USA) for 30 seconds and then transferred to a 2 ml cryovial (Scientific Laboratory Supplies, UK). The cryovial was stored at -80 °C if RNA extraction was not undertaken immediately.

The following steps were performed according to the RNeasy® Plus Mini kit handbook (QIAGEN, UK).

Collected cells in RLT buffer were vortexed for 30 s to disrupt the lysate. The homogenised lysate was added to a genomic DNA (gDNA) eliminator spin column as a purification step. The gDNA column was placed in a 2 ml collection tube and centrifuged for 30 secs at 8000 x g (10,000 rpm). The gDNA column was discarded and 1 volume (350 µL) of 70 % molecular grade ethanol (96 – 100 %) (Fisher, UK) added to the flow through and mixed by pipetting. The total mixture (700 µL) was added to a RNeasy spin column placed in a 2 ml collection tube and centrifuged for 15 s at 8000 x g (10,000 rpm). The flow-through was

discarded. 700 µL RW1 buffer was added to the RNeasy Mini spin column and centrifuged for 15 s at 8000 x g (10,000 rpm) and the flow-through discarded.

A working solution of RPE buffer was made by adding 4 volumes of molecular grade ethanol (Fisher, UK). 500 µL of RPE solution was used to wash the column of any residual ethanol by centrifugation at 8000 x g for 15 s then a further 2 min after discarding the flow through. The column was then spun at 13, 200 rpm for 1 min to further dry the column membrane to ensure no residual ethanol remained which could interfere with the elution of RNA. The RNeasy spin column was placed in a new 1.5 ml collection tube. 30 µL of RNase-free water was added directly to the membrane and centrifuged for 1 min at 8000 x g (10,000 rpm) to elute the bound RNA.

2.6.2 RNA quantification

The quantity and quality of eluted RNA was measured by a micro volume NanoDrop spectrophotometer (Jenway 6300, Genova Nano, UK). The reader was cleaned with 70 % ethanol prior to use. The reader was first 'blanked' using 1 µL RNase-free water (QIAGEN, UK) allowing a background absorbance value to be determined and minimising interference with sample readings. 1 µL of eluted sample RNA was then added to the middle of the reader for measurement. The concentration (µg/ml) and purity (260/280) readings were taken for every RNA sample. Samples with purities within the acceptable range of 1.9 – 2.1 were then used for the following complementary DNA (cDNA) synthesis.

2.6.3 Reverse transcription for cDNA synthesis

Single stranded cDNA was synthesised from eluted RNA following Tetro cDNA Synthesis Kit protocol (Meridian Biosciences, Bioline, UK). A 'master mix' was made by the addition of supplied reagents (quantities added per sample): 1 µL primer oligo II, 1 µL 10 mM dNTP, 4 µL 5X RT buffer, 1 µL, RNase inhibitor, 1 µL reverse transcriptase. After mixing by pipetting, 8 µL of the master mix was aliquoted to each PCR reaction tube (4titude, Fisher Scientific, UK) for each sample. 0.5 - 1 µg of RNA was then added to the PCR tubes. After RNA addition DPEC-treated water (Meridian Biosciences, UK) was added, if necessary, to reach a final reaction volume of 20 µL. All tubes were briefly centrifuged to ensure all mixture was collected to the bottom of the tube. The PCR tubes were then placed in a Biometra TAdvanced thermocycler (Analytik Jena, Germany) where samples were incubated at 45 °C for 60 min to generate complementary DNA (cDNA). The reaction was then terminated at 85 °C for 5 min. All cDNA samples were stored at -20 °C for future work.

2.6.4 Semi quantitative reverse transcriptase polymerase chain reaction (sqRT-PCR)

The primer sequences used for the following polymerase chain reaction analyses are described in Table 2.6. Glyceraldehyde-3-phosphate dehydrogenase (*GAPDH*) was used as the housekeeping gene in all sqRT-PCR experiments to act as a normalisation reference for the expression of the genes of interest. A 'mastermix' was made for each primer pair containing 10 µL forward primer, 10 µL reverse primer and 60 µL RNase-free water. A mix of 12.5 µL REDTaq® ReadyMix™ PCR reaction mix, 2 µL of primer 'mastermix' and 9.5 µL RNase-free water was made for each cDNA sample. 24 µL of this mixture was aliquoted to each reaction tube with 1 µL cDNA. The reaction mix was then placed in a Biometra TAdvanced thermocycler (Analytik Jena, Germany) to follow a process of initial

denaturation and polymerase activation at 94 °C for 5 min followed by annealing of primers and extension of the DNA at 63 °C. The reaction was then terminated at 72 °C for 10 min and cooled to 4 °C.

2.6.4.1 Gel electrophoresis and visualisation

sq-RT PCR product sizes were validated via gel electrophoresis technique and preliminary expression level changes were assessed. Briefly, a gel consisting of 1.5 % agarose (EuroGentec, Belgium) dissolved in tris-acetate-EDTA buffer (TAE, Thermofisher, UK) was made. 6 µL of SYBR® safe DNA gel stain (Invitrogen, Thermofisher Scientific, UK) was added to allow visualisation of DNA. 3 µL of a reference GeneRuler 1 kb DNA Ladder (ThermoFisher Scientific, UK) was added to each gel, followed by 3 µL of reaction samples. A current of 100 V was applied to the gel for 40 min to induce separation of the genes and the reference gene ladder. After electrophoresis, gene expression was visualised as bands following exposure to ultraviolet light using a SynGene G:BOX gel visualisation system (SynGene, UK). Expression levels were quantified by normalising target gene band intensity to the housekeeping reference gene *GAPDH*.

Table 2.6 Description of the primers used for sqRT-PCR and qPCR analysis.

Gene Name	**Gene**	**Accession number / Source**	**Primer sequence 5′ - 3′**	**Product (bp)**	**No. cycles (sqRT PCR)**	**Efficiency value (qPCR)**
Beta-2-microtubulin	*B2M*	NM_004048	F-5'-ACC CCC ACT GAA AAA GAT GA-3' R-5'-ATC TTC AAA CCT CCA TGA TG-3'	114	N/A	2.05
Glyceraldehyde-3- phosphate dehydrogenase	*GAPDH* (sqRT PCR)	In house primer School of Dentistry	F-5'-TCT AGA CGG CAG GTC AGG TCC-3' R-5'-CCA CCC ATG GCA AAT TCC ATG-3'	598	20	N/A
Glyceraldehyde-3- phosphate dehydrogenase	*GAPDH* (qPCR)	NM_002046	F-5'-CTC CTG TTC GAC AGT CAG-3' R-5'-GCC CAA TAC GAC CAA ATC-3'	111	N/A	2.07
Tyrosine 3-monooxygenase	*YWHAZ*	NM_003406	F-5'-ACT TTT GGT ACA TTG TGG CTT CAA-3' R-5'-CCG CCA GGA CAA ACC AGT AT-3'	94	N/A	2.09
Ribosomal protein L27	*RPL27*	NM_001349921	F-5'-ATG GGC AAG AAG AAG ATC GC-3' R-5'-AGA CAT CCT TAT TGA CGA CAG TT-3'	133	N/A	1.913
Endothelial nitric oxide synthase	*eNOS*	NM_000603	F-5'- CTC CAG CCC CGG TAC TAC TC -3' R-5'- TTA GCC ACG TGG AGC AGA CT -3'	139	N/A	1.979
Platelet endothelial cell adhesion molecule 1	*PECAM-1*	NM_000442	F-5′-TCA AAT GAT CCT GCG GTA TTC-3′ R-5′-CCA CCA CCT TAC TTG ACA GGA-3′	169	32	1.92

Vascular endothelial growth factor A	*VEGF-A*	NM_001033756	F-5′-CCC ACT GAG GAG TCC AAC AT-3′ R-5′-AAA TGC TTT CTC CGC TCT GA-3′	173	32	1.89
Vascular endothelial growth factor receptor 2	*VEGF-R2*	NM_002253	F-5′-GCA ATC CCT GTG GAT CTG AA-3′ R-5′-ACT CCA TGC CCT TAG CCA CT-3′	193	30	2.00
Von Willebrand factor	*VWF*	NM_000552	F-5′-GAC CTT GCT GAA GAG TCA TCG-3′ R-5′-GCC AGT CAG CTT GAA ATT CTG-3′	184	26	1.87

2.6.5 Real time quantitative polymerase chain reaction (qPCR)

qPCR has become the gold standard of gene expression analysis as it allows "real time" quantification of products throughout the duration of the PCR reaction. The following method uses a sensitive fluorescent DNA stain (SYBR Green I) which has a high affinity for double stranded DNA (dsDNA). Once bound to the minor groove of dsDNA the fluorescence increases up to 1000-fold. The fluorescence signal can consequently be used to quantify the amount of dsDNA present as the fluorescence is proportional to the amount of dsDNA PCR product (Wittwer et al., 1997).

2.6.5.1 Primer efficiency

The efficiency of primers used in qPCR was established via calibration curves of serially diluted cDNA concentrations prior to running gene of interest samples. A primer 'master mix' was made for each gene of interest and housekeeper gene using the following components of the LightCycler® 480 SYBR Green I Master (Roche, UK): 100 µL Green I Master, 78 µL H_2O and 1 µL of the specific forward primer and 1 µL of the specific reverse primer. The tubes were vortexed for 5 seconds to ensure efficient mixing. 9 µL of the primer mixture was added to the wells of a Light Cycler 96 well plate (Roche, UK).

A pool of all cDNA samples was made. This 100 % cDNA mixture was diluted with molecular grade RNase-free water to create concentrations of 50 %, 10 %, 1 %, 0.1 % and a control 0 % cDNA with only molecular grade H_2O (Corning, USA). 1 µL of diluted cDNA was added in duplicate wells of the 96 well plate on ice (Fig 2.10).

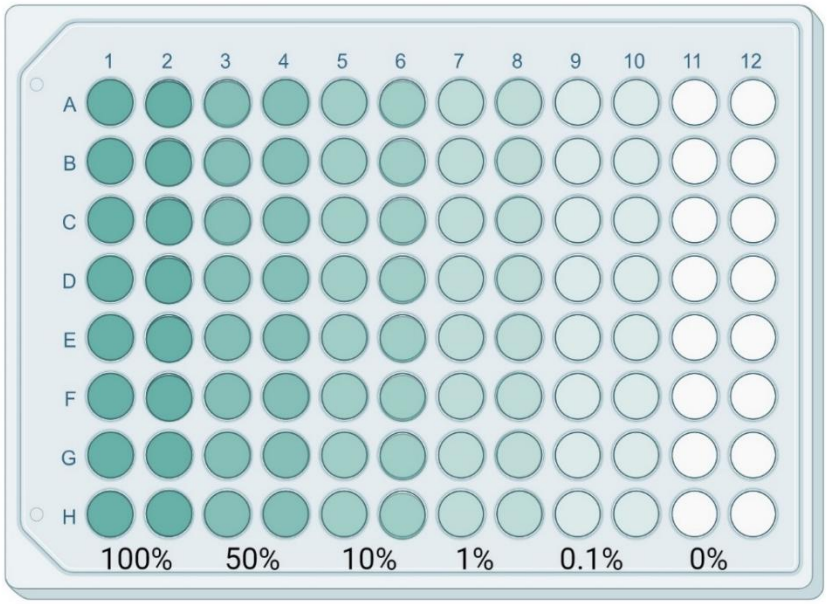

Figure 2.10 Plate layout for primer efficiency PCR run.
Serial dilutions of 100% pooled sample cDNA were added to a 96 well PCR microplate in duplicate wells. Each row corresponds to a different primer.

After sample addition, the plate was sealed with plate sealing film (Roche, UK) and centrifuged at 3220 rpm for 3 min (Universal 320 R, Hettich, Germany) to ensure all mixture was collected to the bottom of the wells. The plate was then transferred to a LightCycler® 480 Instrument II (Roche Diagnostics, Switzerland) for real-time qPCR analysis. The cycle settings for the primer efficiency and all subsequent runs are detailed in Table 2.7. The system software LightCycler® 480 software version 1.5 (Roche, UK) was used to calculate primer efficiency. Primers were deemed 'efficient' if the amplification efficiency value was 2 ± 0.2 as stated in MIQE guidelines (Bustin et al., 2009). This indicated that the amount of PCR product doubles with each cycle.

Table 2.7 qPCR programme settings for primer efficiency PCR reaction plate.
The following settings were input into the LightCycler® 480 Instrument II for primer efficiency PCR cycle runs.

Stage		**Temperature (°C)**	**Time (min : sec)**	**No. cycles**
Pre-incubation		95	5:00	1
Amplification	**Denaturation**	95	0:20	60
	Annealing	60	0:20	
	Extension	72	0:30	
Melting Curve		97	Continuous	1
Cooling		40	0:30	1

2.6.5.2 LightCycler® 480 application

Primer master mix for housekeeper and target genes of interest were added to the wells of a Light Cycler 96 well plate. 1 µL of diluted cDNA was added in triplicate wells to each primer mastermix on ice (Fig 2.11) to create a final volume of 10 µL.

Following the MIQE guidelines (Bustin et al., 2009) multiple controls were added to each plate. Inter-plate controls contained the primer mastermix for each gene present on the plate with 100 % pooled cDNA to ensure reliability in the comparison of results between plates. Negative control wells contained only primer mastermix to detect any non-specific amplification (e.g. primer dimers) and any sample contamination. Positive control wells contained *GAPDH* primer mastermix and 100 % pooled cDNA this was present to identify any errors or variation in the qPCR runs as a signal should always be detected in these wells.

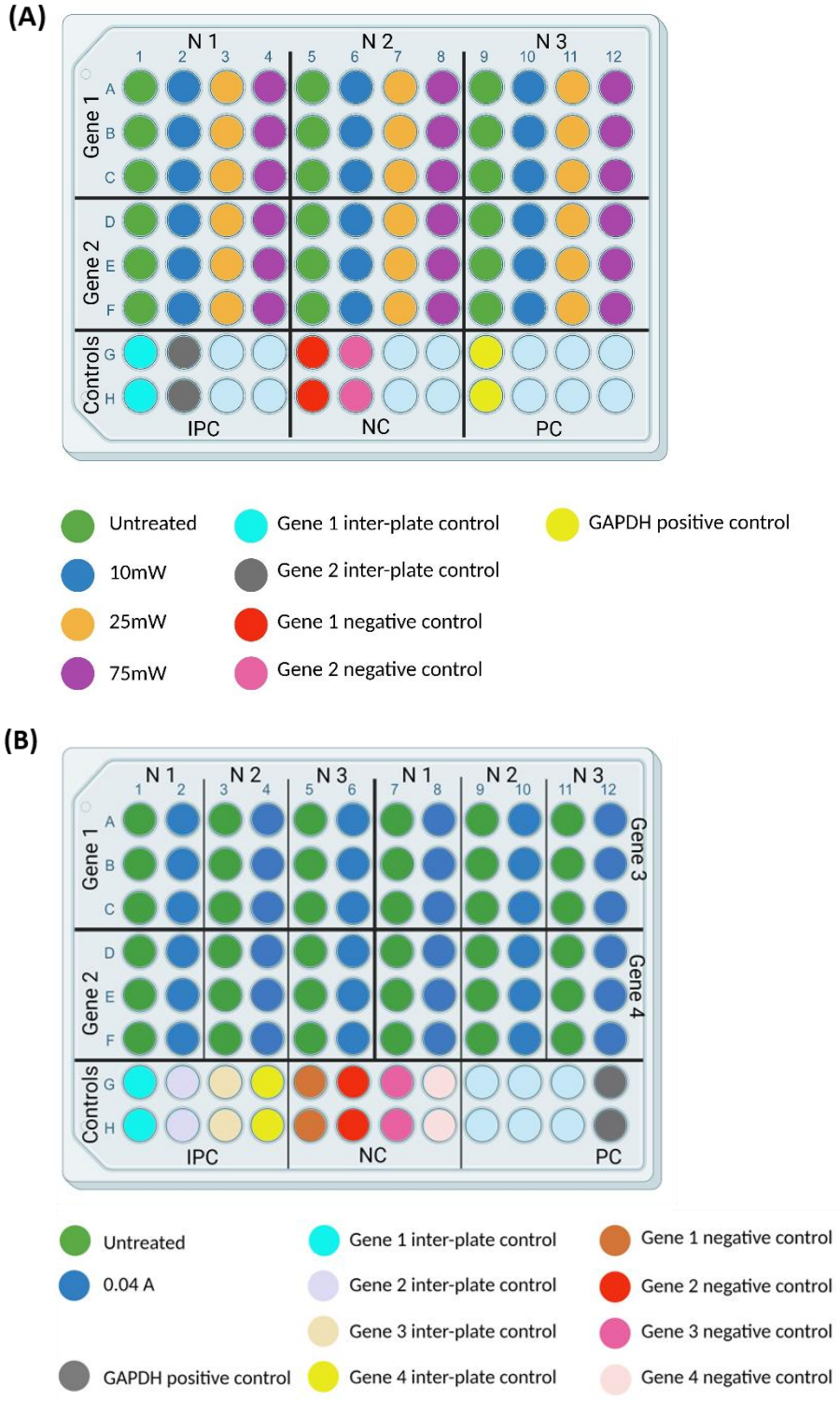

Figure 2.11 Light Cycler 96 well plate layout for RT qPCR analysis.
(A) Plate layout for DuoSon cDNA samples. (B) Plate layout for cassette cDNA samples. Samples were added in triplicate wells with three biological replicates (N1, N2, N3). Inter-plate controls were added to allow reliable analysis between plates. Negative controls contained the primer mastermix only and a GAPDH positive control with pooled cDNA was present.

The plates were centrifuged at 3220 rpm for 3 min, placed in the Lightcyler® 480 machine and run at the settings described in Table 2.8. Crossing point (Cp) values were calculated in the Lightcycler® 480 software via the second derivative maximum method. These values are defined as the cycle number where the fluorescence detected from the samples exceeds the background threshold indicating presence of the target sequence.

Table 2.8 qPCR programme settings for target gene PCR reaction plate.
The following settings were input into the LightCycler® 480 Instrument II for target gene PCR cycle runs.

Stage		Temperature (°C)	Time (min : sec)	No. cycles
Pre-incubation		95	5:00	1
Amplification	**Denaturation**	95	0:20	45
	Annealing	60	0:20	
	Extension	72	0:30	
Melting Curve		97	Continuous	1
Cooling		40	0:30	1

2.6.5.3 Relative quantification in qBase^{PLUS}

The quantification cycle values (Cq) of each plate were imported into the qBase^{PLUS} software (Biogazelle, Belgium) for analysis. The calibrated normalised relative quantity (CNRQ) method (Hellemans et al., 2007) was used to convert the Cq values into normalised relative quantities (NRQs) against multiple reference (housekeeper) genes. The housekeeper genes used were *GAPDH, B2M, YWHAZ* and *RPL27*. The stability of these housekeepers was first analysed using a geNorm algorithm. The housekeeper genes with lowest variability were then

used as reference genes for target sample normalisation. Quality control was also used for sample technical replicates by setting a replicate variability threshold of 1 cycle. This meant the difference between the highest Cq value and lowest Cq value must not be more than 1 cycle. Any replicates outside of this range were excluded from the calculations.

2.7 Tube formation assay

Tube formation assay was performed to investigate the effect of 45 kHz ultrasound on the angiogenic behaviour of HUVECs at different times post ultrasound exposure: immediately, 24 h and 72 h after ultrasound exposure. Matrigel^{TM}-Matrix (Corning, NY, USA) was thawed overnight on ice at 4 °C prior to use. All pipette tips, well plates and culture dishes used in tube formation experiments were chilled overnight at 4 °C.

2.7.1 Tube formation in 48 well plate

Once thawed, 50 µL of 10 mg/ml Matrigel^{TM} was pipetted onto chilled 48 well plates (Fisher Scientific, UK) using cooled pipette tips. The plates were then incubated at 37 °C for 1 h to allow polymerisation of the basement membrane matrix. During polymerisation ultrasonically treated HUVECs were detached from culture dishes using Trypsin/EDTA solution and counted using a haemocytometer (Section 2.5.1). 5 x 10^4 cells were seeded in cEGM onto the Matrigel^{TM} coated wells with 3 technical replicates per condition.

The wells were visualised using a Nikon Eclipse TE300 phase contrast inverted microscope (Nikon, Japan) 4 h, 6 h and 24 h after seeding using a at 4 x objective (Plan Fluor 4x/0.13 PhL DL, Nikon, Japan). 4 – 5 images per well were captured using a Nikon D5100 camera (Nikon, Japan). Image analysis was performed using the JavaScript plugin ‘Angiogenesis Analyzer’

(Carpentier, 2012) in Fiji (Schindelin et al., 2012). Images were converted from the RAW .NEF file using NX studio software (Nikon studio) to a 16-bit TIFF file. Images were then stacked to an RGB image and rescaled to 25 % the original image in Fiji. This increased the pixel size to ensure the Angiogenesis Analyser plug-in analysed and plotted a correct 'map' onto the images, known as an angiogenesis tree. The data from the Angiogenesis Analyser were exported to Microsoft Excel (Microsoft 365, version 2412, USA). The measurements for total tube length and the number of branches were statistically analysed in GraphPad Prism (GraphPad Software, USA). Comparisons between multiple time points were performed by setting the untreated 4 h average measurement as 100 % and all other data was set as a % increase/decrease to this control value.

2.7.2 Tube formation in 35 mm culture dish

Tube formation ability was assessed immediately after ultrasound treatment of HUVECs in a 35 mm culture dish (CytoOne®, StarLab, UK). After overnight thawing, 750 µL of 10 mg/ml Matrigel™ was pipetted into chilled 35 mm culture dishes. After 1 h of polymerisation in a 37 °C incubator 9.6 x 10^4 cells were seeded in 2 ml cEGM onto the Matrigel™-coated dishes. Cells were left for 1 h to settle and attach to the matrix. After 1 h, an additional 2 ml cEGM was added to the culture to allow immersion of the DuoSon transducer in the 35 mm dish. The clamp stand was adjusted to move the stage a further 0.5 mm away from the transducer face to account for the 0.5 mm thick layer of Matrigel™. This ensured a consistent distance of 5 mm between the transducer face and the cell layer. Cells were then treated with 45 kHz continuous wave ultrasound (Section 2.4.1). Cells were treated for 1, 3 and 5 min with an untreated control group, where the DuoSon transducer was immersed but not turned on, as a control.

Images were captured in 5 regions of the well: top left, top right, bottom right, bottom left and centre of the well. Images were captured 4 h, 6 h and 24 h after ultrasonic treatment at 4x objective (Plan Fluor 4x/0.13 PhL DL, Nikon, Japan) using a Nikon D5100 camera (Nikon, Japan) attached to a Nikon Eclipse TE300 microscope (Nikon, Japan). The images were analysed using Angiogenesis Analyser JavaScript plugin in Fiji using the same analysis process as imaging in 48 well plates. The data was then analysed using a principal component analysis (PCA) in R (v 4.3.0, RStudio Team, 2020) to visualise effects of intensity, exposure length and time point on total tube length and number of branches measured. The parameters of exposure length and intensity were combined to calculate the supplied dose of ultrasound in Joules (J) using the calibrated total acoustic power measurements (Table 2.2) and the following Equation 2.2. The energy and corresponding DuoSon treatment conditions are described in Appendix Table 7.5.

Equation 2.2. Calculation of enery supplied (J) during DuoSon exposure in 35 mm culture dishes.

$$Energy\ (J) = Total\ acoustic\ power\ (W)\ \text{x}\ Exposure\ length\ (s)$$

2.8 Immunocytochemistry

Cell morphology and internal organisation was examined after ultrasound exposure using phalloidin staining, as the organisation of actin can be an indicator of the angiogenic behaviour of an endothelial cell.

2.8.1 F-actin cytoskeleton staining

ActinGreen^{TM} 488 ReadyProbes (Thermofisher, UK) were used as a room temperature (RT) stable solution to Alexa Fluor 488 Phalloidin. Phalloidin is a bi-cyclic peptide with high

affinity and selectivity to F-actin. ActinGreen™ 488 conjugates the F-actin probe to a photostable green-fluorescent Alexa Fluor 488 dye providing visualisation of green-fluorescent stained cells. ActinGreen™ 488 was used to assess any morphological changes post 45 kHz exposure.

2.8.1.1 Cell morphology post DuoSon exposure

Cell morphology, specifically F-actin organisation, was visualised 24 h, 48 h and 72 h after exposure to DuoSon 45 kHz ultrasound (Section 2.4.1). Cell culture media was removed from the culture dishes and cells washed twice with Dulbecco's phosphate buffered saline (DPBS). Cells were then fixed with 1 ml 3.7 % paraformaldehyde (PFA, Thermo Scientific, UK) for 10 min at RT. After fixation cells were washed twice with DPBS and permeabilized using 0.5 % Triton™ X-100 (Sigma, UK) for 1 h at RT. Any remaining detergent was removed by washing with DPBS. Cells were then stained with 2 drops of ActinGreen™ 488 ReadyProbe (Thermofisher, UK) ensuring the entire monolayer was stained and the wells covered in aluminium foil for 45 min at RT. Prior to visualisation, the stain was removed, cells washed with DPBS and 2 drops of fluoroshield mounting medium with DAPI (Abcam, UK) were added to the wells. A Nikon Eclipse TE300 fluorescent microscope (Nikon, Japan) attached to a CoolLED pE2 excitation system (CoolLED, UK) was used for cell visualisation. The ActinGreen™ 488 dye was visualised at 490 nm and DAPI visualised at 400 nm wavelength. Images were captured using a Nikon D5100 camera (Nikon, Japan).

2.8.1.2 Cell morphology post acoustic absorbing tank exposure

Following exposure to ultrasound using the acoustic absorbing tank method (Section 2.4.2), HUVECs were stained for F-actin at 24 h and 72 h timepoints. At each time point cEGM was

removed from the cassettes via the inlet/outlet valve using a 20 ml syringe. Cells were washed twice with 5 ml DPBS prior to fixation. 10 ml PFA was added to the cassette to fill the culture chamber in the cassette and left at RT for 10 min. After 10 min PFA was removed and cells were washed twice with DPBS. A sterile scalpel (Swann-Morton™, Fisher, UK) was used to cut the polycarbonate film from the cassette, and tweezers (Fisher, UK) used to place the films facing cell-side upwards into 90 mm petri dishes (Fisher, UK). 0.5 % Triton™ X-100 was added to the films covering the film surface for 1 h at RT. The films were washed with DPBS and then stained with ActinGreen™ 488 ReadyProbe ensuring the stain was added to the entire surface of the film. After 30 min covered in foil at RT the stain was removed, washed with DPBS and fluoroshield mounting medium with DAPI added to the film. Cells were visualised following the same procedure as analysis of actin following DuoSon exposure.

2.9 Statistical analysis

All experiments contained 3 technical replicates n = 3 and at least 3 biological replicates $N \geq 3$ to allow for statistical analysis. Biological replicates were defined as separate cell cultures from different HUVEC passages (passage 2 – 5 only) used in experimentation on different days.

2.9.1 GraphPad Prism

Statistical analysis was carried out in GraphPad Prism, versions 9.3.1 to 10.4.1 (GraphPad Software, San Diego, California, US) unless otherwise stated. Temperature measurements during DuoSon exposure were analysed via one-phase decay non-linear regression analysis to quantify the rate of temperature change during DuoSon exposure. The tests implemented for

comparisons of 3 or more data sets were one-way analysis of variance (ANOVA) with Tukey's post-hoc HSD (honestly significant difference) calculator or two-way ANOVA with Tukey's post hoc test. Comparisons between the means of 2 groups were made using unpaired t-test analysis. The tests used for each analysis are defined in the corresponding results section.

2.9.2 Principal component analysis (PCA)

PCA is a technique used to identify significant differences within large data sets. PCA was used to analyse data obtained from 'Angiogenesis Analyser' results from the tube formation assay in 35 mm culture dishes. Large data sets were obtained from the 'Angiogenesis Analyser' as multiple ultrasound conditions were investigated: intensity, lengths of exposure and times after exposure. Rather than choose what variables to analyse, PCA analysis was performed on the whole dataset and visualized in R (v 4.3.0, RStudio Team, 2020, Boston, MA, USA) using the packages FactoMineR (Lê et al., 2008), factoextra (Kassambara & Mundt, 2017), ggplot2 (Wickham, 2016), devtools (Wickham et al., 2022), ggfortify (Tang et al., 2016) and dplyr (Wickham et al., 2023). Ellipses produced on the graphs indicated a confidence of 95%. The script written and run in R can be found in Appendix 7.4.1.

2.10 Illustration design

Illustrations within this thesis were created in Biorender.com.

Chapter 3.

RESULTS

3.1 HUVEC exposure to 45 kHz using DuoSon transducer

3.1.1 Introduction

The following section describes experimentation undertaken to identify an effect on HUVEC behaviour following exposure to 5 min 45 kHz continuous wave ultrasound via the DuoSon device. As HUVECs would be exposed to the surrounding atmosphere during DuoSon transducer submergence, the work was carried out in a sterile class II hood. To maintain sterility, class II hoods are supplied with a constant flow of recirculating filtered air. For this reasoning, the effect of working in a class II hood on the temperature of cell culture medium (cEGM) was assessed via K-type thermocouple readings. Following this, HUVEC response to 45 kHz DuoSon ultrasound was analysed outlined in Fig 3.1. HUVEC morphology was observed via F-actin staining, as the main component of a cell cytoskeleton which is crucial to numerous cell activities such as cell-cell connections, motility and shape. After visualisation, quantitative analysis on HUVEC response to ultrasound was investigated. HUVEC viability and number was analysed via trypan blue staining and CCK-8 assay to identify any stimulating or damaging effect caused by low frequency ultrasound exposure.

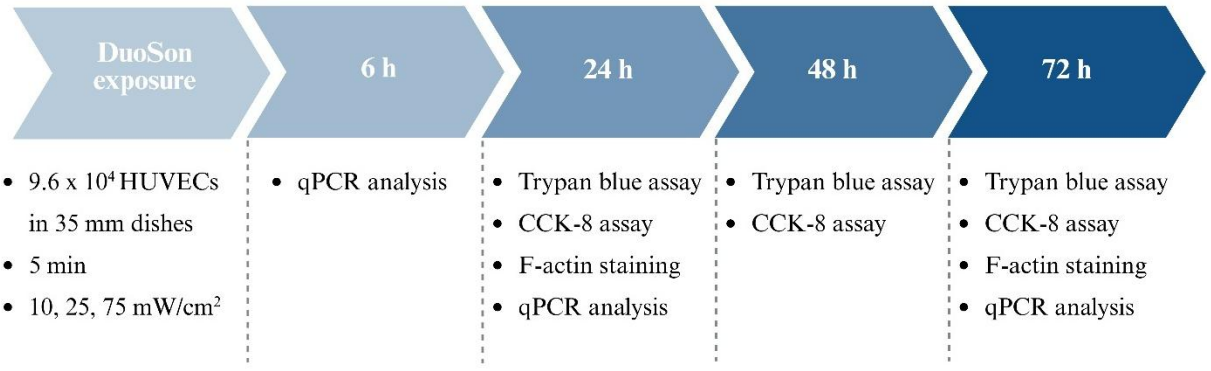

Figure 3.1 Representatice timeline of HUVEC response analysis to DuoSon exposure. Following DuoSon exposure for 5 min at 3 different intensities, HUVEC response was analysed at multiple timepoints. qPCR was used to study gene expression response, cell number and viability was assessed via trypan blue and CCK-8 assay and HUVEC cytoskeleton organisation was observed via F-actin staining and microscopy techniques.

3.1.2 Temperature of culture medium during ultrasound exposure

Temperature recordings taken immediately after the culture dish was removed from a 37 °C incubator and placed in the clamp configuration showed the medium always cooled at the first sample recording (0 s). With the class II cabinet air flow turned on (Fig 3.2 A) and off (Fig 3.2 B) the temperature of the medium decreased during the 30 min ultrasound exposure for all intensities (0, 10, 25 & 75 mW/cm^2). The temperature began to plateau after approximately 10 min of exposure with air flow, earlier than without air flow where the media continued to cool. However, one-phase decay analysis showed the rate of temperature decrease was significantly different between all conditions tested with or without air flow, as all curves were significantly different to each other ($p < 0.0001$). Therefore the rate of medium cooling was dependent on the air flow supply to the class II cabinet, as well as the intensity of ultrasound applied. The higher the intensity of ultrasound the slower the rate of medium cooling.

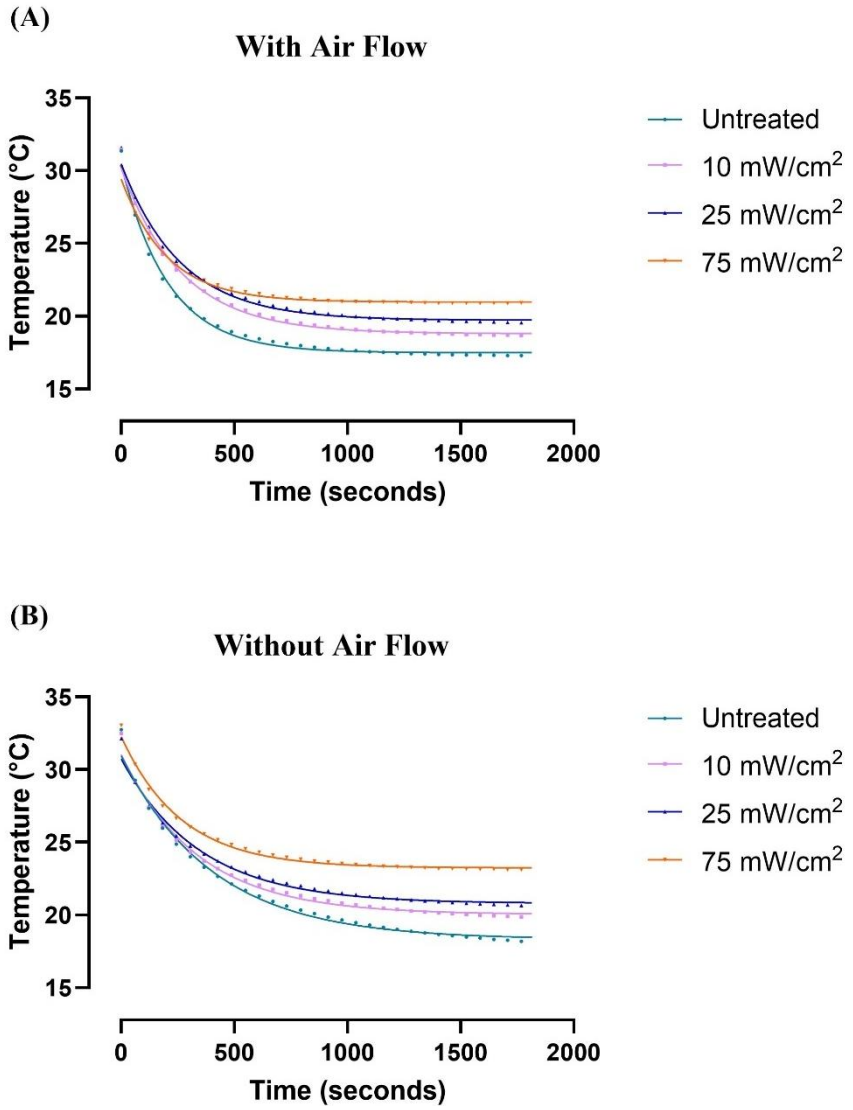

Figure 3.2 Culture medium temperature with 45 kHz ultrasound treatment for 30 min following removal of culture dish from 37 °C incubator.

One-phase decay analysis was performed on temperature readings over 30 min ultrasound exposure. With air flow (A) and without air flow (B) the higher the intensity of ultrasound, the slower the rate of medium cooling. (N = 3, mean value with line of best fit determined with nonlinear regression analysis).

The final temperature reading taken after 30 min ultrasound of untreated cEGM decreased to 17.3 °C with air flow in the class II cabinet (Fig 3.3 A). This was significantly lower than occurred with exposure to ultrasound intensities of 25 mW/cm^2 (19.6 °C, $p < 0.05$) and 75 mW/cm^2 (20.9 °C, $p < 0.0001$). The final temperature of cEGM exposed to 75 mW/cm^2

was also significantly higher than when exposed to the lowest ultrasound intensity of 10 mW/cm^2 ($p < 0.05$). There was no significant difference in the final temperature of cEGM when exposed to 10 mW/cm^2 and 25 mW/cm^2 ($p = 0.1381$) ultrasound intensities. Similarly, without air flow the final temperature of untreated cEGM (18.2 °C) was significantly lower than ultrasound treated cEGM (Fig 3.3 B). 10 mW/cm^2 (19.9 °C; $p < 0.05$), 25 mW/cm^2 (20.6 °C; $p < 0.01$) and 75 mW/cm^2 (23.1 °C $p < 0.0001$). The final temperature of cEGM exposed to the highest intensity 75 mW/cm^2 was significantly higher than other conditions ($p < 0.0001$). A significant difference was observed between the final temperature readings of 25 mW/cm^2 and 10 mW/cm^2 ($p < 0.05$).

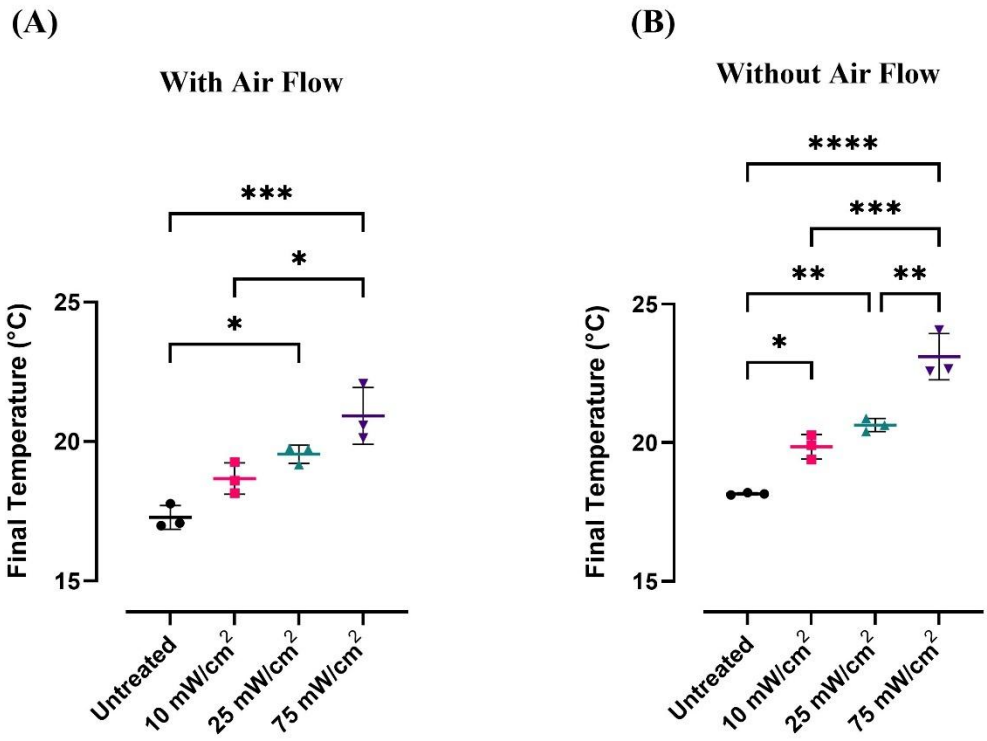

Figure 3.3 Final temperature recording after 30 min ultrasound with and without air flow.

Temperature recordings taken of cEGM after 30 min of ultrasound exposure at 10, 25 and 75 mW/cm^2 and in untreated cEGM. Recordings taken with (A) and (B) without air flow. Significant differences were identified through one-way ANOVA with Tukey's multiple comparisons post-hoc test. (N = 3, mean ± SD; * $p < 0.05$, ** $p < 0.01$, *** $p < 0.001$, **** $p < 0.0001$).

Due to the significant decrease in temperature seen over 30 min exposure, subsequent cell culture experiments were conducted during a 5 min exposure period. The temperature recordings after 5 min showed mostly insignificant differences in medium temperature between untreated and ultrasound treated cEGM with air flow (Fig 3.4). The only significant difference ($p < 0.05$) was recorded between untreated cEGM (20.6 °C) and cEGM exposed to 25 mW/cm^2 (23.1 °C). Therefore, it could be argued that any subsequent differences in cellular response following 5 min ultrasound exposure would likely not be a result of temperature difference between untreated and treated cells but of the non-thermal effects of ultrasound excitation.

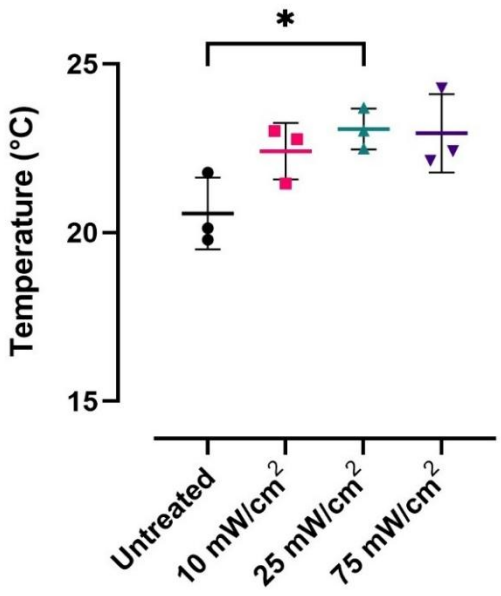

Figure 3.4 Temperature readings taken after 5 min ultrasound exposure with air flow. Temperature recordings taken of cEGM after 5 min of ultrasound exposure at 10, 25 and 75 mW/cm^2 and in untreated cEGM with air flow supply. Significant differences were identified through one-way ANOVA with Tukey's multiple comparisons post-hoc test. (N = 3, mean ± SD; * $p < 0.05$).

3.1.3 Influence of 45 kHz DuoSon exposure on HUVEC cytoskeleton

Following temperature measurements, HUVECs were exposed *in vitro* to 5 min 45 kHz DuoSon US. An effect on the HUVEC cytoskeleton was subsequently investigated. HUVECs were visualised 24 h and 72 h after DuoSon ultrasound exposure via F-actin and nuclear (DAPI) staining. The fluorescent images were overlaid allowing visualisation of the HUVEC monolayer and more specifically cytoskeleton organisation.

Over the imaging period from 24 h to 72 h cell density appeared to increase in untreated and treated cells with apparent increased visualisation of cell-cell contact points, represented in Fig 3.5 B, D, F & H. However, areas of more closely aggregated cells were seen in cells exposed to ultrasound at intensities of 25 and 75 mW/cm^2 after 72 h (Fig 3.5 F & H) compared with untreated cells (Fig 3.5 B). Localised actin staining could be observed in some instances at these cell-cell contact points (white arrows in Fig 3.5 B, D, F, G, H), which correlates to actin's function in in endothelial cell-cell contact (Schnittler et al., 2014). So-called actin localisation could also be seen in cells that were not within contact of another cell in all conditions, most predominantly 24 h after exposure (orange arrows in Fig 3.5 A, C, E, G). These areas of localised actin may indicate the location of the leading edge of a migrating cell as actin is implicated in cellular motility (Lamalice et al., 2007). As all cells, ultrasound exposed and unexposed, displayed localised staining this may suggest cell motility was not inhibited by ultrasound exposure. Though this effect cannot be determined quantitatively through these stained images.

Not only were localised points of actin observed, but actin staining spanning the HUVEC membrane was also seen in some instances (yellow arrows in Fig 3.5 E, F & G). This staining

corresponds to actin filaments present in the cell membrane cytoskeleton. As this staining was observed in untreated cells and those exposed to ultrasound it can be suggested that the cell membrane integrity was not damaged due to ultrasound exposure. HUVECs also exhibited similar morphology when exposed and unexposed to DuoSon ultrasound suggesting no noticeable effect on the cellular structure.

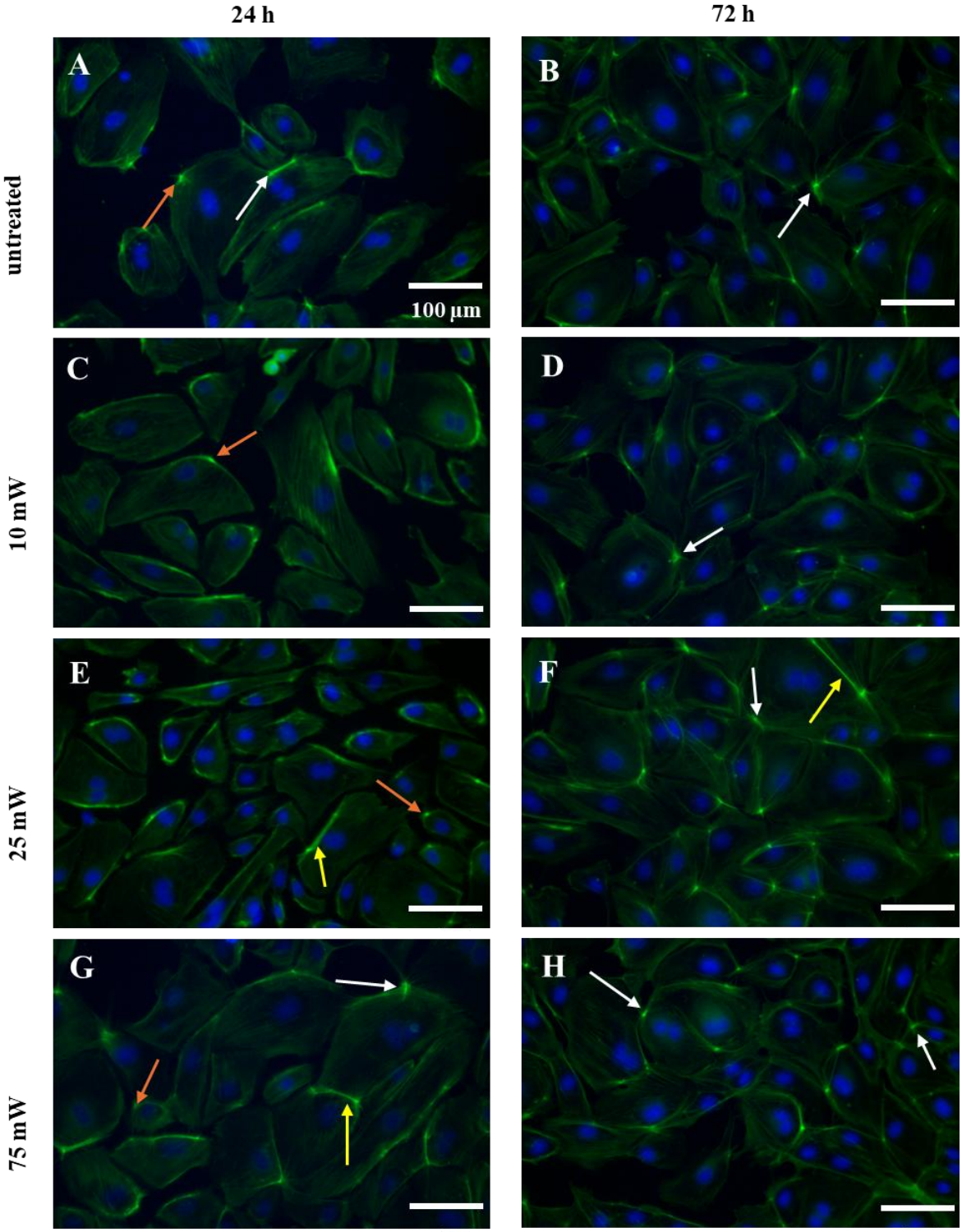

Figure 3.5 Fluorescent micrographs of F-actin stained HUVECs 24 h, 48 h and 72 h post ultrasound exposure.

Localised areas of F-actin can be seen on the edge of HUVECs with (white arrows) and without (orange arrows) cell-cell contact. Elongated staining could also be seen at the edge of some HUVEC bodies (yellow arrows). (N = 3, scale bars represent 100 µm).

3.1.4 Viable cell number analysis

Cells counted 24 h after ultrasound exposure at 10 mW/cm^2 showed a 10 % increase in viable cell number compared with untreated cells. Exposure to intensities of 25 mW/cm^2 and 75 mW/cm^2 showed greater increase in cell number by 19 % and 15 % compared with untreated cells (Fig 3.6 A). However, these increased numbers respectively counted were not significantly higher than the untreated cells numbers counted ($p = 0.5989$ and $p = 0.8681$, respectively). Analysis of HUVEC numbers 48 h after ultrasound treatment showed a similar trend to that observed at 24 h (Fig 3.6 B). Increased viable cell numbers were counted after exposure to intensities of 25 and 75 mW/cm^2. Similarly to numbers counted after 24 h, 25 mW/cm^2 delivery resulted in the highest increase in viable cell number of 12 % compared with untreated cells. A slight decrease in viable cell number was seen in cells exposed to 10 mW/cm^2, 10 % lower than untreated cells. Although all differences were not statistically significant after one-way ANOVA analysis. Nonetheless, these observations indicate no significantly detrimental effects to cell viability. On the contrary, a positive effect can be suggested due to the increase of viable cell number, though not statistically significant, most likely due to the short time after treatment.

Viable HUVEC number was also evaluated 72 h after ultrasound treatment. A significant increase in viable cell number compared with controls was seen in all ultrasound treated groups (Fig 3.6 C). Cells exposed to 10 mW/cm^2 intensity ultrasound showed a 14 % ($p < 0.05$) increase in cell number compared with cells unexposed to ultrasound. 45 kHz continuous ultrasound at the highest intensity of 75 mW/cm^2 resulted in a significant 25 % increase in cell number ($p < 0.001$). As with viable cell number analysis 24 h and 48 h after ultrasound exposure, the greatest increase in viable cell number was seen after delivery of

25 mW/cm^2 intensity. Viable cell number was significantly greater than untreated cells by 27 % ($p < 0.001$) and also significantly greater than cells exposed to 10 mW/cm^2 (14 % increase, $p < 0.05$).

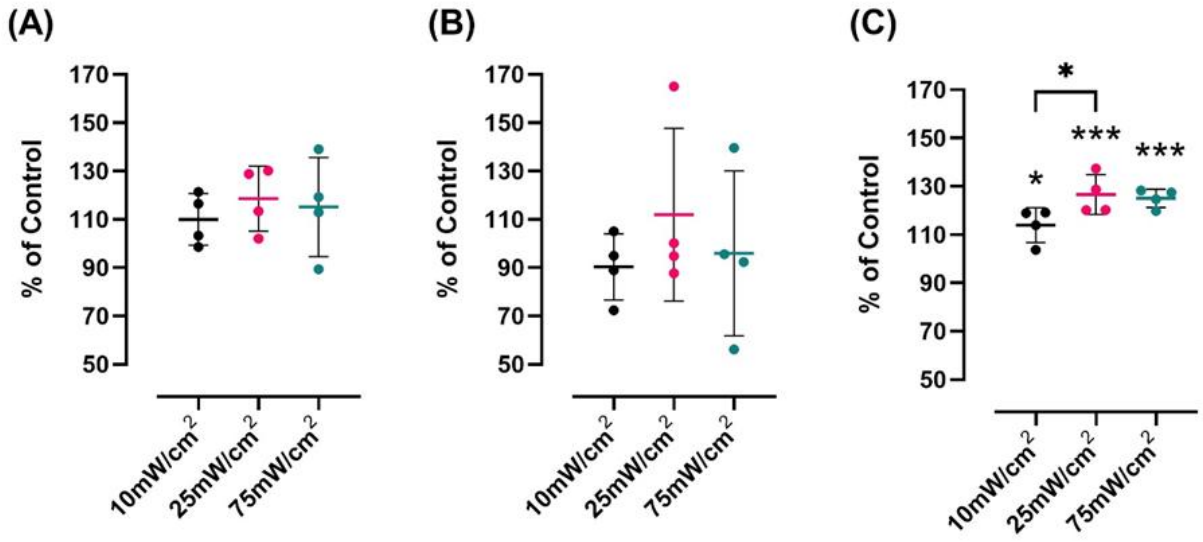

Figure 3.6 Viable HUVEC number 24 h, 48 h and 72 h after ultrasound exposure. Viable cell numbers were counted 24 h (A), 48 h (B) and 72 h (C) after ultrasound exposure using trypan blue exclusion assay. Results are expressed as a percentage of the untreated control (N = 4, mean ± SD).

Viable cell number was also determined via the cell counting (CCK-8) assay. A standard curve for the experiments was created to assess the assay validity and subsequently quantify the number of cells after ultrasound exposure (Fig 3.7). The graph showed a linear correlation ($R^2 = 0.9902$) between cell number and absorbance readings.

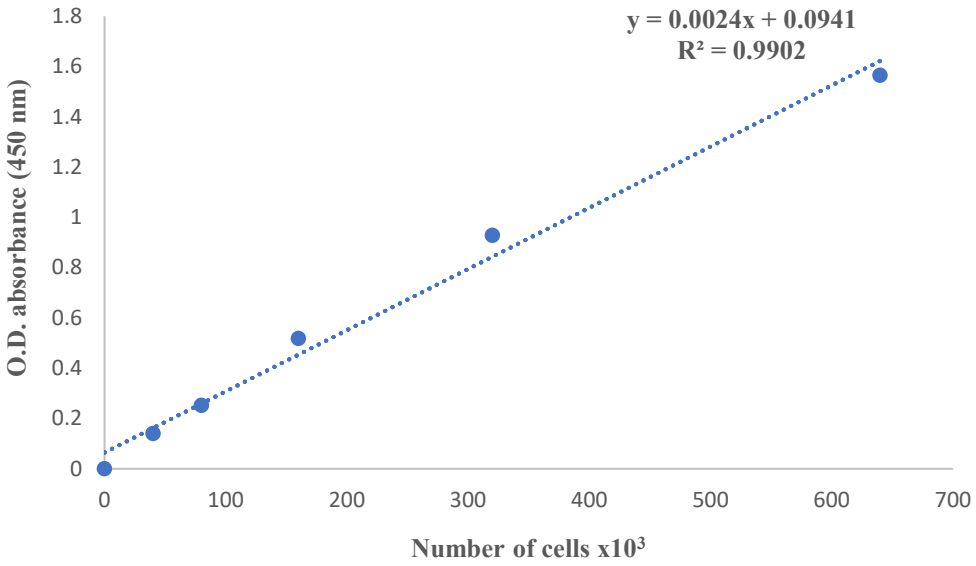

Figure 3.7 Representative calibration curve of CCK-8 for HUVECs.
A line of best fit was generated for O. D readings against known viable cell numbers. The linear regression equation and R^2 coefficient produced are plotted on the graph, showing linear correlation between O.D. readings and cell number ($R^2 > 0.9$).

O.D readings taken 24 h and 72 h after ultrasound exposure were converted to actual cell number using the calibration curve obtained. Fig 3.8 A showed there was no significant effect on viable cell numbers after 24 h using this assay. After 72 h (Fig 3.8 B) there was a moderate, albeit non-significant increase in cell number in HUVECs exposed to 25 mW/cm^2 compared with untreated cells ($p = 0.9037$) and cells exposed to 10 mW/cm^2 ($p = 0.9083$). However, as with results obtained via trypan blue assay, there was no detrimental effect on HUVEC viability caused by 45 kHz ultrasound exposure.

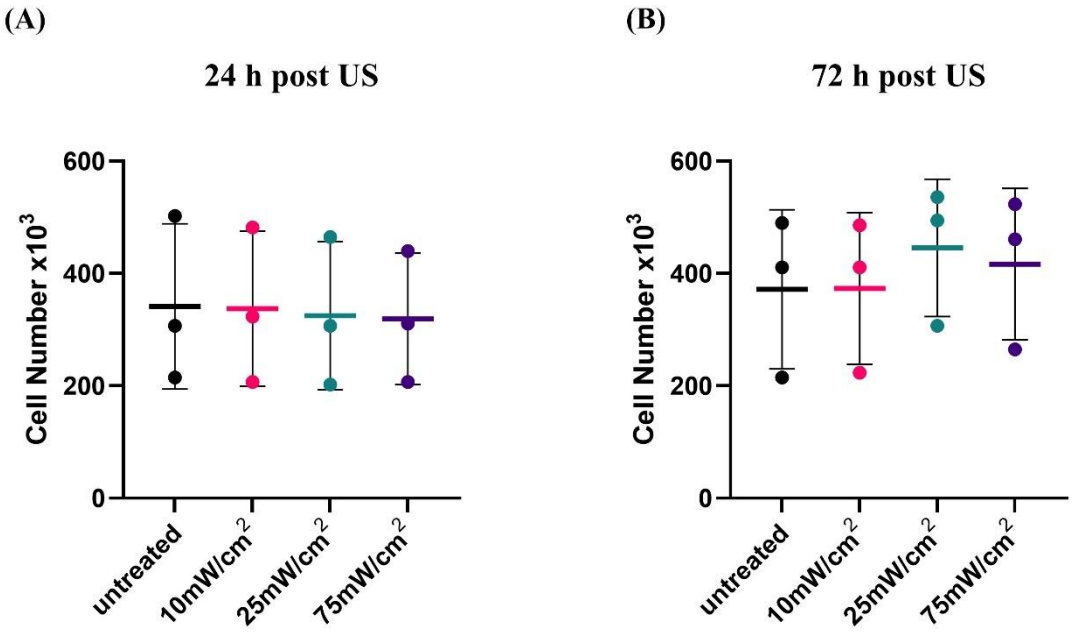

Figure 3.8 CCK-8 analysis 24 h and 72 h post ultrasound exposure.
O.D. readings from CCK-8 analysis were converted to viable cell numbers using calibration curves generated. No statistically significant difference in viable cell number seen between untreated cells and cells exposed to ultrasound at either time point. (N = 3, mean ± SD).

The work described in this section identified an initial effect on HUVEC behaviour regarding a non-significant change to cell viability and an increase in viable cell number was observed. The next objective was to assess if any ultrasound effects could be seen in more specific angiogenesis-related behaviour.

3.2 Angiogenic behaviour of HUVECs post 45 kHz ultrasound exposure

3.2.1 Introduction

The following experiments aimed to identify an effect on angiogenic behaviour in response to 45 kHz ultrasound. As ultrasound exposure appeared to have a stimulatory effect on HUVEC cell number, it was hypothesised a stimulatory effect would also be seen in the angiogenic response of HUVECs. An *in vitro* tube formation assay assessed this hypothesis by visualising and quantifying the ability of HUVECs to form tube-like structures mimicking sprout formation *in vitro*. HUVECs were exposed to ultrasound before seeding onto Matrigel^{TM}-coated 48 well plates immediately after exposure, 24 h after exposure and 72 h after exposure. This methodology was then developed further to expose HUVECs to ultrasound and assess the tube formation effect without a reseeding step. As such, HUVECs seeded on Matrigel^{TM}-coated 35 mm dishes were exposed to 45 kHz DuoSon US. Additional ultrasound settings of varying lengths of exposure (1, 3 and 5 min) were analysed within this experiment. As a large data set of multiple conditions would be generated, it was decided PCA would be best suited to identify any significant effect on tube formation ability relating to the intensity applied, length of ultrasound exposure and imaging time point (4, 6 and 24 h). The experimental design of both tube formation assay methods used in this study is shown in Fig 3.9.

Identifying the genetic changes that may occur in HUVECs after ultrasound exposure is a crucial step to gaining insight into the overall molecular mechanisms involved in the HUVEC response. Therefore, qPCR analysis was undertaken on selected molecular mediators of angiogenesis to understand the response observed in the preceding *in vitro* assays.

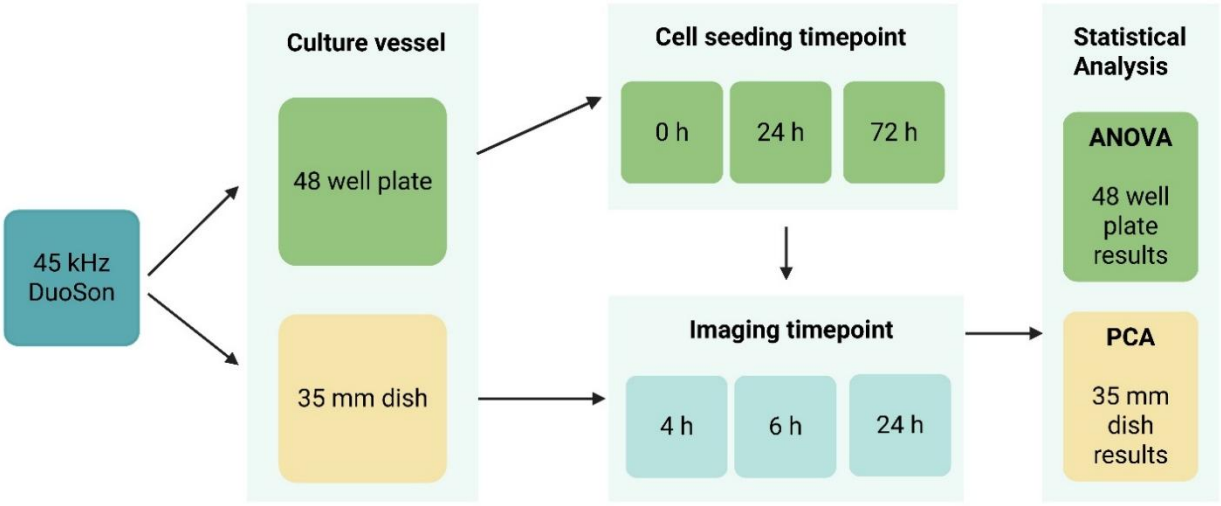

Figure 3.9 Experimental design of *in vitro* tube formation assays used in this study. HUVECs were seeded in 48 well plates at 3 different timepoints following DuoSon exposure. The cells were then imaged at 3 timepoints following seeding and tube formation characteristics analysed using ANOVA statistical tests. HUVECs were also exposed to ultrasound directly on Matrigel-coated 35 mm dishes and imaged at 3 different timepoints. These imaging results were analysed using PCA techniques.

3.2.2 Tube formation analysis after reseeding in a 48-well plate

Images were taken 4 h, 6 h and 24 h after seeding as shown representatively in Fig 3.10. Although no differential observations could be seen between untreated and ultrasound exposed cells in any of the time points assessed, by 24 h tube formation was visibly decreased with the detachment of cells observed (Fig 3.10 C). The images were then analysed using 'Angiogenesis Analyser' in Fiji, to discern any statistical tube formation effect. Imaging in 48-well plates at 4 x objective resulted in a shadowing effect in the centre of the well, as seen in Fig 3.10, though this did not create any issues in the Fiji image analysis. All statistical two-way ANOVA comparisons for the following data can be found in Appendix 7.3.1

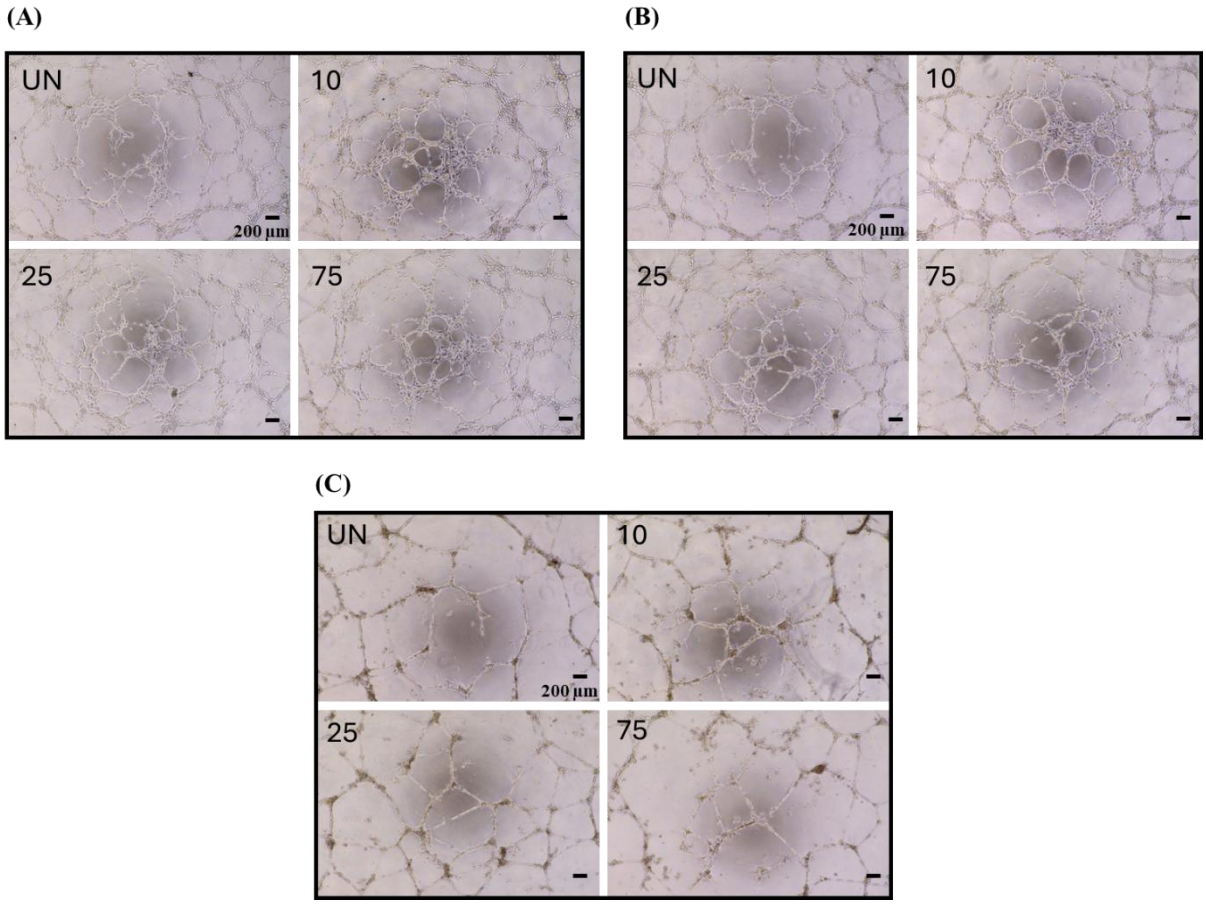

Figure 3.10 Representative photomicrographs of HUVECs seeded onto Matrigel™-coated well plates after ultrasound exposure.

HUVECs were imaged (A) 4 h, (B) 6 h, and (C) 24 h after seeding. Images were then quantified in Fiji using 'Angiogenesis Analyser' Javascript plugin. UN = untreated, 10 = 10 mW/cm^2, 25 = 25 mW/cm^2, 75 = 75 mW/cm^2.
(N = 3, 5 images taken per well, scale bars represent 200 µm)

3.2.2.1 Tube formation assay immediately after ultrasound exposure

After 45 kHz exposure, HUVECs were immediately reseeded into Matrigel™-coated well plates and tube formation behaviour was assessed for untreated and treated cells. The total tube length in µm was compared between imaging time points of 4 h, 6 h and 24 h with 4 h untreated cells set as 100 % control.

No significant differences were found between the tube length measured in treated and untreated cells at 4 h and 6 h (Fig 3.11 A). However, as shown in Fig 3.11 A, total tube length measured 24 h after seeding was lower than those measured at 4 h and 6 h after seeding. For all conditions, unexposed and exposed to ultrasound, the total tube length measured at 24 h was significantly lower than those measured 4 h after seeding (Appendix ANOVA Table 7.2 A). Comparisons by one-way ANOVA analysis were also made between untreated and ultrasound treated cells at the same time point (Fig 3.11 B – D). These analyses revealed exposure of cells to 75 mW/cm^2 resulted in slightly decreased total length of tubes formed. However this was not significantly lower between conditions following one way ANOVA with Tukey post-hoc test analysis.

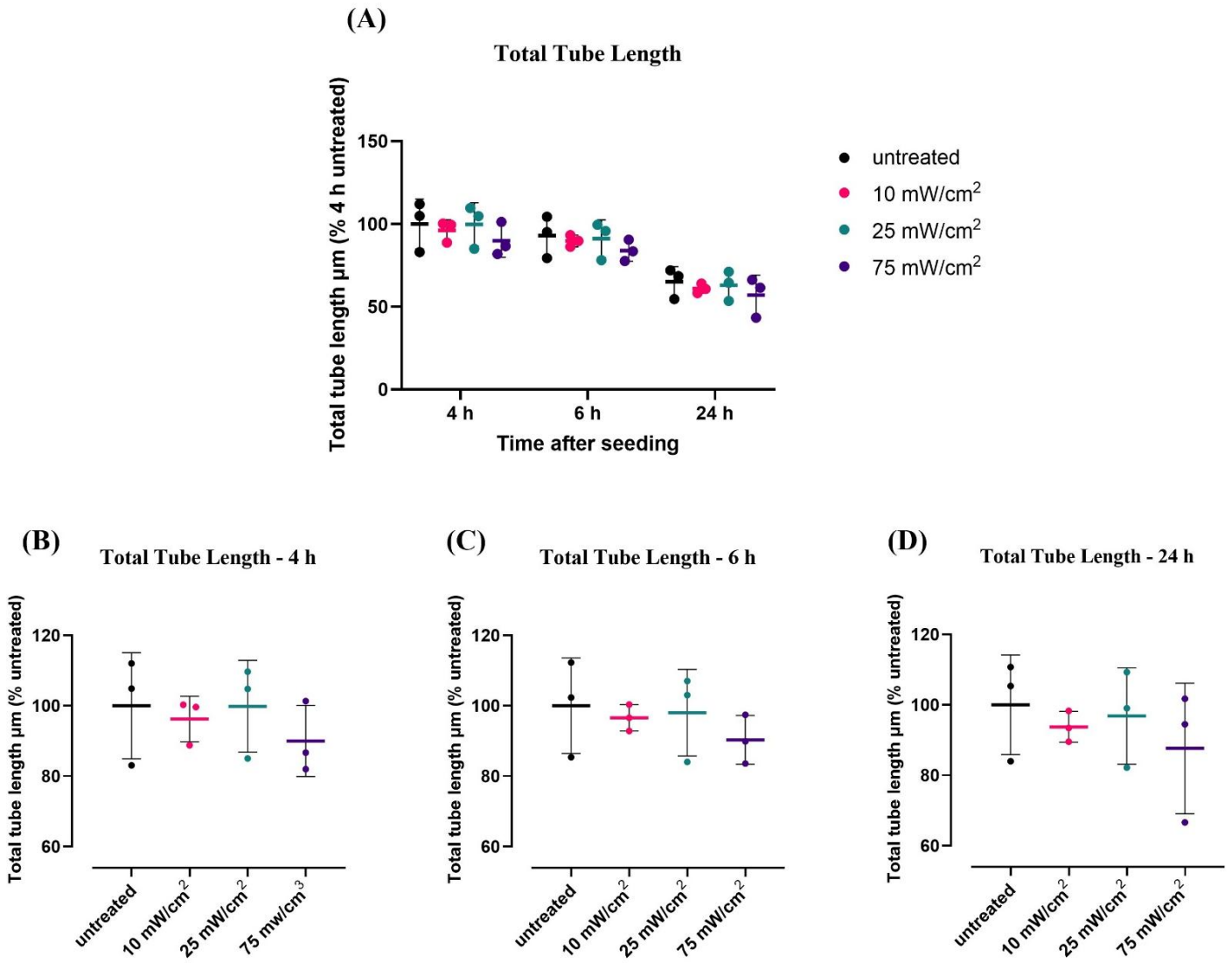

Figure 3.11 Total tube length measured of HUVECs seeded immediately after ultrasound.
(A) Two-way ANOVA comparisons showed significant decrease in tube length after 24 h compared with almost all cells at 4 h and 6 h. *p*-values shown in Appendix Table 7.2 A. (B – D) showed no significant effect of ultrasound on tube length (N = 3, mean ± SD).

The number of branches counted by 'Angiogenesis Analyser' was also compared between imaging time points after seeding of 4, 6 and 24 h (Fig 3.12 A). No significant difference was identified between the number of branches counted at 4 h and 6 h for all ultrasound-exposed and unexposed cell comparisons. However, as with tube length analysis presented previously, the number of branches counted 24 h after seeding was significantly lower than the number counted after 4 h at all ultrasonic conditions measured (Appendix ANOVA Table 7.2 B). Comparison of the number of branches at the same time point using one-way ANOVA showed no significant differences according to the exposure intensity (Fig 3.12 B – D).

Analysis of tube formation in cells seeded immediately after ultrasound showed a significant decrease in tube formation behaviour when measured at the 24 h time point of the assay, compared with 4 h. However no significant difference in tube formation behaviour was identified when comparing untreated cells and cells exposed to ultrasound within time points. This suggests there was no significant effect of ultrasound on tube formation, rather the timeframe of the tube formation assay affected tube formation ability of HUVECs.

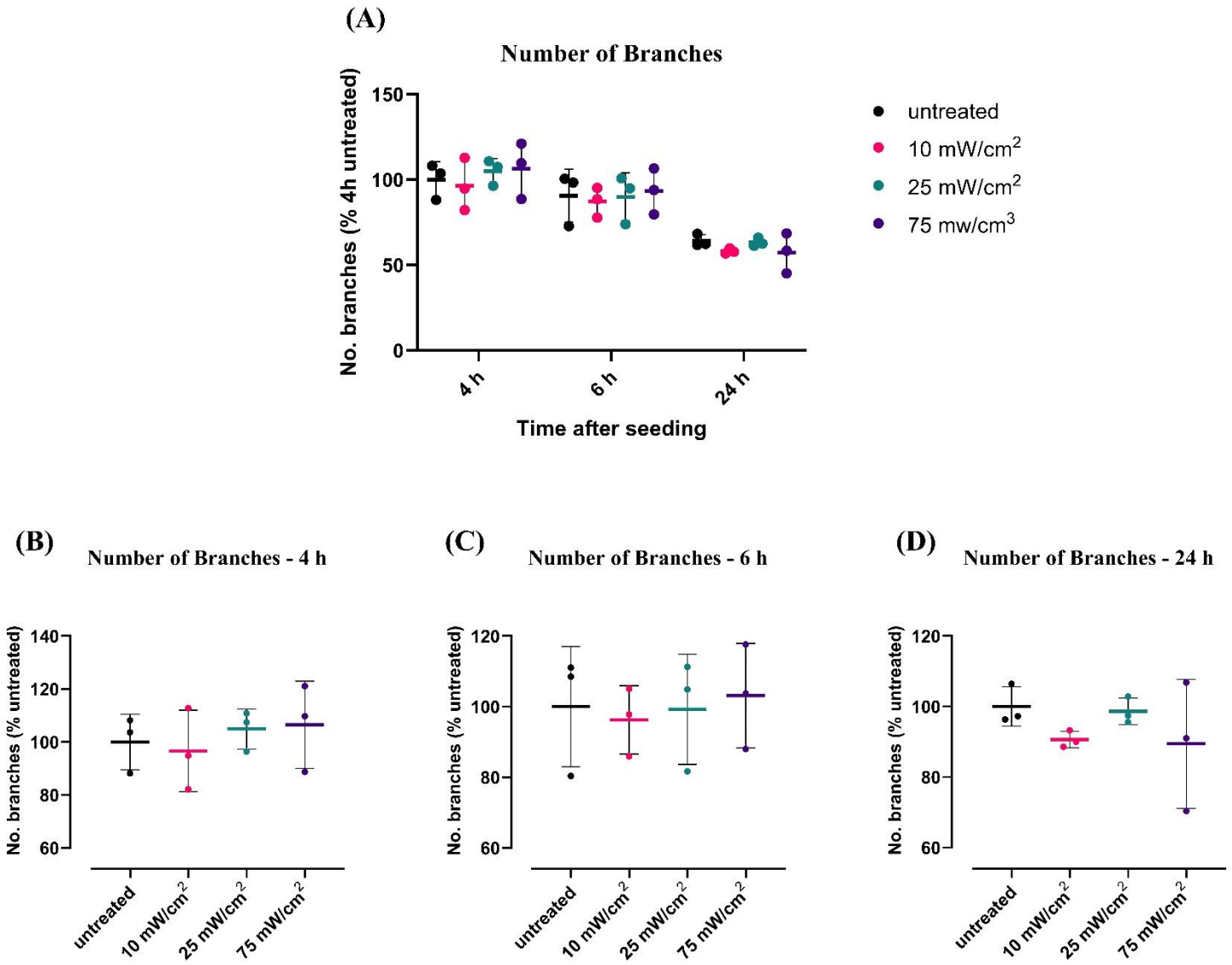

Figure 3.12 Number of branches in HUVECs seeded immediately after ultrasound exposure. (A) Two-way ANOVA comparisons showed significant decrease in branch number after 24 h compared with all conditions at 4 h. (B – D) Comparisons within the same time points showed similar number of branches for all ultrasonic conditions. (N = 3, mean ± SD).

3.2.2.2 Tube formation assay 24 h after ultrasound exposure

To assess whether there was a time-dependent effect on HUVECs, as observed in viable cell number analysis, tube formation assays were undertaken 24 h after ultrasound exposure. 24 h after 45 kHz exposure, HUVECs were reseeded into Matrigel^{TM}-coated well plates and tube formation ability was assessed. Micrographs were captured 4 h, 6 h and 24 h after seeding, however the 4 h time point only contained 2 biological repeats so was subsequently excluded from statistical analysis.

The total tube length in µm was statistically compared between imaging time points of 6 h and 24 h due to a lack of biological repeat data at 4 h (Fig 3.13 A). The tube length quantified at all conditions after 24 h was significantly lower than tube length quantified in all conditions after 6 h (Appendix ANOVA Table 7.3 A). Total tube length 6 h after seeding was similar in treated cells compared with the untreated control (Fig 3.13 B). After 24 h the tube length was moderately increased in cells exposed to 25 mW/cm^2 (9 %) and 75 mW/cm^2 (10 %) compared with untreated cells (Fig 3.13 C). However one-way ANOVA comparisons showed no significant differences (p = 0.674 and p = 0.6432, respectively).

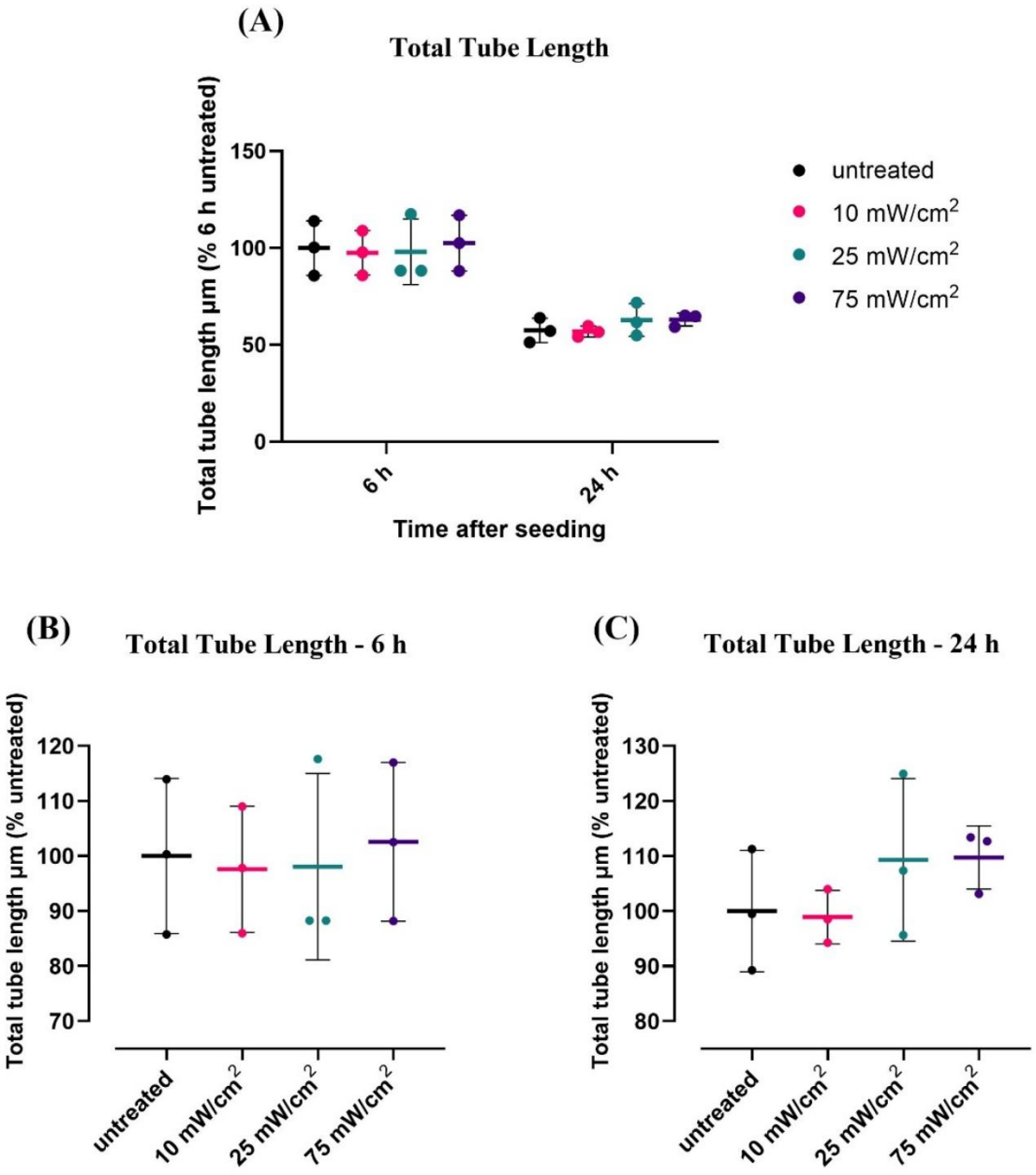

Figure 3.13 Total tube length measured in HUVECs seeded onto Matrigel™ 24 h after ultrasound exposure.

(A) Two-way ANOVA comparisons showed a significant decrease in tube length after 24 h compared with all ultrasound conditions at 6 h. (B - C) Comparisons of tube length of HUVECs within 6 h and 24 h time points showed no significant effect of ultrasound. (N = 3, mean ± SD).

Reduced numbers of branches were measured in all cells, unexposed and exposed to ultrasound, at the 24 h time point compared with 6 h after reseeding following 'Angiogenesis Analyser' measurements (Fig 3.14 A). However no significant difference was detected by two-way ANOVA comparisons (Appendix ANOVA Table 7.3 B). Analysis 6 h after seeding on Matrigel^{TM} revealed moderate differences in branch number between ultrasound-exposed and unexposed cells (Fig 3.14 B). The number of branches compared with untreated cells was 8 % lower in cells exposed to 10 mW/cm^2 and 5 % lower in cells exposed to 75 mW/cm^2. Though both trends were statistically not significantly different following one-way ANOVA with Tukey HSD analysis ($p = 0.4804$ and $p = 0.7645$, respectively). Within the 24 h time point no difference in branch number was identified (Fig 3.14 C).

Similar results were obtained in tube formation assays performed 24 h after ultrasound exposure, as those performed immediately after ultrasound exposure (Section 3.2.2.1). Ultrasound did not appear to have a significant effect on the tube formation behaviour of HUVECs after 24 h.

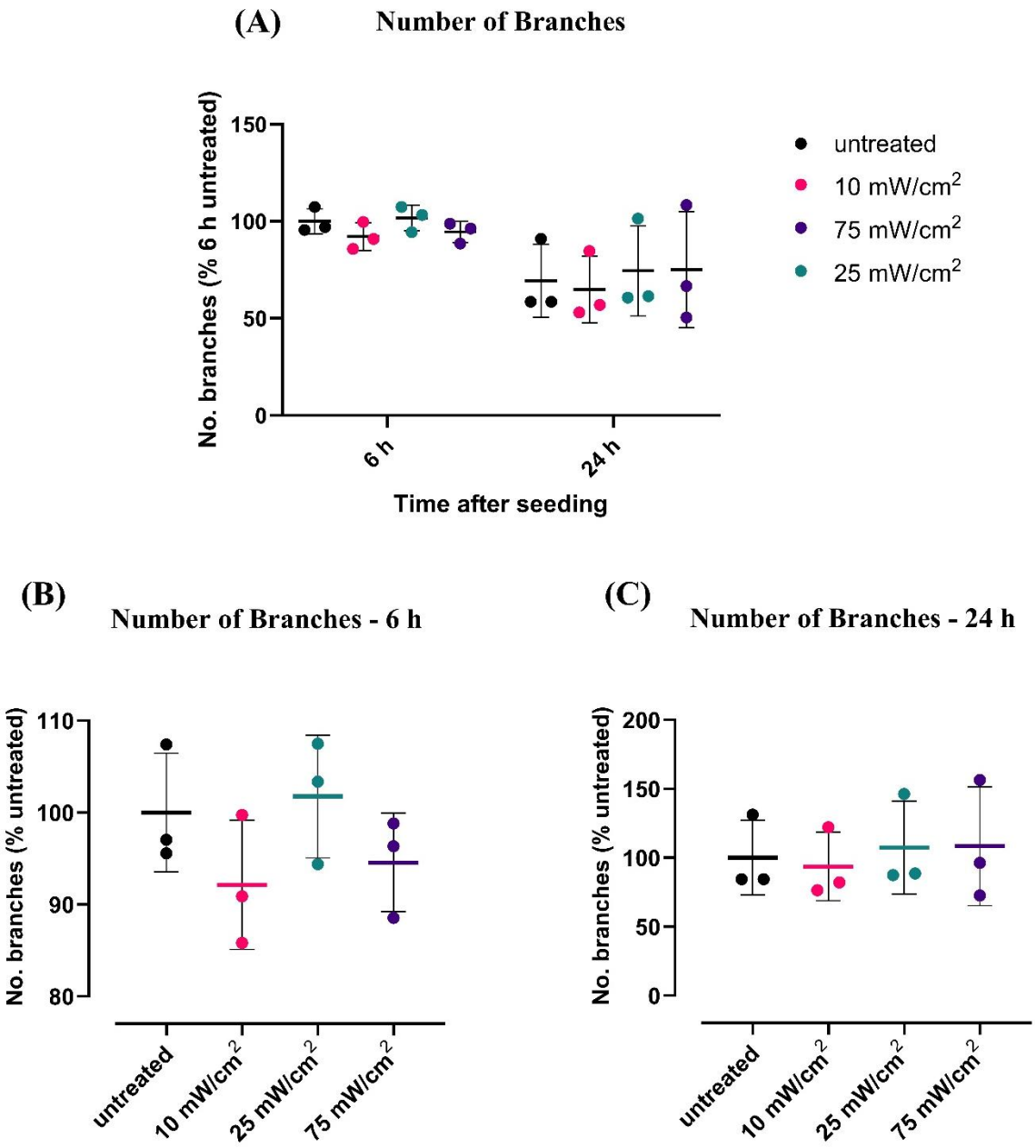

Figure 3.14 Number of branches measured in HUVECs seeded onto Matrigel™ 24 h after ultrasound exposure.

(A) Two-way ANOVA comparisons showed no significant difference in branch number between 24 h and 6 h after seeding. (B) Although a lower number of branches was seen 6 h after seeding in cells treated with 10 and 75 mW/cm^2, the decrease was not significantly different. (C) No significant effect was seen in branch number after 24 h. (N = 3, mean ± SD).

3.2.2.3 Tube formation assay 72 h after ultrasound exposure.

Tube formation ability was further assessed 72 h after 45 kHz ultrasound exposure to explore the time-dependent response to ultrasound seen in viable cell number analysis. Micrographs were captured 4 h, 6 h and 24 h after seeding on Matrigel^{TM}-coated well plates to assess tube formation behaviour.

Whereas significant decrease in total tube length was measured 24 h after seeding compared with 4 h after seeding in cells analysed immediately after ultrasound exposure (Section 3.2.2.1), no significant decrease in tube length was observed between 4 h and 24 h imaging timepoints in cells analysed 72 h after ultrasound exposure (Appendix ANOVA Table 7.4 A; Fig 3.15 A). The only significant difference measured was between cells exposed to 25 mW/cm^2 imaged at 24 h compared with cells treated with 10 mW/cm^2 at 4 h (Fig 3.15 A; $p < 0.05$). Comparisons at the same time points using one-way ANOVA showed no significant differences in tube length between cells exposed to ultrasound and untreated (Fig 3.15 B - D). These analyses within the same time point were concurrent with cells assayed immediately after ultrasound exposure and 24 h after ultrasound exposure, further suggesting ultrasound exposure had no significant direct impact on HUVEC tube formation ability.

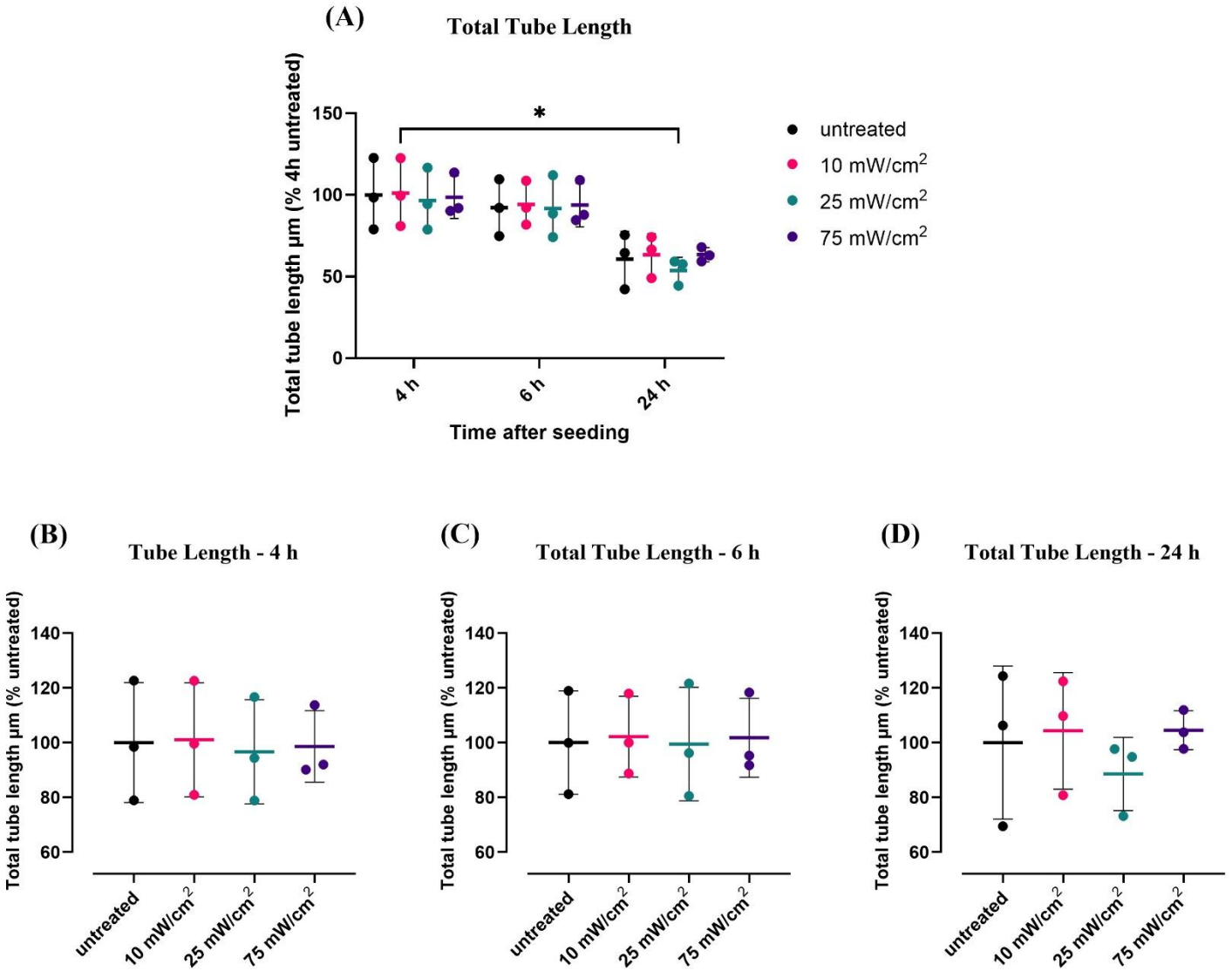

Figure 3.15 Total tube length measured in HUVECs seeded onto Matrigel™ 72 h after ultrasound exposure. (A) Two-way ANOVA comparisons showed a significant decrease in tube length in cells exposed to 25 mW/cm^2 after 24 h compared with 10 mW/cm^2 at 6 h (B - D) One-way ANOVA comparisons of tube length within time-points of 4 h, 6 h and 24 h showed no significant differences compared with the untreated control. (N = 3, mean ± SD; * $p < 0.05$

Comparisons between the number of branches counted between ultrasound conditions 4 h, 6 h and 24 h after seeding showed a reduced number counted 24 h after seeding compared with the earlier time points (Fig 3.16 A), concurrent with cells analysed immediately and 24 h after ultrasound exposure. However, significant differences were only identified between untreated cells at the 24 h time point and other untreated cells 6 h after seeding and all cells 4 h after seeding (Appendix ANOVA Table 7.4 B). Cells exposed to ultrasound were not significantly different in branch number compared with 4 h, unlike the significant comparisons seen between these time points in cells immediately and 24 h after ultrasound exposure. This may suggest a delayed effect of ultrasound on tube formation behaviour in the ability of branch formation.

No significant effect on branch number was observed following one-way ANOVA comparisons within time points (Fig 3.16 B – D). Although a slightly lower branch number was seen in cells exposed to 10 mW/cm^2, 4 h after seeding (7 %, $p = 0.6849$) and in cells exposed to 75 mW/cm^2 after 6 h (10 %, $p = 0.7413$) compared with untreated cells. After 24 h a slightly higher number of branches was seen in all treated cells, though this increase was not significant (10 mW/cm^2 $p = 0.6461$; 25 mW/cm^2 $p = 0.2989$; 75 mW/cm^2 $p = 0.4435$).

In summary the measurements of tube formation ability in HUVECs 72 h after ultrasound exposure showed a possible temporal response to ultrasound, notable in the ability to form branches. There was no significant decrease in branch formation in cells exposed to ultrasound at 24 h imaging compared with 4 h imaging. Additionally, slightly higher branch number was seen 24 h after seeding compared with untreated cells, which is a trend not seen at any other tube formation analysis timepoint after ultrasound exposure.

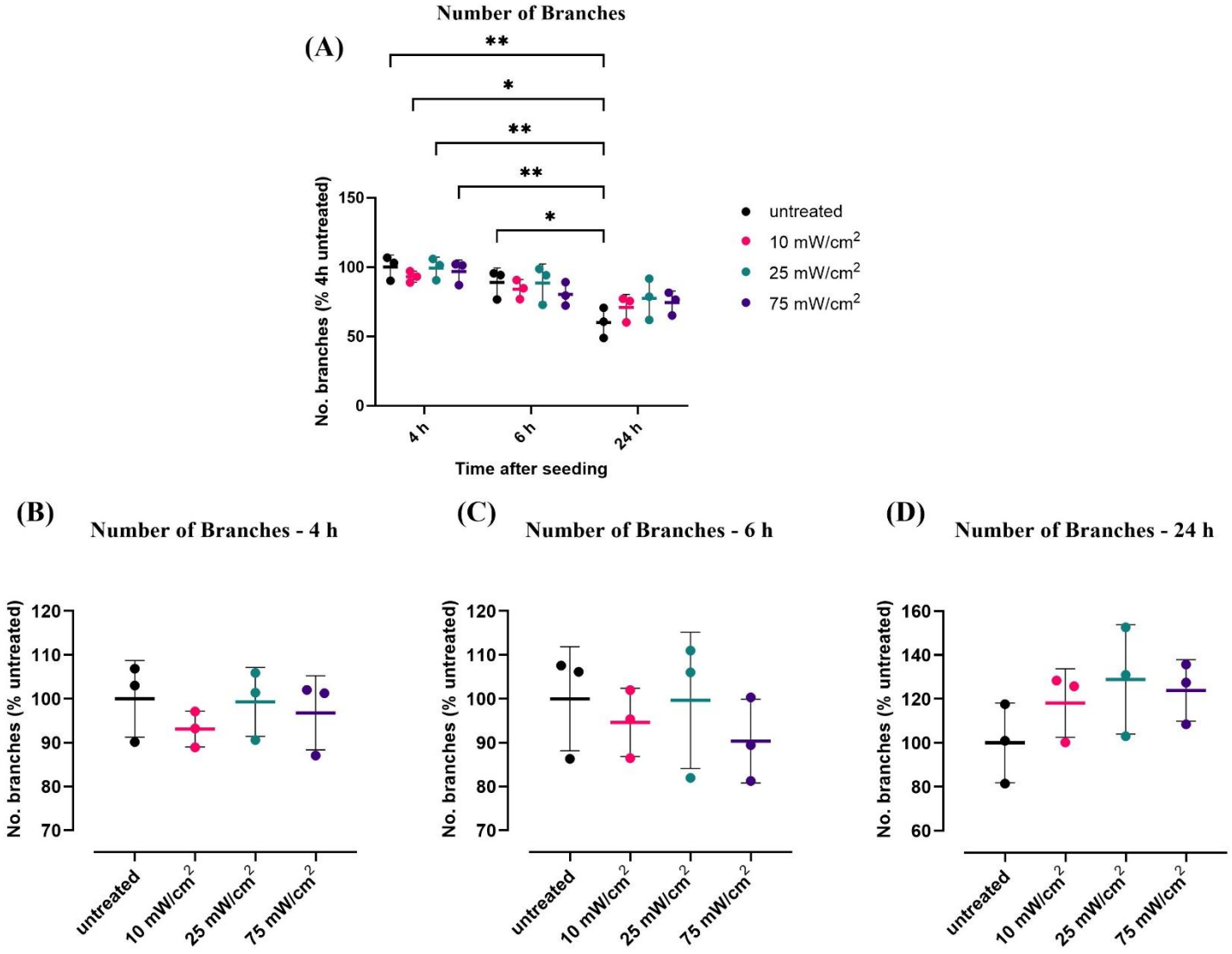

Figure 3.16 Branch number of branches in HUVECs seeded 72 h after ultrasound exposure
(A) Two-way ANOVA comparisons showed significantly lower branch number in untreated cells after 24 h compared with all ultrasound intensities 4 h after seeding. (B - D) Branch number was not significantly different between untreated and ultrasound exposed cells when compared at each time point.
(N = 3, mean ± SD;
* $p < 0.05$, ** $p < 0.01$).

Tube formation analysis showed no significant effect on tube formation ability independent on the ultrasound intensity delivered to HUVECs. However this methodology may not have been identifying the direct effect of ultrasound on tube formation ability. After ultrasound exposure, cells were trypsinised, counted and ultimately reseeded which could have introduced multiple factors that may be masking or interfering with the HUVEC response to ultrasound. Subsequently, a new approach was designed to deliver ultrasound to cells directly on Matrigel^{TM} coated wells.

3.2.3 Tube formation in 35 mm culture dishes

HUVECs analysed 4 h after ultrasound exposure showed no significant difference in tube formation ability compared with untreated controls as determined by PCA. Significant differences between data analysed by PCA could be visualised by separation in ellipses that group results from the same data set. In Fig 3.17 A, analysis of ultrasound exposure length effect is displayed; 1 min (red), 3 min (green) and 5 min (blue) ellipses overlap with one another. The ellipses for 3 min and 1 min showed near complete overlapping of one another indicating very minimal difference in effect, compared with the overlapping of 1 min and 5 min. These results showed there was more of a difference in the tube formation ability in HUVECs when comparing between 1 min and 5 min, though still not a significant effect ($p = 0.57$).

Similarly, when assessing the effect of ultrasound intensity applied, Fig 3.17 B showed overlapping ellipses of untreated (red), 10 mW/cm^2 (green), 25 mW/cm^2 (blue) and 75 mW/cm^2 (purple). This demonstrated a non-significant effect on tube formation ability regardless of the intensity applied ($p = 0.49$). However, the data obtained from exposure to

25 mW/cm^2 showed the least area of overlapping ellipses with other datasets suggesting this intensity results in an effect on tube formation ability compared with other intensities and the untreated control.

Analysis combining all data obtained from different intensity and exposure length of ultrasound also showed a statistically non-significant effect 4 h after ultrasound ($p = 0.65$, Fig 3.17 C). Overlapping of ellipses could be seen, showing no distinct difference in tube formation ability of HUVECs regardless of the ultrasound conditions assessed. The amount of energy supplied to the cells in Joules per second during DuoSon exposure was calculated following Equation 2.2 (Section 2.7.2). The amount of energy supplied ranged from 0 J in untreated cells to the highest amount of 365.1 J. However there was no significant effect in tube formation response regardless of the energy supplied to the cells ($p = 0.73$), as evidenced by overlapping ellipses depicted in Fig 3.17 D.

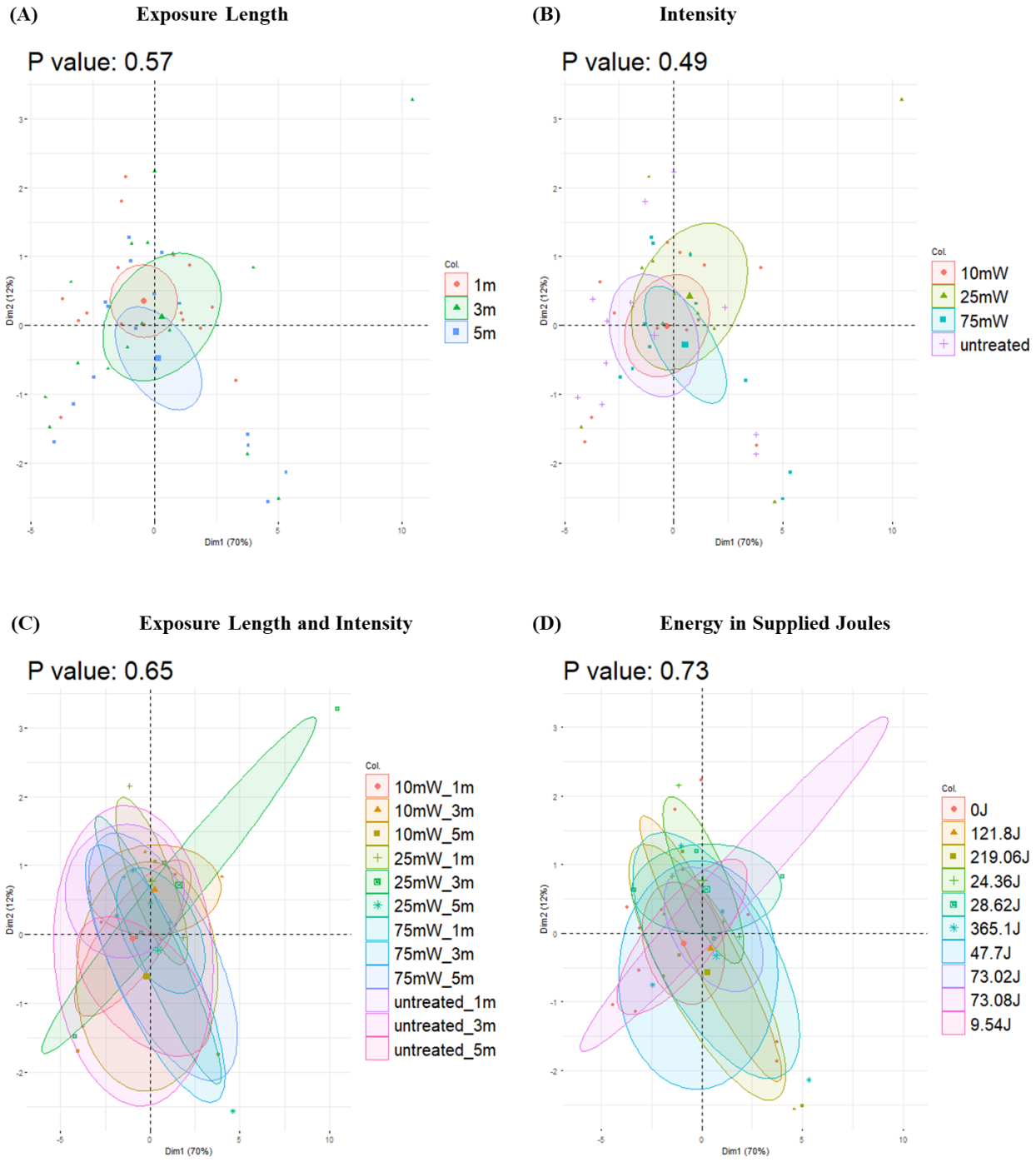

Figure 3.17 Principal component analysis 4 h after 45 kHz DuoSon exposure.
Data were grouped according to (A) exposure length, (B) intensity (C) a combination of ultrasound exposure length and intensity and (D) depicting the energy supplied to cells during each DuoSon exposure setting. Overlapping ellipses in all datasets indicated no statistical difference in tube formation between untreated cells and cells exposed to ultrasound at all intensities. Analysis and graph visualisation performed in R Studio, N = 4.

PCA was performed on data obtained after Fiji 'Angiogenesis Analyser' 6 h after ultrasound exposure. Similar trends were observed as with analysis 4 h after ultrasound exposure; partial overlapping of ellipses was seen in comparisons between the exposure length of ultrasound displayed in Fig 3.18 A. This demonstrated a non-significant difference in tube formation ability at the different exposure lengths tested (1, 3 and 5 min; $p = 0.48$)

The intensity of ultrasound applied to HUVECs also did not have a significant effect on tube formation ability when comparing data from untreated cells and cells exposed to 10, 25 and 75 mW/cm^2 ($p = 0.62$, Fig 3.18 B). Total overlapping of ellipses could be seen in Fig 3.18 C depicting PCA of both intensity and exposure length comparisons. This demonstrated 6 h after ultrasound exposure there was no significant difference in the tube length ability of HUVECs regardless of the intensity applied or if ultrasound was applied for 1, 3 or 5 min ($p = 0.7$). The energy supplied to the cells can be seen in Fig 3.18 D, with non-significant effect on tube formation behaviour between all doses of ultrasound ($p = 0.73$).

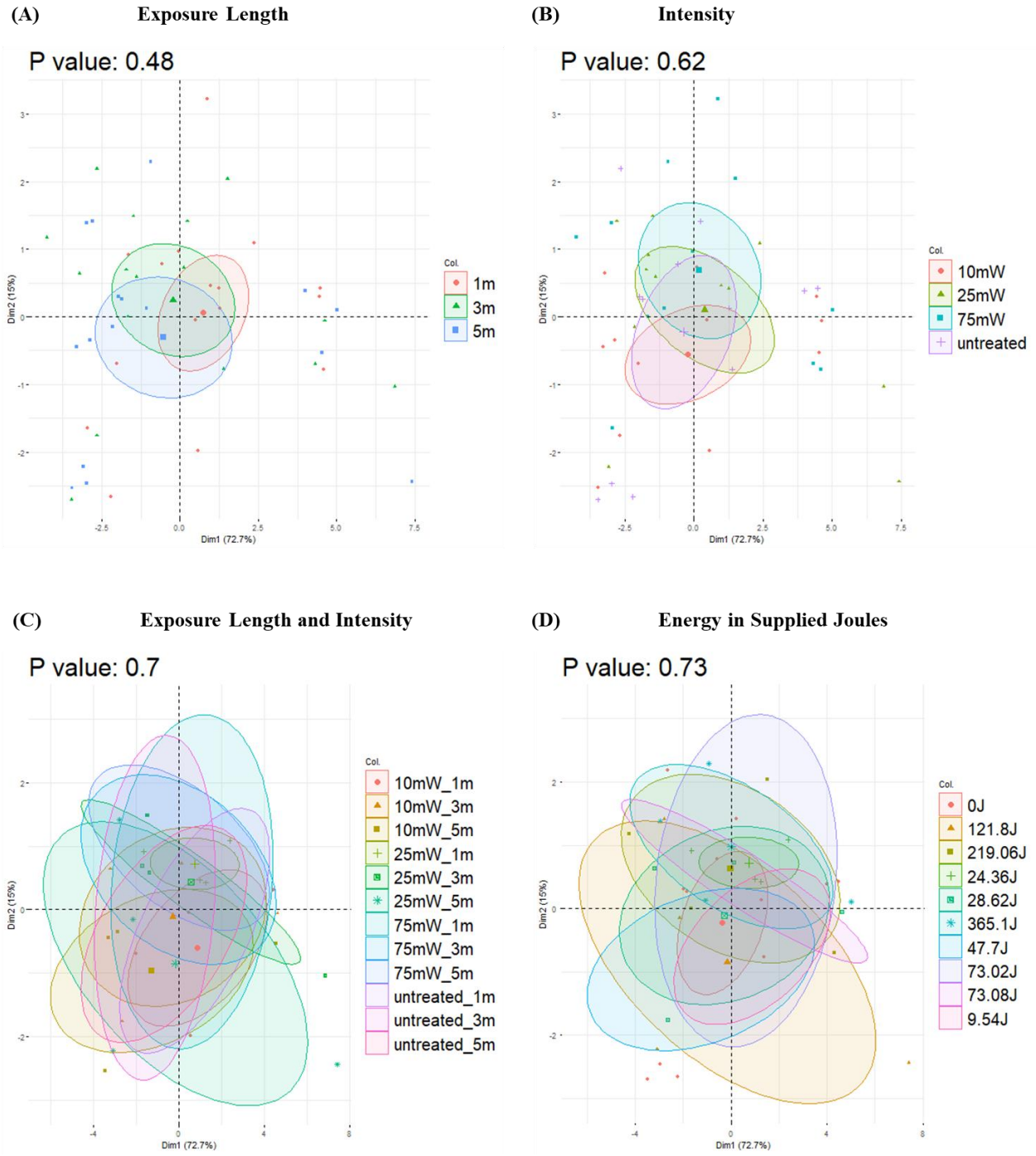

Figure 3.18 Principal component analysis 6 h after 45 kHz DuoSon exposure. Overlapping ellipses in all PCA graphs show (A) exposure length, (B) Ultrasound intensity and (C) both factors combined do not significantly affect the tube formation ability of HUVECs. (D) exposure length and intensity settings were converted to show the energy supplied in Joules to the cells during DuoSon exposure. Analysis and graph visualisation performed in R Studio, N = 4.

HUVECs were analysed 24 h after ultrasound exposure by 'Angiogenesis Analyser' script in Fiji. Similarly with results obtained 4 h and 6 h after ultrasound, no significant difference in tube formation behaviour, regardless of the exposure time length ($p = 0.36$, Fig 3.19 A), intensity ($p = 0.54$, Fig 3.19 B), a combination of intensity and exposure length of ultrasound ($p = 0.66$, Fig 3.19 C) or amount of energy supplied ($p = 0.7$, Fig 3.19 D) was observed. The exposure length of 1 min showed partial overlapping of ellipses compared with 3 min and 5 min indicating the shorter time of exposure slightly differed in tube formation response. However the data obtained from different exposure length were not statistically different ($p = 0.36$) suggesting exposure length of 1 min, 3 min or 5 min did not affect the tube formation response of HUVECs.

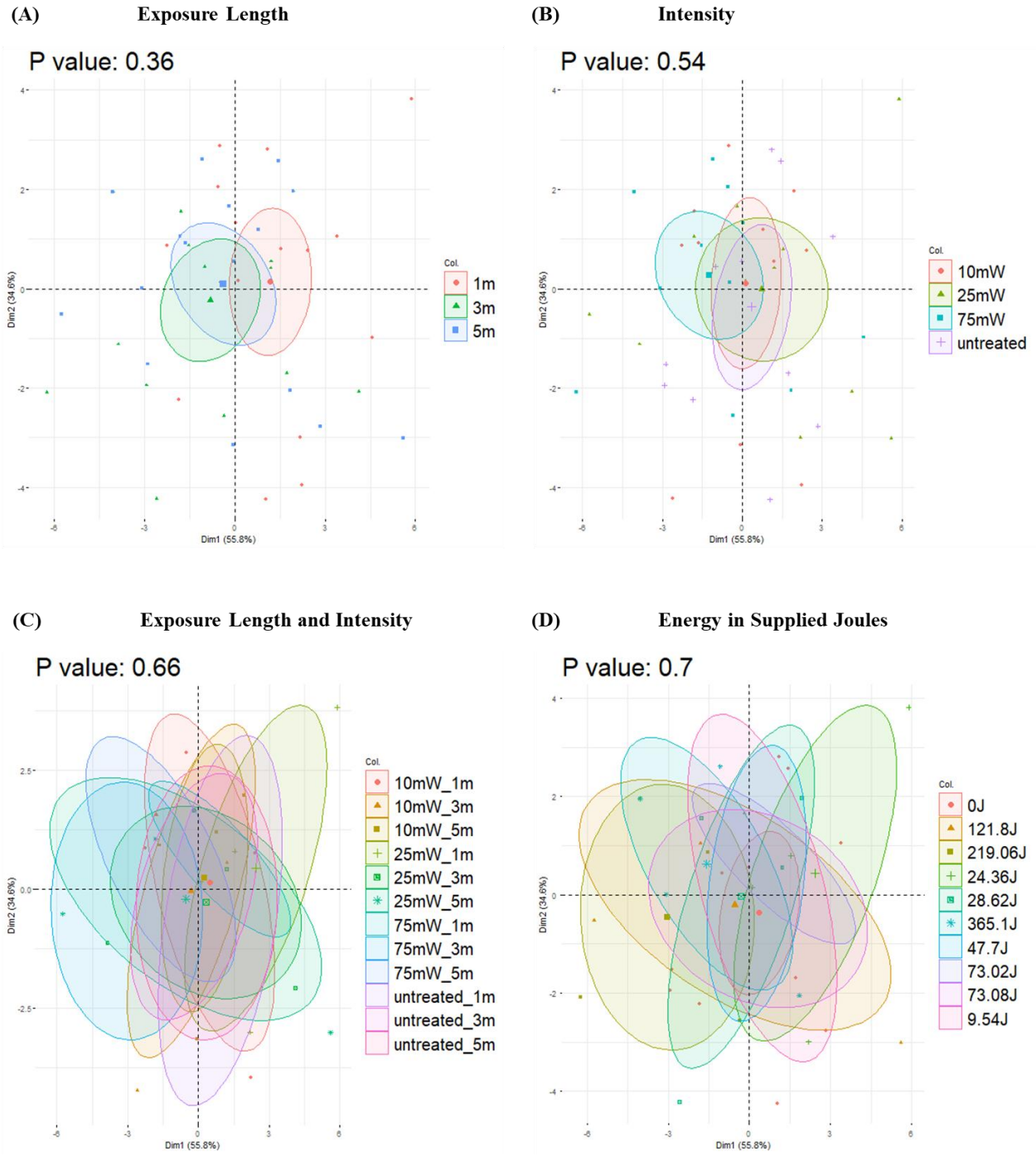

Figure 3.19 Principal component analysis 24 h after 45 kHz DuoSon exposure.
PCA of tube formation 24 h after ultrasound exposure also showed no significant effect on tube formation ability independent of (A) ultrasound exposure length, (B) intensity (C) combination of ultrasound exposure length and intensity and (D) calculated dosage of ultrasound energy supplied. The overlapping of ellipses showed data from all groups was not significantly different from each other. Analysis and graph visualisation performed in R Studio, N = 4.

All imaging time points of 4, 6 and 24 h after ultrasound exposure were combined and analysed by PCA to assess any temporal effect on HUVEC tube formation behaviour. When comparing the response to different exposure lengths within all the imaging time points, a total overlap of 95 % confidence ellipses was observed concluding the length of exposure had no significant effect on HUVEC tube formation at all imaging time points ($p = 0.86$, Fig 3.20 A). Analysis of an effect caused by ultrasound intensity also showed no significant difference in tube formation ability at all imaging time points ($p = 0.59$, Fig 3.20 B). Data from both ultrasound intensity and exposure length was then combined and analysed, however this analysis further indicated the ultrasound settings delivered did not significantly affect HUVEC tube formation behaviour ($p = 0.77$, Fig 3.20 C). The amount of energy delivered to the cells was calculated in Joules per second following the same calculations as for 4 h and 6 h data. The results showed no significant difference in tube formation response regardless of the energy supplied to the cells ($p = 0.69$, Appendix Fig 7.2).

Separation of confidence ellipses was observed when the effect of imaging time point was analysed (Fig 3.20 D, E & F). When comparing tube formation ability dependent on time point after ultrasound exposure (Fig 3.20 D), there was an overlap of data obtained from 4 h (green) and 6 h (blue). However, data obtained after 24 h showed only a partial overlap of data points with no overlapping of ellipses. Though the difference seen was statistically not significant ($p = 0.2$), this result suggests the time after ultrasound exposure and the imaging time point within the tube formation assay, influenced the tube formation ability of HUVECs. Separation or partial overlapping of ellipses depending on exposure length combined with timepoint (Fig 3.20 E) and intensity combined with time point (Fig 3.20 F) further highlight the effect the imaging time point had on the results obtained from the tube formation assay.

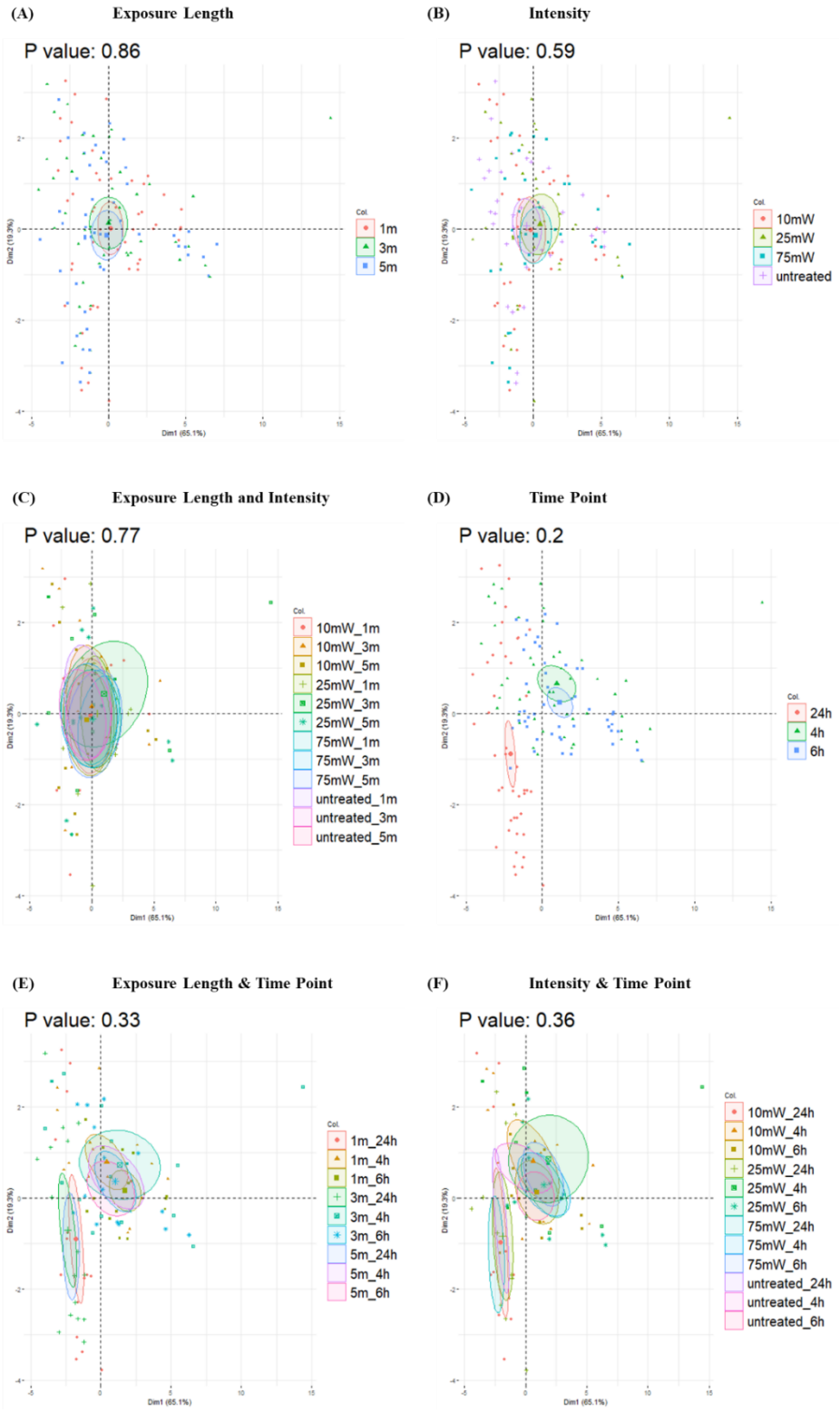

Figure 3.20 Principal component analysis of all imaging time points, exposure length and intensity of 45 kHz DuoSon exposure.

PCA demonstrated no significant effect of exposure length (A), intensity (B) or a combination of both variables on tube formation. There was an effect depending on the imaging time point demonstrated by partial separation in ellipses of 24 h and the ellipses of 4 and 6 h after ultrasound. (N = 4).

Overall PCA analysis indicated there was no significant effect on HUVEC tube formation response to ultrasound regardless of the intensity applied nor the length of exposure. The condition that appeared to have an impact on tube formation results was the time after ultrasound exposure. When analysed after 24 h there was a difference in results obtained compared with 4 h and 6 h after exposure, whereas no difference was seen in HUVEC response between 4 h and 6 h. This was concurrent to results and micrographs taken using the 48 well plate methodology (Section 3.2.2) where tube formation declined at the 24 h time point. Though no stimulatory effect was observed in this set of data, there was also no sign of an inhibitory effect of ultrasound on HUVEC tube formation ability.

3.2.4 Gene expression changes due to ultrasound exposure

Primers used in qPCR were first tested and validated via sqRT-PCR. All primers tested produced expected sizes of PCR products after gel visualisation indicating the suitability for further quantitative PCR analysis. Preliminary sqRT-PCR analysis was also undertaken to identify any effect of angiogenesis-related gene expression 72 h after 5 min DuoSon delivery which could then be explored further using qPCR techniques (Fig 3.21). *PECAM-1* expression was reduced in all treated cells compared with untreated cells, with the greatest reduction following 10 mW/cm^2 exposure (29 %). In contrast, *VEGF-A*, *VEGF-R2*, and *VWF* expression was increased following ultrasound exposure. The greatest increases were seen in *VEGF-R2* expression following 25 mW/cm^2 and 75 mW/cm^2 exposure resulting in 18 % and 27 % increased expression respectively. Although no statistical analysis could be performed on this preliminary data to lack of biological replicates, these results indicated there was an effect on angiogenic gene expression. Further qPCR analysis was performed to try to gain insight into the molecular effect 45 kHz ultrasound was enacting in HUVECs.

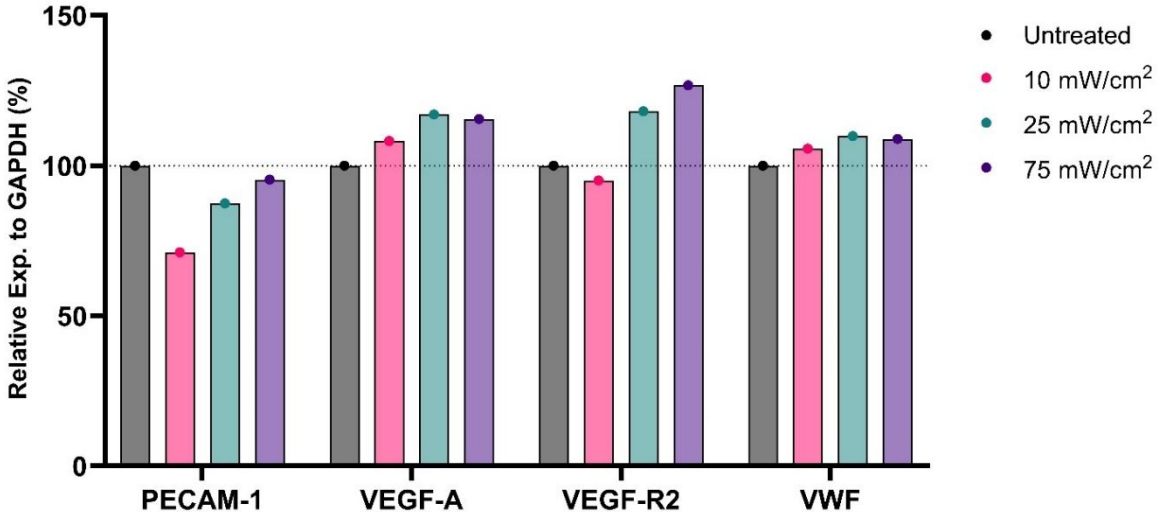

Figure 3.21 sq-RT PCR analysis of angiogenesis-related genes 72 h after ultrasound exposure.

Gene expression levels of *PECAM-1*, *VEGF-A*, *VEGF-R2* and *VWF* were normalised to *GAPDH* shown as 100% dotted line on the graph. *PECAM-1* showed decreased expression following ultrasound exposure at all intensities. *VEGF-A*, *VEGF-R2* and *VWF* showed increased expression following ultrasound exposure. (No statistical analysis was performed on these preliminary results, N = 1).

3.2.4.1 Angiogenesis-related gene expression analysis using qPCR

Following preliminary sqRT-PCR analysis, the expression of angiogenesis-related genes was measured 6 h (Fig 3.22), 24 h (Fig 3.23) and 72 h (Fig 3.24) after 5 min 45 kHz DuoSon exposure.

Analysis 6 h post ultrasound exposure (Fig 3.22) revealed the expression of HUVEC marker *PECAM-1* was at a comparable level in all cells whether exposed to ultrasound or not. Expression levels of *VEGF-A* and the corresponding receptor *VEGF-R2* exhibited similar expression patterns. A slight decrease in expression level of both genes was seen in all ultrasound-exposed cells compared with untreated cells. As ultrasound intensity increased, as did the level of expression reduction. The greatest decrease in expression level in *VEGF-A*

and *VEGFR2* was seen in cells exposed to 75 mW/cm^2 compared with untreated cells. *VEGF-A* expression decreased to CNRQ 0.68 ± 0.24 (p = 0.3799) after 75 mW/cm^2 exposure and *VEGFR2* showed a CNRQ value of 0.74 ± 0.16 (p = 0.5551). This response of reduced expression with exposure to increased ultrasound intensity was also seen in *VWF*. *VWF* expression decreased in all ultrasound exposed cells compared with the control after 6 h. Expression levels in cells exposed to 75 mW/cm^2 intensity were approximately half the level seen in untreated cells; a CNRQ of 0.55 ± 0.19 compared with untreated cells with a CNRQ of 1.01 ± 0.19 (p = 0.1195). *eNOS* expression also decreased 6 h after ultrasound exposure compared with untreated cells, especially at the highest intensity exposure 75 mW/cm^2. *eNOS* expression in cells exposed to 75 mW/cm^2 showed a CNRQ of 0.58 ± 0.04, significantly lower than untreated cell *eNOS* CNRQ of 1.00 ± 0.04 (p = 0.0162).

Overall, gene expression appeared to decrease 6 h after ultrasound exposure across the majority of genes tested. The reduction of gene expression was related to the intensity of ultrasound delivered, the higher the intensity, the greater the level of gene expression reduction.

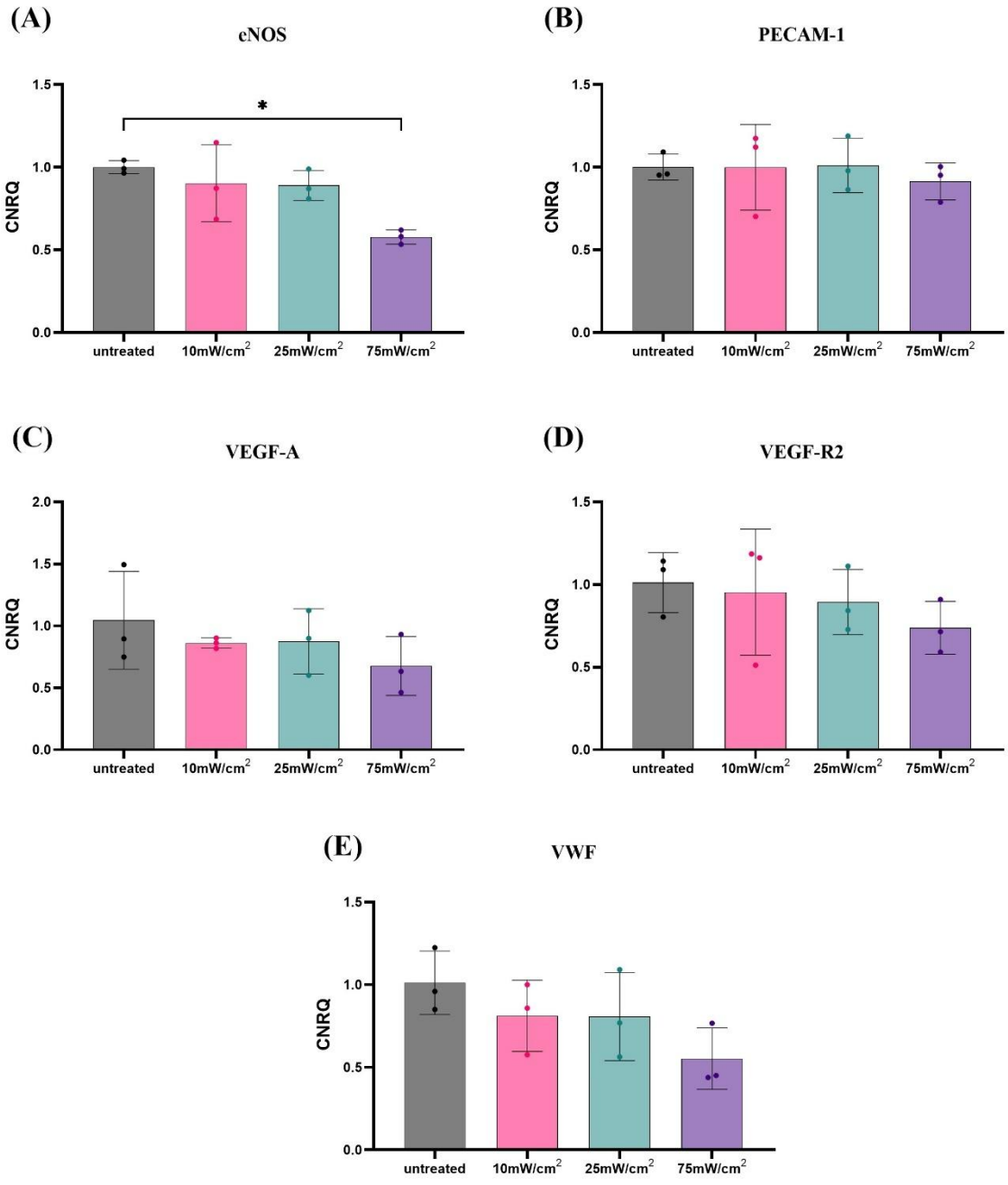

Figure 3.22 qPCR analysis of angiogenesis-related genes 6 h after ultrasound exposure. Calibrated normalised relative quantity (CNRQ) values plotted as normalised expression to 4 housekeeper gene expression levels. Exposure to 75 mW/cm^2 generated a significant reduction in *eNOS* expression compared with untreated cells. All other changes in gene expression were not statistically significant.
(N = 3, mean ± SD, * $p < 0.05$)

Similarities in the expression levels of the angiogenesis-related genes remained between those measured at 6 h and 24 h after ultrasound exposure (Fig 3.23). For example, *PECAM-1* expression remained at similar levels for all cells analysed, which was observed after 6 h. Additionally, moderately decreased expression in *eNOS*, *VEGF-A*, *VEGF-R2* and *VWF* was again observed in cells exposed to 75 mW/cm^2. *eNOS* expression was reduced to half the level of expression observed in untreated cells; CNRQ 1.12 ± 0.7 compared with untreated expression levels of CNRQ 1.95 ± 0.62. *VWF* expression was seen at a lower CNRQ of 3.33 ± 2.69, compared with an expression level of 5.91 ± 4.02 in untreated cells. *VEGF-A* expression was also reduced (1.18 ± 0.18) compared with untreated cells (1.82 ± 0.43), as well as 10 mW/cm^2 exposure (1.95 ± 0.71) and 25 mW/cm^2 (2.05 ± 0.66). Overall, gene expression was reduced compared with untreated cells in all genes except *PECAM*-1 when exposed to 75 mW/cm^2. This trend of reduced expression was similar to the expression patterns seen after 6 h exposure. However, in contrast to 6 h expression measurements, analysis after 24 h showed no significant differences in *eNOS* gene expression between exposed and unexposed cells.

There was also a greater amount of variability within the cells analysed as evident by the standard deviation bars, particularly in *PECAM-1* and *VWF* expression. This large spread of data may be masking significant expression changes, though trends of reduced expression after 75 mW/cm^2 could still be identified.

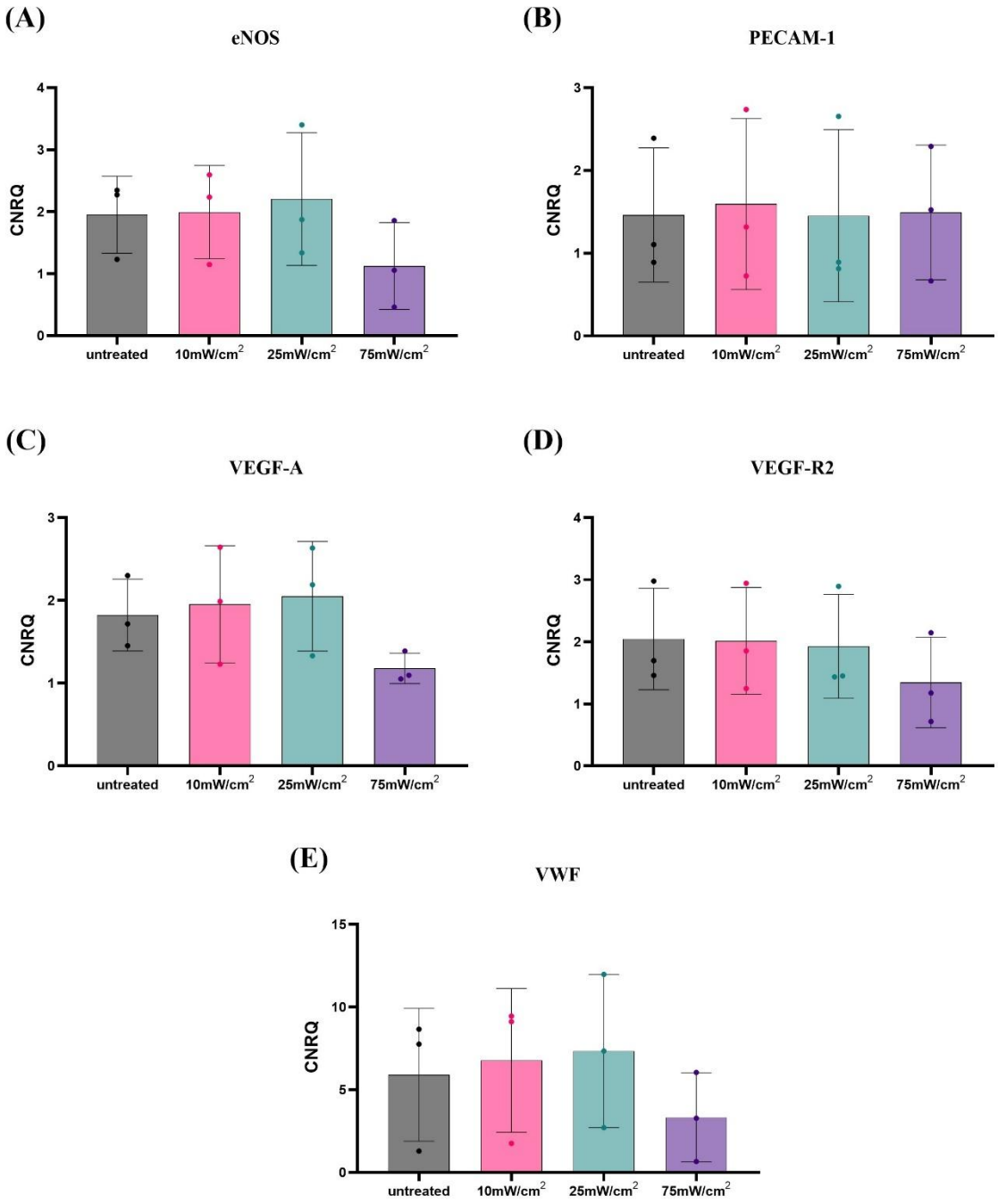

Figure 3.23 qPCR analysis on angiogenesis-related gene expression 24 h post ultrasound exposure.

qPCR analysis of HUVECs exposed to 45 kHz ultrasound and intensities of 10, 25 and 75 mW/cm^2 and an untreated control was performed 24 h after exposure. CNRQ values are plotted as normalised expression to 4 stable expression housekeeper genes. (N = 3, mean ± SD).

Conversely, gene expression analysis 72 h after ultrasound exposure showed a different expression response to those seen after 6 h and 24 h. Whereas after 6 h and 24 h reduced levels of gene expression was observed after exposure to 75 mW/cm^2, significantly in *eNOS*, rather comparable expression levels were seen across all genes at this intensity compared with untreated cells (Fig 3.24). This suggests the effect of higher intensity exposure causing a reduction of gene expression appeared to have recovered after 72 h. Alternatively, moderately reduced expression was observed after exposure to the lower intensity of 10 mW/cm^2 in all genes assessed compared with untreated cells. *eNOS* expression was measured with a CNRQ of 0.6 ± 0.8 after 10 mW/cm^2 exposure compared with CNRQ of 0.91 ± 0.7 in untreated cells. Similar to measurements 6 h and 24 h after ultrasound, *VWF* expression demonstrated comparable expression patterns to *eNOS; VWF* was also reduced after 10 mW/cm^2 (CNRQ 0.75 ± 0.7) compared with untreated cells (CNRQ 1.21 ± 0.73).

However large deviation of expression was observed indicating a variability within the replicates particularly in the expression of *VWF*. This large spread of data may be masking true effects of ultrasound resulting in statistically insignificant results after one-way ANOVA comparison.

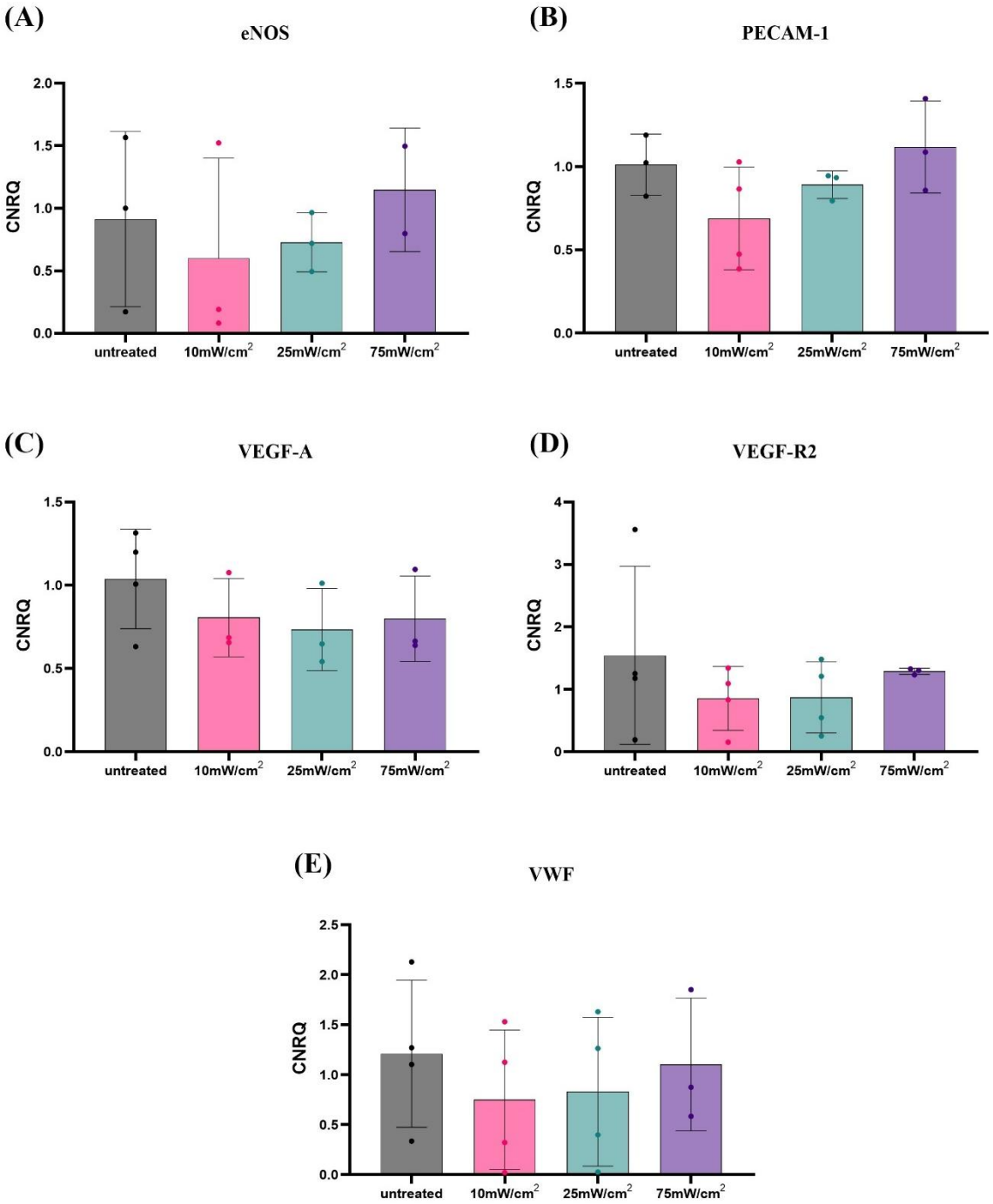

Figure 3.24 qPCR analysis of angiogenesis-related gene expression 72 h post ultrasound exposure.

CNRQ values are plotted as normalised expression to 4 stable expression housekeeper genes. No significant effect on gene expression was measured 72 h after DuoSon exposure. (N = 4, mean ± SD, data points that did not pass qBase^{PLUS} replicate quality were omitted from the analysis).

Initial experiments using the DuoSon device indicated an influence in HUVEC behaviour when exposed to low frequency ultrasound. This was seen in the form of increased viable cell number as a delayed response to ultrasound, 72 h after exposure. Though a direct effect on tube formation was not measured during *in vitro* tube formation assay, the significant reduction in branch number at the latest time point of the assay was not present in HUVECs seeded 72 h after exposure; a suggestion of a time-dependent response. Conversely significant effects were seen in gene expression at the earliest time point of 6 h post ultrasound exposure.

The next objective was to develop an ultrasound exposure method that could be characterised and standardised for future investigations.

3.3 Characterisation of acoustic absorbing tank

3.3.1 Introduction

After observing ultrasound influence on HUVEC behaviour using the DuoSon, the next purpose of this study was to develop a standardised approach of ultrasound exposure to more clearly understand the bioeffects of specific levels of ultrasonic energy. An exposure method of a degassed water tank was implemented in the following *in vitro* experiments. Characterisation was undertaken to investigate the suitability of this method to deliver a controlled environment for *in vitro* ultrasonic treatment of cells. Temperatures were recorded both within the tank and the medium in a CLINIcell® cassette during ultrasound exposure. Controlling the temperature of the water surrounding the submerged cassette was a main goal in the improvement upon the DuoSon design and would identify mechanical effects of ultrasound if thermal effects were kept to a minimum. The acoustic field was characterised using a 4 mm needle hydrophone to measure pressure values during 45 kHz ultrasound exposure. It was hypothesised a degassed water tank would provide an environment with minimised reflection interference on the incident wave due to complete lining with acoustic absorbing tiles designed for low frequency ultrasound.

3.3.2 Temperature recording during ultrasound exposure

3.3.2.1 Tank water temperature during ultrasound exposure

The temperature of the water was heated to 37 °C and then measured every second for 10 min. After the removal of the water heater for ultrasound delivery, the water temperature decreased during the 10 min measurements for all conditions. The decrease in temperature was related to the driving current setting; the lower the driving current, the greater the decrease in temperature (Fig 3.25). Without ultrasound, the temperature during 10 min

decreased significantly by 0.8 °C to 36.2 °C ($p < 0.0001$). The decrease in tank water temperature was at a slower rate during ultrasound delivery as indicated by the final temperature values. At 0.02 A, 0.04 A and 0.06 A the temperature decreased by 0.5 °C to 36.5 °C after 10 min.

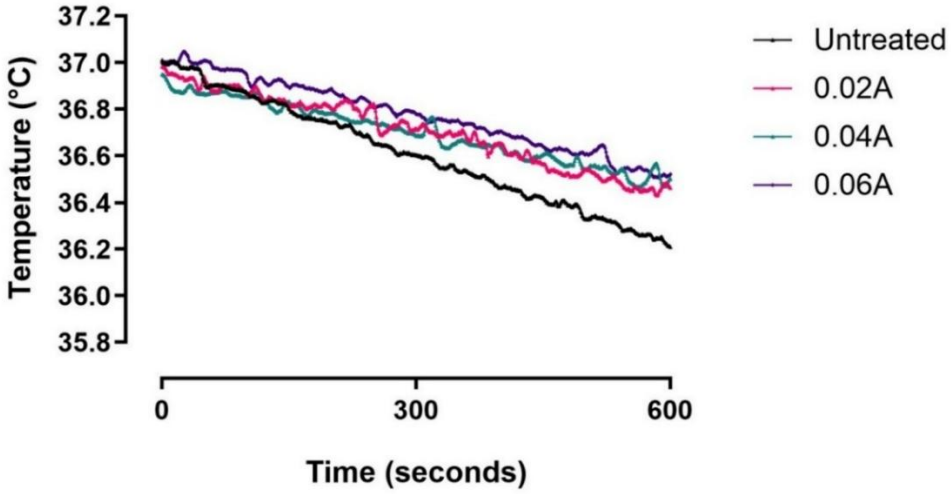

Figure 3.25 Continuous temperature measurements of the tank water for 10 min. The water temperature decreased in all conditions dependent on the driving current. Linear regression analysis showed that the differences between all graph gradients were significantly different ($p < 0.0001$).

Temperatures were also compared between driving current using two-way ANOVA analysis with results outlined in Table 3.1 and graphically described in Fig 3.26. There was no significant difference in temperature between the driving current conditions measured within the same time point. The temperature decreased significantly in all conditions after 10 min, most significantly when no ultrasound was applied ($p < 0.001$) as shown in Fig 3.26. After 5 min the water temperature in the absence of ultrasound application decreased significantly ($p < 0.01$) by 0.4 °C. Although the water temperature decreased after 5 min of ultrasound application, this was not significantly different for any of the current settings. At 0.02 A and

0.04 A the temperature decreased by 0.3 °C to 36.7 °C. At the highest current setting the decrease in temperature was the lowest by 0.2 °C to 36.8 °C.

Table 3.1 Temperature of tank water at 5 min intervals.
A table for tank water temperature readings at 5 min and 10 min of ultrasound exposure. Comparisons were made between all conditions using two-way ANOVA with Tukey's multiple comparisons post-hoc test (N = 3, mean values recorded; * $p < 0.05$, ** $p < 0.01$, *** $p < 0.001$, **** $p < 0.0001$)

Current (A)	Starting Temp (°C)	Temp after 5 min (°C)	Temp after 10 min (°C)
0	37.0	36.6 **	36.2 ****
0.02	37.0	36.7	36.5 ***
0.04	37.0	36.7	36.5 **
0.06	37.0	36.8	36.5 ***

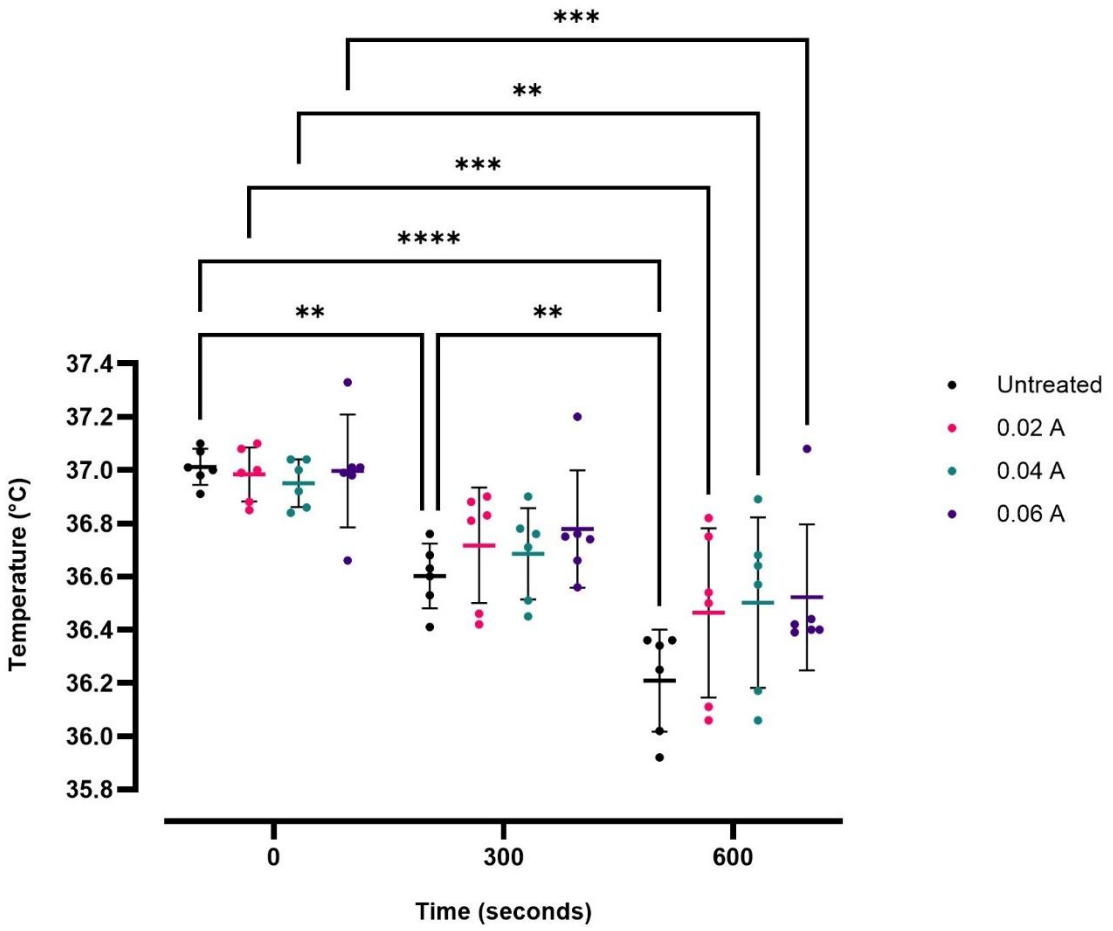

Figure 3.26 Tank water temperatures following ultrasound exposure at 5 min intervals. Temperatures of tank water plotted at 5 min intervals over 10 min ultrasound delivery. Comparisons were made between all conditions using two – way ANOVA with Tukey's post-hoc multiple comparisons test (n = 6; mean ±SD; ** $p < 0.01$, *** $p < 0.001$, **** $p < 0.0001$).

Although significantly lower temperatures were measured after 10 min, after 5 min the temperature was not as significantly reduced. Only without ultrasound was there a significant decrease in temperature after 5 min and the temperature recorded was only 0.1 – 0.2 °C lower than with ultrasound delivery. Consequently, it was investigated whether 5 min ultrasound delivery would have an effect on the temperature of cEGM within the CLINIcell® cassette.

3.3.2.2 Media temperature after ultrasound exposure

After 5 min of ultrasound, the temperature of cEGM within a CLINIcell® cassette rose at all driving current settings. At 0.02 A the temperature of cEGM within a CLINIcell® cassette rose by 0.7 °C from 35.8 °C to 36.5 °C (Fig 3.27 A). After 5 min at 0.04 A the temperature of cEGM within a CLINIcell® cassette rose by 0.6 °C from 35.9 °C to 36.5 °C (Fig 3.27 B). At 0.06 A the media temperature rose by 0.7 °C from 35.8 °C to 36.5 °C (Fig 3.27 C). However, the temperature increase seen in all conditions was not statistically significant after unpaired t-test analysis. The final temperatures of all conditions were also not significantly different to each other after one-way ANOVA analysis (Fig 3.27 D). There was only 0.03 °C difference between the lowest current setting of 0.02 A (36.52 °C) and the highest of 0.06 A (36.55 °C). These results confirmed that ultrasound delivery in the tank configuration did not have a significant effect on cEGM temperature within the CLINIcell® cassette.

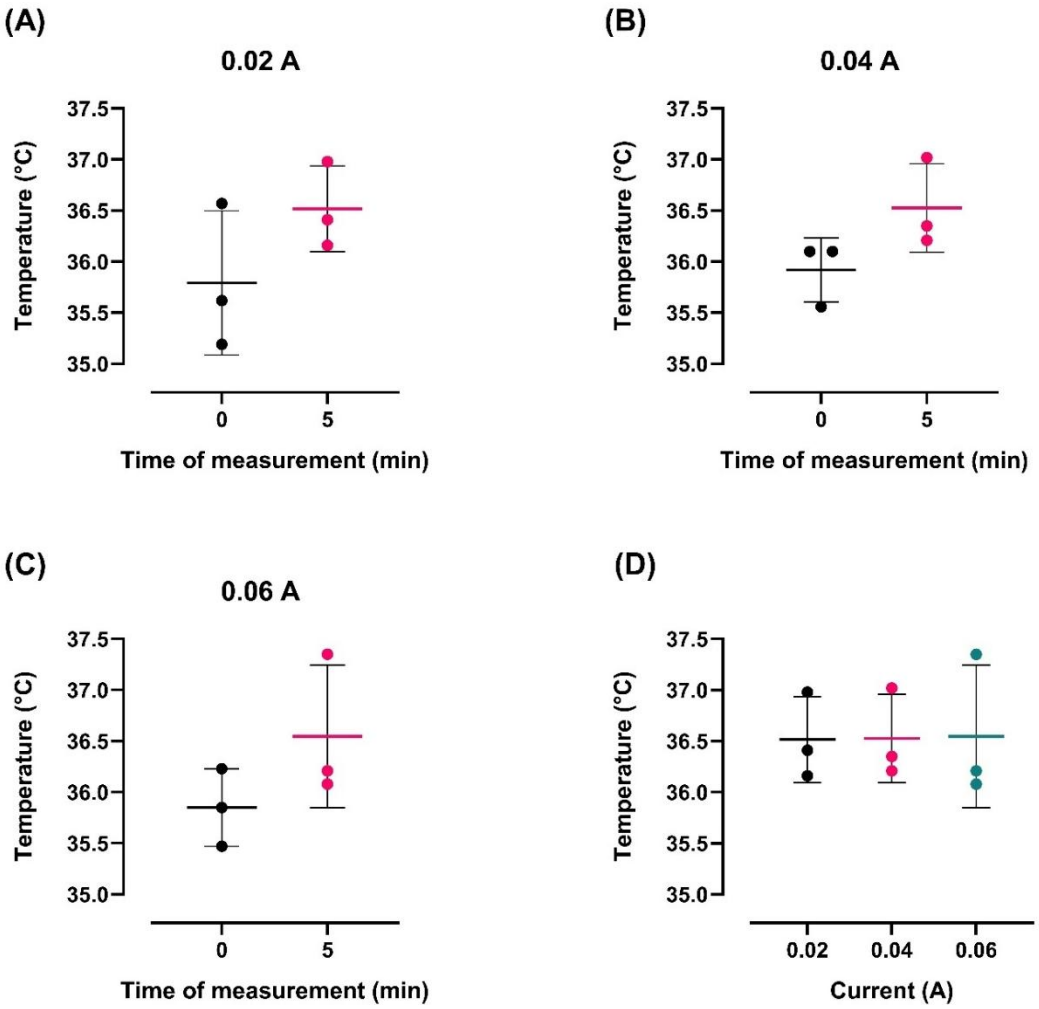

Figure 3.27 Thermal measurements of cEGM within a CLINIcell® cassette.
Non-significant increase in cEGM temperature was measured after 5 min at all current settings tested; (A) 0.02 A, (B) 0.04 A and (C) 0.06 A following unpaired t-test analysis. The final cEGM temperature was not statistically significantly different between the current gains tested (D) after one-way ANOVA with Tukey's post-hoc comparisons. (N = 3, mean ± SD).

3.3.3 Scanning of the acoustic field

Following assessment of thermal control in the tank configuration, characterisation of the acoustic field was undertaken. A longitudinal scan starting 5 mm from the transducer face and moving 25 mm in the Z plane away from the transducer face showed a decrease in peak negative pressure with increasing distance (Fig 3.28 A). The highest peak negative pressure value was identified at the start point (5 mm away from the transducer) at 0.19 MPa. This

decreased to 0.05 MPa with a separation of 25 mm from the transducer, a 74 % decrease in peak negative pressure for 20 mm movement. This scan indicated the pressure within the acoustic field decreased with distance from the transducer with no other areas of high pressure within the field.

The transverse scan 5 mm (Fig 3.28 B) from the centre of the transducer showed a pattern consistent with the transducer face dimensions. The area encompassing the colour plot from colours green to green in the X and Y axes had dimensions of 10 pixels x 10 pixels. This equated to 25 mm calculated by multiplying the number of pixels by the step per scan (2.5 mm). The dimensions of the transducer face were also 25 mm x 25 mm. The highest peak negative pressure area was not seen at [0, 0] coordinates but was from 0 to 7.5 mm in the -X direction. The highest peak negative pressure scanned at these coordinates was 0.215 MPa. The lowest pressure scanned within the transducer face dimensions was 0.15 MPa, 30 % lower than the highest pressure scanned within the transducer face. These results showed differences of pressure emitted from different regions of the transducer face.

The transverse scan of 10.5 cm x 8.5 cm, taken 25 mm away from the transducer face (Fig 3.28 C) showed a decrease in peak negative pressure at the centre of the scanned area compared with scans 5 mm away. The highest peak negative pressure with 25 mm separation was 0.075 MPa, compared with 0.215 MPa at 5 mm, which represented a decrease of 65 %. Similarly with scans at 5 mm, the peak negative pressure decreased in all directions from the centre of the transducer. Within the 25 mm x 25 mm area of the transducer face there was a 20 % decrease in peak negative pressure from 0.075 MPa at [0, -7.5] coordinates to 0.06 MPa at the edge of the transducer face. Therefore, the difference in pressure values across the

transducer face seen at 5 mm separation were also seen at 25 mm separation. Although there was a 65 % decrease in the highest peak negative pressure value compared with 5 mm distance, the pressure values obtained in the scanned area surrounding the transducer face dimensions were similar to those obtained at 5 mm separation.

A CLINIcell® cassette filled with degassed deionised water was then positioned 5 mm away from the transducer with the 4 mm needle hydrophone placed 25 mm away to see any attenuation caused by the cassette. A similar pressure map was obtained (Fig 3.28 D) to that obtained without a cassette present. The highest peak negative pressure was 0.077 MPa, almost equal to the highest pressure seen without a cassette (0.075 MPa). Again, this highest peak of negative pressure value was identified 7.5 mm in the -X direction from the centre of the transducer as with the scans at 5 mm and 25 mm. A decrease in peak negative pressure values were again seen across the transducer face dimensions (25 mm x 25 mm). There was a 22 % difference in pressure values measured at the peak pressure point [0, -7.5] compared with 0.06 MPa at the edge of the transducer face. Interestingly, the pressure map showed an increase in pressure values (0.02 MPa) measured around the edges of the scanned area compared with the scan without a cassette present (0.01 MPa).

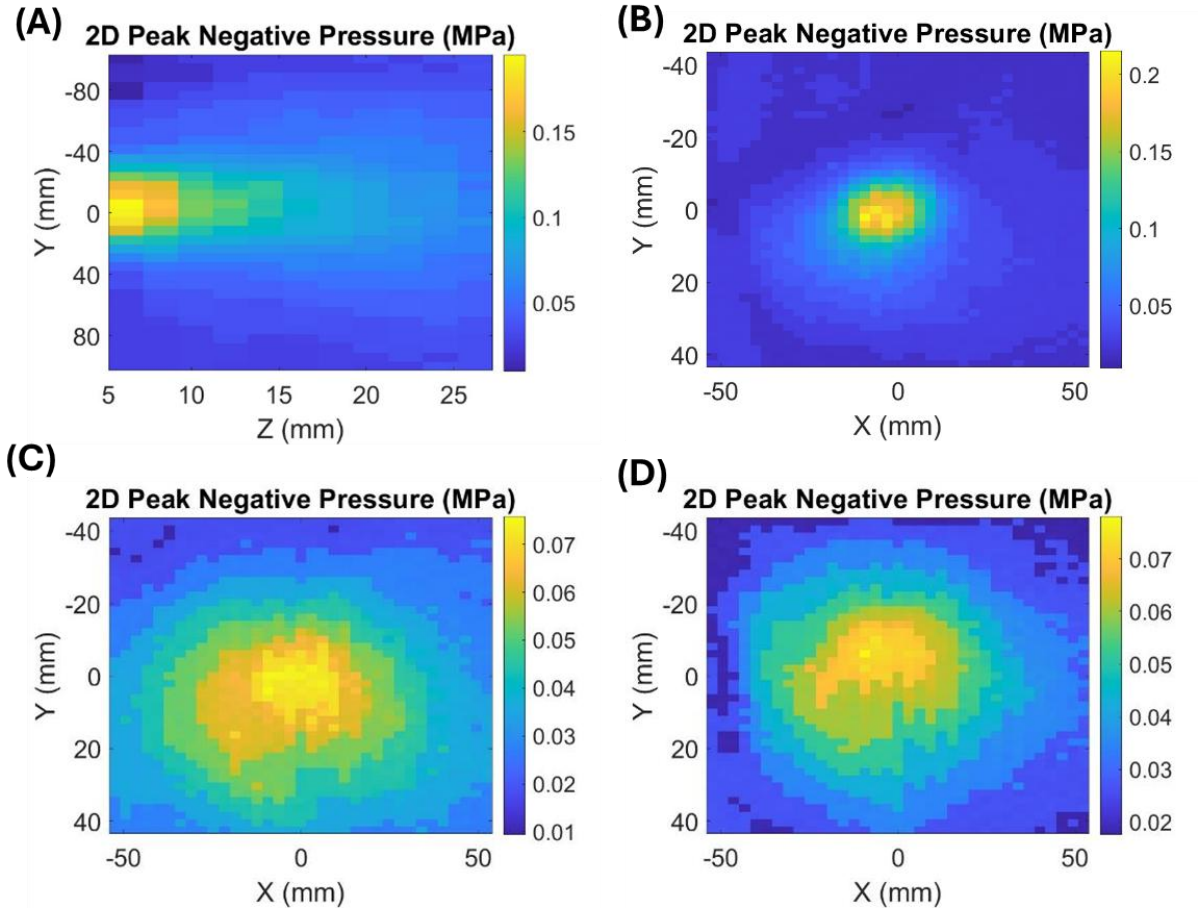

Figure 3.28 Acoustic pressure field scans using 4 mm needle hydrophone.
(A) Longitudinal scan starting 5 mm away from the transducer face, scanning 8.5 cm x 2.5 cm in the YZ plane. (B) Transverse scan of 10.5 cm x 8.5 cm dimension 5 mm from the transducer face shows higher pressure in the centre of the plot. (C) Transverse scan of 10.5 cm x 8.5 cm, 25 mm from the transducer face shows pressure values three times less than at 5 mm. (D) Transverse scan of 10.5 cm x 8.5 cm 25 mm from the transducer face with a CLINIcell® cassette between the hydrophone and transducer showed similar plot and pressure values as in (C).

Scans were made at a single point from the transducer face at 5 mm, 25 mm and 25 mm with a CLINIcell® cassette present at 8 different current settings (0.001 to 0.075 A). The scans at 5 mm showed a somewhat linear increase in peak negative pressure (MPa) after regression analysis which correlated with the increased current (A) (R^2 = 0.9739; Fig 3.29 A). Scans 25 mm from the transducer also showed a linear relationship between peak negative pressure and current applied (R^2 = 0.9712; Fig 3.29 B). The presence of a CLINIcell® cassette did not disrupt the linear increase (R^2 = 0.9814; Fig 3.29 C). The peak negative pressure was lower at all current settings when measured 25 mm from the transducer compared with 5 mm separation which concurred with the acoustic field scan data showing a reduction in pressure values with separation. At the driving current of 0.04 A there was a 66 % decrease from 0.175 MPa to 0.06 MPa. This decrease with distance is concurrent with the decreasing peak negative pressure measured with increased separation from the transducer in transverse and longitudinal scans. The comparable values and linear increase at 25 mm with and without a CLINIcell® cassette further indicated minimal wave attenuation and interference caused by the presence of a CLINIcell® cassette. However the graphs depicted in Fig 3.29 also highlight an observation that when zero current is applied, the pressure is not zero as would be expected. Rather a low pressure between 0.02 and 0.06 MPa was measured in all scans.

Nonetheless, these results demonstrated the tank exposure method provided an acoustic field with minimal wave interference and improved control over temperature in the tank and CLINIcell® cassette during ultrasound exposure. Additionally, the exact ultrasonic energy delivered to the cells could be measured which was absent in the DuoSon exposure method. The next stage of this work was to introduce HUVECs to the CLINIcell® system to assess any changes in behaviour.

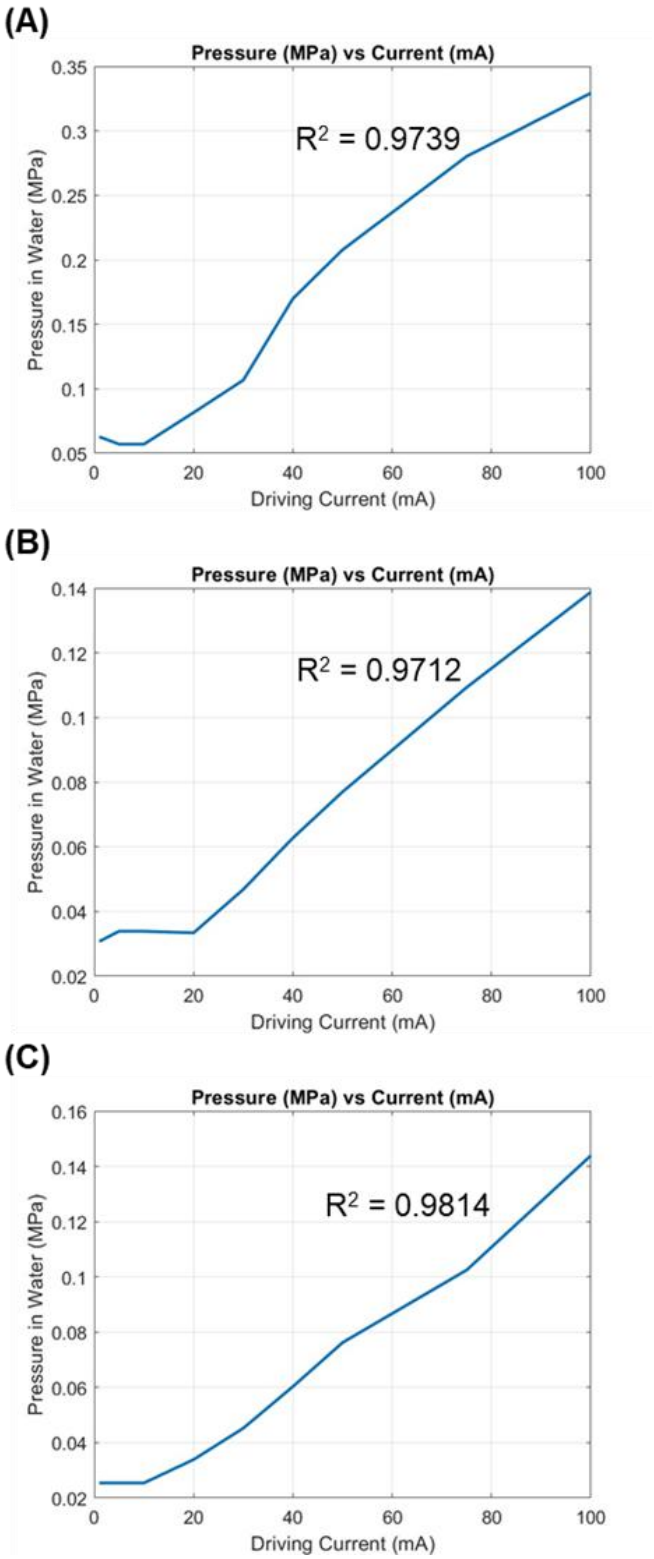

Figure 3.29 Single point pressure scans at varying distance, with and without a cassette.
Linear regression analysis performed on hydrophone pressure readings from increasing driving current (mA). R^2 coefficient value is plotted on the graph. Scans were performed (A) 5 mm from the transducer face, (B) 25 mm from the transducer without a CLINIcell® cassette present and (C) 25 mm from the transducer with a CLINIcell® cassette between transducer and hydrophone.

3.4 Effect of 45 kHz ultrasound on HUVECs via acoustic absorbing tank exposure

3.4.1 Introduction

Following characterisation of the tank, analysis was performed to understand HUVEC response to ultrasound in the tank configuration. HUVECs were exposed to 45 kHz continuous ultrasound for 5 min at the same power used in characterisation scans: 0.04 A, (175 kPa, extrapolated from Fig 3.29A). The assays employed were F-actin immunostaining, viable cell number analysis, and qPCR analysis of angiogenesis-related genes.

3.4.2 Influence of 45 kHz exposure in the tank on HUVEC cytoskeleton

In accordance with DuoSon experimentation, effects on HUVEC cytoskeleton were investigated following ultrasound exposure in the tank configuration. As shown in representative photomicrographs in Fig 3.30 A, untreated cells exhibited a more polygonal shape. Cells that were exposed to ultrasound, in contrast, were observed with instances of non-uniform morphology. After 24 h, HUVECs were observed in some areas of aggregations rather than a uniform monolayer following ultrasound exposure (circled in Fig 3.30 B). These cluster formations resulted in some indistinguishable cell body shapes, with the appearance of "overlapping" cell bodies suggesting an effect on the attachment of HUVECs to the membrane following ultrasound exposure. Similar to staining after DuoSon exposure, localised actin staining could be seen in these areas of cell aggregation with increased cell-cell contact (orange arrows in Fig 3.30 B & C). Elongated cell body shape could also be seen in some cells after ultrasound exposure as highlighted 72 h after ultrasound (white arrows in Fig 3.30 C). These observations suggest an effect on cell shape and attachment as a result of ultrasound exposure leading to non-uniform morphology and increased cell clustering.

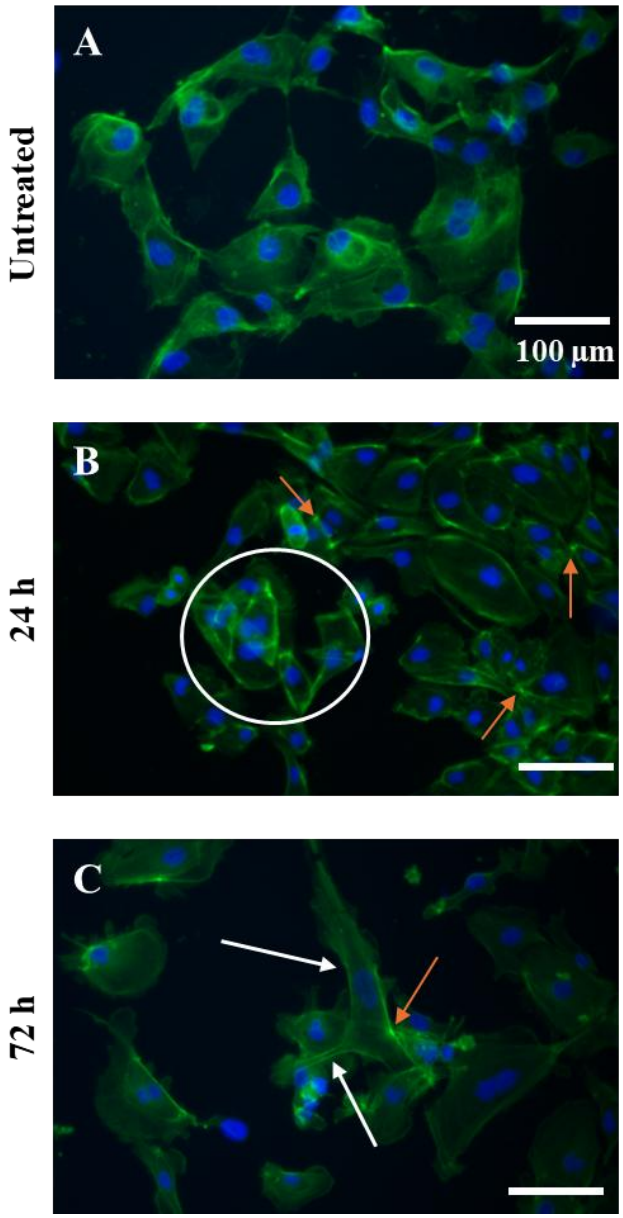

Figure 3.30 Fluorescent micrographs of F-actin stained HUVECs 24 h and 72 h post ultrasound exposure in an acoustic absorbing tank.
(A) Untreated HUVECs and cells exposed to ultrasound were visualised (B)24 h and (C) 72 h after ultrasound. Exposed cells were seen forming aggregates with overlapping cell bodies (circled in B) and non-uniform elongated cell shapes (white arrows in C) compared with untreated cells. Areas of localised actin staining at cell – cell contact point with examples highlighted with orange arrows. Untreated cells exhibited more uniform monolayer with polygonal shaped cell bodies. (N = 1).
Scale bars represent 100 µm.

3.4.3 Viable cell number analysis

Viable cell numbers were counted 24 h and 72 h post ultrasound and analysed using unpaired t-test comparisons as depicted in Fig 3.31. A moderate increase in viable cell number was seen in ultrasound treated groups 24 h after exposure with 10.14 $x10^4 \pm 0.67$ cells counted compared with 8.02 $x10^4 \pm 1.36$ in untreated conditions (Fig 3.31 A). However, this increase was not significantly different, $p = 0.0794$ after unpaired t-test analysis. There was also no significant difference in viable cell number 72 h after ultrasound exposure between treated and untreated cells ($p = 0.2903$) shown in Fig 3.31 B. However, slightly higher cell numbers were observed in treated groups, 14.22 x $10^4 \pm 1.61$, compared with 10.71 x $10^4 \pm 4.73$ in cells unexposed to US.

No significant effect in viable cell number was seen after ultrasound delivery in the tank configuration, although slightly elevated numbers of viable cells were seen at each time point. There was also no significantly damaging effect to cell viability seen after ultrasound exposure. These results are somewhat concurrent with the cell viability results seen in the DuoSon configuration.

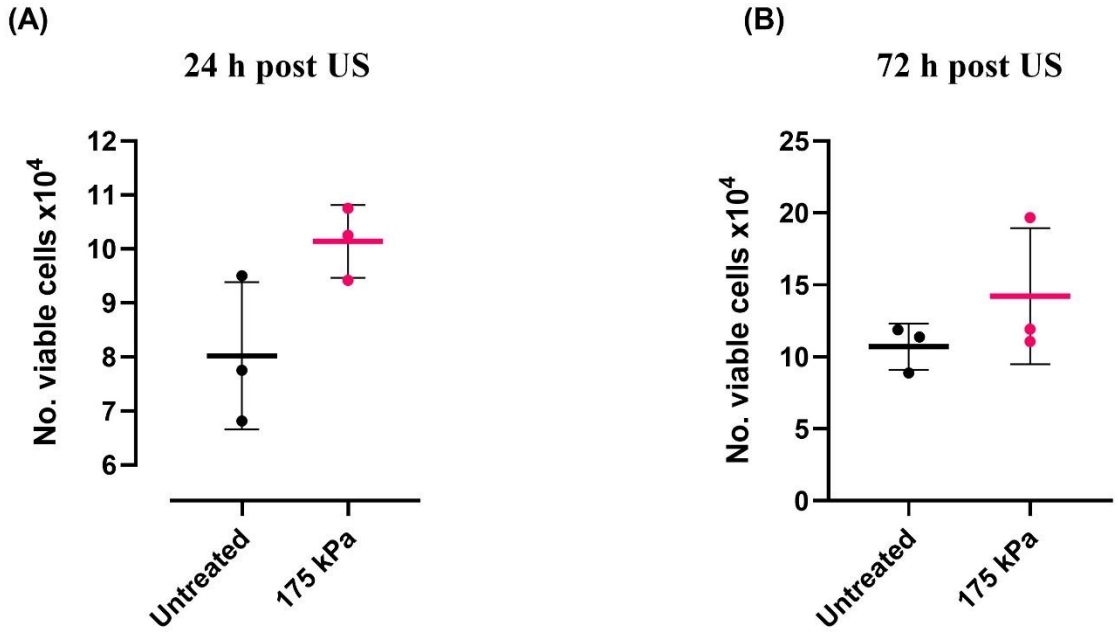

Figure 3.31 Viable HUVEC cell numbers 24 h and 72 h post ultrasound exposure in the acoustic absorbing tank.

Cells were counted 24 h and 72 h after ultrasound exposure. (A) 24 h after ultrasound showed a moderate increase in cell number after ultrasound compared with untreated cells, however this was not found to be significantly different. (B) Similar cell numbers were identified within untreated and treated cultures 72 h after exposure. (N = 3, mean ± SD)

3.4.4 Expression of angiogenesis-related genes

Gene expression analysis after ultrasound exposure in the acoustic absorbing tank was performed 6 h, 24 h and 72 h after exposure (Fig 3.32). The genes analysed were the same as those analysed in the DuoSon exposure configuration relative to the expression of stable housekeeper genes - *B2M*, *GAPDH*, *RPL27* and *YWHAZ*. There was no significant change in expression levels in any genes analysed after 6 h. Although a slight decrease was seen in *eNOS* expression in treated cells with a CNRQ of 0.79 ± 0.21, whereas expression in untreated cells showed a CNRQ of 1.03 ± 0.3 (p = 0.3193). After 24 h similar gene expression

levels were seen between untreated and treated cells; only moderate increase in gene expression in the treated cells, although statistically there was no effect.

Conversely, 72 h after ultrasound exposure there was a decrease in all gene expression. Reduced *VWF* expression levels were seen in treated cells (0.82 ± 0.21) in comparison with untreated cells levels of 1.01 ± 0.14 although not significantly different ($p = 0.2771$). A similar trend was also seen in *VEGFR2* expression. Moderate, though insignificantly ($p = 0.2296$) reduced expression was seen in cells exposed to 175 kPa ultrasound (0.74 ± 0.21) than untreated cells (1.03 ± 0.28). A statistically significant effect on *eNOS* expression was seen in cells 72 h after US. *eNOS* expression was observed at CNRQ of 1.00 ± 0.06 in untreated cells, whereas cells exposed to 175 kPa showed a significantly reduced CNRQ of 0.8 ± 0.04 ($p = 0.0064$). Expression analysis of the selected angiogenesis-related genes indicated a reduction in expression levels at the latest time point of 72 h post exposure across all genes. The most significantly affected gene in response to ultrasound was *eNOS* as with observations after DuoSon ultrasound delivery.

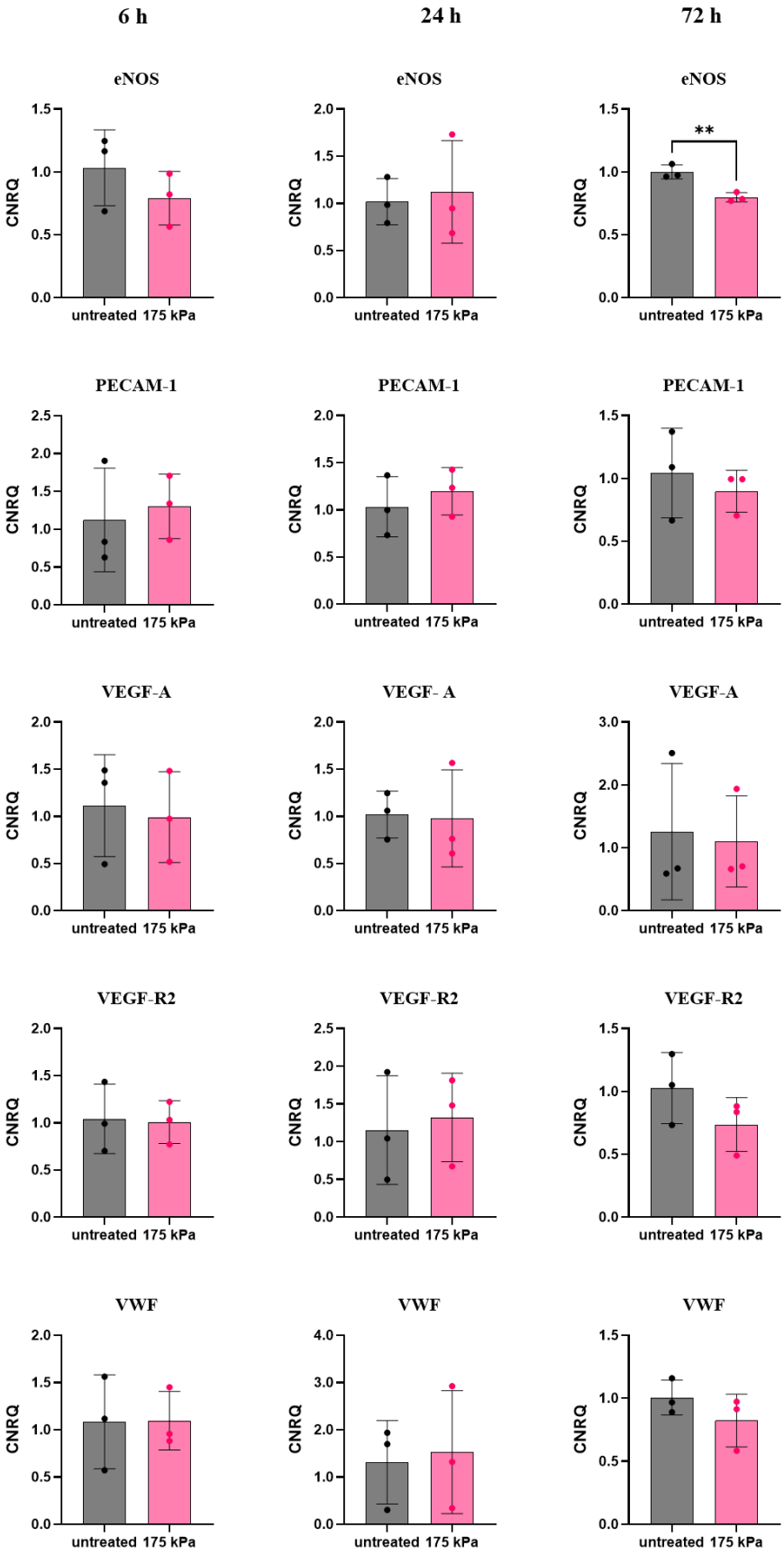

Figure 3.32 qPCR analysis of angiogenesis-related genes 6 h, 24 h and 72 h after ultrasound exposure. Calibrated normalised relative quantity (CNRQ) values were normalised expression to 4 housekeeper genes. Unpaired t-test compared differences in expression levels between ultrasound-exposed and untreated cells. A significant reduction in *eNOS* expression was measured 72 h after ultrasound exposure (N = 3, mean ± SD; ** $p < 0.01$)

Chapter 4.

DISCUSSION

4.1 Development of *in vitro* configurations for ultrasound exposure to cells

One of the main challenges of exposing cells to ultrasound *in vitro* is understanding precisely how much energy is being emitted from a transducer to a cell monolayer and ultimately experienced by the cells. This challenge was highlighted in Mizrahi's 2007 *in vitro* study where a culture dish of medium was exposed to an acoustic beam of known intensity and pressure and generated higher-than-expected acoustic pressures within the culture dish (Mizrahi et al., 2007). Mizrahi et al.(2007) suggested this discrepancy in pressure values was due to significant reflection and standing wave formation within the dish and at the medium/air boundary. The conclusion from this study was that calculating how much energy was present and predicting what amount the cells are receiving was not possible to control.

The conventional method for measuring ultrasound energy uses hydrophones which are sensitive devices and exposure to high acoustic pressure could damage the hydrophone, which was a challenge within the DuoSon configuration (Section 2.2.1). Ultrasound emitted at a frequency of 45 kHz ultrasound with a wave velocity in culture medium of the petri dish taken as approximately 1,480 m/s has a calculated wavelength of 3.3 cm (Equation 1.1). This wavelength is similar to the size of the petri dishes used for DuoSon exposure (35 mm diameter). Therefore the sound energy will be emitted around the 5 ml culture medium in the petri dish and due to impedance mismatches between the medium and air, the energy will be reflected within the dish producing a range of standing waves and possibility for cavitation to occur. There is a possibility this sound energy trapped within the culture dish could damage the hydrophone. More challenging is the positioning of a hydrophone into the DuoSon configuration. The immersion of the transducer face into the culture dish does not allow any additional space for a hydrophone, therefore the exact ultrasound energy during a cell culture

experiment would not be possible. Therefore although the tank configuration results are displayed in response to peak negative acoustic pressure, such *in situ* acoustic readings were not possible for the DuoSon configuration and are arguably of limited use due to the expected reverberant environment within the culture dish. As such HUVEC response to DuoSon exposure is displayed in response to calibrated intensity measurements. However, the DuoSon configuration (Section 2.2.1) ensured precise and reproducible positioning of the transducer perpendicular and 5 mm above the cell with control over the immersion in culture dishes ensuring minimal disturbance to the cell monolayer.

The exposure arrangement of cells evolved during the project and a second *in vitro* configuration was implemented. The aim of the tank exposure apparatus in the present study was to reduce any standing waves and cavitation effects to allow accurate measurement of the ultrasound energy experienced by cells as discussed in the review of *in vitro* ultrasonic exposure methods by Snehota et al., (2020). To assist in this, deionised water was degassed via boiling (Liu et al., 2014) a commonly used technique in acoustic field tank experiments to reduce the activity of any gas bubbles in the water and subsequent mechanical cavitation effects on cells. However, the pouring of degassed water into the tank may reintroduce air bubbles into the system on the internal walls of the tank or in the water itself. No bubbles were visible to the naked eye in the tank system before or during ultrasound exposure, however it remains a possibility there may still have been micron sized bubbles which were difficult to detect. The exposure system required a large volume of water to be used so that any reflections arising between water/air boundaries were lost over the propagation distance of the ultrasonic waves. The size of the tank (60 cm x 30 cm x 30 cm) used in this research project is smaller in comparison with available low frequency ultrasound scanning tanks. For

example, low frequency scanning tanks designed for 50 kHz and above manufactured by Precision Acoustics have been designed as 3 m x 1.5 m x 1.5 m, 5 times larger than the tank used in this study. However the workspace necessitated a tank in close proximity to a cell incubator and microbiological safety cabinet for cell culturing in controlled lab conditions. Therefore the sized tank used in this study was of the most feasible practical size. Efforts were made to minimise the effect of standing waves and cavitation where possible. The transducer and cell cassette were aligned longitudinal to the tank to reduce the risk of the ultrasound wave meeting the water/air interface and subsequently reduce the risk of reflection at this interface. Low frequency ultrasound exposure produces an ultrasound beam with a greater beam spread, increasing the possibility of encountering all tank wall boundaries. Therefore all sides of the tank were lined with ultrasonic energy absorbing tiles, designed for low frequency 20 – 200 kHz ultrasound, which was a modification from only one side of the tank as with the previous design (Savva et al., 2019).

Acoustic field mapping demonstrated the anechoic nature of the tank. The acoustic output of the transducer was measured in peak-negative acoustic pressure values (MPa) as it is during rarefactional periods of an acoustic wave cycle that gas bubbles are most likely to form and lead to potential cavitation effects. An absence of multiple pressure hotspots strongly indicated an absence of reflections at the water/air boundary or water/absorber boundaries interfering with the scanned acoustic field. This was an important finding to visualise the acoustic environment during ultrasound exposure which is not always present in the literature. CLINIcell® cassettes showed minimal ultrasound energy attenuation using comparisons of pressure values and visualisation of scans with (Fig 3.28 D) and without (Fig 3.28 C) a cassette in the acoustic field. This provided further confidence that the pressure values

mapped to the scanned area was consistent with the ultrasound energy the cells would experience during *in vitro* exposure. A lack of attenuation also reduced the possibility of thermal effects on the cells cultured in the cassettes as absorbed ultrasound waves can lead to localised temperature rises as described in section 1.5.1. Slight differences in pressure values were observed at the edges of the transverse scan dimensions which may have been caused by a scattering effect of the ultrasound wave between the polycarbonate case and the polycarbonate film layer. Scattering of an ultrasonic wave can be caused by an irregular surface (DeSanto, 2002), which could have occurred at the joining of the polycarbonate film and the polycarbonate plastic casing. Nonetheless, the slight differences in pressure values were determined to not significantly interfere with the wave propagation or cell exposure. Although there was a potential for the introduction of unwanted bubbles to the acoustic field within the CLINIcell® cassette. Cell culture medium used in cassette cell culture was not degassed, however the deionised water used to fill the CLINIcell® cassette during acoustic characterisation was also not degassed. As there was an absence of subharmonics in the hydrophone measurements during the tank characterisation, this suggested a lack or a very low level of cavitation occurred during ultrasound exposure.

Single-point pressure scans analysing the effect of increased current applied to the pressure measured within the tank surprisingly showed that when zero current was applied, the pressure measured did not correspond at zero as expected (Fig 3.29). This observation could be explained by the presence of background noise detected by the hydrophone. As seen in Fig 2.7, acoustic mapping of the tank involved multiple electrical equipment working simultaneously. A motorised X Y Z stage was used to continuously reposition the hydrophone during the scan process, laptops were used to trigger a Picoscope to save hydrophone readings

and to drive the transducer via a PiezoDrive driver and a separate computer was also used to control the motorised stage through LABVIEW software. All of this machinery and electrical equipment could create background noise which could subsequently be detected by the 4 mm hydrophone. This provides an explanation to the appearance of low levels of pressure being measured (0.02 – 0.06 MPa) even when there was no current applied to the transducer within the tank. Nonetheless, when current was applied the pressure measured also increased in a somewhat linear fashion. Therefore the further development of the tank exposure configuration demonstrated in the present study was a significant addition to the research of *in vitro* exposure of cells to ultrasound.

The tank exposure method also provided an improved means of controlling temperature compared with the DuoSon configuration. Removal of the water heater once the temperature had reached 37 °C eliminated the presence of artefacts within the acoustic field. Exposure lengths of 5 min did not cause a significant decrease in tank temperature. Although a significant decrease was observed without ultrasound delivery over 5 min, the actual temperature recorded was only 0.3 °C lower than that recorded after ultrasound delivery. This difference in temperature would not be sufficient to attribute to any difference in cellular response during 5 min *in vitro* experiments. The decrease in water tank temperature also did not impact on the temperature of cEGM within the cassette during a 5 min exposure. The final temperature measured was 36.5 °C which was unlikely to produce any significant biological effect as most mammalian cell lines are cultured between 36 – 37 °C (Segeritz & Vallier, 2017). Therefore, the tank configuration was shown to have suitable thermal control during ultrasound delivery.

Although the acoustic absorbing tank achieved one of the project's objectives which was to develop a standardised ultrasonic exposure system, there are still improvements that can be made in future studies. During cell culture experiments the transducer and cassette were aligned manually using a laser spirit level within the aluminium pole rig. Such manual adjustments may have introduced a potential for non-reproducible positioning during each cassette loading. An improved positioning apparatus, such as a motorised XYZ 3-axis stage, could optimise the alignment procedure in accuracy and time to ensure the reliability of ultrasound exposure is upheld.

Two methods have been identified to minimise any cavitation effects. First, the cEGM used for cell culture when seeding HUVECs into the CLINIcell® cassettes should be degassed prior to addition. There was an outlet valve opened to facilitate gas removal during culture media addition. However, degassing by proven methods such as vacuum filtration is a more measured way to reduce the presence of bubbles and subsequently cavitation in the system. Secondly, using a mechanical pump at a low speed to fill the tank would allow more controlled introduction of the degassed solution. Although pressure field mapping during characterisation of the acoustic field did not identify any presence of cavitation, there is still uncertainty if cavitation was present during cellular experiments. As each biological experiment involves introduction of new degassed water, cell cultures and CLINIcell® cassettes, the acoustic field may alter and the introduction of gas bubbles may occur. Placing a hydrophone behind the CLINIcell® cassette would provide confirmation of the presence of cavitation during each cell culture ultrasound experiment. Once again, the introduction of a hydrophone introduces another layer of complexity to the system.

4.2 Comparison of HUVEC response within exposure configurations

This work investigated the effect on cell viability and cell numbers following ultrasound exposure using both DuoSon and tank configurations. Measurements via CCK-8 assay following DuoSon exposure and trypan blue assay, following DuoSon and tank exposure, showed that there was no significantly damaging effect to cell viability. This finding supports literature investigating the effect of therapeutic ultrasound on angiogenesis where no cell death has been recorded. For example Huang et al., (2017) observed a significant reduction in apoptosis and significant enhancement in cell viability after therapeutic ultrasound treatment using 1 MHz, 0.3 W/cm^2 for 9 min. Though the frequencies differ between Huang's research and the presented work, this study provided new findings into the effect of kHz ultrasound on cellular viability.

Viable cell number analysis showed comparable numbers counted in the tank exposure system compared with untreated cells 72 h after ultrasound exposure, with moderately increased numbers 24 h after ultrasound. It is possible that increasing the statistical power of the analysis with an increase in the number of biological replicates, may lead to a more significant effect, as comparisons at 24 h were only marginally statistically insignificantly different (p = 0.0794). Similarly, DuoSon exposure resulted in moderately increased viable cell number compared with untreated cells 24 h after ultrasound exposure. This may have been due to the time taken for HUVECs to divide and proliferate in response to ultrasound resulting in the effect becoming visible after 24 h. In contrast to tank exposure, there was a significant increase in the number of viable cells 72 h after DuoSon exposure. A similar response was previously reported after endothelial cell exposure to ultrasound though the frequency applied was higher at 510 kHz (Schuster et al., 2013). Schuster's research also

observed a significant increase in cell numbers 72 h after ultrasound exposure rather than 24 h and 48 h. In contrast, a more recent study observed a proliferative effect on endothelial cells 24 h after LIPUS treatment (Li et al., 2022). Li also delivered ultrasound to cells seeded in 96 well plates and 24 well plates. However work by the Birmingham team has shown that this experimental system is flawed as the well plates are adjacent to each other and therefore ultrasonic energy can be transferred throughout the plate (Gupta et al., 2022; Patel et al., 2015). Previous researchers have not provided information regarding measuring the amount of ultrasonic energy in the well plates such as the work reported by Li et al. 2022. Without hydrophone measurements, it is impossible to understand the exact amount of ultrasonic energy transferred to the cells. As stated earlier in Section 4.1, such measurements were not possible in the DuoSon research in this study.

The differences in viable cell numbers measured in the present study may have been due to the different dose of ultrasound applied in each system. Cells respond to ultrasound in a dose-dependent manner; increased cell number has been shown to occur with increasing energy applied (Schuster et al., 2013). The amount of ultrasound experienced by HUVECs in the DuoSon system is unknown. There may be variations in energy caused by reflections within the culture dish walls and between the medium/air boundaries which were not as prominent in the tank system as demonstrated in Section 3.3.3. Reflections within a culture dish have been shown to result in higher-than-expected acoustic pressure levels within the dish (Mizrahi et al., 2007). Therefore the energy intensity applied to cells within the DuoSon may be higher than those in the tank system resulting in a difference in cell proliferation response.

Cytoskeletal actin staining employed in the present study may provide visual indication of the presence of increased HUVEC growth. Non-confluent, proliferating endothelial cells have a specific F-actin distribution which was first reported two decades ago by Searles et al., (2004). Searles' research demonstrated F-actin localisation towards the cell periphery in proliferating cells which was similar to the observations made in the present study where HUVECs exhibited localised actin staining to the cell outer margin in both ultrasound exposure configurations (Fig 3.5 and Fig 3.30). This peripheral staining can be seen more abundantly in HUVECs 72 h after 25 mW/cm^2 DuoSon ultrasound, potentially correlating with the significant increase in viable cell number. Areas of localised actin staining at the cell periphery may also indicate the location of the leading edge of a cell, suggesting the cell motility of HUVECs was unaffected (Lamalice et al., 2007). However, further quantitative analysis would have to be undertaken to support such possibilities.

HUVEC morphology was not noticeably altered when imaging took place following DuoSon exposure. Endothelial cell morphological changes can be reversible, as identified by Altland et al., (2004) when observed changes in endothelial cell shape after ultrasound exposure were not visible after further 24 h culture. So, it may be possible that cell morphological changes after DuoSon treatment occurred at an earlier time point than 24 h. However the observation of cell morphology changes 72 h after ultrasound exposure in the tank system indicated prolonged morphological changes may also occur after ultrasound exposure. F-actin staining revealed instances of cell clustering 24 h and 72 h after ultrasound exposure in the tank system resulting in non-uniformity in cell shape. Occurrences of elongation in cell bodies and contrasting smaller, clumped indistinct cell bodies were observed in ultrasound exposed cells (Fig 3.30). A combination of finite element modelling (FEM) and F-actin

immunocytochemistry techniques have demonstrated ultrasound exposure causes increasing amount of strain within the cell, particularly in the cell cytoplasm and actin cytoskeleton causing changes in cell shape (Samandari et al., 2017). This may account for the changes in shape observed in the present study following 45 kHz exposure.

Though these initial findings indicated a pro-angiogenic response to 45 kHz ultrasound in HUVECs (increased cell number, morphological alteration, lack of cell death) tube formation analysis did not show any significant direct effect of US. Initial analyses involved exposure of HUVECs to DuoSon ultrasound followed by tube formation assay in 48 well plates. Temporal responses were examined to identify whether there was a correlation between cell number and tube formation ability. Therefore, cells were seeded onto the Matrigel^{TM}-coated assay plates immediately, 24 h and 72 h post exposure. At all time points after exposure, there was no significant difference in total tube length or number of branches formed between cells exposed to ultrasound and those unexposed. This suggests that 45 kHz ultrasound did not have a significant effect on the sprouting ability of HUVECs after 5 min treatment regardless of when analysed which differs from previously reported results in the field. Huang et al., (2015) reported significantly increased tube formation in cells treated with 9 min 1 MHz ultrasound at a 6 h timepoint compared with untreated HUVECs. Though it is unclear what characteristics were measured and analysis used by Huang to determine tube formation. The magnification used to image cells by Huang also differed from the protocol used in the presented work. Huang's research imaged cells at 100x magnification which does not capture the view of an entire well unlike 4x magnification employed in the presented work allows. Only a partial view of the well can be captured which may not fully represent the total tube formation response. Contrasting results have been reported by another research group. Su et

al., (2019) measured significantly decreased number of branches 8 h after 1 min LIPUS treatment (0.5 MHz, 210 mW/cm^2). The difference in reported responses highlights the sensitivity of cells to different frequencies and emissions of ultrasound. The results presented in the present study align more closely with Huang's research findings as no significant negative effect on the tube formation behaviour of HUVECs was observed with continuous wave emission.

However, an indication of a time-dependent response to ultrasound, similar to the response in HUVEC cell number, was observed. In cells seeded immediately and 24 h after ultrasound exposure, the number of branches was significantly lower at 24 h in all exposed and unexposed cells compared with the earliest time point analysed. Cells that were seeded 72 h after ultrasound exposure showed a different response. Only in untreated cells was a significantly lower number of branches counted at 24 h compared with 4 h. Cells that were exposed to ultrasound at all 3 intensities (10, 25 and 75 mW/cm^2) did not result in significantly decreased number of branches. This suggested ultrasound exposure allowed HUVECs to retain an ability to form branches for a longer time than untreated cells. Cells within the *in vitro* tube formation assay began to undergo apoptosis and subsequently tubes began to deteriorate at 24 h (DeCicco-Skinner et al., 2014; Ranta et al., 1998). Therefore the loss of significantly reduced branches counted in cells exposed to ultrasound at the 24 h time point may have indicated delayed tube deterioration and an increase in the tube integrity of HUVECs seeded 72 h after ultrasound exposure, This further implied a delayed response to ultrasound in HUVECs.

Tube formation assays are well-established methods of assessing angiogenic behaviour of endothelial cells since the protocol's first description by Kubota et al., in 1988. The protocol involves seeding endothelial cells onto a substrate that contains basement membrane proteins such as laminins, collagen IV, various growth factors and cytokines that mimic *in vivo* tissue extracellular matrix. Tube formation has been assessed following ultrasound exposure previously by seeding onto Matrigel^{TM}-coated wells after ultrasound exposure (Huang et al., 2015; Su et al., 2019). This protocol involved detaching cells from adherent cultures using trypsinisation and centrifugation, followed by cell counting and reseeding. In total, the reseeding step of the protocol lasted over 30 min in the present study following DuoSon exposure due to the number of technical replicates and conditions within each experiment. Not only was there a doubt over whether the direct effect of ultrasound was being measured due to the time taken, the process of detachment could also have had a masking role on the effect of ultrasound. Detachment of cells using the protease trypsin involves cleavage of peptide bonds in cell adhesion proteins; the addition of EDTA accelerates this process. Due to the nature of this process side effects on cell cytoplasm content (Lordon et al., 2024), cytoskeleton and actin filaments (Nehls et al., 2019; Raizada et al., 1981) have been published. As described previously, the function and reorganisation of actin is a key factor in the angiogenic ability of HUVECs. Any alteration in the actin cytoskeleton could influence the tube formation ability of HUVECs which may interfere with the response to the initial ultrasound delivery. Due to this, a second approach was utilised. HUVECs were seeded onto Matrigel^{TM}-coated culture dishes prior to ultrasound exposure. Although this method has been followed previously (Huang at al., 2015) HUVECs were seeded onto multiwell plates prior to ultrasound exposure, rather than singular culture dishes used in the present study. No significant difference in tube formation ability was observed in HUVECs exposed to

ultrasound compared with untreated cells regardless of exposure length or intensity of ultrasound in this method. PCA showed the only difference seen in tube formation ability was due to the time point of the assay which was also seen in tube formation results in 48 well plates – 24 h results in a reduction in tube formation characteristics measured. However, HUVECs were only assessed immediately after ultrasound exposure as cells begin to undergo apoptosis 24 – 48 h in Matrigel™ culture (Ranta et al., 1998). As a result of this, HUVECs could not be visualised 72 h after ultrasound exposure as in the 48 well plate and viable cell number analysis.

Even though no significant direct effect on tube formation ability was observed, the observations of this study are important for understanding potential cellular effects of miniaturised surgical devices. Exposure of HUVECs to low frequency ultrasound did not significantly inhibit tube formation at any intensity applied. Therefore 45 kHz applied at these intensities will not cause inhibition of angiogenesis which, if it did occur, would be detrimental to the desired post-ultrasonic surgery healing process. Although a significant increase in tube formation ability may be a desirable outcome for stimulating therapeutic angiogenesis, this study showed an increase in the ability to retain tube formation ability for a longer time. This was found in cells seeded 72 h after ultrasound, compared with cells not exposed to ultrasound which was further indication of a delayed response similar to viable cell number results.

The present study examined gene expression using qPCR to identify any responses to the ultrasound exposure at the intracellular level. A notable observation within both DuoSon and tank exposure configurations was the similarity in expression response between *eNOS* and *VWF*. A link between *eNOS* and *VWF* has been reported in literature associating a decrease in

eNOS expression with an increased secretion of *VWF* in renal injury mice models (Nakayama et al., 2010). This association was previously described to occur via the downstream production of NO inhibiting the release of *VWF* from WPBs as demonstrated in human aortic endothelial cells (HAECs) *in vitro* and in *eNOS*-deficient mice *in vivo* by Matsushita et al., (2003). Therefore, it could be expected reduced *eNOS* expression measured in the presented study would coincide with reduced NO synthesis and subsequent increased *VWF* expression and secretion. However gene expression analysis indicated low frequency ultrasound influenced *eNOS* and *VWF* mRNA expression independently of this pathway as both genes exhibited similar expression levels.

A decrease in angiogenesis-related gene expression was measured following ultrasound exposure in both DuoSon and tank configurations. Such effects on expression levels appeared to be a time-dependent response. The decrease in gene expression following DuoSon exposure was also dependent on the intensity delivered. Lower intensities (10 mW/cm^2) appeared to have a delayed effect in reducing gene expression with moderate decreases seen after 72 h. Whereas the highest intensity (75 mW/cm^2) resulted in reduced gene expression at earlier time points 6 h and 24 h after ultrasound exposure and by 72 h gene expression levels were comparable with untreated cells. Overall following DuoSon exposure, a downregulation of genes, notably *eNOS* and *VWF*, occurred 6 h and 24 h after ultrasound exposure with *eNOS* expression significantly decreased 6 h after 75 mW/cm^2 exposure compared with untreated cells. Gene expression levels measured 72 h after ultrasound exposure were comparable with untreated cells. Interestingly, gene expression was downregulated at the later time point 72 h after ultrasound exposure in the tank system with comparable expression levels with untreated cells measured at 6 h and 24 h. This difference in response could be seen most clearly in the

expression levels of *eNOS*. In both exposure systems, *eNOS* was significantly downregulated in ultrasound exposed cells. However, following 75 mW/cm^2 DuoSon exposure, significant downregulation was measured 6 h after ultrasound whereas significant downregulation was measured 72 h after ultrasound exposure in the tank system.

The difference in time of response poses an interesting question on the intracellular responses to mechanical stimuli such as ultrasound. A possible reason for this contrast in response time maybe, as mentioned before, due to the difference in ultrasonic energy delivered to the cells. Subsequently, the mechanical effects on the HUVEC monolayer may differ causing varying intracellular responses.

Such mechanical effects can alter cell morphology as discussed. Therefore the F-actin observations in this present study may provide further insight to the difference in *eNOS* expression responses. F-actin staining was not undertaken 6 h after DuoSon to observe morphological effects in HUVECs. However no significant morphological changes were observed 24 h or 72 h after DuoSon US, neither were any significant gene expression changes measured at these time points. Conversely, 72 h after ultrasound exposure in the tank system, some HUVECs were observed with irregular cell morphology. The “cobblestone” polygonal cell shape was not as apparent. The cell aggregations were undefined and on occasion elongated cell bodies were observed. At this time point, there was a significant decrease in *eNOS* activity measured. Changes in cell shape result in changes to intracellular responses via mechanotransduction (Haftbaradaran Esfahani & Knöll, 2020), which may be one of the factors affecting *eNOS* expression. Mechanotransduction is the process by which mechanical stimuli are sensed by cells and converted into intracellular biochemical responses by various

force-sensitive cell surface molecules (Dahl et al., 2008). For example, endothelial cells are subject to shear stress due to blood flow causing changes in the cell morphology and membrane resulting in intracellular responses (Li et al., 2005). Such changes in morphology caused by low intensity ultrasound have been implicated in the remodelling of chromatin in fibroblasts and chondrocytes (Noriega et al., 2012). Changes in chromatin organisation can influence gene expression by altering the accessibility of transcription factors and RNA polymerase to the target DNA sequence (Phillips, 2008). Shear stress can also be produced *in vitro* by exposure of endothelial cells to ultrasound (vanBavel, 2007). Whilst some studies have shown shear stress causes upregulation *eNOS* expression (Malek et al., 1999; Moore et al., 2010; Weber et al., 2005), oscillatory shear stress has resulted in a decrease in *eNOS* mRNA expression in HUVECs (Ziegler et al., 1998). Such oscillatory shear stress can be caused by microstreaming effects of ultrasound. Low shear stress levels have also resulted in decreased *eNOS* expression compared with exposure to high shear stress levels (Zhang et al., 2016b) which may be concurrent with the low frequency and intensity ultrasound deployed in the present study.

A change to the cytoskeleton of an endothelial cell specifically has been reported to attenuate *eNOS* activity (Govers & Rabelink, 2001). This may be due to the direct interaction between the actin components and *eNOS* mRNA (Searles et al., 2004). Therefore there is a suggestion that mechanical forces on the HUVEC membrane due to ultrasound exposure resulted in the significant reduction in *eNOS* expression in the present study. However, *eNOS* regulation is a complex process dependent on mRNA expression, mRNA stability and post transcriptional processes as described in Section 1.2.3.2. Though it is acknowledged that the influence on the endothelial cell membrane may impact multiple *eNOS* activation pathways via numerous

mechanoreceptors present in the endothelial cell membrane (Chatterjee & Fisher, 2014). Further experimentation is needed to test the hypothesis of alterations to endothelial cell membrane and actin organisation caused by mechanical forces exerted on the cell monolayer caused downregulation in *eNOS* expression.

The reduced expression of *eNOS* observed in the present study may also explain the effect seen in HUVEC tube formation ability after ultrasound exposure. When measured immediately and 24 h after ultrasound, the tube length of HUVECs was slightly decreased compared with untreated cells and the ability to sustain tube formation after 24 h in Matrigel^{TM} was significantly decreased. This may correspond with the reduced levels of *eNOS* expression at these earlier time points. Conversely, 72 h after ultrasound, HUVECs were able to retain tube formation ability at the 24 h imaging time point compared with untreated cells. There was also a moderately greater number of branches measured at this later timepoint in all treated cells compared with untreated cells. These observations may be a result of the recovered levels of *eNOS* expression 72 h after ultrasound. These results suggest the observations of tube formation behaviour are related to the intracellular activity, specifically the *eNOS* pathway of HUVECs. This suggestion is supported in literature reporting a reduction in the tube formation ability of *eNOS* deficient endothelial cells *in vitro* (Bu et al., 2022a; Zhao et al., 2002). These observations could be explained by the role of *eNOS* in tip cell selection and migration (Priya et al., 2015). Therefore, the downregulation of *eNOS* seen in the presented study and previously reported research may be due to an inhibition on tip cell selection and subsequent sprouting ability.

The reduction in *eNOS* gene expression observed in the present study was surprising as it differs from other literature reporting an increase in angiogenesis-related gene expression following low intensity ultrasound exposure (Altland et al., 2004; Huang et al., 2015; Sahni et al., 2024). However, there are other reports observing an inhibition in *eNOS* expression in HUVEC cell line EA-hy-926 following exposure to low shear stress and oscillatory shear stress (Ziegler et al., 1998). Differences in endothelial cell responses to ultrasound reported once again highlight the complexity of intracellular response to varying mechanical stimuli. This area merits further research, especially in understanding biological effects of ultrasonic surgical devices on the surrounding hard and soft tissues. Interestingly, a recent study (Bu et al., 2022b) demonstrated a loss of *eNOS* was not only associated with a reduction in tube formation ability, as mentioned, but a significant increase in cell proliferation. The authors of this study found this observation surprising due to the disagreement with previously reported observations associating an activation of *eNOS* to increased endothelial cell proliferation and migration via the PI3K-Akt pathway and release of NO (Chen et al., 2008; Namkoong et al., 2005). Observations in the present study appear to align with Bu et al,. (2022b) findings of decreased *eNOS* expression associated with no inhibitory effect on HUVEC survival and apparent increase in proliferation. Therefore, a down regulation of *eNOS* does not unequivocally indicate an inhibition of angiogenesis as a loss of *eNOS* function can induce endothelial cell proliferation and migration - hallmarks of angiogenesis. Such conflicting reports in the literature highlights the need for more understanding in the downstream effects of *eNOS* and complex molecular processes involved in endothelial cell behaviour and angiogenesis.

4.3 Clinical importance of the presented findings

The findings of this study may be translated to the clinical situation. When using the 45 kHz ultrasonic DuoSon there was no significantly detrimental effect on HUVEC viability or tube formation ability. Therefore there is unlikely to be such a detrimental effect of the ultrasound from a 45 kHz surgical instrument on the wound healing process. Maintaining endothelial cell viability, in addition to significant increased cell number as seen in DuoSon experimentation or moderate increases seen in the tank configuration, indicates a supportive and proangiogenic effect. Endothelial cells are crucial is all phases of wound healing: inflammation, proliferation and remodelling (Cañedo-Dorantes & Cañedo-Ayala, 2019). Therefore demonstrating cell viability is maintained for at least 72 h in this study, with moderate to significant increase in cell number, strongly suggests sustained support and potential enhancement of the healing process after the initial use of 45 kHz surgical devices.

Although a significant proangiogenic response was not seen in this study with regards to tube formation, increased tube integrity was seen 72 h after ultrasonic treatment. This may suggest 45 kHz may lead to more stable and mature vessels *in vivo*. A decrease in mature, stable vessels results in less efficient or lack of nutrient and oxygen delivery, ultimately delaying the repair process (Johnson & Wilgus, 2014). Delays to surgical wound healing places heavy financial burden on the NHS and on the patient's quality of life (Section 1.3.2). Therefore, demonstrating an increase in tube integrity that could support correct wound healing without significant interference in the overall process is an important and interesting finding. Although further work is needed to investigate the hypothesis of increased tube integrity following 45 kHz ultrasound exposure, for example in the standardised tank system

developed in this study, these results are a promising step into discovering the effect ultrasonic devices have on post-surgical wound healing.

Although there was no direct stimulation of tube formation within the set of experiments presented, this lack of stimulatory effect may be desirable for specific 45 kHz ultrasonic devices. For example, the aim of tumour resection surgery is the safe removal of all or part of the cancerous tissue, however there is always a risk of residual cancer cells remaining after resection. The finding that 45 kHz does not stimulate tube formation *in vitro* may suggest safe deployment of ultrasonic devices driven at this frequency in tumour resection procedures. This is due to the potentially reduced risk of residual tumour cell stimulation to an angiogenic state which, if occurs, could lead to tumour regrowth, vascularisation and metastasis (Atkin & Chopada, 2006).

The decreased risk of unregulated angiogenesis whilst maintaining tube integrity is important in other clinical settings such as ophthalmic surgery. Ocular angiogenesis can lead to the production of dysfunctional, immature, leaky vessels that can lead to a number of eye disorders such as age-related macular degeneration (AMD) and diabetic retinopathy and can ultimately cause complete sight loss (Sapieha et al., 2010). The present study suggests 45 kHz does not significantly stimulate the formation of "capillary-like" tubes *in vitro* but also leads to increased tube integrity; hallmarks of supporting stable wound healing processes essential for post-ophthalmic surgical healing. Phacoemulsification is a technique used in cataract surgery that uses ultrasound energy to emulsify and aspirate the cataractous lens allowing replacement with an artificial intraocular lens (Linebarger et al., 1999). Phacoemulsification devices are driven between 35 and 45 kHz, efficient frequencies for nuclear emulsification

(Packer et al., 2005). Therefore, the presented findings of no significant stimulation of tube formation *in vitro* add further support to the use of devices at the highest range of 45 kHz regarding the biological safety of such surgeries.

Overall the work presented in this study is important for understanding and following important for safety guidelines in ultrasonic device design and subsequent use in a range of surgical procedures.

4.4 Further work

Further specific studies into the angiogenic response of HUVECs after ultrasound exposure in the tank configuration would include the following:

- Investigate the tube formation ability following ultrasound delivery in the acoustic absorbing tank. Optimisation steps would have to be undertaken to develop a protocol of exposing HUVECs onto Matrigel^{TM}-coated CLINIcell® cassettes. The method of introducing media into the CLINIcell® cassette may pose a problem for the viscous, temperature-sensitive Matrigel^{TM} solution. Matrigel^{TM} must be kept cool during the coating stage as it begins to solidify and adhere to any surface when at room temperature. It may be difficult to keep the Matrigel^{TM} at such a temperature whilst adding to a syringe and injecting via the Luer lock valves system. There may be warming to room temperature of some areas within the cassette that could hinder the even distribution of Matrigel^{TM}.
- Investigate the angiogenic response further using migration and wound healing assays. A scratch wound assay can be used following ultrasound exposure in the tank system by seeding exposed cells and creating a scratch, or by using ultrasound-conditioned

media to culture cells and assess wound closure compared with unconditioned media. However the issue remains to develop a method to perform this assay directly after tank exposure which will have to be optimised.

The regulation of *eNOS* mRNA expression is highly complex involving transcriptional, posttranscriptional and posttranslational protein interactions. Therefore, further investigation into other factors influenced by *eNOS* activity is necessary to gain more understanding of the molecular pathways involved in *eNOS* regulation, downstream effects and ultimately the response to 45 kHz ultrasound:

- *eNOS* protein activity can be affected by post-translational modifications not only effects on mRNA expression. Activation of *eNOS* is related to its phosphorylation which can be measured using western blot techniques. However phosphorylation does not strictly result in activation, it is dependent on the specific site of phosphorylation that can cause activation or inhibition. As a result, *eNOS* activity cannot be solely determined by phosphorylation measurements but it is a necessary analysis to increase understanding.
- Further investigation into effects on *eNOS* activity can be assessed through the enzyme's production of NO. NO levels are directly proportional to *eNOS* activity as the enzyme catalyses the oxidation of L-arginine to L-citrulline and NO (Förstermann & Münzel, 2006). Levels of NO produced in the cEGM after ultrasound exposure can be measured *in* using a nitric oxide colorimetric assay.
- An interesting post-transcriptional interaction to research is the association of *eNOS* with the actin cytoskeleton. As ultrasound applies mechanical forces on cell membranes, there is a suggestion that this will affect the actin cytoskeleton, which

ultimately can affect *eNOS* expression and activity. Measuring the ratio of the monomer G-actin to its polymer F-actin would identify an effect of remodelling caused by ultrasound treatment. This could impact *eNOS* activity as association with G-actin has been shown to cause a greater increase in *eNOS* activity than association with F-actin (Su et al., 2003). Immunocytochemistry of *eNOS* and both G-actin and F-actin will provide a visualisation to the protein-protein interaction and any possible effects ultrasound exposure may exert on *eNOS* localisation in HUVECs.

The exposure systems in this study may not directly mimic *in vivo* responses due to the presence of varying wave attenuation coefficients in the human body. However, the initial *in vitro* results described provide new findings in the HUVEC response to low frequency ultrasound. Further work is necessary to determine if such low frequency ultrasound produces a cellular response in an environment more indicative of *in vivo* conditions:

- HUVECs can be cocultured with a variety of cell types to investigate how ultrasound effects cell-cell interactions and processes. Coculturing with fibroblasts can be used to study vascularisation (Costa-Almeida et al., 2014; Sukmana & Vermette, 2010) and tissue regeneration (Fujita et al., 2023; Nakatsu et al., 2003). Investigations into osteogenesis and angiogenesis crosstalk following ultrasound exposure to analyse tissue healing can also be studied through osteoblast (Jabbarzadeh et al., 2008; Ma et al., 2011) and mesenchymal stem cell coculture (Chen et al., 2018; Kang et al., 2013).
- 3-D culture techniques also provide a culture environment more mimicking of *in vivo* conditions. 3-D scaffold/matrix-based techniques use biomaterials such as collagen (type I), gelatin methacrylate (GelMA) and Matrigel^{TM} among others, to provide structural support for HUVEC growth and vascular growth. Optimisation experiments

would be needed to investigate the plausibility of coating CLINIcell® cassettes with such material and exposing to ultrasound in the tank configuration.

- A form of hydrogel that has been used to mimic tissue for *in vitro* ultrasound studies is agar-based gel phantoms. Agar phantoms can be modified to mimic specific tissue properties such as stiffness and attenuation coefficient by altering the concentration of agar and additional additives (Drakos et al., 2021). Such methods can be integrated into the acoustic absorbing tank system by positioning the agar between the transducer and CLINIcell® cassette.

Chapter 5.

CONCLUSIONS

The work presented in this thesis investigated the response of endothelial cells to low frequency kHz ultrasound and any subsequent effect on angiogenesis. For this purpose, a newly developed *in vitro* setup was established and characterised for such *in vitro* cell culture ultrasonic experimentations and compared with a previously in-house developed *in vitro* set-up using the DuoSon device. The findings of this research highlighted the potential of kHz ultrasound to directly impact on human endothelial cells and angiogenesis as summarised below:

- The study demonstrated a direct and visible effect of ultrasound on HUVEC morphology via F-actin staining. Elongation and cell clustering was observed in some instances following ultrasound exposure, most prominently following exposure in the tank configuration rather than the DuoSon configuration.
- The presented work also showed 45 kHz ultrasound was not damaging to HUVEC viability, rather, the ultrasound exposure resulted in an increase in viable cell number. This increase was measured as significant following DuoSon exposure and appeared to be a time-dependent response, resulting in significant effect 72 h after ultrasound exposure.
- Tube formation analysis revealed no direct significant effect on tube length or number of branches measured following ultrasound exposure. However, a potential ability of HUVECs to retain tube formation behaviour for longer periods after 45 kHz ultrasonic exposure was observed.
- The cellular responses observed may be a result of the effect seen in HUVEC gene expression. In both exposure systems utilised in this study, the expression of *eNOS*, a key regulator of cellular function and sprouting angiogenesis, was significantly

downregulated. This strongly indicates an effect on the *eNOS* pathway following 45 kHz ultrasonic exposure.

- This work emphasised the influence experimental configurations have on cellular responses. Slight differences were found in endothelial cell morphology, cell number and gene expression measurements when comparing cellular response following DuoSon and acoustic absorbing tank ultrasound configurations.

In conclusion, the present study adds to the literature on biological effects of ultrasound and describes a standardised ultrasonic exposure system for cells. The work presented in the study has demonstrated a time and dose-dependent endothelial cell response to low frequency continuous wave ultrasound. Though the hypothesis of a pro-angiogenic response was not observed in all experiments undertaken, as a decrease in *eNOS* and no significant increase in tube formation *in vitro* were measured, exposure at multiple intensities of 45 kHz ultrasound did not significantly inhibit the angiogenic ability of endothelial cells. Therefore these results suggest 45 kHz does not significantly inhibit the wound healing process of HUVECs *in vitro*. This is of potential clinical importance as it suggests ultrasonic surgical devices resonating at 45 kHz will not significantly impair the post-surgical wound healing process.

Finally, this study has also provided a robust, standardised *in vitro* ultrasound exposure system with minimal interference from configuration limitations such as thermal instability or reflection interference. The acoustic absorbing tank system may be used for a range of cell types and ultrasound parameters allowing researchers to understand the many complex biological effects of low frequency ultrasound. This research will aid the development and ultimately the application of therapeutic or surgical ultrasonic clinical devices.

Chapter 6.

REFERENCES

Adair, T. H., & Montani, J. P. (2010). In *Angiogenesis*. https://www.ncbi.nlm.nih.gov/pubmed/21452444

Al-Maswary, A. A., Walmsley, A. D., Cooper, P. R., & Scheven, B. A. (2024). Low-intensity pulsed ultrasound induces proliferation of human neural stem cells. *Clinical and Translational Discovery*, *4*(2), e259. https://doi.org/10.1002/ctd2.259

Altland, O., Dalecki, D., Suchkova, V., & Francis, C. (2004). Low-intensity ultrasound increases endothelial cell nitric oxide synthase activity and nitric oxide synthesis. *Journal of Thrombosis and Haemostasis*, *2*(4), 637-643. https://doi.org/10.1111/j.1538-7836.2004.00655.x

Ariani, M., Fishbein, M. C., Chae, J. S., Sadeghi, H., Michael, A. D., Dubin, S., & Siegel, R. (1991). Dissolution of peripheral arterial thrombi by ultrasound. *Circulation*, *84*(4), 1680-1688. https://doi.org/10.1161/01.CIR.84.4.1680

Aro, H., Kallioniemi, H., Aho, A., & Kellokumpu-Lehtinen, P. (1981). Ultrasonic device in bone cutting: A histological and scanning electron microscopical study. *Acta Orthopaedica Scandinavica*, *52*(1), 5-10. https://doi.org/10.3109/17453678108991750

Atkin, G. K., & Chopada, A. (2006). Tumour angiogenesis: the relevance to surgeons. *Annals of the Royal College of Surgeons of England*, *88*(6), 525–529. https://doi.org/10.1308/003588406X117106

Balamuth, L. (1963). Ultrasonics and dentistry. *Sound: Its uses and control*, *2*(2), 15-19. https://doi.org/10.1121/1.2369595

Bates, D. O., & Harper, S. J. (2002). Regulation of vascular permeability by vascular endothelial growth factors. *Vascular Pharmacology*, *39*(4-5), 225–237. https://doi.org/10.1016/s1537-1891(03)00011-9

Blanco, R., & Gerhardt, H. (2013). VEGF and Notch in tip and stalk cell selection. *Cold Spring Harbor Perspectives in Medicine*, *3*(1), a006569. https://doi.org/10.1101/cshperspect.a006569

Boluriaan, S., & Morris, P. J. (2003). Acoustic streaming: from Rayleigh to today. *International Journal of Aeroacoustics*, *2*(3), 255-292. https://doi.org/10.1260/147547203322986

Bradnock, B., Law, H. T., & Roscoe, K. (1996). A quantitative comparative assessment of the immediate response to high frequency ultrasound and low frequency ultrasound ('longwave therapy') in the treatment of acute ankle sprains. *Physiotherapy*, *82*(2), 78-84. https://doi.org/10.1016/S0031-9406(05)66955-6

Bredt, D. S., & Snyder, S. H. (1992). Nitric oxide, a novel neuronal messenger. *Neuron*, *8*(1), 3-11. https://doi.org/10.1016/0896-6273(92)90104-l

Bu, S., Nguyen, H. C., Nikfarjam, S., Michels, D. C., Rasheed, B., Maheshkumar, S., Singh, S., & Singh, K. K. (2022a). Endothelial cell-specific loss of eNOS differentially affects

endothelial function. *PLoS One*, *17*(9), e0274487. https://doi.org/10.1371/journal.pone.0274487

Bu, S., Nguyen, H. C., Nikfarjam, S., Michels, D. C., Rasheed, B., Ramesh, S., Patel, D., Patel, M., Singh, S., & Frisbee, J. (2022b). Loss of eNOS in Endothelial Cells Promotes Proliferation. *The Federation of American Societies for Experimental Biology Journal*, *36*. https://doi.org/10.1096/fasebj.2022.36.S1.L7652

Burri, P. H., & Tarek, M. R. (1990). A novel mechanism of capillary growth in the rat pulmonary microcirculation. *The Anatomical Record*, *228*(1), 35-45. https://doi.org/10.1002/ar.1092280107

Buschmann, I., & Schaper, W. (1999). Arteriogenesis Versus Angiogenesis: Two Mechanisms of Vessel Growth. *News in Physiological Sciences*, *14*, 121-125. https://doi.org/10.1152/physiologyonline.1999.14.3.121

Bustin, S. A., Benes, V., Garson, J. A., Hellemans, J., Huggett, J., Kubista, M., Mueller, R., Nolan, T., Pfaffl, M. W., Shipley, G. L., Vandesompele, J., & Wittwer, C. T. (2009). The MIQE Guidelines: Minimum Information for Publication of Quantitative Real-Time PCR Experiments. *Clinical Chemistry*, *55*(4), 611-622. https://doi.org/10.1373/clinchem.2008.112797

Caduff, J. H., Fischer, L. C., & Burri, P. H. (1986). Scanning electron microscope study of the developing microvasculature in the postnatal rat lung. *The Anatomical Record*, *216*(2), 154-164. https://doi.org/10.1002/ar.1092160207

Cañedo-Dorantes, L., & Cañedo-Ayala, M. (2019). Skin Acute Wound Healing: A Comprehensive Review. *International Journal of Inflammation*, *2019*, 3706315. https://doi.org/10.1155/2019/3706315

Cao, G., O'Brien, C. D., Zhou, Z., Sanders, S. M., Greenbaum, J. N., Makrigiannakis, A., & DeLisser, H. M. (2002). Involvement of human PECAM-1 in angiogenesis and in vitro endothelial cell migration. *American Journal of Physiology-Cell Physiology*, *282*(5), C1181-1190. https://doi.org/10.1152/ajpcell.00524.2001

Carano, R. A., & Filvaroff, E. H. (2003). Angiogenesis and bone repair. *Drug Discovery Today*, *8*(21), 980-989. https://doi.org/10.1016/s1359-6446(03)02866-6

Carmeliet, P., & Jain, R. K. (2000). Angiogenesis in cancer and other diseases. *Nature*, *407*(6801), 249-257. https://doi.org/10.1038/35025220

Carmeliet, P., & Jain, R. K. (2011). Molecular mechanisms and clinical applications of angiogenesis. *Nature*, *473*(7347), 298-307. https://doi.org/10.1038/nature10144

Carpentier, G. (2012). Contribution: angiogenesis analyzer. *ImageJ News*, *5*(1).

Cébe-Suarez, S., Zehnder-Fjällman, A., & Ballmer-Hofer, K. (2006). The role of VEGF receptors in angiogenesis;: complex partnerships. *Cellular and Molecular Life Sciences*, *63*(5), 601-615. https://doi.org/10.1007/s00018-005-5426-3

Chatterjee, S., & Fisher, A. B. (2014). Mechanotransduction in the endothelium: role of membrane proteins and reactive oxygen species in sensing, transduction, and transmission of the signal with altered blood flow. *Antioxidants & Redox Signaling*, *20*(6), 899-913. https://doi.org/10.1089/ars.2013.5624

Chau, T. C. Y., Keyser, M. S., Da Silva, J. A., Morris, E. K., Yordanov, T. E., Duscyz, K. P., Paterson, S., Yap, A. S., Hogan, B. M., & Lagendijk, A. K. (2022). Dynamically regulated focal adhesions coordinate endothelial cell remodelling in developing vasculature. *Development*, *149*(23). https://doi.org/10.1242/dev.200454

Chaussy, C., Brendel, W., & Schmiedt, E. (1980). Extracorporeally induced destruction of kidney stones by shock waves. *Lancet*, *2*(8207), 1265-1268. https://doi.org/10.1016/s0140-6736(80)92335-1

Chen, C. H., Hung, H. S., & Hsu, S. h. (2008). Low-energy laser irradiation increases endothelial cell proliferation, migration, and eNOS gene expression possibly via PI3K signal pathway. *Lasers in Surgery and Medicine: The Official Journal of the American Society for Laser Medicine and Surgery*, *40*(1), 46-54. https://doi.org/10.1002/lsm.20589

Chen, W., Liu, X., Chen, Q., Bao, C., Zhao, L., Zhu, Z., & Xu, H. H. K. (2018). Angiogenic and osteogenic regeneration in rats via calcium phosphate scaffold and endothelial cell co-culture with human bone marrow mesenchymal stem cells (MSCs), human umbilical cord MSCs, human induced pluripotent stem cell-derived MSCs and human embryonic stem cell-derived MSCs. *Journal of Tissue Engineering and Regenerative Medicine*, *12*(1), 191–203. https://doi.org/10.1002/term.2395

Chen, Z. Z., Pei, Z. C., Zhao, X., Zhang, J. H., Wei, J. J., & Hao, N. J. (2022). Acoustic microreactors for chemical engineering. *Chemical Engineering Journal*, *433*. https://doi.org/10.1016/j.cej.2021.133258

Claes, L., & Willie, B. (2007). The enhancement of bone regeneration by ultrasound. *Progress in Biophysics and Molecular Biology*, *93*(1-3), 384-398. https://doi.org/10.1016/j.pbiomolbio.2006.07.021

Cleary, R., Li, X., & Lucas, M. (2021). Incorporating direct metal laser sintered complex shaped Ti-6Al-4V components in ultrasonic surgical devices. *Journal of the Acoustical Society of America*, *150*(3), 2163-2173. https://doi.org/10.1121/10.0006379

Costa-Almeida, R., Gomez-Lazaro, M., Ramalho, C., Granja, P. L., Soares, R., & Guerreiro, S. G. (2015). Fibroblast-endothelial partners for vascularization strategies in tissue engineering. *Tissue Engineering. Part A*, *21*(5-6), 1055–1065. https://doi.org/10.1089/ten.TEA.2014.0443

D'Ettorre, C., Mariani, A., Stilli, A., y Baena, F. R., Valdastri, P., Deguet, A., Kazanzides, P., Taylor, R. H., Fischer, G. S., & DiMaio, S. P. (2021). Accelerating surgical robotics research: A review of 10 years with the da Vinci research kit. *IEEE Robotics & Automation Magazine*, *28*(4), 56-78. https://doi.org/10.1109/MRA.2021.3101646

Dahl, K. N., Ribeiro, A. J., & Lammerding, J. (2008). Nuclear shape, mechanics, and mechanotransduction. *Circulation Research*, *102*(11), 1307-1318. https://doi.org/10.1161/CIRCRESAHA.108.173989

Davis, G. E., & Camarillo, C. W. (1996). An alpha 2 beta 1 integrin-dependent pinocytic mechanism involving intracellular vacuole formation and coalescence regulates capillary lumen and tube formation in three-dimensional collagen matrix. *Experimental Cell Research*, *224*(1), 39–51. https://doi.org/10.1006/excr.1996.0109

Dayton, P., Klibanov, A., Brandenburger, G., & Ferrara, K. (1999). Acoustic radiation force in vivo: a mechanism to assist targeting of microbubbles. *Ultrasound in Medicine & Biology*, *25*(8), 1195-1201. https://doi.org/10.1016/s0301-5629(99)00062-9

De Smet, F., Segura, I., De Bock, K., Hohensinner, P. J., & Carmeliet, P. (2009). Mechanisms of vessel branching: filopodia on endothelial tip cells lead the way. *Arteriosclerosis, Thrombosis, and Vascular Biology*, *29*(5), 639-649. https://doi.org/10.1161/ATVBAHA.109.185165

DeCicco-Skinner, K. L., Henry, G. H., Cataisson, C., Tabib, T., Gwilliam, J. C., Watson, N. J., Bullwinkle, E. M., Falkenburg, L., O'Neill, R. C., & Morin, A. (2014). Endothelial cell tube formation assay for the in vitro study of angiogenesis. *Journal of Visualized Experiments: JoVE,* (91), e51312. https://doi.org/10.3791/51312

DeLisser, H. M., ChristofidouSolomidou, M., Strieter, R. M., Burdick, M. D., Robinson, C. S., Wexler, R. S., Kerr, J. S., Garlanda, C., Merwin, J. R., Madri, J. A., & Albelda, S. M. (1997). Involvement of endothelial PECAM-1/CD31 in angiogenesis. *American Journal of Pathology*, *151*(3), 671-677. PMID: 9284815; PMCID: PMC1857836.

Deng, J., Huang, Q., Wang, F., Liu, Y., Wang, Z., Wang, Z., Zhang, Q., Lei, B., & Cheng, Y. (2012). The role of caveolin-1 in blood-brain barrier disruption induced by focused ultrasound combined with microbubbles. *Journal of Molecular Neuroscience : MN*, *46*(3), 677–687. https://doi.org/10.1007/s12031-011-9629-9

DeSanto, J. (2002). Scattering by rough surfaces. In *Scattering* (pp. 15-36). Elsevier. https://doi.org/10.1016/B978-012613760-6/50003-6

Dimmeler, S., & Zeiher, A. M. (1999). Nitric oxide–an endothelial cell survival factor. *Cell Death & Differentiation*, *6*(10), 964-968. https://doi.org/10.1038/sj.cdd.4400581

DiPietro, L. A. (2016). Angiogenesis and wound repair: when enough is enough. *Journal of Leucocyte Biology*, *100*(5), 979-984. https://doi.org/10.1189/jlb.4MR0316-102R

Doan, N., Reher, P., Meghji, S., & Harris, M. (1999). In vitro effects of therapeutic ultrasound on cell proliferation, protein synthesis, and cytokine production by human fibroblasts, osteoblasts, and monocytes. *Journal of Oral and Maxillofacial Surgery*, *57*(4), 409-419; discussion 420. https://doi.org/10.1016/s0278-2391(99)90281-1

Doherty, J. R., Trahey, G. E., Nightingale, K. R., & Palmeri, M. L. (2013). Acoustic radiation force elasticity imaging in diagnostic ultrasound. *IEEE Transactions on Ultrasonics,*

Ferroelectrics, and Frequency Control, *60*(4), 685-701. https://doi.org/10.1109/TUFFC.2013.2617

Doinikov, A. A. (2003). Acoustic radiation forces: Classical theory and recent advances. *Recent Research Developments in Acoustics*, *1*, 39-67. https://doi.org/10.1017/S0022112094001096

Donald, I., Macvicar, J., & Brown, T. (1958). Investigation of abdominal masses by pulsed ultrasound. *The Lancet*, *271*(7032), 1188-1195. https://doi.org/10.1016/s0140-6736(58)91905-6

Drakos, T., Antoniou, A., Evripidou, N., Alecou, T., Giannakou, M., Menikou, G., Constantinides, G., & Damianou, C. (2021). Ultrasonic Attenuation of an Agar, Silicon Dioxide, and Evaporated Milk Gel Phantom. *Journal of Medical Ultrasound*, *29*(4), 239–249. https://doi.org/10.4103/JMU.JMU_145_20

Dunn, F., & Fry, W. J. (1961). Ultrasonic absorption and reflection by lung tissue. *Physics in Medicine & Biology*, *5*(4), 401. https://doi.org/10.1088/0031-9155/5/4/302

Dupré, L., & Prunier, G. (2023). Deciphering actin remodelling in immune cells through the prism of actin-related inborn errors of immunity. *European Journal of Cell Biology*, *102*(1), 151283. https://doi.org/10.1016/j.ejcb.2022.151283

Duran, C. L., Howell, D. W., Dave, J. M., Smith, R. L., Torrie, M. E., Essner, J. J., & Bayless, K. J. (2017). Molecular Regulation of Sprouting Angiogenesis. *Comprehensive Physiology*, *8*(1), 153–235. https://doi.org/10.1002/cphy.c160048

Dussik, K. (1942). On the possibility of using ultrasound waves as a diagnostic aid. *Neurol Psychiat*, *174*, 153-168.

Duval, M., Bedard-Goulet, S., Delisle, C., & Gratton, J. P. (2003). Vascular endothelial growth factor-dependent down-regulation of Flk-1/KDR involves Cbl-mediated ubiquitination. Consequences on nitric oxide production from endothelial cells. *Journal of Biological Chemistry*, *278*(22), 20091-20097. https://doi.org/10.1074/jbc.M301410200

Dyson, M. (1982). Non-thermal cellular effects of ultrasound. *British Journal of Cancer*, *5*, 165-171. PMID: 6950755

Etame, A. B., Diaz, R. J., Smith, C. A., Mainprize, T. G., Hynynen, K., & Rutka, J. T. (2012). Focused ultrasound disruption of the blood-brain barrier: a new frontier for therapeutic delivery in molecular neurooncology. *Neurosurgical Focus*, *32*(1), E3. https://doi.org/10.3171/2011.10.FOCUS11252

Fang, T. D., Salim, A., Xia, W., Nacamuli, R. P., Guccione, S., Song, H. M., Carano, R. A., Filvaroff, E. H., Bednarski, M. D., Giaccia, A. J., & Longaker, M. T. (2005). Angiogenesis is required for successful bone induction during distraction osteogenesis. *Journal of Bone and Mineral Research*, *20*(7), 1114-1124. https://doi.org/10.1359/Jbmr.050301

Fantinati, M. S., Mendonca, D. E., Fantinati, A. M., Santos, B. F., Reis, J. C., Afonso, C. L., Vinaud, M. C., & Lino Rde, S. J. (2016). Low intensity ultrasound therapy induces

angiogenesis and persistent inflammation in the chronic phase of the healing process of third degree burn wounds experimentally induced in diabetic and non-diabetic rats. *Acta Cirúrgica Brasileira*, *31*(7), 463-471. https://doi.org/10.1590/S0102-865020160070000006

Favaloro, R. G. (1998). Critical analysis of coronary artery bypass graft surgery: a 30-year journey. *Journal of the American College of Cardiology*, *31*(4S2), 1B-63B. https://doi.org/10.1016/s0735-1097(97)00559-7

Ferguson, C., Alpern, E., Miclau, T., & Helms, J. A. (1999). Does adult fracture repair recapitulate embryonic skeletal formation? *Mechanisms of Development*, *87*(1-2), 57-66. https://doi.org/10.1016/S0925-4773(99)00142-2

Ferrara, N. (2004). Vascular endothelial growth factor: Basic science and clinical progress. *Endocrine Reviews*, *25*(4), 581-611. https://doi.org/10.1210/er.2003-0027

Ferrara, N., & Davis-Smyth, T. (1997). The biology of vascular endothelial growth factor. *Endocrine Reviews*, *18*(1), 4-25. https://doi.org/10.1210/er.18.1.4

Fledelius, H. C. (1997). Ultrasound in ophthalmology. *Ultrasound in Medicine & Biology*, *23*(3), 365-375. https://doi.org/10.1016/S0301-5629(96)00213-X

Fleming, I., & Busse, R. (2003). Molecular mechanisms involved in the regulation of the endothelial nitric oxide synthase. *American Journal of Physiology-Regulatory, Integrative and Comparative Physiology*, *284*(1), R1-R12. https://doi.org/10.1152/ajpregu.00323.2002

Fletcher, D. A., & Mullins, D. (2010). Cell mechanics and the cytoskeleton. *Nature*, *463*(7280), 485-492. https://doi.org/10.1038/nature08908

Folkman, J., & Shing, Y. (1992). Angiogenesis. *Journal of Biological Chemistry*, *267*(16), 10931-10934. PMID: 1375931.

Förstermann, U., & Münzel, T. (2006). Endothelial nitric oxide synthase in vascular disease: from marvel to menace. *Circulation*, *113*(13), 1708–1714. https://doi.org/10.1161/CIRCULATIONAHA.105.602532

Fraker Jr, T. D., Fihn, S. D., Committee, W. o. b. o. t. C. S. A. W., Members, W. C., Gibbons, R. J., Abrams, J., Chatterjee, K., Daley, J., Deedwania, P. C., & Douglas, J. S. (2007). 2007 chronic angina focused update of the ACC/AHA 2002 guidelines for the management of patients with chronic stable angina: a report of the American College of Cardiology/American Heart Association Task Force on Practice Guidelines Writing Group to develop the focused update of the 2002 guidelines for the management of patients with chronic stable angina. *Circulation*, *116*(23), 2762-2772. https://doi.org/10.1016/j.jacc.2007.08.002

Fujita, T., Yuki, T., & Honda, M. (2023). The construction of a microenvironment with the vascular network by co-culturing fibroblasts and endothelial cells. *Regenerative Therapy*, 25, 138–146. https://doi.org/10.1016/j.reth.2023.12.004

Gao, Q., Walmsley, A. D., Cooper, P. R., & Scheven, B. A. (2016). Ultrasound stimulation of different dental stem cell populations: role of mitogen-activated protein kinase signaling. *Journal of Endodontics*, *42*(3), 425-431. https://doi.org/10.1016/j.joen.2015.12.019

Gerhardt, H., Golding, M., Fruttiger, M., Ruhrberg, C., Lundkvist, A., Abramsson, A., Jeltsch, M., Mitchell, C., Alitalo, K., Shima, D., & Betsholtz, C. (2003). VEGF guides angiogenic sprouting utilizing endothelial tip cell filopodia. *The Journal of Cell Biology*, *161*(6), 1163–1177. https://doi.org/10.1083/jcb.200302047

Gerner, E. W., Boone, R., Connor, W. G., Hicks, J. A., & Boone, M. L. (1976). A transient thermotolerant survival response produced by single thermal doses in HeLa cells. *Cancer Research*, *36*(3), 1035–1040. PMID: 1253166.

Ghorayeb, S. R., Patel, U. S., Walmsley, A. D., & Scheven, B. A. (2013). Biophysical characterization of low-frequency ultrasound interaction with dental pulp stem cells. *Journal of Therapeutic Ultrasound*, *1*, 12. https://doi.org/10.1186/2050-5736-1-12

Goodson, H. V., & Hawse, W. F. (2002). Molecular evolution of the actin family. *Journal of Cell Science*, *115*(13), 2619-2622. https://doi.org/10.1242/jcs.115.13.2619

Gordon, J. D., Shifren, J. L., Foulk, R. A., Taylor, R. N., & Jaffe, R. B. (1995). Angiogenesis in the human female reproductive tract. *Obstetrical & Gynecological Survey*, *50*(9), 688-697. https://doi.org/10.1097/00006254-199509000-00024

Govers, R., & Rabelink, T. J. (2001). Cellular regulation of endothelial nitric oxide synthase. *American Journal of Physiology-Renal Physiology*, *280*(2), F193-F206. https://doi.org/10.1152/ajprenal.2001.280.2.F193

Granger, D. N., & Senchenkova, E. (2010). *Inflammation and the Microcirculation*. San Rafael (CA): Morgan & Claypool Life Sciences. PMID: 21452440.

Gruntzig, A. (1978). Trans-Luminal Dilatation for Coronary-Artery Stenosis - Reply. *Lancet*, *1*(8073), 1093-1093. https://doi.org/10.1016/S0003-4975(10)63764-2

Guest, J. F., Ayoub, N., McIlwraith, T., Uchegbu, I., Gerrish, A., Weidlich, D., Vowden, K., & Vowden, P. (2017). Health economic burden that different wound types impose on the UK's National Health Service. *International Wound Journal*, *14*(2), 322–330. https://doi.org/10.1111/iwj.12603

Guest, J. F., Fuller, G. W., & Vowden, P. (2020). Cohort study evaluating the burden of wounds to the UK's National Health Service in 2017/2018: update from 2012/2013. *British Medical Journal open*, *10*(12), e045253. https://doi.org/10.1136/bmjopen-2020-045253

Gupta, D., Savva, J., Li, X., Chandler, J. H., Shelton, R. M., Scheven, B., Mulvana, H., Valdastri, P., Lucas, M., & Walmsley, A. D. (2022). Traditional multiwell plates and petri dishes limit the evaluation of the effects of ultrasound on cells in vitro. *Ultrasound in Medicine & Biology*, *48*(9), 1745-1761. https://doi.org/10.1016/j.ultrasmedbio.2022.05.001

Habib, R. H., Dimitrova, K. R., Badour, S. A., Yammine, M. B., El-Hage-Sleiman, A. K. M., Hoffman, D. M., Geller, C. M., Schwann, T. A., & Tranbaugh, R. F. (2015). CABG Versus PCI Greater Benefit in Long-Term Outcomes With Multiple Arterial Bypass Grafting. *Journal of the American College of Cardiology*, *66*(13), 1417-1427. https://doi.org/10.1016/j.jacc.2015.07.060

Haftbaradaran Esfahani, P., & Knöll, R. (2020). Cell shape: effects on gene expression and signaling. *Biophysical Reviews*, *12*(4), 895–901. https://doi.org/10.1007/s12551-020-00722-4

Hanawa, K., Ito, K., Aizawa, K., Shindo, T., Nishimiya, K., Hasebe, Y., Tuburaya, R., Hasegawa, H., Yasuda, S., Kanai, H., & Shimokawa, H. (2014). Low-intensity pulsed ultrasound induces angiogenesis and ameliorates left ventricular dysfunction in a porcine model of chronic myocardial ischemia. *PLoS One*, *9*(8), e104863. https://doi.org/10.1371/journal.pone.0104863

Hausman, M. R., Schaffler, M. B., & Majeska, R. J. (2001). Prevention of fracture healing in rats by an inhibitor of angiogenesis. *Bone*, *29*(6), 560-564. https://doi.org/10.1016/S8756-3282(01)00608-1

Heckman, J. D., Ryaby, J. P., McCabe, J., Frey, J. J., & Kilcoyne, R. F. (1994). Acceleration of tibial fracture-healing by non-invasive, low-intensity pulsed ultrasound. J*ournal of Bone and Joint Surgery*, *76*(1), 26-34. https://doi.org/10.2106/00004623-199401000-00004

Heigh, E., Bohman, L., Briskin, G., Slayton, M., Amodei, R., Compton, K., & Baravarian, B. (2019). Intense Therapeutic Ultrasound for Treatment of Chronic Plantar Fasciitis: A Pivotal Study Exploring Efficacy, Safety, and Patient Tolerance. *Journal of Foot and Ankle Surgery*, *58*(3), 519-527. https://doi.org/10.1053/j.jfas.2018.10.002

Heiss, E. H., & Dirsch, V. M. (2014). Regulation of eNOS enzyme activity by posttranslational modification. *Current Pharmaceutical Design*, *20*(22), 3503–3513. https://doi.org/10.2174/13816128113196660745

Hellemans, J., Mortier, G., De Paepe, A., Speleman, F., & Vandesompele, J. (2007). qBase relative quantification framework and software for management and automated analysis of real-time quantitative PCR data. *Genome Biology*, *8*, R19. https://doi.org/10.1186/gb-2007-8-2-r19

Henzi, S., Krayenbühl, N., Bozinov, O., Regli, L., & Stienen, M. N. (2019). Ultrasonic aspiration in neurosurgery: comparative analysis of complications and outcome for three commonly used models. *Acta Neurochirurgica*, *161*(10), 2073–2082. https://doi.org/10.1007/s00701-019-04021-0

Hellström, M., Phng, L. K., Hofmann, J. J., Wallgard, E., Coultas, L., Lindblom, P., Alva, J., Nilsson, A. K., Karlsson, L., Gaiano, N., Yoon, K., Rossant, J., Iruela-Arispe, M. L., Kalén, M., Gerhardt, H., & Betsholtz, C. (2007). Dll4 signalling through Notch1 regulates formation of tip cells during angiogenesis. *Nature*, *445*(7129), 776–780. https://doi.org/10.1038/nature05571

Herve, M. A., Buteau-Lozano, H., Mourah, S., Calvo, F., & Perrot-Applanat, M. (2005). VEGF189 stimulates endothelial cells proliferation and migration in vitro and up-regulates the expression of Flk-1/KDR mRNA. *Experimental Cell Research*, *309*(1), 24-31. https://doi.org/10.1016/j.yexcr.2005.05.022

Holmes, D. I. R., & Zachary, I. (2005). The vascular endothelial growth factor (VEGF) family: angiogenic factors in health and disease. *Genome Biology*, *6*(2), 1-10. https://doi.org/10.1186/gb-2005-6-2-209

Horton, J. E., Tarpley Jr, T. M., & Jacoway, J. R. (1981). Clinical applications of ultrasonic instrumentation in the surgical removal of bone. *Oral Surgery, Oral Medicine, Oral Pathology*, *51*(3), 236-242. https://doi.org/10.1016/0030-4220(81)90051-7

Houser, K. L., & Noschang, S. A. (2018). Ultrasonic surgical shears and method for sealing a blood vessel using same. In: Google Patents.

Huang, J.-J., Shi, Y.-Q., Li, R.-L., Hu, A., Lu, Z.-Y., Weng, L., Han, Y.-P., Wang, S.-Q., Zhang, L., & Hao, C.-N. (2017). Therapeutic ultrasound protects HUVECs from ischemia/hypoxia-induced apoptosis via the PI3K-Akt pathway. *American Journal of Translational Research*, *9*(4), 1990 –1999. PMID: 28469805

Huang, J.-J., Shi, Y.-Q., Li, R.-L., Hu, A., Lu, Z.-Y., Weng, L., Wang, S.-Q., Han, Y.-P., Zhang, L., & Li, B. (2015). Angiogenesis effect of therapeutic ultrasound on HUVECs through activation of the PI3K-Akt-eNOS signal pathway. *American Journal of Translational Research*, *7*(6), 1106 –1115. PMID: 26279754

Huang, J.-J., Shi, Y.-Q., Li, R.-L., Hu, A., Zhou, H.-S., Cheng, Q., Xu, Z., Yang, Z.-M., Hao, C.-N., & Duan, J.-L. (2014). Angiogenesis effect of therapeutic ultrasound on ischemic hind limb in mice. *American Journal of Translational Research*, *6*(6), 703-713. PMID: 25628781

Ikai, H., Tamura, T., Watanabe, T., Itou, M., Sugaya, A., Iwabuchi, S., Mikuni-Takagaki, Y., & Deguchi, S. (2008). Low-intensity pulsed ultrasound accelerates periodontal wound healing after flap surgery. *Journal of Periodontal Research*, *43*(2), 212-216. https://doi.org/10.1111/j.1600-0765.2007.01016.x

Jabbarzadeh, E., Starnes, T., Khan, Y. M., Jiang, T., Wirtel, A. J., Deng, M., Lv, Q., Nair, L. S., Doty, S. B., & Laurencin, C. T. (2008). Induction of angiogenesis in tissue-engineered scaffolds designed for bone repair: a combined gene therapy-cell transplantation approach. *Proceedings of the National Academy of Sciences of the United States of America*, *105*(32), 11099–11104. https://doi.org/10.1073/pnas.0800069105

Jaffe, E. A., Nachman, R. L., Becker, C. G., & Minick, C. R. (1973). Culture of human endothelial cells derived from umbilical veins. Identification by morphologic and immunologic criteria. *The Journal of Clinical Investigation*, *52*(11), 2745-2756. https://doi.org/10.1172/JCI107470

James, J. A., Dalton, G., Bullen, M., Freundlich, H., & Hopkins, J. (1960). The ultrasonic treatment of Meniere's disease. *The Journal of Laryngology & Otology*, *74*(10), 730-757. https://doi.org/10.3109/00016487609107485

Johnson, K. E., & Wilgus, T. A. (2014). Vascular Endothelial Growth Factor and Angiogenesis in the Regulation of Cutaneous Wound Repair. *Advances in Wound Care*, *3*(10), 647–661. https://doi.org/10.1089/wound.2013.0517

Johnson, T., Zhao, L., Manuel, G., Taylor, H., & Liu, D. (2019). Approaches to therapeutic angiogenesis for ischemic heart disease. *Journal of Molecular Medicine (Berl)*, *97*(2), 141-151. https://doi.org/10.1007/s00109-018-1729-3

Kamei, M., Saunders, W. B., Bayless, K. J., Dye, L., Davis, G. E., & Weinstein, B. M. (2006). Endothelial tubes assemble from intracellular vacuoles in vivo. *Nature*, *442*(7101), 453–456. https://doi.org/10.1038/nature04923

Kang, Y., Kim, S., Fahrenholtz, M., Khademhosseini, A., & Yang, Y. (2013). Osteogenic and angiogenic potentials of monocultured and co-cultured human-bone-marrow-derived mesenchymal stem cells and human-umbilical-vein endothelial cells on three-dimensional porous beta-tricalcium phosphate scaffold. *Acta Biomaterialia*, *9*(1), 4906–4915. https://doi.org/10.1016/j.actbio.2012.08.008

Kaproth-Joslin, K. A., Nicola, R., & Dogra, V. S. (2015). The History of US: From Bats and Boats to the Bedside and Beyond. *Radiographics*, *35*(3), 960-970. https://doi.org/10.1148/rg.2015140300

Karamysheva A. F. (2008). Mechanisms of angiogenesis. *Biochemistry. Biokhimiia*, *73*(7), 751–762. https://doi.org/10.1134/s0006297908070031

Karsch, U., Henn, W., Seyfert, U. T., Steudel, W. I., & Reif, J. (2002). Effect of high power ultrasound on endothelial cells - an in vitro study of the endothelium-hemostasis interaction. *Clinical Hemorheology and Microcirculation*, *27*(2), 123–135. PMID: 12237482.

Karthikesh, M. S., & Yang, X. (2021). The effect of ultrasound cavitation on endothelial cells. *Experimental Biology and Medicine*, *246*(7), 758-770. https://doi.org/10.1177/1535370220982301

Kassambara, A., & Mundt, F. (2017). Package 'factoextra'. *Extract and Visualize the Results of Multivariate Data Analyses*, *76*(2).

Kato, Y., Saito, N., Niimi, K., Saito, D., Sakuma, H., Hasebe, D., Katagiri, W., & Kobayashi, T. (2021). A comparison and evaluation of the use of ultrasonic cutting devices with conventional powered instruments in orthognathic surgery. *Advances in Oral and Maxillofacial Surgery*, *2*, 100081. https://doi.org/10.1016/j.adoms.2021.100081

Katzir, S. (2012). Who knew piezoelectricity? Rutherford and Langevin on submarine detection and the invention of sonar. *Notes and Records of the Royal Society*, *66*(2), 141-157. https://doi.org/10.1098/rsnr.2011.0049

Kazazi-Hyseni, F., Beijnen, J. H., & Schellens, J. H. M. (2010). Bevacizumab. *Oncologist*, *15*(8), 819-825. https://doi.org/10.1634/theoncologist.2009-0317

Khambay, B. S., & Walmsley, A. D. (1999). Acoustic microstreaming: detection and measurement around ultrasonic scalers. *Journal of Periodontology*, *70*(6), 626-631. https://doi.org/10.1902/jop.1999.70.6.626

Khambay, B. S., & Walmsley, A. D. (2000). Investigations into the use of an ultrasonic chisel to cut bone. Part 1: Forces applied by clinicians. *Journal of dentistry*, *28*(1), 31–37. https://doi.org/10.1016/s0300-5712(99)00043-3

Khan, T. A., Sellke, F. W., & Laham, R. J. (2002). Therapeutic Angiogenesis for Coronary Artery Disease. *Current Treatment Options in Cardiovascular Medicine*, *4*(1), 65-74. https://doi.org/10.1007/s11936-002-0027-z

Kilburn, L. B., Packer, R. J., Fonseca, A., Keating, R. F., Mueller, S., Narsinh, K., Ho, W. S., Niazi, T., Fenn, P., Clanton, R., Henry, L., Potter, W., Andresen, C., Marcus, S., Benaim, E., & Syed, H. R. (2024). Interim report of a phase 2 study of sonodynamic therapy (SDT) using SONALA-001 together with MR-guided low-intensity focused ultrasound (MRgFUS) in children with diffuse intrinsic pontine glioma (DIPG). *Journal of Clinical Oncology*, *42*(16). https://doi.org/10.1200/JCO.2024.42.16_suppl.206

Koch, S., Tugues, S., Li, X. J., Gualandi, L., & Claesson-Welsh, L. (2011). Signal transduction by vascular endothelial growth factor receptors. *Biochemical Journal*, *437*, 169-183. https://doi.org/10.1042/Bj20110301

Krock, B. L., Skuli, N., & Simon, M. C. (2011). Hypoxia-induced angiogenesis: good and evil. *Genes Cancer*, *2*(12), 1117-1133. https://doi.org/10.1177/1947601911423654

Kubota, Y., Kleinman, H. K., Martin, G. R., & Lawley, T. J. (1988). Role of laminin and basement membrane in the morphological differentiation of human endothelial cells into capillary-like structures. *The Journal of Cell Biology*, *107*(4), 1589-1598. https://doi.org/10.1083/jcb.107.4.1589

Kumar, I., Staton, C. A., Cross, S. S., Reed, M. W. R., & Brown, N. J. (2009). Angiogenesis, vascular endothelial growth factor and its receptors in human surgical wounds. *British Journal of Surgery*, *96*(12), 1484-1491. https://doi.org/10.1002/bjs.6778

Kurz, H., Burri, P. H., & Djonov, V. G. (2003). Angiogenesis and vascular remodeling by intussusception: From form to function. *News in Physiological Sciences*, *18*, 65-70. https://doi.org/10.1152/nips.01417.2002

Lamalice, L., Le Boeuf, F., & Huot, J. (2007). Endothelial cell migration during angiogenesis. *Circulation Research*, *100*(6), 782-794. https://doi.org/10.1161/01.RES.0000259593.07661.1e

Landes, C. A., Stübinger, S., Ballon, A., & Sader, R. (2008). Piezoosteotomy in orthognathic surgery versus conventional saw and chisel osteotomy. *Oral and Maxillofacial Surgery*, *12*(3), 139–147. https://doi.org/10.1007/s10006-008-0123-7

Langevin, P. (1920). French Patent No. 505,703. *Filed September 17, 1917. Issued August*, *5*.

Laviña, B., Castro, M., Niaudet, C., Cruys, B., Alvarez-Aznar, A., Carmeliet, P., Bentley, K., Brakebusch, C., Betsholtz, C., & Gaengel, K. (2018). Defective endothelial cell migration in the absence of Cdc42 leads to capillary-venous malformations. *Development*, *145*(13), dev161182 https://doi.org/ARTN dev161182

Lê, S., Josse, J., & Husson, F. (2008). FactoMineR: an R package for multivariate analysis. *Journal of Statistical Software*, *25*, 1-18.

Lea, S. C., Price, G. J., & Walmsley, A. D. (2005). A study to determine whether cavitation occurs around dental ultrasonic scaling instruments. *Ultrasonics Sonochemistry*, *12*(3), 233-236. https://doi.org/10.1016/j.ultsonch.2003.10.006

Lehmann, J. F. (1953). The biophysical basis of biologic ultrasonic reactions with special reference to ultrasonic therapy. *Archives of Physical Medicine and Rehabilitation*, *34*(3), 139-152. PMID: 13031770.

Leighton, T. (1998). The principles of cavitation. In M. J.W. Povey, T. J. Mason, *Ultrasound in Food Processing* Blackie Academic and Professional, London, 151-178

Lepock, J. R. (2005). Measurement of protein stability and protein denaturation in cells using differential scanning calorimetry. *Methods*, *35*(2), 117-125. https://doi.org/10.1016/j.ymeth.2004.08.002

Lertkiatmongkol, P., Liao, D., Mei, H., Hu, Y., & Newman, P. J. (2016). Endothelial functions of platelet/endothelial cell adhesion molecule-1 (CD31). *Current Opinion in Hematology*, *23*(3), 253–259. https://doi.org/10.1097/MOH.0000000000000239

Li, J., Guo, W., Yu, F., Liu, L., Wang, X., Li, L., Fang, B., & Xia, L. (2022). Low-intensity pulsed ultrasound promotes angiogenesis via the AKT pathway and DNA methylation in human umbilical vein endothelial cells. *Ultrasonics*, *118*, 106561. https://doi.org/10.1016/j.ultras.2021.106561

Li, X., Stritch, T., Manley, K., & Lucas, M. (2021). Limits and opportunities for miniaturizing ultrasonic surgical devices based on a Langevin transducer. *IEEE Transactions on Ultrasonics, Ferroelectrics, and Frequency Control*, *68*(7), 2543-2553. https://doi.org/10.1109/TUFFC.2021.3065207

Li, Y.-S. J., Haga, J. H., & Chien, S. (2005). Molecular basis of the effects of shear stress on vascular endothelial cells. *Journal of Biomechanics*, *38*(10), 1949-1971. https://doi.org/10.1016/j.jbiomech.2004.09.030

Lighthill, J. (1978). Acoustic Streaming. *Journal of Sound and Vibration*, *61*(3), 391-418. https://doi.org/10.1016/0022-460X(78)90388-7

Linebarger, E. J., Hardten, D. R., Shah, G. K., & Lindstrom, R. L. (1999). Phacoemulsification and modern cataract surgery. *Survey of Ophthalmology*, *44*(2), 123–147. https://doi.org/10.1016/s0039-6257(99)00085-5

Lisko, J., Kamioka, N., & Grubb, K. J. (2019). The Eternal Debate: CABG Vs PCI. Current Status of the Literature. *Seminars in Thoracic and Cardiovascular Surgery*, *31*(4), 734-739. https://doi.org/10.1053/j.semtcvs.2019.05.009

Liu, L., Yang, Y., Liu, P., & Tan, W. (2014). The influence of air content in water on ultrasonic cavitation field. *Ultrasonics Sonochemistry*, *21*(2), 566-571. https://doi.org/10.1016/j.ultsonch.2013.10.007

Liu, X., Wang, B., Ding, H., Shi, H., Liu, J., & Sun, H. (2018). Low-intensity pulsed ultrasound in combination with SonoVue induces cytotoxicity of human renal glomerular endothelial cells via repression of the ERK1/2 signaling pathway. *Renal failure*, *40*(1), 458–465. https://doi.org/10.1080/0886022X.2018.1487868

Lizzi, F. L., Muratore, R., Deng, C. X., Ketterling, J. A., Alam, S. K., Mikaelian, S., & Kalisz, A. (2003). Radiation-force technique to monitor lesions during ultrasonic therapy. *Ultrasound in Medicine & Biology*, *29*(11), 1593-1605. https://doi.org/10.1016/s0301-5629(03)01052-4

Lordon, B., Campion, T., Gibot, L., & Gallot, G. (2024). Impact of trypsin on cell cytoplasm during detachment of cells studied by terahertz sensing. *Biophysical Journal*, *123*(16), 2476-2483. https://doi.org/10.1016/j.bpj.2024.06.011

Lu, A., Wang, L., & Qian, L. (2015). The role of eNOS in the migration and proliferation of bone-marrow derived endothelial progenitor cells and in vitro angiogenesis. *Cell Biology International*, *39*(4), 484-490. https://doi.org/10.1002/cbin.10405

Lu, H., Cui, H., Lu, G., Jiang, L., Hensleigh, R., Zeng, Y., Rayes, A., Panduranga, M. K., Acharya, M., & Wang, Z. (2023). 3D Printing and processing of miniaturized transducers with near-pristine piezoelectric ceramics for localized cavitation. *Nature Communications*, *14*(1), 2418. https://doi.org/10.1038/s41467-023-37335-w

Lucas, M., Gachagan, A., & Cardoni, A. (2009). Research applications and opportunities in power ultrasonics. *Proceedings of the Institution of Mechanical Engineers, Part C: Journal of Mechanical Engineering Science*, *223*(12), 2949-2965. http://dx.doi.org/10.1243/09544062JMES1671

Lucas, M., Mathieson, A., & Cleary, R. (2023). Ultrasonic cutting for surgical applications. In *Power Ultrasonics* (pp. 617-635). Elsevier. https://doi.org/10.1016/B978-0-12-820254-8.00037-3

Ludwig, G. D. (1949). *Considerations underlying the use of ultrasound to detect gallstones and foreign bodies in tissue*. Naval Medical Research Institute.

Ma, J., van den Beucken, J. J., Yang, F., Both, S. K., Cui, F. Z., Pan, J., & Jansen, J. A. (2011). Coculture of osteoblasts and endothelial cells: optimization of culture medium and cell ratio. *Tissue engineering. Part C, Methods*, *17*(3), 349–357. https://doi.org/10.1089/ten.TEC.2010.0215

Maddi, A., Hai, H., Ong, S.-T., Sharp, L., Harris, M., & Meghji, S. (2006). Long wave ultrasound may enhance bone regeneration by altering OPG/RANKL ratio in human osteoblast-like cells. *Bone*, *39*(2), 283-288. https://doi.org/10.1016/j.bone.2006.01.162

Malek, A. M., Izumo, S., & Alper, S. L. (1999). Modulation by pathophysiological stimuli of the shear stress-induced up-regulation of endothelial nitric oxide synthase expression in endothelial cells. *Neurosurgery*, *45*(2), 334. https://doi.org/10.1097/00006123-199908000-00028

Man, J., Shelton, R. M., Cooper, P. R., Landini, G., & Scheven, B. A. (2012a). Low intensity ultrasound stimulates osteoblast migration at different frequencies. *Journal of Bone and Mineral Metabolism*, *30*(5), 602-607. https://doi.org/10.1007/s00774-012-0368-y

Man, J., Shelton, R. M., Cooper, P. R., & Scheven, B. A. (2012b). Low-intensity low-frequency ultrasound promotes proliferation and differentiation of odontoblast-like cells. *Journal of Endodontics*, *38*(5), 608-613. https://doi.org/10.1016/j.joen.2012.01.015

Mannucci, P. M. (1995). Platelet von Willebrand factor in inherited and acquired bleeding disorders. *Proceedings of the National Academy of Sciences of the United States of America*, *92*(7), 2428-2432. https://doi.org/10.1073/pnas.92.7.2428

Matsushita, K., Morrell, C. N., Cambien, B., Yang, S. X., Yamakuchi, M., Bao, C., Hara, M. R., Quick, R. A., Cao, W., O'Rourke, B., Lowenstein, J. M., Pevsner, J., Wagner, D. D., & Lowenstein, C. J. (2003). Nitric oxide regulates exocytosis by S-nitrosylation of N-ethylmaleimide-sensitive factor. *Cell*, *115*(2), 139–150. https://doi.org/10.1016/s0092-8674(03)00803-1

Matsumura, T., Wolff, K., & Petzelbauer, P. (1997). Endothelial cell tube formation depends on cadherin 5 and CD31 interactions with filamentous actin. *Journal of Immunology (Baltimore, Md. : 1950)*, *158*(7), 3408–3416. PMID: 9120301.

Meola, M., Ibeas, J., Lasalle, G., & Petrucci, I. (2021). Basics for performing a high-quality color Doppler sonography of the vascular access. *The Journal of Vascular Access*, *22*(1_suppl), 18-31. https://doi.org/10.1177/11297298211018060

Mi, Q., Chen, N., Shaifta, Y., Xie, L., Lu, H., Liu, Z., Chen, Q., Hamid, C., Becker, S., & Ji, Y. (2011). Activation of endothelial nitric oxide synthase is dependent on its interaction with globular actin in human umbilical vein endothelial cells. *Journal of Molecular and Cellular Cardiology*, *51*(3), 419-427. https://doi.org/10.1016/j.yjmcc.2011.06.017

Miller, D. L., Smith, N. B., Bailey, M. R., Czarnota, G. J., Hynynen, K., Makin, I. R. S., & Bioeffects Committee of the American Institute of Ultrasound in Medicine. (2012). Overview of therapeutic ultrasound applications and safety considerations. *Journal of Ultrasound in Medicine*, *31*(4), 623-634. https://doi.org/10.7863/jum.2012.31.4.623

Mizrahi, N., Seliktar, D., & Kimmel, E. (2007). Ultrasound-induced angiogenic response in endothelial cells. *Ultrasound in Medicine & Biology, 33*(11), 1818-1829. https://doi.org/10.1016/j.ultrasmedbio.2007.05.007

Molina, C. A., Ribo, M., Rubiera, M., Montaner, J., Santamarina, E., Delgado-Mederos, R., Arenillas, J. F., Huertas, R., Purroy, F., Delgado, P., & Alvarez-Sabin, J. (2006). Microbubble administration accelerates clot lysis during continuous 2-MHz ultrasound monitoring in stroke patients treated with intravenous tissue plasminogen activator. *Stroke*, *37*(2), 425-429. https://doi.org/10.1161/01.STR.0000199064.94588.39

Monkley, S. J., Kostourou, V., Spence, L., Petrich, B., Coleman, S., Ginsberg, M. H., Pritchard, C. A., & Critchley, D. R. (2011). Endothelial cell talin1 is essential for embryonic

angiogenesis. *Developmental Biology*, *349*(2), 494-502. https://doi.org/10.1016/j.ydbio.2010.11.010

Moore, J. P., Weber, M., & Searles, C. D. (2010). Laminar shear stress modulates phosphorylation and localization of RNA polymerase II on the endothelial nitric oxide synthase gene. *Arteriosclerosis, Thrombosis, and Vascular Biology*, *30*(3), 561-567. https://doi.org/10.1161/ATVBAHA.109.199554

Mould, R. F. (2007). Pierre curie, 1859-1906. *Current Oncology*, *14*(2), 74-82. https://doi.org/10.3747/co.2007.110

Mukherji, S. K. (2010). Bevacizumab (Avastin). *American Journal of Neuroradiology*, *31*(2), 235-236. https://doi.org/10.3174/ajnr.A1987

Müller, A. M., Hermanns, M. I., Skrzynski, C., Nesslinger, M., Müller, K.-M., & Kirkpatrick, C. J. (2002). Expression of the endothelial markers PECAM-1, vWf, and CD34 in vivo and in vitro. *Experimental and Molecular Pathology*, *72*(3), 221-229. https://doi.org/10.1006/exmp.2002.2424

Nair, N. Y., Samuel, V., Ramesh, L., Marib, A., David, D. T., & Sundararaman, A. (2022). Actin cytoskeleton in angiogenesis. *Biology Open*, *11*(12). https://doi.org/10.1242/bio.058899

Nakatsu, M. N., Sainson, R. C., Aoto, J. N., Taylor, K. L., Aitkenhead, M., Pérez-del-Pulgar, S., Carpenter, P. M., & Hughes, C. C. (2003). Angiogenic sprouting and capillary lumen formation modeled by human umbilical vein endothelial cells (HUVEC) in fibrin gels: the role of fibroblasts and Angiopoietin-1. *Microvascular research*, *66*(2), 102–112. https://doi.org/10.1016/s0026-2862(03)00045-1

Nakayama, T., Sato, W., Yoshimura, A., Zhang, L., Kosugi, T., Campbell-Thompson, M., Kojima, H., Croker, B. P., & Nakagawa, T. (2010). Endothelial von Willebrand factor release due to eNOS deficiency predisposes to thrombotic microangiopathy in mouse aging kidney. *The American journal of pathology*, *176*(5), 2198–2208. https://doi.org/10.2353/ajpath.2010.090316

Namkoong, S., Lee, S.-J., Kim, C.-K., Kim, Y.-M., Chung, H.-T., Lee, H., Han, J.-A., Ha, K.-S., Kwon, Y.-G., & Kim, Y.-M. (2005). Prostaglandin E2 stimulates angiogenesis by activating the nitric oxide/cGMP pathway in human umbilical vein endothelial cells. *Experimental & Molecular Medicine*, *37*(6), 588-600. https://doi.org/10.1038/emm.2005.72

Nehls, S., Nöding, H., Karsch, S., Ries, F., & Janshoff, A. (2019). Stiffness of MDCK II cells depends on confluency and cell size. *Biophysical Journal*, *116*(11), 2204-2211. https://doi.org/10.1016/j.bpj.2019.04.028

Ng, A. T., & Tam, P. C. (2014). Current status of robot-assisted surgery. *Hong Kong Medical Journal = Xianggang yi xue za zhi*, *20*(3), 241–250. https://doi.org/10.12809/hkmj134167

Nightingale, K. R., Kornguth, P. J., Walker, W. F., McDermott, B. A., & Trahey, G. E. (1995). A novel ultrasonic technique for differentiating cysts from solid lesions: preliminary results in the breast. *Ultrasound in Medicine & Biology*, *21*(6), 745-751. https://doi.org/10.1016/0301-5629(95)00020-r

Nio, A. Q., Faraci, A., Christensen-Jeffries, K., Eckersley, R. J., Monaghan, M. J., Raymond, J. L., Forsberg, F., & Lamata, P. (2017). The subharmonic amplitude of SonoVue increases with hydrostatic pressure at low incident acoustic pressures. *In 2017 IEEE International Ultrasonics Symposium (IUS)*, (pp. 1-4). IEEE. https://doi.org/10.1109/ULTSYM.2017.8092984

Noriega, S., Budhiraja, G., & Subramanian, A. (2012). Remodeling of chromatin under low intensity diffuse ultrasound. *The International Journal of Biochemistry & Cell Biology*, *44*(8), 1331–1336. https://doi.org/10.1016/j.biocel.2012.04.027

O'Brien, W. D., Jr. (2007). Ultrasound-biophysics mechanisms. *Progress in Biophysics and Molecular Biology*, *93*(1-3), 212-255. https://doi.org/10.1016/j.pbiomolbio.2006.07.010

Ogata, T., Ito, K., Shindo, T., Hatanaka, K., Eguchi, K., Kurosawa, R., Kagaya, Y., Monma, Y., Ichijo, S., Taki, H., Kanai, H., & Shimokawa, H. (2017). Low-intensity pulsed ultrasound enhances angiogenesis and ameliorates contractile dysfunction of pressure-overloaded heart in mice. *PLoS One*, *12*(9), e0185555. https://doi.org/10.1371/journal.pone.0185555

Osborn, E. A., Rabodzey, A., Dewey, C. F., & Hartwig, J. H. (2006). Endothelial actin cytoskeleton remodeling during mechanostimulation with fluid shear stress. *American Journal of Physiology-Cell Physiology*, *290*(2), C444-C452. https://doi.org/10.1152/ajpcell.00218.2005

Packer, M., Fishkind, W. J., Fine, I. H., Seibel, B. S., & Hoffman, R. S. (2005). The physics of phaco: a review. *Journal of Cataract and Refractive Surgery*, *31*(2), 424–431. https://doi.org/10.1016/j.jcrs.2004.11.027

Patel, S. A., Nilsson, M. B., Le, X. N., Cascone, T., Jain, R. K., & Heymach, J. V. V. (2023). Molecular Mechanisms and Future Implications of VEGF/VEGFR in Cancer Therapy. *Clinical Cancer Research*, *29*(1), 30-39. https://doi.org/10.1158/1078-0432.Ccr-22-1366

Patel, U. S., Ghorayeb, S. R., Yamashita, Y., Atanda, F., Walmsley, A. D., & Scheven, B. A. (2015). Ultrasound field characterization and bioeffects in multiwell culture plates. *Journal of Therapeutic Ultrasound*, *3*, 8. https://doi.org/10.1186/s40349-015-0028-5

Patey, S. J., & Corcoran, J. P. (2021). Physics of ultrasound. *Anaesthesia and Intensive Care Medicine*, *22*(1), 58-63. https://doi.org/10.1016/j.mpaic.2020.11.012

Phillips, T. (2008) Regulation of transcription and gene expression in eukaryotes. *Nature Education*, 1(1):199

Pearse, R. M., Moreno, R. P., Bauer, P., Pelosi, P., Metnitz, P., Spies, C., Vallet, B., Vincent, J. L., Hoeft, A., Rhodes, A., Intensive, T. G. E. S., & Soc, T. G. E. (2012). Mortality after surgery in Europe: a 7 day cohort study. *Lancet*, *380*(9847), 1059-1065. https://doi.org/10.1016/S0140-6736(12)61148-9

Pennes, H. H. (1998). Analysis of tissue and arterial blood temperatures in the resting human forearm. *Journal of Applied Physiology*, *85*(1), 5-34. https://doi.org/10.1152/jappl.1948.1.2.93

Pettet, G., Chaplain, M. A. J., McElwain, D. L. S., & Byrne, H. M. (1996). On the role of angiogenesis in wound healing. *Proceedings of the Royal Society B-Biological Sciences*, *263*(1376), 1487-1493. https://doi.org/10.1098/rspb.1996.0217

Polat, B. E., Hart, D., Langer, R., & Blankschtein, D. (2011). Ultrasound-mediated transdermal drug delivery: mechanisms, scope, and emerging trends. *Journal of Controlled Release : Official Journal of the Controlled Release Society*, *152*(3), 330–348. https://doi.org/10.1016/j.jconrel.2011.01.006

Pollard, T. D. (2016). Actin and Actin-Binding Proteins. *Cold Spring Harbor Perspectives in Biology*, *8*(8). https://doi.org/10.1101/cshperspect.a018226

Poolman, R. W., Agoritsas, T., Siemieniuk, R. A., Harris, I. A., Schipper, I. B., Mollon, B., Smith, M., Albin, A., Nador, S., Sasges, W., Schandelmaier, S., Lytvyn, L., Kuijpers, T., van Beers, L. W., Verhofstad, M. H., & Vandvik, P. O. (2017). Low intensity pulsed ultrasound (LIPUS) for bone healing: a clinical practice guideline. *British Medical Journal*, *356*, j576. https://doi.org/10.1136/bmj.j576

Privratsky, J. R., Paddock, C. M., Florey, O., Newman, D. K., Muller, W. A., & Newman, P. J. (2011). Relative contribution of PECAM-1 adhesion and signaling to the maintenance of vascular integrity. *Journal of Cell Science*, *124*(Pt 9), 1477–1485. https://doi.org/10.1242/jcs.082271

Priya, M. K., Sahu, G., Soto-Pantoja, D. R., Goldy, N., Sundaresan, A. M., Jadhav, V., Barathkumar, T., Saran, U., Jaffar Ali, B., & Roberts, D. D. (2015). Tipping off endothelial tubes: nitric oxide drives tip cells. *Angiogenesis*, *18*, 175-189. https://doi.org/10.1007/s10456-014-9455-0

Quarato, C. M. I., Lacedonia, D., Salvemini, M., Tuccari, G., Mastrodonato, G., Villani, R., Fiore, L. A., Scioscia, G., Mirijello, A., & Saponara, A. (2023). A review on biological effects of ultrasounds: key messages for clinicians. *Diagnostics*, *13*(5), 855. https://doi.org/10.3390/diagnostics13050855

Raizada, M. K., Tan, G., & Fellows, R. E. (1981). Trypsin-induced alterations of insulin binding, microfilament organization and cell shape in fibroblastic cultures from non-diabetic and diabetic mice. *Experimental Cell Research*, *133*(2), 261-271. https://doi.org/10.1016/0014-4827(81)90318-9

Ramieri, V., Saponaro, G., Lenzi, J., Caporlingua, F., Polimeni, A., Silvestri, A., Pizzuti, A., Roggini, M., Tarani, L., & Papoff, P. (2015). The use of piezosurgery in cranial surgery in children. *Journal of Craniofacial Surgery*, *26*(3), 840-842. https://doi.org/10.1097/SCS.0000000000001574

Ranta, V., Mikkola, T., Ylikorkala, O., Viinikka, L., & Orpana, A. (1998). Reduced viability of human vascular endothelial cells cultured on Matrigel™. *Journal of Cellular Physiology*, *176*(1), 92-98. https://doi.org/10.1002/(SICI)1097-4652(199807)176:1<92::AID-JCP11>3.0.CO;2-Q

Reher, P., Doan, N., Bradnock, B., Meghji, S., & Harris, M. (1999). Effect of ultrasound on the production of IL-8, basic FGF and VEGF. *Cytokine*, *11*(6), 416-423. https://doi.org/10.1006/cyto.1998.0444

Ribatti, D., & Djonov, V. (2012). Intussusceptive microvascular growth in tumors. *Cancer Letters*, *316*(2), 126-131. https://doi.org/10.1016/j.canlet.2011.10.040

Risau, W. (1997). Mechanisms of angiogenesis. *Nature*, *386*(6626), 671-674. https://doi.org/10.1038/386671a0

Risau, W., & Flamme, I. (1995). Vasculogenesis. *Annual review of cell and developmental biology*, *11*(1), 73-91. https://doi.org/10.1146/annurev.cb.11.110195.000445

Robinson, S. P., & Green, G. J. (1997) Intercomparison to validate calibration methods for hydrophones in the frequency range 10-315 kHz. *NPL Report CIRA (EXT) 020* National Physical Laboratory, UK

Saber, A. A., & Saber, A. (2017). Therapeutic ultrasound: Physiological role, clinical applications and precautions. *Journal of Surgery*, *9*(3), 61-69. https://doi.org/10.11648/j.js.s.2017050301.22

Sadler, J. E., Budde, U., Eikenboom, J. C., Favaloro, E. J., Hill, F. G., Holmberg, L., Ingerslev, J., Lee, C. A., Lillicrap, D., Mannucci, P. M., Mazurier, C., Meyer, D., Nichols, W. L., Nishino, M., Peake, I. R., Rodeghiero, F., Schneppenheim, R., Ruggeri, Z. M., Srivastava, A., Montgomery, R. R., Federici, A. B. & Working Party on von Willebrand Disease, C. (2006). Update on the pathophysiology and classification of von Willebrand disease: a report of the Subcommittee on von Willebrand Factor. *Journal of Thrombosis and Haemostasis*, *4*(10), 2103-2114. https://doi.org/10.1111/j.1538-7836.2006.02146.x

Sahni, J., McCue, I. S., Johnson, A. R., Schake, M. A., Sotelo, L. D., Turner, J. A., & Pedrigi, R. M. (2024). Ultrasound Induces Similar Temporal Endothelial Expression Patterns of eNOS and KLF2 as Normal Flow. *Ultrasound in Medicine & Biology*, *50*(12), 1893-1902. https://doi.org/10.1016/j.ultrasmedbio.2024.08.017

Samandari, M., Abrinia, K., Mokhtari-Dizaji, M., & Tamayol, A. (2017). Ultrasound induced strain cytoskeleton rearrangement: An experimental and simulation study. *Journal of biomechanics*, *60*, 39-47. https://doi.org/10.1016/j.jbiomech.2017.06.003

Sanai, N., Tien, A. C., Tovmasyan, A., Chang, Y. W., Margaryan, T., Hendrickson, K., Eschbacher, J., Yoo, W., Harmon, J., Hong, A., Quarles, C., Barani, I., Alhilali, L., Mirzadeh, Z., & Mehta, S. (2022). A First-in-Human Phase 0/1 Trial of 5-Aminolevulinic Acid Sonodynamic Therapy (5-Ala Sdt) in Recurrent Glioblastoma. *Neuro-Oncology*, *24*, 72-73. https://doi.org/10.1093/neuonc/noac209.279

Sapieha, P., Hamel, D., Shao, Z., Rivera, J. C., Zaniolo, K., Joyal, J. S., & Chemtob, S. (2010). Proliferative retinopathies: Angiogenesis that blinds. *International Journal of Biochemistry & Cell Biology*, *42*(1), 5-12. https://doi.org/10.1016/j.biocel.2009.10.006

Sarvazyan, A. P., Rudenko, O. V., & Nyborg, W. L. (2010). Biomedical applications of radiation force of ultrasound: historical roots and physical basis. *Ultrasound in Medicine & Biology*, *36*(9), 1379-1394. https://doi.org/10.1016/j.ultrasmedbio.2010.05.015

Saura, M., Zaragoza, C., Cao, W., Bao, C., Rodríguez-Puyol, M., Rodríguez-Puyol, D., & Lowenstein, C. J. (2002). Smad2 mediates transforming growth factor-β induction of endothelial nitric oxide synthase expression. *Circulation Research*, *91*(9), 806-813. https://doi.org/10.1161/01.res.0000040397.23817.e5

Sauteur, L., Krudewig, A., Herwig, L., Ehrenfeuchter, N., Lenard, A., Affolter, M., & Belting, H. G. (2014). Cdh5/VE-cadherin Promotes Endothelial Cell Interface Elongation via Cortical Actin Polymerization during Angiogenic Sprouting. *Cell Reports*, *9*(2), 504-513. https://doi.org/10.1016/j.celrep.2014.09.024

Savva, J., Lucas, M., & Mulvana, H. (2019). A controlled in vitro study of optimal low intensity pulsed ultrasound fields for stimulation of proliferation in murine osteoblasts. In *2019 IEEE International Ultrasonics Symposium (IUS)*, (pp. 1543-1546). IEEE. https://doi.org/10.1109/ULTSYM.2019.8925594

Schafer, M., & Cleary, R. (2023). Ultrasonic surgical devices and procedures. In *Power Ultrasonics* (pp. 539-556). Elsevier. https://doi.org/10.1016/B978-0-12-820254-8.00010-5

Scheven, B. A., Man, J., Millard, J. L., Cooper, P. R., Lea, S. C., Walmsley, A. D., & Smith, A. J. (2009). VEGF and odontoblast-like cells: stimulation by low frequency ultrasound. *Archives of Oral Biology*, *54*(2), 185-191. https://doi.org/10.1016/j.archoralbio.2008.09.008

Schindelin, J., Arganda-Carreras, I., Frise, E., Kaynig, V., Longair, M., Pietzsch, T., Preibisch, S., Rueden, C., Saalfeld, S., & Schmid, B. (2012). Fiji: an open-source platform for biological-image analysis. *Nature Methods*, *9*(7), 676-682. https://doi.org/10.1038/nmeth.2019

Schnittler, H., Taha, M., Schnittler, M. O., Taha, A. A., Lindemann, N., & Seebach, J. (2014). Actin filament dynamics and endothelial cell junctions: the Ying and Yang between stabilization and motion. *Cell and Tissue Research*, *355*, 529-543. https://doi.org/10.1007/s00441-014-1856-2

Schuster, A., Schwab, T., Bischof, M., Klotz, M., Lemor, R., Degel, C., & Schäfer, K. H. (2013). Cell specific ultrasound effects are dose and frequency dependent. *Annals of Anatomy = Anatomischer Anzeiger : Official Organ of the Anatomische Gesellschaft*, *195*(1), 57–67. https://doi.org/10.1016/j.aanat.2012.03.008

Searles, C. D., Ide, L., Davis, M. E., Cai, H., & Weber, M. (2004). Actin cytoskeleton organization and posttranscriptional regulation of endothelial nitric oxide synthase during cell growth. *Circulation Research*, *95*(5), 488-495. https://doi.org/10.1161/01.RES.0000138953.21377.80

Secomski, W., Bilmin, K., Kujawska, T., Nowicki, A., Grieb, P., & Lewin, P. A. (2017). In vitro ultrasound experiments: Standing wave and multiple reflections influence on the outcome. *Ultrasonics*, *77*, 203-213. https://doi.org/10.1016/j.ultras.2017.02.008

Segeritz, C. P., & Vallier, L. (2017). Cell Culture: Growing Cells as Model Systems In Vitro. *Basic Science Methods for Clinical Researchers*, 151–172. https://doi.org/10.1016/B978-0-12-803077-6.00009-6

Sellke, F. W., Laham, R. J., Edelman, E. R., Pearlman, J. D., & Simons, M. (1998). Therapeutic angiogenesis with basic fibroblast growth factor: technique and early results. *The Annals of Thoracic Surgery*, *65*(6), 1540-1544. https://doi.org/10.1016/s0003-4975(98)00340-3

Shankar, H., & Pagel, P. S. (2011). Potential adverse ultrasound-related biological effects: a critical review. *Anesthesiology*, *115*(5), 1109-1124. https://doi.org/10.1097/ALN.0b013e31822fd1f1

Shehata, I. A. (2012). Treatment with high intensity focused ultrasound: secrets revealed. *European Journal of Radiology*, *81*(3), 534-541. https://doi.org/10.1016/j.ejrad.2011.01.047

Shekhar, H., Palaniappan, A., Peng, T., Lafond, M., Moody, M. R., Haworth, K. J., Huang, S., McPherson, D. D., & Holland, C. K. (2019). Characterization and Imaging of Lipid-Shelled Microbubbles for Ultrasound-Triggered Release of Xenon. *Neurotherapeutics : the Journal of the American Society for Experimental NeuroTherapeutics*, *16*(3), 878–890. https://doi.org/10.1007/s13311-019-00733-4

Shibuya, M., & Claesson-Welsh, L. (2006). Signal transduction by VEGF receptors in regulation of angiogenesis and lymphangiogenesis. *Experimental Cell Research*, *312*(5), 549-560. https://doi.org/10.1016/j.yexcr.2005.11.012

Shindo, T., Ito, K., Ogata, T., Hatanaka, K., Kurosawa, R., Eguchi, K., Kagaya, Y., Hanawa, K., Aizawa, K., Shiroto, T., Kasukabe, S., Miyata, S., Taki, H., Hasegawa, H., Kanai, H., & Shimokawa, H. (2016). Low-Intensity Pulsed Ultrasound Enhances Angiogenesis and Ameliorates Left Ventricular Dysfunction in a Mouse Model of Acute Myocardial Infarction. *Arteriosclerosis, Thrombosis, and Vascular Biology*, *36*(6), 1220-1229. https://doi.org/10.1161/ATVBAHA.115.306477

Shojaei, F. (2012). Anti-angiogenesis therapy in cancer: Current challenges and future perspectives. *Cancer Letters*, *320*(2), 130-137. https://doi.org/10.1016/j.canlet.2012.03.008

Siemerink, M. J., Klaassen, I., Van Noorden, C. J., & Schlingemann, R. O. (2013). Endothelial tip cells in ocular angiogenesis: potential target for anti-angiogenesis therapy. *Journal of Histochemistry and Cytochemistry*, *61*(2), 101-115. https://doi.org/10.1369/0022155412467635

Simoons, M. L., & Windecker, S. (2010). Chronic stable coronary artery disease: drugs vs. revascularization. *European Heart Journal*, *31*(5), 530-U525. https://doi.org/10.1093/eurheartj/ehp605

Snehota, M., Vachutka, J., Ter Haar, G., Dolezal, L., & Kolarova, H. (2020). Therapeutic ultrasound experiments in vitro: Review of factors influencing outcomes and reproducibility. *Ultrasonics*, *107*, 106167. https://doi.org/10.1016/j.ultras.2020.106167

Spadaccio, C., & Benedetto, U. (2018). Coronary artery bypass grafting (CABG) vs. percutaneous coronary intervention (PCI) in the treatment of multivessel coronary disease: quo vadis?—a review of the evidences on coronary artery disease. *Annals of Cardiothoracic Surgery*, *7*(4), 506. https://doi.org/10.21037/acs.2018.05.17

Spinelli, G., Lazzeri, D., Conti, M., Agostini, T., & Mannelli, G. (2014). Comparison of piezosurgery and traditional saw in bimaxillary orthognathic surgery. *Journal of Cranio-Maxillofacial Surgery*, *42*(7), 1211-1220. https://doi.org/10.1016/j.jcms.2014.02.011

Sporn, L. A., Marder, V. J., & Wagner, D. D. (1986). Inducible secretion of large, biologically potent von Willebrand factor multimers. *Cell*, *46*(2), 185-190. https://doi.org/10.1016/0092-8674(86)90735-x

Starke, R. D., Ferraro, F., Paschalaki, K. E., Dryden, N. H., McKinnon, T. A., Sutton, R. E., Payne, E. M., Haskard, D. O., Hughes, A. D., Cutler, D. F., Laffan, M. A., & Randi, A. M. (2011). Endothelial von Willebrand factor regulates angiogenesis. *Blood*, *117*(3), 1071-1080. https://doi.org/10.1182/blood-2010-01-264507

Stegen, S., Van Gastel, N., & Carmeliet, G. (2015). Bringing new life to damaged bone: the importance of angiogenesis in bone repair and regeneration. *Bone*, *70*, 19-27. https://doi.org/10.1016/j.bone.2014.09.017

Stewart, H. F., Stratmeyer, M. E. (1982). *An Overview of ultrasound : theory, measurement, medical applications, and biological effects.* Rockville, Md. :U.S. Dept. of Health and Human Services, Public Health Service, Food and Drug Administration, Center for Devices and Radiological Health,

Strober W. (2001). Trypan blue exclusion test of cell viability. *Current Protocols in Immunology*, *Appendix 3*, . https://doi.org/10.1002/0471142735.ima03bs21

Strutt, J. W. (1884). I. On the circulation of air observed in Kundt's tubes, and on some allied acoustical problems. *Philosophical Transactions of the Royal Society of London*(175), 1-21. https://doi.org/10.1098/rstl.1884.0002

Su, Y., Edwards-Bennett, S., Bubb, M. R., & Block, E. R. (2003). Regulation of endothelial nitric oxide synthase by the actin cytoskeleton. *American Journal of Physiology. Cell Physiology*, *284*(6), C1542–C1549. https://doi.org/10.1152/ajpcell.00248.2002

Su, Z., Xu, T., Wang, Y., Guo, X., Tu, J., Zhang, D., Kong, X., Sheng, Y., & Sun, W. (2019). Low intensity pulsed ultrasound promotes apoptosis and inhibits angiogenesis via p38 signaling mediated endoplasmic reticulum stress in human endothelial cells. *Molecular Medicine Reports*, *19*(6), 4645-4654. https://doi.org/10.3892/mmr.2019.10136

Sukmana, I., & Vermette, P. (2010). The effects of co-culture with fibroblasts and angiogenic growth factors on microvascular maturation and multi-cellular lumen formation in HUVEC-oriented polymer fibre constructs. *Biomaterials*, *31*(19), 5091–5099. https://doi.org/10.1016/j.biomaterials.2010.02.076

Suslick K. S. (1990). Sonochemistry. *Science (New York, N.Y.)*, *247*(4949), 1439–1445. https://doi.org/10.1126/science.247.4949.1439

Takahashi, H., & Shibuya, M. (2005). The vascular endothelial growth factor (VEGF)/VEGF receptor system and its role under physiological and pathological conditions. *Clinical Science*, *109*(3), 227-241. https://doi.org/10.1042/Cs20040370

Tang, Y., Horikoshi, M., & Li, W. (2016). ggfortify: unified interface to visualize statistical results of popular R packages. The *R Journal.*, *8*(2), 474.

Tempany, C. M., McDannold, N. J., Hynynen, K., & Jolesz, F. A. (2011). Focused ultrasound surgery in oncology: overview and principles. *Radiology*, *259*(1), 39-56. https://doi.org/10.1148/radiol.11100155

Tenopoulou, M., & Doulias, P.-T. (2020). Endothelial nitric oxide synthase-derived nitric oxide in the regulation of metabolism. *F1000Research*, *9*, F1000 Faculty Rev-1190. https://doi.org/10.12688/f1000research.19998.1

ter Haar, G. (1999). Therapeutic ultrasound. *European journal of ultrasound : official journal of the European Federation of Societies for Ultrasound in Medicine and Biology, 9*(1), 3–9. https://doi.org/10.1016/s0929-8266(99)00013-0.

Thomas, S. R., Chen, K., & Keaney, J. F. (2002). Hydrogen peroxide activates endothelial nitric-oxide synthase through coordinated phosphorylation and dephosphorylation via a phosphoinositide 3-kinase-dependent signaling pathway. *Journal of Biological Chemistry*, *277*(8), 6017-6024. https://doi.org/10.1074/jbc.M109107200

Tran, N., Garcia, T., Aniqa, M., Ali, S., Ally, A., & Nauli, S. M. (2022). Endothelial nitric oxide synthase (eNOS) and the cardiovascular system: in physiology and in disease states. *American Journal of Biomedical Science & Research*, *15*(2), 153. PMID: 35072089

Tung, J. J., Tattersall, I. W., & Kitajewski, J. (2012). Tips, stalks, tubes: notch-mediated cell fate determination and mechanisms of tubulogenesis during angiogenesis. *Cold Spring Harbor perspectives in medicine*, *2*(2), a006601. https://doi.org/10.1101/cshperspect.a006601

Vakil, N., & Everbach, E. C. (1993). Transient acoustic cavitation in gallstone fragmentation: a study of gallstones fragmented in vivo. *Ultrasound in Medicine & Biology*, *19*(4), 331–342. https://doi.org/10.1016/0301-5629(93)90105-w

VanBavel, E. (2007). Effects of shear stress on endothelial cells: possible relevance for ultrasound applications. *Progress in Biophysics and Molecular Biology*, *93*(1-3), 374-383. https://doi.org/10.1016/j.pbiomolbio.2006.07.017

Vercellotti, T., De Paoli, S., & Nevins, M. (2001). The piezoelectric bony window osteotomy and sinus membrane elevation: Introduction of a new technique for simplification of the sinus augmentation procedure. *International Journal of Periodontics & Restorative Dentistry*, *21*(6), 561-567. PMID: 11794567.

Vernon, M. M., & Lewin, M. B. (2018). Fetal and Neonatal Echocardiography. In *Avery's Diseases of the Newborn* (pp. 779-789). Elsevier. https://doi.org/10.1016/B978-0-323-40139-5.00053-X

Vitt, U. A., Hsu, S. Y., & Hsueh, A. J. W. (2001). Evolution and classification of cystine knot-containing hormones and related extracellular signaling molecules. *Molecular Endocrinology*, *15*(5), 681-694. https://doi.org/10.1210/me.15.5.681

Volkov, M., & Shepeleva, I. (1974). The use of ultrasonic instrumentation for the transection and uniting of bone tissue in orthopaedic surgery. *Reconstruction Surgery and Traumatology*, *14*, 147-152. PMID: 4842674.

Wagner, D. D., Saffaripour, S., Bonfanti, R., Sadler, J. E., Cramer, E. M., Chapman, B., & Mayadas, T. N. (1991). Induction of specific storage organelles by von Willebrand factor propolypeptide. *Cell*, *64*(2), 403-413. https://doi.org/10.1016/0092-8674(91)90648-i

Walmsley, A. (1988). Applications of ultrasound in dentistry. *Ultrasound in Medicine & Biology*, *14*(1), 7-14. https://doi.org/10.1016/0301-5629(88)90158-5

Walmsley, A. (2015). Ultrasonics in dentistry. *Physics Procedia*, *63*, 201-207. https://doi.org/10.1016/j.phpro.2015.03.033

Walsh, D. A. (1999). Angiogenesis and arthritis. *Rheumatology*, *38*(2), 103-112. https://doi.org/10.1093/rheumatology/38.2.103

Ward, M., Wu, J., & Chiu, J. F. (2000). Experimental study of the effects of Optison concentration on sonoporation in vitro. *Ultrasound in Medicine & Biology*, *26*(7), 1169–1175. https://doi.org/10.1016/s0301-5629(00)00260-x

Wasteneys, G. O., & Galway, M. E. (2003). Remodelling the cytoskeleton for growth and form: An overview with some new views. *Annual Review of Plant Biology*, *54*, 691-722. https://doi.org/10.1146/annurev.arplant.54.031902.134818

Weber, M., Hagedorn, C. H., Harrison, D. G., & Searles, C. D. (2005). Laminar shear stress and 3' polyadenylation of eNOS mRNA. *Circulation Research*, *96*(11), 1161–1168. https://doi.org/10.1161/01.RES.0000170651.72198.fa

Wickham H, François R, Henry L, Müller K, Vaughan D (2023). dplyr: A Grammar of Data Manipulation. *R package version 1.1.4*, https://github.com/tidyverse/dplyr

Wickham, H., Hester, J., Chang, W., & Hester, M. J. (2022). *devtools: Tools to Make Developing R Packages Easier*. *R Package, Version*, *2*(4). https://github.com/r-lib/devtools.

Wickham, H. (2016). Getting Started with ggplot2. In *ggplot2: Elegant graphics for data analysis* (pp. 11-31). Springer. https://ggplot2.tidyverse.org.

Wild, J. J., & Neal, D. (1951). Use of high-frequency ultrasonic waves for detecting changes of texture in living tissues. *Lancet*, *1*(6656), 655-657. https://doi.org/10.1016/s0140-6736(51)92403-8

Wild, J. J., & Reid, J. M. (1954). Echographic visualization of lesions of the living intact human breast. *Cancer Research*, *14*(4), 277-282. PMID: 13160950.

Williams, A. R. (1973). A possible alteration in the permeability of ascites cell membranes after exposure to acoustic microstreaming. *Journal of Cell Science*, *12*(3), 875-885. https://doi.org/10.1242/jcs.12.3.875

Wittwer, C. T., Herrmann, M. G., Moss, A. A., & Rasmussen, R. P. (1997). Continuous fluorescence monitoring of rapid cycle DNA amplification. *Biotechniques*, *22*(1), 130-&. https://doi.org/10.2144/97221bi01

Wong, R. A., Schumann, B., Townsend, R., & Phelps, C. A. (2007). A survey of therapeutic ultrasound use by physical therapists who are orthopaedic certified specialists. *Physical Therapy*, *87*(8), 986-994. https://doi.org/10.2522/ptj.20050392

Wood, R. W., & Loomis, A. L. (1927). XXXVIII. The physical and biological effects of high-frequency sound-waves of great intensity. *The London, Edinburgh, and Dublin Philosophical Magazine and Journal of Science*, *4*(22), 417-436. https://doi.org/10.1080/14786440908564348

Wu, F., Wang, Z. B., Chen, W. Z., Zou, J. Z., Bai, J., Zhu, H., Li, K. Q., Xie, F. L., Jin, C. B., Su, H. B., & Gao, G. W. (2004). Extracorporeal focused ultrasound surgery for treatment of human solid carcinomas: early Chinese clinical experience. *Ultrasound in Medicine & Biology*, *30*(2), 245-260. https://doi.org/10.1016/j.ultrasmedbio.2003.10.010

Wu, J. (2018). Acoustic streaming and its applications. *Fluids*, *3*(4), 108. https://doi.org/10.3390/fluids3040108

Wu, J., & Nyborg, W. L. (2008). Ultrasound, cavitation bubbles and their interaction with cells. *Advanced Drug Delivery Reviews*, *60*(10), 1103-1116. https://doi.org/10.1016/j.addr.2008.03.009

Xu, H., Cao, Y., Yang, X., Cai, P., Kang, L., Zhu, X., Luo, H., Lu, L., Wei, L., Bai, X., Zhu, Y., Zhao, B. Q., & Fan, W. (2017). ADAMTS13 controls vascular remodeling by modifying VWF reactivity during stroke recovery. *Blood*, *130*(1), 11-22. https://doi.org/10.1182/blood-2016-10-747089

Yoo, S. Y., & Kwon, S. M. (2013). Angiogenesis and its therapeutic opportunities. *Mediators of Inflammation*, *2013*(1), 127170. https://doi.org/10.1155/2013/127170

Yoshida, S., Yoshida, A., Matsui, H., Takada, Y. I., & Ishibashi, T. (2003). Involvement of macrophage chemotactic protein-1 and interleukin-1β during inflammatory but not basic fibroblast growth factor-dependent neovascularization in the mouse cornea. *Laboratory Investigation*, *83*(7), 927-938. https://doi.org/10.1097/01.Lab.0000075642.11787.83

Yoshizumi, M., Perrella, M. A., Burnett Jr, J., & Lee, M. E. (1993). Tumor necrosis factor downregulates an endothelial nitric oxide synthase mRNA by shortening its half-life. *Circulation Research*, *73*(1), 205-209. https://doi.org/10.1161/01.res.73.1.205

Yu, Z. N., Xu, L. L., Li, L., Zhang, H., Ma, Y. Y., Wang, L., Jiang, J. T., & Zhang, M. (2024). Comparison of the outcomes between ultrasonic devices and clamping in hepatectomy: a meta-analysis. *World Journal of Surgical Oncology*, *22*(1), 304. https://doi.org/10.1186/s12957-024-03575-3

Yumita, N., Nishigaki, R., Umemura, K., & Umemura, S. (1989). Hematoporphyrin as a Sensitizer of Cell-Damaging Effect of Ultrasound. *Japanese Journal of Cancer Research*, *80*(3), 219-222. https://doi.org/10.1111/j.1349-7006.1989.tb02295.x

Zeng, C., Li, H., Yang, T., Deng, Z. H., Yang, Y., Zhang, Y., Ding, X., & Lei, G. H. (2014). Effectiveness of continuous and pulsed ultrasound for the management of knee osteoarthritis: a systematic review and network meta-analysis. *Osteoarthritis and Cartilage*, *22*(8), 1090-1099. https://doi.org/10.1016/j.joca.2014.06.028

Zhang, C., Xie, Y., Luo, X., Ji, Q., Lu, C., He, C., & Wang, P. (2016a). Effects of therapeutic ultrasound on pain, physical functions and safety outcomes in patients with knee osteoarthritis: a systematic review and meta-analysis. *Clinical Rehabilitation*, *30*(10), 960-971. https://doi.org/10.1177/0269215515609415

Zhang, Y., Liao, B., Li, M., Cheng, M., Fu, Y., Liu, Q., Chen, Q., Liu, H., Fang, Y., & Zhang, G. (2016b). Shear stress regulates endothelial cell function through SRB 1-eNOS signaling pathway. *Cardiovascular Therapeutics*, *34*(5), 308-313. https://doi.org/10.1111/1755-5922.12199

Zhao, X., Lu, X., & Feng, Q. (2002). Deficiency in endothelial nitric oxide synthase impairs myocardial angiogenesis. *American Journal of Physiology-Heart and Circulatory Physiology*, *283*(6), H2371-H2378. https://doi.org/10.1152/ajpheart.00383.2002

Zhou, Z., Christofidou-Solomidou, M., Garlanda, C., & DeLisser, H. M. (1999). Antibody against murine PECAM-1 inhibits tumor angiogenesis in mice. *Angiogenesis*, *3*(2), 181-188. https://doi.org/10.1023/a:1009092107382

Ziche, M., & Morbidelli, L. (2000). Nitric oxide and angiogenesis. *Journal of Neuro-oncology*, *50*, 139-148. https://doi.org/10.1023/a:1006431309841

Ziegler, T., Silacci, P., Harrison, V. J., & Hayoz, D. (1998). Nitric oxide synthase expression in endothelial cells exposed to mechanical forces. *Hypertension*, *32*(2), 351-355. https://doi.org/10.1161/01.hyp.32.2.351

Zimmerman, D. (2002). Paul Langevin and the discovery of active sonar or asdic. *The Northern Mariner/Le Marin du Nord*, *12*(1), 39-52.

Chapter 7.

APPENDICES

7.1 Hydrophone kHz calibration

A 4 mm needle hydrophone (Precision Acoustics, Dorchester, UK) was used to measure peak pressure values in the acoustic field of the absorbing tank. The hydrophone was calibrated by the supplier following standard substitution calibration technique. Corresponding uncertainty values for each frequency are shown in dB and as percentages shown in Table 7.1.

Table 7.1 Calibration data for 4 mm needle hydrophone in kHz range.

Frequency (kHz)	Sensitivity (dB)	Sensitivity (mV/MPa)	Uncertainty (db)	Uncertainty (%)
20	-228.466377	3772.950833	± 0.7	8
21	-228.11403	3929.148889	± 0.7	8
22	-228.618029	3707.648296	± 0.7	8
23	-228.921258	3580.445794	± 0.7	8
24	-229.787506	3240.594743	± 0.7	8
25	-230.611922	2947.161135	± 0.7	8
26	-230.090999	3129.320438	± 0.7	8
27	-231.046499	2803.335421	± 0.7	8
28	-231.862381	2552.00167	± 0.7	8
29	-231.454017	2674.848114	± 0.7	8
30	-230.943845	2836.662942	± 0.7	8
31	-229.545291	3332.233684	± 0.7	8
32	-228.53416	3743.621964	± 0.7	8
33	-227.439764	4246.311011	± 0.7	8
34	-226.931518	4502.193022	± 0.7	8
35	-225.73485	5167.226487	± 0.7	8
36	-225.021239	5609.679447	± 0.7	8

37	-224.962865	5647.506379	± 0.7	8
38	-224.700501	5820.696281	± 0.7	8
39	-224.618351	5876.009207	± 0.7	8
40	-224.718291	5808.786854	± 0.7	8
41	-224.772011	5772.972312	± 0.7	8
42	-225.043923	5595.048375	± 0.7	8
43	-224.90683	5684.058149	± 0.7	8
44	-225.386161	5378.881446	± 0.7	8
45	-225.737563	5165.613071	± 0.7	8

7.2 qPCR primer specificity

Melt curve analysis was performed to assess the specificity of the qPCR reaction for each primer used. Melt curve analysis at the end of the amplification PCR run, involved the measurement of fluorescence during incremental increase of sample temperature. The SYBR green dye used in the qPCR reaction only fluoresced when bound to double-stranded DNA (ds DNA). As the temperature increased, the dsDNA denatured to single stranded (ssDNA) and the dye dissociated from the DNA therefore reducing the levels of fluorescence detected. The temperature at which 50 % of the dsDNA was dissociated into ssDNA is known as the melting temperature (T_m) which is identified with a singular peak at the T_m position when plotted on a melt curve of a single amplicon. Multiple peaks on the curve suggested the presence of multiple PCR products which could be caused by non-specific priming or primer dimer formations.

(A) – *B2M*

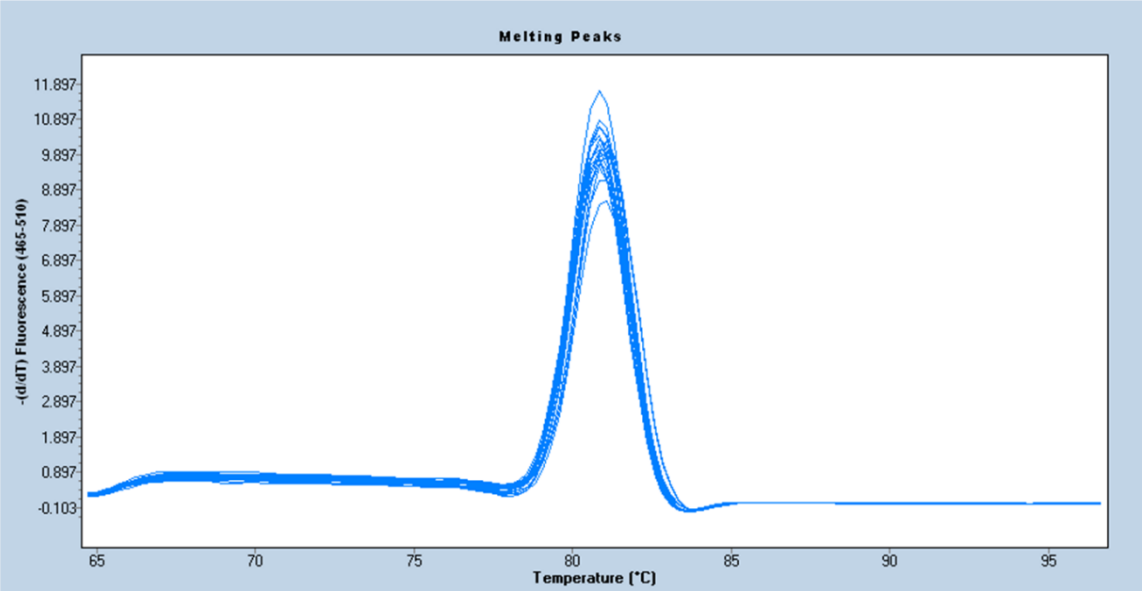
Melting Peaks
-(d/dT) Fluorescence (465-510)
11.897
10.897
9.897
8.897
7.897
6.897
5.897
4.897
3.897
2.897
1.897
0.897
-0.103
65
70
75
80
85
90
95
Temperature (°C)

(B) – *ENOS*

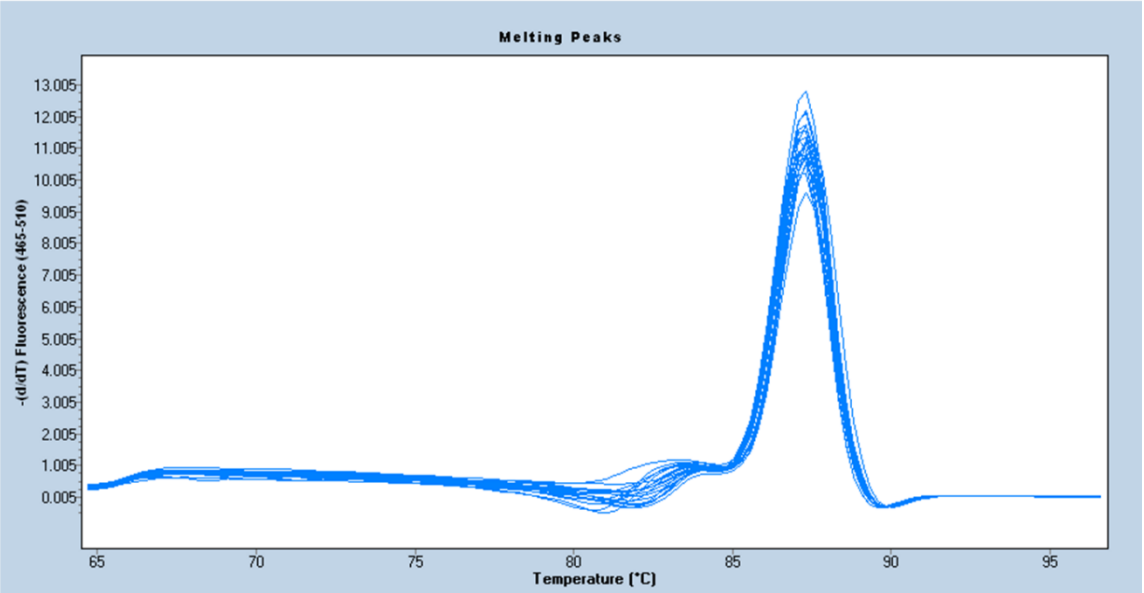
Melting Peaks
-(d/dT) Fluorescence (465-510)
13.005
12.005
11.005
10.005
9.005
8.005
7.005
6.005
5.005
4.005
3.005
2.005
1.005
0.005
65
70
75
80
85
90
95
Temperature (°C)

(C) - *GAPDH*

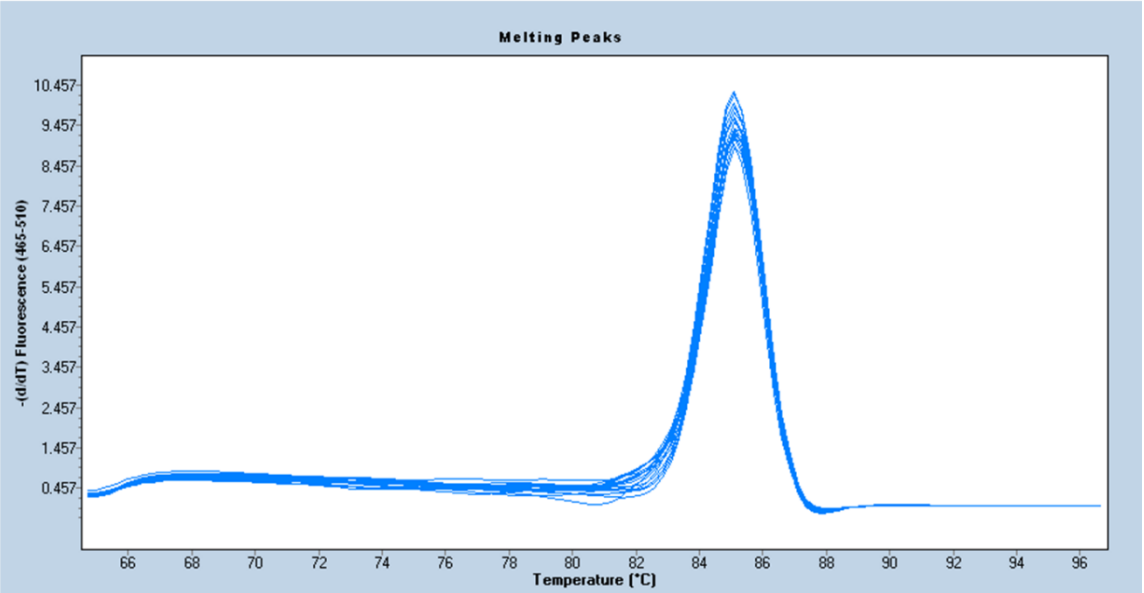

(D) – *PECAM-1*

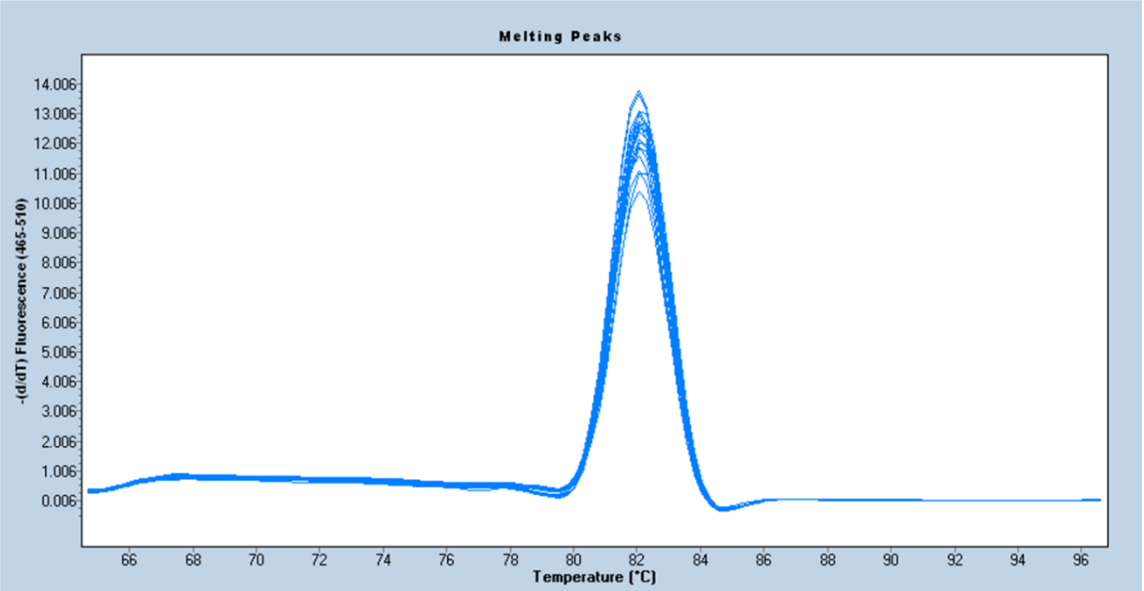

(E) – *RPL27*

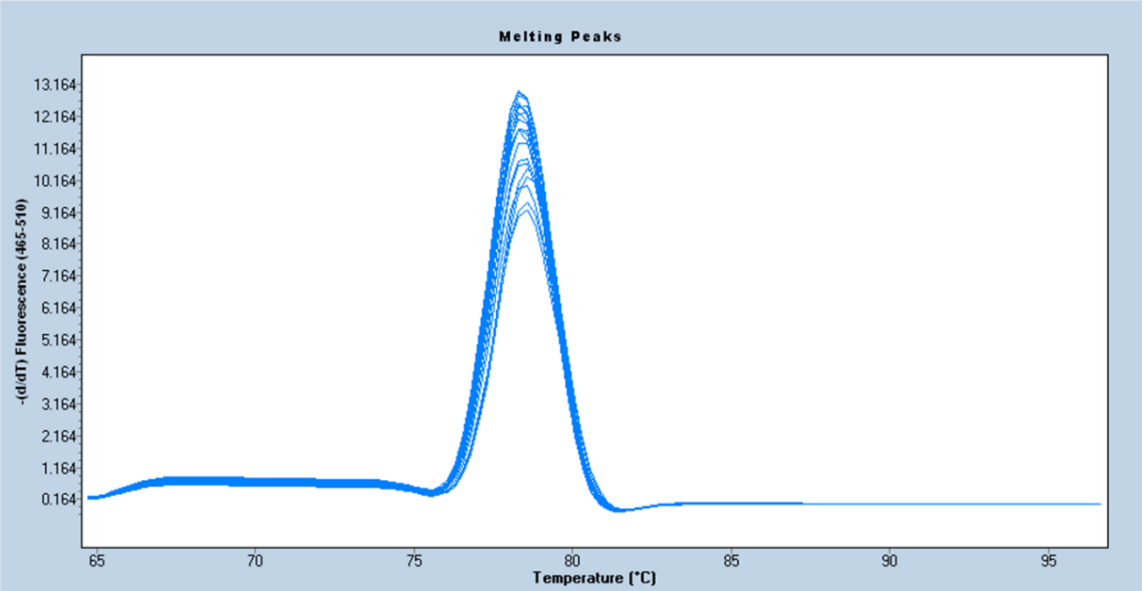

(F) – *VEGF-A*

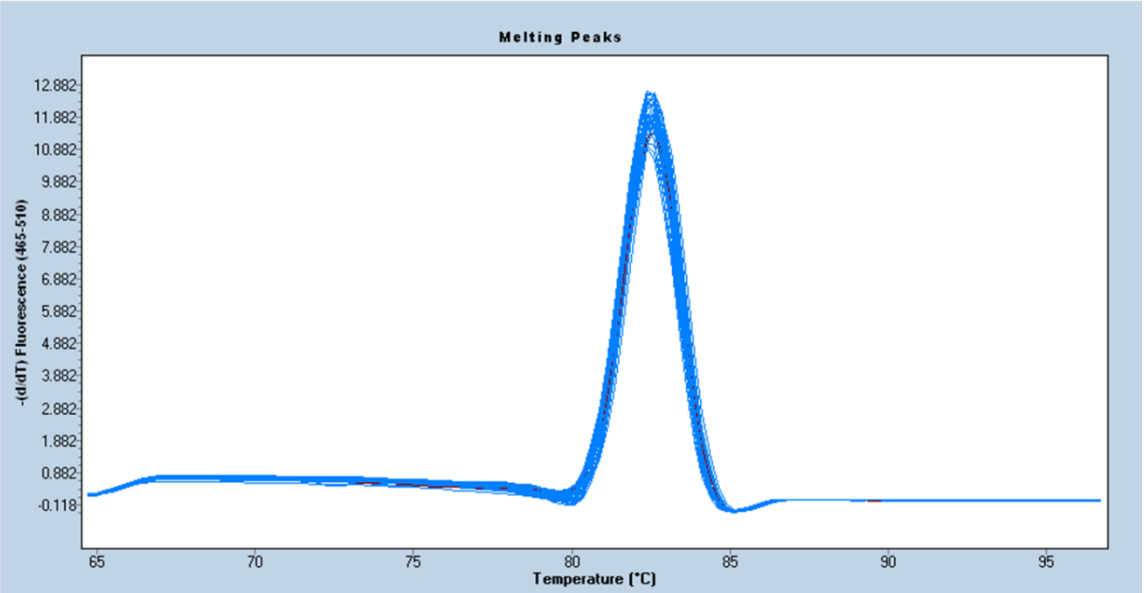

(G) – *VEGFR2*

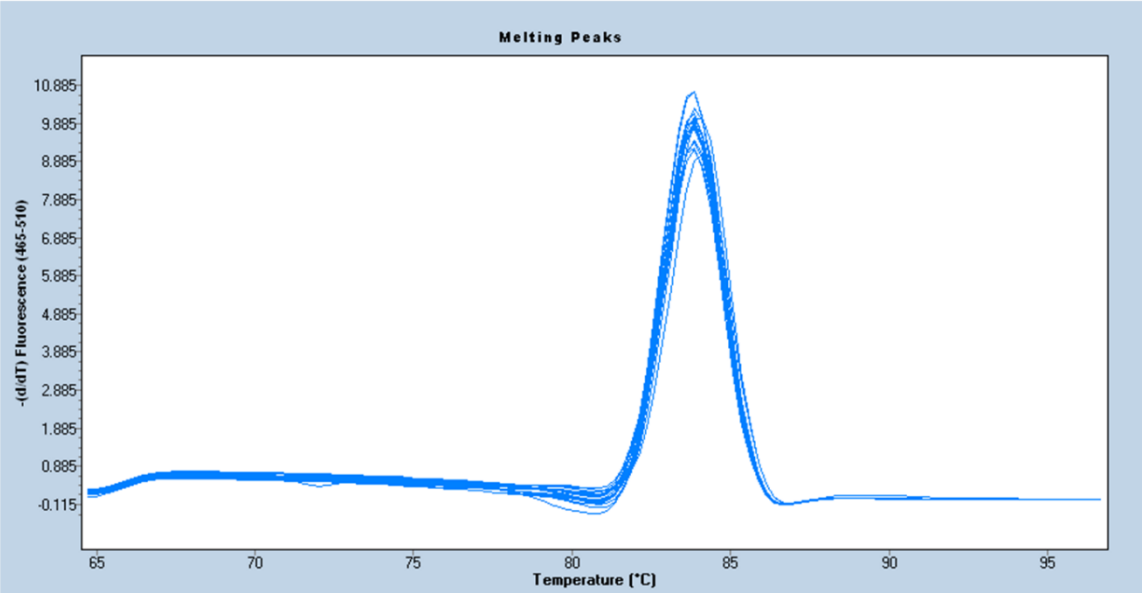

(H) – *VWF*

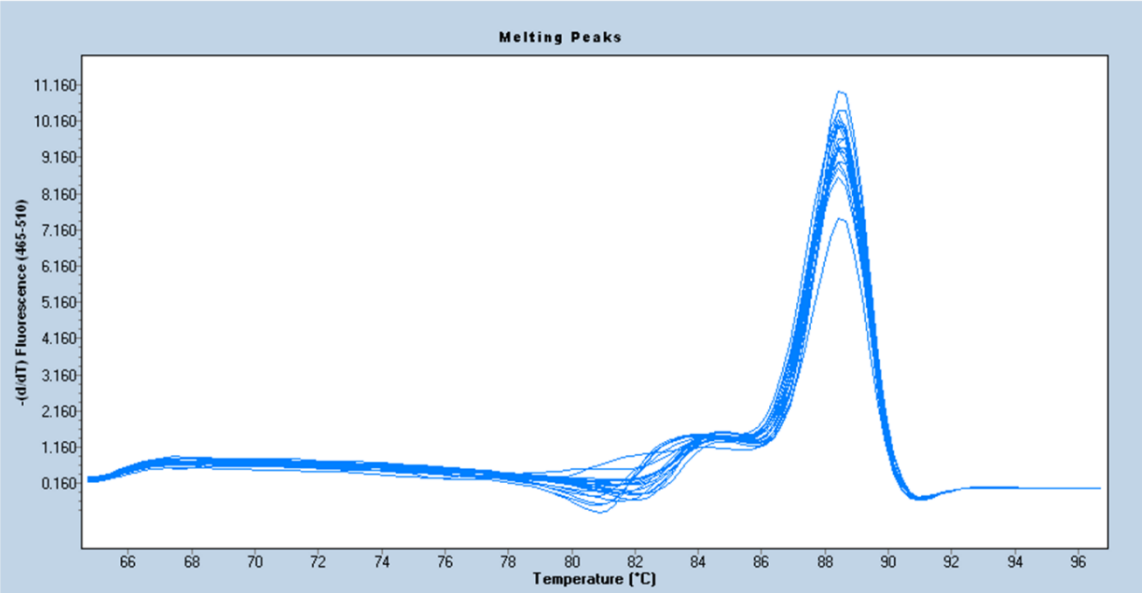

(I) – *YWHAZ*

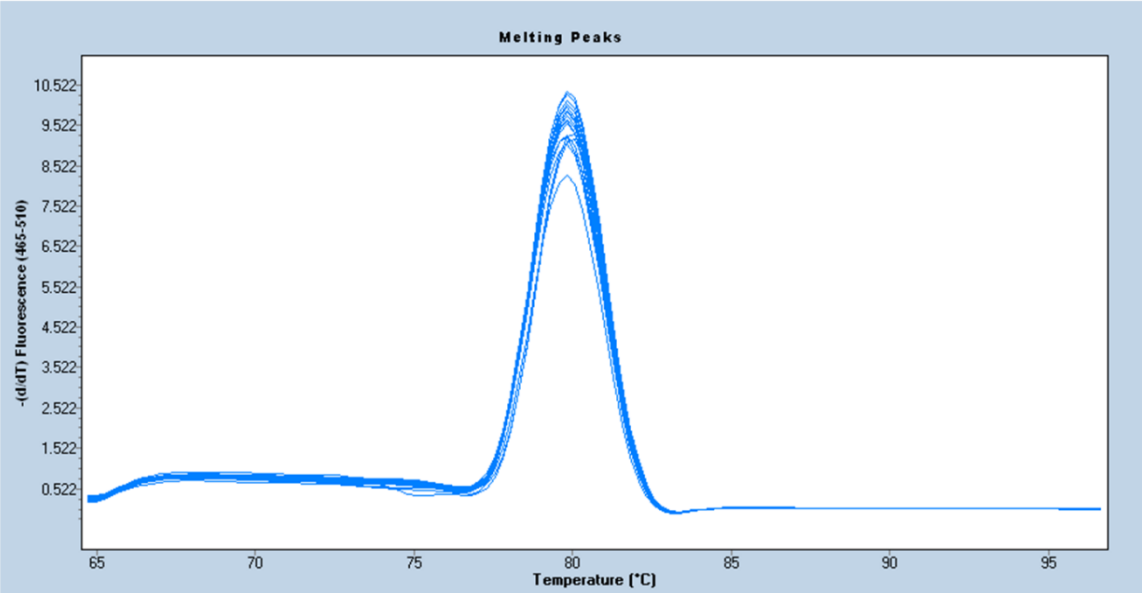

Figure 7.1 Melt curve analysis for primer specificity assessment.
Melt curve analysis was undertaken for primers (A) *B2M* , (B) *eNOS*, (C) *GAPDH*, (D) *PECAM-1*, (E) *RPL27*, (F) *VEGF-A*, (G) *VEGF-R2*, (H) *VWF*, (I) *YWHAZ*. Single peaks at each primer T_m indicated target-specific primer binding.

7.3 Tube formation assay

7.3.1 Two-way ANOVA analysis for tube formation assay

The following tables show results from two-way ANOVA analysis with Tukey's post-hoc multiple comparisons test. These analyses were performed on 'Angiogenesis Analyser' data after tube formation assays in 48-well plates. Multiple comparisons were made between 4 h, 6 h and 24 h timepoints on untreated and ultrasound exposed cells. ANOVA comparisons showed significantly reduced tube length (Table 7.2 A), and number of branches measured (Table 7.2 B) after 24 h compared with 4 h and 6 h time points in HUVECs seeded immediately after ultrasound exposure.

HUVECs seeded 24 h after ultrasound exposure were also analysed using two-way ANOVA with Tukey post-hoc comparisons. However comparisons were only made between 24 h and 6 h time points due to a loss of 4 h biological replicate data. Comparisons showed significantly lower tube length at 24 h compared with 6 h (Table 7.3 A), No significant difference was measured in number of branches measured both between timepoints and within time points (Table 7.3 B).

Two-way ANOVA comparison 72 h post ultrasound exposure demonstrated no significant difference in tube length measured in treated and untreated cells between any time point, except significantly lower length in 25mW/cm^2 exposed cells imaged 24 h after seeding than 10 mW/cm^2 exposed cells 4 h after seeding (Table 7.4 A). Interestingly, the number of branches measured 24 h after seeding were significantly lower only in unexposed cells, compared with cells analysed 4 h after seeding as shown in Table 7.4 B.

Table 7.2 Two-way ANOVA with Tukey post-hoc comparisons test for tube formation immediatley after ultrasound exposure.

(A) Total Tube Length

Tukey's multiple comparisons test	Summary	Adjusted P Value
4 h:untreated vs. 6 h:untreated	ns	0.999
4 h:untreated vs. 6 h:10 mW/cm2	ns	0.9789
4 h:untreated vs. 6 h:25 mW/cm2	ns	0.9929
4 h:untreated vs. 6 h:75 mW/cm2	ns	0.7134
4 h:untreated vs. 24 h:untreated	*	0.0114
4 h:untreated vs. 24 h:10 mW/cm2	**	0.0035
4 h:untreated vs. 24 h:25 mW/cm2	**	0.0063
4 h:untreated vs. 24 h:75 mW/cm2	**	0.0011
4 h:10 mW/cm2 vs. 6 h:untreated	ns	>0.9999
4 h:10 mW/cm2 vs. 6 h:10 mW/cm2	ns	0.9996
4 h:10 mW/cm2 vs. 6 h:25 mW/cm2	ns	>0.9999
4 h:10 mW/cm2 vs. 6 h:75 mW/cm2	ns	0.9268
4 h:10 mW/cm2 vs. 24 h:untreated	*	0.0325
4 h:10 mW/cm2 vs. 24 h:10 mW/cm2	*	0.0104
4 h:10 mW/cm2 vs. 24 h:25 mW/cm2	*	0.0184
4 h:10 mW/cm2 vs. 24 h:75 mW/cm2	**	0.0033
4 h:25 mW/cm2 vs. 6 h:untreated	ns	0.9992
4 h:25 mW/cm2 vs. 6 h:10 mW/cm2	ns	0.9816
4 h:25 mW/cm2 vs. 6 h:25 mW/cm2	ns	0.994
4 h:25 mW/cm2 vs. 6 h:75 mW/cm2	ns	0.7267
4 h:25 mW/cm2 vs. 24 h:untreated	*	0.012
4 h:25 mW/cm2 vs. 24 h:10 mW/cm2	**	0.0037
4 h:25 mW/cm2 vs. 24 h:25 mW/cm2	**	0.0066
4 h:25 mW/cm2 vs. 24 h:75 mW/cm2	**	0.0011
4 h:75 mW/cm2 vs. 6 h:untreated	ns	>0.9999
4 h:75 mW/cm2 vs. 6 h:10 mW/cm2	ns	>0.9999
4 h:75 mW/cm2 vs. 6 h:25 mW/cm2	ns	>0.9999
4 h:75 mW/cm2 vs. 6 h:75 mW/cm2	ns	0.9998
4 h:75 mW/cm2 vs. 24 h:untreated	ns	0.1576
4 h:75 mW/cm2 vs. 24 h:10 mW/cm2	ns	0.058
4 h:75 mW/cm2 vs. 24 h:25 mW/cm2	ns	0.0965
4 h:75 mW/cm2 vs. 24 h:75 mW/cm2	*	0.0197
6 h:untreated vs. 24 h:untreated	ns	0.0759
6 h:untreated vs. 24 h:10 mW/cm2	*	0.0257
6 h:untreated vs. 24 h:25 mW/cm2	*	0.0444
6 h:untreated vs. 24 h:75 mW/cm2	**	0.0083
6 h:10 mW/cm2 vs. 24 h:untreated	ns	0.1632
6 h:10 mW/cm2 vs. 24 h:10 mW/cm2	ns	0.0603
6 h:10 mW/cm2 vs. 24 h:25 mW/cm2	ns	0.1002
6 h:10 mW/cm2 vs. 24 h:75 mW/cm2	*	0.0205
6 h:25 mW/cm2 vs. 24 h:untreated	ns	0.1194
6 h:25 mW/cm2 vs. 24 h:10 mW/cm2	*	0.0424
6 h:25 mW/cm2 vs. 24 h:25 mW/cm2	ns	0.0717
6 h:25 mW/cm2 vs. 24 h:75 mW/cm2	*	0.0141
6 h:75 mW/cm2 vs. 24 h:untreated	ns	0.5005
6 h:75 mW/cm2 vs. 24 h:10 mW/cm2	ns	0.24
6 h:75 mW/cm2 vs. 24 h:25 mW/cm2	ns	0.3551
6 h:75 mW/cm2 vs. 24 h:75 mW/cm2	ns	0.0966

(B) Number of Branches

Tukey's multiple comparisons test	Summary	Adjusted P Value
4 h:untreated vs. 6 h:untreated	ns	0.9954
4 h:untreated vs. 6 h:10 mW/cm2	ns	0.954
4 h:untreated vs. 6 h:25 mW/cm2	ns	0.9919
4 h:untreated vs. 6 h:75 mw/cm3	ns	0.9998
4 h:untreated vs. 24 h:untreated	*	0.0269
4 h:untreated vs. 24 h:10 mW/cm2	**	0.0059
4 h:untreated vs. 24 h:25 mW/cm2	*	0.0216
4 h:untreated vs. 24 h:75 mw/cm3	**	0.0048
4 h:10 mW/cm2 vs. 6 h:untreated	ns	>0.9999
4 h:10 mW/cm2 vs. 6 h:10 mW/cm2	ns	0.9954
4 h:10 mW/cm2 vs. 6 h:25 mW/cm2	ns	0.9998
4 h:10 mW/cm2 vs. 6 h:75 mw/cm3	ns	>0.9999
4 h:10 mW/cm2 vs. 24 h:untreated	ns	0.0604
4 h:10 mW/cm2 vs. 24 h:10 mW/cm2	*	0.0141
4 h:10 mW/cm2 vs. 24 h:25 mW/cm2	*	0.0491
4 h:10 mW/cm2 vs. 24 h:75 mw/cm3	*	0.0116
4 h:25 mW/cm2 vs. 6 h:untreated	ns	0.9095
4 h:25 mW/cm2 vs. 6 h:10 mW/cm2	ns	0.7353
4 h:25 mW/cm2 vs. 6 h:25 mW/cm2	ns	0.8826
4 h:25 mW/cm2 vs. 6 h:75 mw/cm3	ns	0.9787
4 h:25 mW/cm2 vs. 24 h:untreated	**	0.0079
4 h:25 mW/cm2 vs. 24 h:10 mW/cm2	**	0.0017
4 h:25 mW/cm2 vs. 24 h:25 mW/cm2	**	0.0063
4 h:25 mW/cm2 vs. 24 h:75 mw/cm3	**	0.0014
4 h:75 mw/cm3 vs. 6 h:untreated	ns	0.8377
4 h:75 mw/cm3 vs. 6 h:10 mW/cm2	ns	0.6281
4 h:75 mw/cm3 vs. 6 h:25 mW/cm2	ns	0.8015
4 h:75 mw/cm3 vs. 6 h:75 mw/cm3	ns	0.9474
4 h:75 mw/cm3 vs. 24 h:untreated	**	0.0052
4 h:75 mw/cm3 vs. 24 h:10 mW/cm2	**	0.0011
4 h:75 mw/cm3 vs. 24 h:25 mW/cm2	**	0.0041
4 h:75 mw/cm3 vs. 24 h:75 mw/cm3	***	0.0009
6 h:untreated vs. 24 h:untreated	ns	0.2156
6 h:untreated vs. 24 h:10 mW/cm2	ns	0.0604
6 h:untreated vs. 24 h:25 mW/cm2	ns	0.1816
6 h:untreated vs. 24 h:75 mw/cm3	ns	0.0504
6 h:10 mW/cm2 vs. 24 h:untreated	ns	0.3878
6 h:10 mW/cm2 vs. 24 h:10 mW/cm2	ns	0.1277
6 h:10 mW/cm2 vs. 24 h:25 mW/cm2	ns	0.3364
6 h:10 mW/cm2 vs. 24 h:75 mw/cm3	ns	0.1084
6 h:25 mW/cm2 vs. 24 h:untreated	ns	0.2444
6 h:25 mW/cm2 vs. 24 h:10 mW/cm2	ns	0.0704
6 h:25 mW/cm2 vs. 24 h:25 mW/cm2	ns	0.2069
6 h:25 mW/cm2 vs. 24 h:75 mw/cm3	ns	0.059
6 h:75 mw/cm3 vs. 24 h:untreated	ns	0.122
6 h:75 mw/cm3 vs. 24 h:10 mW/cm2	*	0.0309
6 h:75 mw/cm3 vs. 24 h:25 mW/cm2	ns	0.1008
6 h:75 mw/cm3 vs. 24 h:75 mw/cm3	*	0.0256

Table 7.3 Two-way ANOVA with Tukey post-hoc comparisons test for tube formation 24 h after ultrasound exposure.

(A) Total Tube Length

Tukey's multiple comparisons test	Summary	Adjusted P Value
6 h:untreated vs. 24 h:untreated	**	0.004
6 h:untreated vs. 24 h:10 mW/cm2	**	0.0035
6 h:untreated vs. 24 h:25 mW/cm2	*	0.013
6 h:untreated vs. 24 h:75 mW/cm2	*	0.0138
6 h:10 mW/cm2 vs. 24 h:untreated	**	0.0068
6 h:10 mW/cm2 vs. 24 h:10 mW/cm2	**	0.006
6 h:10 mW/cm2 vs. 24 h:25 mW/cm2	*	0.022
6 h:10 mW/cm2 vs. 24 h:75 mW/cm2	*	0.0232
6 h:25 mW/cm2 vs. 24 h:untreated	**	0.0062
6 h:25 mW/cm2 vs. 24 h:10 mW/cm2	**	0.0054
6 h:25 mW/cm2 vs. 24 h:25 mW/cm2	*	0.0199
6 h:25 mW/cm2 vs. 24 h:75 mW/cm2	*	0.021
6 h:75 mW/cm2 vs. 24 h:untreated	**	0.0023
6 h:75 mW/cm2 vs. 24 h:10 mW/cm2	**	0.002
6 h:75 mW/cm2 vs. 24 h:25 mW/cm2	**	0.0074
6 h:75 mW/cm2 vs. 24 h:75 mW/cm2	**	0.0079

(B) Number of Branches

Tukey's multiple comparisons test	Summary	Adjusted P Value
6 h:untreated vs. 24 h:untreated	ns	0.3815
6 h:untreated vs. 24 h:10 mW/cm2	ns	0.2382
6 h:untreated vs. 24 h:25 mW/cm2	ns	0.5929
6 h:untreated vs. 24 h:75 mW/cm2	ns	0.6221
6 h:10 mW/cm2 vs. 24 h:untreated	ns	0.7086
6 h:10 mW/cm2 vs. 24 h:10 mW/cm2	ns	0.5165
6 h:10 mW/cm2 vs. 24 h:25 mW/cm2	ns	0.891
6 h:10 mW/cm2 vs. 24 h:75 mW/cm2	ns	0.9083
6 h:25 mW/cm2 vs. 24 h:untreated	ns	0.32
6 h:25 mW/cm2 vs. 24 h:10 mW/cm2	ns	0.1947
6 h:25 mW/cm2 vs. 24 h:25 mW/cm2	ns	0.5176
6 h:25 mW/cm2 vs. 24 h:75 mW/cm2	ns	0.5463
6 h:75 mW/cm2 vs. 24 h:untreated	ns	0.6047
6 h:75 mW/cm2 vs. 24 h:10 mW/cm2	ns	0.4176
6 h:75 mW/cm2 vs. 24 h:25 mW/cm2	ns	0.8147
6 h:75 mW/cm2 vs. 24 h:75 mW/cm2	ns	0.8378

Table 7.4. Two-way ANOVA with Tukey post-hoc comparisons test for tube formation 72 h after ultrasound exposure.

(A) Total Tube Length

Tukey's multiple comparisons test	Summary	Adjusted P Value
4 h:untreated vs. 6 h:untreated	ns	>0.9999
4 h:untreated vs. 6 h:10 mW/cm2	ns	>0.9999
4 h:untreated vs. 6 h:25 mW/cm2	ns	>0.9999
4 h:untreated vs. 6 h:75 mW/cm2	ns	>0.9999
4 h:untreated vs. 24 h:untreated	ns	0.1577
4 h:untreated vs. 24 h:10 mW/cm2	ns	0.2259
4 h:untreated vs. 24 h:25 mW/cm2	ns	0.0534
4 h:untreated vs. 24 h:75 mW/cm2	ns	0.2295
4 h:10 mW/cm2 vs. 6 h:untreated	ns	0.9999
4 h:10 mW/cm2 vs. 6 h:10 mW/cm2	ns	>0.9999
4 h:10 mW/cm2 vs. 6 h:25 mW/cm2	ns	0.9998
4 h:10 mW/cm2 vs. 6 h:75 mW/cm2	ns	>0.9999
4 h:10 mW/cm2 vs. 24 h:untreated	ns	0.1361
4 h:10 mW/cm2 vs. 24 h:10 mW/cm2	ns	0.1972
4 h:10 mW/cm2 vs. 24 h:25 mW/cm2	*	0.0452
4 h:10 mW/cm2 vs. 24 h:75 mW/cm2	ns	0.2005
4 h:25 mW/cm2 vs. 6 h:untreated	ns	>0.9999
4 h:25 mW/cm2 vs. 6 h:10 mW/cm2	ns	>0.9999
4 h:25 mW/cm2 vs. 6 h:25 mW/cm2	ns	>0.9999
4 h:25 mW/cm2 vs. 6 h:75 mW/cm2	ns	>0.9999
4 h:25 mW/cm2 vs. 24 h:untreated	ns	0.2507
4 h:25 mW/cm2 vs. 24 h:10 mW/cm2	ns	0.3447
4 h:25 mW/cm2 vs. 24 h:25 mW/cm2	ns	0.0922
4 h:25 mW/cm2 vs. 24 h:75 mW/cm2	ns	0.3495
4 h:75 mW/cm2 vs. 6 h:untreated	ns	>0.9999
4 h:75 mW/cm2 vs. 6 h:10 mW/cm2	ns	>0.9999
4 h:75 mW/cm2 vs. 6 h:25 mW/cm2	ns	>0.9999
4 h:75 mW/cm2 vs. 6 h:75 mW/cm2	ns	>0.9999
4 h:75 mW/cm2 vs. 24 h:untreated	ns	0.1923
4 h:75 mW/cm2 vs. 24 h:10 mW/cm2	ns	0.2711
4 h:75 mW/cm2 vs. 24 h:25 mW/cm2	ns	0.0673
4 h:75 mW/cm2 vs. 24 h:75 mW/cm2	ns	0.2752
6 h:untreated vs. 24 h:untreated	ns	0.4228
6 h:untreated vs. 24 h:10 mW/cm2	ns	0.5442
6 h:untreated vs. 24 h:25 mW/cm2	ns	0.1785
6 h:untreated vs. 24 h:75 mW/cm2	ns	0.55
6 h:10 mW/cm2 vs. 24 h:untreated	ns	0.3382
6 h:10 mW/cm2 vs. 24 h:10 mW/cm2	ns	0.4493
6 h:10 mW/cm2 vs. 24 h:25 mW/cm2	ns	0.1336
6 h:10 mW/cm2 vs. 24 h:75 mW/cm2	ns	0.4548
6 h:25 mW/cm2 vs. 24 h:untreated	ns	0.4473
6 h:25 mW/cm2 vs. 24 h:10 mW/cm2	ns	0.5705
6 h:25 mW/cm2 vs. 24 h:25 mW/cm2	ns	0.1925
6 h:25 mW/cm2 vs. 24 h:75 mW/cm2	ns	0.5764
6 h:75 mW/cm2 vs. 24 h:untreated	ns	0.3544
6 h:75 mW/cm2 vs. 24 h:10 mW/cm2	ns	0.4679
6 h:75 mW/cm2 vs. 24 h:25 mW/cm2	ns	0.1418
6 h:75 mW/cm2 vs. 24 h:75 mW/cm2	ns	0.4735

(B) Number of Branches

Tukey's multiple comparisons test	Summary	Adjusted P Value
4 h:untreated vs. 6 h:untreated	ns	0.9539
4 h:untreated vs. 6 h:10 mW/cm2	ns	0.6936
4 h:untreated vs. 6 h:25 mW/cm2	ns	0.9453
4 h:untreated vs. 6 h:75 mW/cm2	ns	0.4029
4 h:untreated vs. 24 h:untreated	**	0.0019
4 h:untreated vs. 24 h:10 mW/cm2	*	0.0467
4 h:untreated vs. 24 h:25 mW/cm2	ns	0.2291
4 h:untreated vs. 24 h:75 mW/cm2	ns	0.114
4 h:10 mW/cm2 vs. 6 h:untreated	ns	>0.9999
4 h:10 mW/cm2 vs. 6 h:10 mW/cm2	ns	0.99
4 h:10 mW/cm2 vs. 6 h:25 mW/cm2	ns	>0.9999
4 h:10 mW/cm2 vs. 6 h:75 mW/cm2	ns	0.8921
4 h:10 mW/cm2 vs. 24 h:untreated	*	0.0152
4 h:10 mW/cm2 vs. 24 h:10 mW/cm2	ns	0.2523
4 h:10 mW/cm2 vs. 24 h:25 mW/cm2	ns	0.7114
4 h:10 mW/cm2 vs. 24 h:75 mW/cm2	ns	0.477
4 h:25 mW/cm2 vs. 6 h:untreated	ns	0.9701
4 h:25 mW/cm2 vs. 6 h:10 mW/cm2	ns	0.7447
4 h:25 mW/cm2 vs. 6 h:25 mW/cm2	ns	0.9637
4 h:25 mW/cm2 vs. 6 h:75 mW/cm2	ns	0.453
4 h:25 mW/cm2 vs. 24 h:untreated	**	0.0024
4 h:25 mW/cm2 vs. 24 h:10 mW/cm2	ns	0.0562
4 h:25 mW/cm2 vs. 24 h:25 mW/cm2	ns	0.2649
4 h:25 mW/cm2 vs. 24 h:75 mW/cm2	ns	0.1348
4 h:75 mW/cm2 vs. 6 h:untreated	ns	0.9965
4 h:75 mW/cm2 vs. 6 h:10 mW/cm2	ns	0.8964
4 h:75 mW/cm2 vs. 6 h:25 mW/cm2	ns	0.9952
4 h:75 mW/cm2 vs. 6 h:75 mW/cm2	ns	0.6492
4 h:75 mW/cm2 vs. 24 h:untreated	**	0.0051
4 h:75 mW/cm2 vs. 24 h:10 mW/cm2	ns	0.1078
4 h:75 mW/cm2 vs. 24 h:25 mW/cm2	ns	0.4265
4 h:75 mW/cm2 vs. 24 h:75 mW/cm2	ns	0.2389
6 h:untreated vs. 24 h:untreated	*	0.0494
6 h:untreated vs. 24 h:10 mW/cm2	ns	0.5367
6 h:untreated vs. 24 h:25 mW/cm2	ns	0.944
6 h:untreated vs. 24 h:75 mW/cm2	ns	0.7959
6 h:10 mW/cm2 vs. 24 h:untreated	ns	0.1655
6 h:10 mW/cm2 vs. 24 h:10 mW/cm2	ns	0.8754
6 h:10 mW/cm2 vs. 24 h:25 mW/cm2	ns	0.9992
6 h:10 mW/cm2 vs. 24 h:75 mW/cm2	ns	0.9824
6 h:25 mW/cm2 vs. 24 h:untreated	ns	0.0536
6 h:25 mW/cm2 vs. 24 h:10 mW/cm2	ns	0.5602
6 h:25 mW/cm2 vs. 24 h:25 mW/cm2	ns	0.9528
6 h:25 mW/cm2 vs. 24 h:75 mW/cm2	ns	0.8151
6 h:75 mW/cm2 vs. 24 h:untreated	ns	0.3651
6 h:75 mW/cm2 vs. 24 h:10 mW/cm2	ns	0.9867
6 h:75 mW/cm2 vs. 24 h:25 mW/cm2	ns	>0.9999
6 h:75 mW/cm2 vs. 24 h:75 mW/cm2	ns	0.9997

7.3.2 Energy supplied to HUVECs in 35 mm culture dishes

The energy supplied to the cells was calculated following Equation 2.2 (Section 2.7.2) and is described in Table 7.5. Each DuoSon exposure setting was converted to the amount of energy supplied in Joules by using the total acoustic power of each intensity setting multiplied by the exposure length (in seconds).

Table 7.5 Calculated energy supplied to cells in 35 mm culture dish and the corresponding exposure setting.

DuoSon Exposure Setting (intensity_exposure length)	Supplied Energy (Joules)
untreated_1 min	0
untreated_3 min	0
untreated_5 min	0
10 mW_1 min	9.54
10 mW_3 min	28.62
10 mW_5 min	47.7
25 mW_1 min	24.36
25 mW_3 min	73.08
25 mW_5 min	121.8
75 mW_1 min	73.02
75 mW_3 min	219.06
75 mW_5 min	365.1

The energy supplied to the HUVECs in 35 mm dishes did not significantly affect the tube formation behaviour when analysing data at all imaging timepoints ($p = 0.36$, Fig 7.2). This can be visualised by the overlapping of 95 % confidence ellipses of all energy values supplied to the cells during the *in vitro* experiment.

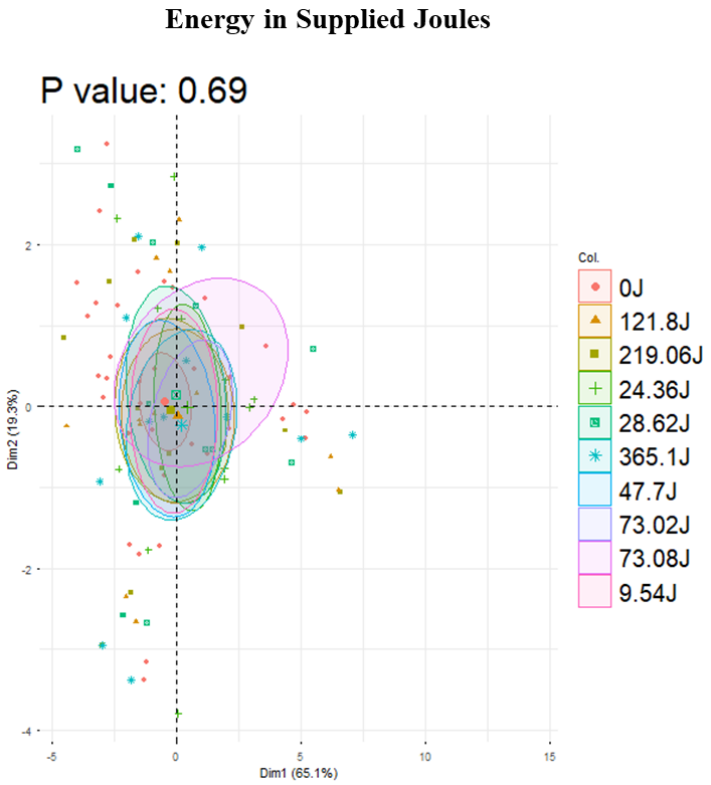

Figure 7.2 Principal component analysis of the energy supplied to HUVECs during 45 kHz DuoSon exposure at all imaging time points.

Data were grouped according to the energy supplied in Joules (J). Overlapping ellipses in all energy settings indicated no statistical difference in tube formation between untreated cells and cells exposed to ultrasound at all intensities. Analysis and graph visualisation performed in R Studio (N = 4; p = 0.69).

7.4 Scripts

7.4.1 RStudio script for PCA

A script was written in RStudio in collaboration with Dr Dario Leonardo Balacco to perform PCA on the tube formation dataset obtained from 'Angiogenesis Analyser' in HUVECs (Fig 7.3). PCA was performed following tube formation assay in 35 mm dishes as multiple variables were measured: intensity, exposure length, imaging time point and assessing numerous tube formation characteristics in 'Angiogenesis Analyser'.

```
library("FactoMineR")
library("factoextra")
library("ggplot2")
library(devtools)
library(ggfortify)
library(dplyr)

setwd($PATH)
table=read.csv($input_file, s="\t")
table_df=as.data.frame(table)
tb2 = table_df [, -1]
rownames(tb2) = table_df[,1]
summary(tb2)
tb3=tb2[,unlist(lapply(tb2, FUN=class))=="numeric"]
#tb3=as.data.frame(tb3)
pca=prcomp(tb3, scale=TRUE)
ymax=max(pca$x[,2])
graphy=ymax-0.5
pca_result <- PCA(tb3, scale.unit = TRUE, ncp = 5, graph = FALSE)
pca_scores <- as.data.frame(pca_result$ind$coord)
pca_scores$group <- factor(tb2$$group_variable)
group <- factor(tb2$group_variable)
centroids <- pca_scores %>%
        group_by(group) %>%
        summarize(PC1 = mean(Dim.1), PC2 = mean(Dim.2))
centroid_dist <- dist(centroids[, c("PC1", "PC2")])
centroid_dist
permute_distances <- function(data, n_perm = 1000) {
        perm_distances <- numeric(n_perm)
    for (i in 1:n_perm) {
                shuffled_groups <- sample(data$group)
                data$group <- shuffled_groups
      perm_centroids <- data %>%
                group_by(group) %>%
                summarize(PC1 = mean(Dim.1), PC2 = mean(Dim.2))
      perm_distances[i] <- dist(perm_centroids[, c("PC1", "PC2")])
      }
   return(perm_distances)
  }
perm_distances <- permute_distances(pca_scores, n_perm = 1000)
observed_dist <- centroid_distS
p_value <- mean(perm_distances >= observed_dist)
p_value=round(p_value, digits=2)
value=print(p_value)
text_label="P value:"
val=paste(text_label,value)
png($output_file.png)
p = fviz_pca_ind(pca,
        col.ind = tb2$Intensity,
        addEllipses = T,
        ellipse.type = "confidence",
        ellipse.level = 0.95,
        repel = TRUE,
        geom="point")
p+ggtitle(val)+ theme(plot.title = element_text(size=30), legend.key.size =
unit(1, 'cm'), legend.text = element_text(size=20))
dev.off()
```

Figure 7.3. R script written to perform and visualise results of PCA.
A script of commands written in R to perform PCA on the tube formation in 35 mm dataset and to visualise the data as ellipses indicative of significance and 95 % confidence.

7.4.2 MATLAB Scripts for acoustic field characterisation

A MATLAB script was written by colleagues Hilde Metzger and Dr Alexandru Moldovan at University of Glasgow to plot hydrophone readings obtained from tank pressure field scanning in Glasgow laboratories described in section 3.3.2. The script allowed for sorting of MATLAB data files saved from Picoscope pressure readings, and plotting of these values as a pressure field image:

```
sizex =_;  % Span in x-direction [mm]
sizey =;_   % Span in y-direction [mm]
sizez = _;   % Span in z-direction [mm]
stepx = 2.5;  % step size in x-direction [mm]
stepy = 2.5;  % Step size in y-direction[mm]
stepz = 2.5;  % Step size in z-direction[mm]
zoffset = 5;  % Distance the hydrophone was from the
transducer front face [mm]

%initialises arrays used
 position=[];
 first=[];
 second=[];
 xyz=[];
 ampl=[];
 pnp_vect=[];
 ppp_vect=[];
```

```
directory = uigetdir();
 files=dir(horzcat(directory,'\*.mat'));
 files={files.name};

% sort_nat sorts the filenames into the natural order so that
they are processed in the correct order
[files, S] = sort_nat(files);

%extracts the files one by one and converts Voltage signal
into Pressure Signal
for i=1:length(files)
 current=files{i};
 cf=horzcat(directory,'\',current);
 load(cf)
 ampl=A;

 %Sampling frequency of scanning tank setup (kHz)
 FS=1/(Tinterval*1e3);
 %define the lowpass Butterworth cutoff frequency (KHz)
 LowPass_freqency=200;
  freq=[20, 21, 22, 23, 24,25, 26, 27, 28, 29, 30, 31, 32, 33,
34, 35, 36, 37, 38, 39, 40, 41, 42, 43, 44, 45];
 NH_sensitivity_magnitude=[3772.950833, 3929.148889,
3707.648296, 3580.445794,
3240.594743,2947.161135,3129.320438,2803.335421,2552.00167,267
```

```
4.848114,2836.662942,3332.233684,3743.621964,4246.311011,4502.
193022,5167.226487,5609.679447,5647.506379,5820.696281,5876.00
9207,5808.786854,5772.972312,5595.048375,5684.058149,5378.8814
46,5165.613071,];


 measured_amplitude=ampl;
 % The interpolated NH calibration data must have as many
points as the measured voltage trace (the amplitude waveform)
 N=size(measured_amplitude,1);
% Get the frequency step size.
 delta_fs=FS/N;


% The frequency vector of the deconvolution matrix must stop
at the sampling frequency of the amplitude waveform in order
for the deconvolution by multiplication to exist!!!!!
 freq_stop_value=FS/2;


% Create the low and high frequency vectors: the low frequency
NH sensitivity vector (i.e. at frequencies < minimum
calibration frequency down till zero) has sensitivity
magnitudes equal to the first entry in the calibration data;
the high frequency sensitivity calibration data (i.e. for
frequencies > highest frequency in the calibration data) has
values equal to theentry with highest calibration frequency in
the calibration data. Reference: [HURRELL AND RAJAGOPAL:
```

```
PRACTICALITIES OF OBTAINING AND USING HYDROPHONE CALIBRATION
DATA]

 freq_low=0:delta_fs:freq(1);

mag_sensitivity_low=ones(1,length(freq_low)).*NH_sensitivity_m
agnitude(1);
 freq_high=freq(end):delta_fs:freq_stop_value;
 mag_sensitivity_high =
ones(1,length(freq_high)).*NH_sensitivity_magnitude(end);
 freq_end=min([freq_stop_value freq(end)]);

%Do an interpolation of the NH calibration data to shift its
points on the frequency points of the amplitude waveform.
 freq_interp=(freq_low(end)+delta_fs):delta_fs:freq_end;

mag_sensitivity_interp=interp1(freq,NH_sensitivity_magnitude,f
req_interp);

 %build the full sized interpolated vectors (with artificial
ends included)
 frequency_spectrum = horzcat(freq_low,freq_interp,freq_high);
 full_mag_sensitivity = [mag_sensitivity_low
mag_sensitivity_interp mag_sensitivity_high];
```

```
 % Infer the Phase data from Magnitude using inverse Hilbert
transform for minimum phase systems. Also nothe that
Inv(H(omega))=-H(omega) Reference: Wear et al.: time-delay
spectrometry
 phase_processed=imag(-
hilbert(log(abs(NH_sensitivity_magnitude))));
 phase_interp=interp1(freq,phase_processed,freq_interp);

 % in the same way as for the magnitude vector, create the
phase vector
 phase_low=zeros(1,length(freq_low));
 phase_high=zeros(1,length(freq_high));
 full_phase= horzcat(phase_low, phase_interp,phase_high);

% Create the complex NH transfer function
  [x,y] = pol2cart(full_phase,full_mag_sensitivity);
  NH_complex_transf_func=x+1i*y;
  NH_complex_transf_func=NH_complex_transf_func';

%% FFT part - transpose the data so that we have the time data
in different columns
     ampl_transpose=measured_amplitude;
 clear measured_amplitude

     full_frequency_signal=(fft(ampl_transpose,N));
```

```
frequency_signal=full_frequency_signal(1:size(NH_complex_trans
f_func,1), :); %make the signal single sideband
 deconvolved_signal=frequency_signal./NH_complex_transf_func;

  High_pass_low=ones(size(deconvolved_signal));
 High_pass_low(1,:)=0;
 deconvolved_signal=deconvolved_signal.*High_pass_low;

 %Only after the deconvolution can we filter our signal
[b,a] = butter(7,LowPass_freqency/(FS/2)); filtered_signal =
filter(b,a,deconvolved_signal);

  filtered_signal =deconvolved_signal;
 time_signal =
ifft(filtered_signal,size(ampl_transpose,1),'symmetric');
%transform back to time traces, bearing in mind that we have a
single sideband in fft domain
 pnp_vect = vertcat(pnp_vect,min(time_signal)*1e3);  % convert
the pnp vector to MPa;
end

pnp_vect = pnp_vect*(-1);
if sizez == 0
 numRows = sizey/stepy+1;
 numColumns = sizex/stepx+1;
```

```
 x =-1*sizex/2:stepx:sizex/2+1;
 y =-1*sizey/2:stepy:sizey/2+1;
 xlbl = 'X (mm)';
 ylbl = 'Y (mm)';
elseif sizex == 0
 numRows = sizey/stepy+1;
 numColumns = sizez/stepz+1;
 y =-1*sizey/2:stepy:sizey/2+1;
 x = zoffset:stepz:sizez;
 xlbl = 'Z (mm)';
 ylbl = 'Y (mm)';
elseif sizey == 0
 numRows = sizex/stepx+1;
 numColumns = sizez/stepz+1;
 y =-1*sizex/2:stepx:sizex/2+1;
 x = zoffset:stepz:sizez;
 xlbl = 'Z (mm)';
 ylbl = 'X (mm)';
PNP = reshape(pnp_vect, [numColumns numRows]);
PNP(:,2:2:end) = flipud(PNP(:,2:2:end));


figure();
imagesc(x, y, PNP)
 clb=colorbar;
  clb_title=get(clb,'title');
```

```
clb_pos(:,2)=610;
clb_title.Position=clb_pos;
title('2D Peak Negative Pressure (MPa)');
 colormap();
set(get(clb,'title'),'string','Pressure Magnitude
(MPa)','FontSize',16);
xlabel(xlbl,'FontSize',16);
ylabel(ylbl,'FontSize',16);
set(gca,'fontsize',18);
plotname = 'MPa';

FigureName=['2D_Color_Plot_tank',plotname,'2.fig'];
save_figure_path=[directory,'\',FigureName];
saveas(gcf,save_figure_path);
FigureName=['2D_Color_Plot_tank',plotname,'2.png'];
save_figure_path=[directory,'\',FigureName];
saveas(gcf,save_figure_path);
```

Another MATLAB script was written by Dr Jack Stevenson. This script allowed reading and plotting of single point scans measured with increasing ultrasound current described in section 3.3.2:

```
%% constants c = 1480;
selpath = uigetdir(); % give this the folder location that
contains the other current folders
```

```
foldersNames = dir(selpath);
foldersNames = foldersNames(3:length(foldersNames));
for i = 1:length(foldersNames)
 currentSettings(i) = str2double(foldersNames(i).name(1:end-
1));
 currentSettingsStr{i} = foldersNames(i).name;
end
%% get files from each subfolder
for ii = 1:length(foldersNames)
 subfolder = fullfile(selpath, currentSettingsStr(ii));
 directory = dir(subfolder{1});
 subDirNames = {directory.name};
 [s, idx] = sort_nat(subDirNames);
 s = s(3:end); %get rid of . and .. so idx will be 2 off....

for j = 1:length(s)
  data(ii,j) = load(fullfile(directory(1).folder, s{j})); %
this is all the data
  freq = fft(data(ii,j).A);
  tidyFreq = abs(freq);
  tidyFreq = tidyFreq(1:length(tidyFreq)/2); % do an fft and
tidy
  sampleRate = 1/data(ii,j).Tinterval; % need the sample rate

if mod(sampleRate, 2) == 0 % make sure its even (for fft freq)
```

```
   maxFFTfreq = sampleRate/2;
else
   maxFFTfreq = (sampleRate/2) + 1;
  end
  fftFreqVect = linspace(1,maxFFTfreq, length(tidyFreq)); %
stretching correct freq over spectrum
    [~, idx] = max(tidyFreq); % find location of peak
    %% plot freq content for every signal
  if j == 1
  figure;
  plot(fftFreqVect, tidyFreq)
%   title(['Resonant Frequency in signal is ',
num2str(round(averageResonance*1e-3)), ' kHz'])
%   xlim([0 1e6]);
  xlim([0 4e5]);
%   ylim([0 4e5]);
  end

  TxResonance(ii,j) = fftFreqVect(idx); % finally get
resonance
  lambda = c/TxResonance(ii,j); % wavelength
  timeBetweenPeaks = 1/TxResonance(ii,j);
    x = (1:length(data(ii,j).A))*data(ii,j).Tinterval;
```

```
  [data_max, locs] = findpeaks(data(ii,j).A, x,
'MinPeakDistance', timeBetweenPeaks*(2/3)); % find max on each
dataset
%   figure
%   findpeaks(data(ii,j).A, x, 'MinPeakDistance',
timeBetweenPeaks*(2/3)) % uncomment this to see graph of find
peaks
  sortDataMax = sort(data_max, 'descend');
  data_max = sortDataMax(2:end-1);
  meanPeaks(ii,j) = mean(data_max); % this is all the max
values from each test (over 10 averages in columns)

%   figure
%   plot(data(ii,j).A)
% pause(0.5)
 End

%% average the max - this is in Volts
averagedData = mean(meanPeaks, 2); % average the data left to
right (all columns)
averageResonance = mean(mean(TxResonance(:,1:10),2)); %
average drive freq

%% find conversion to MPa from calibration
cal(:,1) = (20:45)*1e3; % in Hz
```

```
cal(:,2) = [3772.950833, 3929.148889, 3707.648296,
3580.445794, 3240.594743, 2947.161135, 3129.320438,
2803.335421, 2552.00167, 2674.848114, 2836.662942,
3332.266984, ...
 3743.621964, 4246.311011, 4502.193022, 5167.226487,
5609.679447, 5647.506379, 5820.696281, 5876.009207,
5808.786854, 5772.972312, 5595.048375, 5684.058149,
5378.881446, 5165.613071]; % sensitivity of NH in mV/MPa

[p, s] = polyfit(cal(:,1), cal(:,2), 8); % fit the data to
interpolate

[y, delta] = polyval(p, cal(:,1), s); % get the needed value
figure; plot(cal(:,1), y); hold on; plot(cal(:,1), cal(:,2));
% how does the fit look?
title('calibration data')
legend('raw cal file', 'fit for interpolation', 'Location',
'southeast')

%% results - conversion from mV to MPa
averagedData = averagedData*1e3; % convert to mV
% mV * MPa/mV = MPa
calAtSignalFreq = polyval(p, averageResonance); % getting cal
data at the needed point (at frequency we are driving Tx at)
```

```
pres = (1/calAtSignalFreq) .* averagedData; % this gives out
pressure values now


% data = open(filename);
% plot(data.A)
% figure
% plot(data.B)
figure; plot(fftFreqVect, tidyFreq)
title(['Resonant Frequency in signal is ',
num2str(round(averageResonance*1e-3)), ' kHz'])
xlim([0 1e6]);
figure
findpeaks(data(ii,j).A, x, 'MinPeakDistance',
timeBetweenPeaks*(2/3)) % uncomment this to see graph of find
peaks
title('general signal with find peaks')
figure
plot(currentSettings*1e3, pres, 'LineWidth',2)
grid on
set(gca, 'FontSize', 12)
title('Pressure (MPa) vs Current (mA)');
xlabel('Driving Current (mA)')
ylabel('Pressure in Water (MPa)')
```

7.5 Conference submissions

Thermal effect of ultrasound on culture medium

Lisa Shriane, Farah Raja, Ben Scheven, Richard Shelton and A. Damien Walmsley

British Society for Oral and Dental Research, Annual Scientific Meeting, 2021, Birmingham, UK

Endothelial cell response to low frequency ultrasound

Lisa Shriane, Ben Scheven, Richard Shelton and A. Damien Walmsley

Ultrasonic Industry Association, Annual Symposium 2022, Warwick, UK

45 kHz ultrasound influences endothelial cell growth and gene expression

Lisa Shriane, Ben Scheven, Richard Shelton and A. Damien Walmsley

International Association for Dental Research, Oral Health Research Congress 2022, Marseille, France

Time-dependent angiogenic response to 45khz ultrasound

Lisa Shriane, Ben Scheven, Richard Shelton and A. Damien Walmsley

British Society for Oral and Dental Research, Annual Scientific Meeting 2023, London, UK

Endothelial cell response to low frequency ultrasound treatment

Lisa Shriane, Ben Scheven, Richard Shelton and A. Damien Walmsley

Ultrasonic Industry Association, Annual Symposium 2023, Utrecht, Netherlands

***In vitro* ultrasound treatment of endothelial cells**

Lisa Shriane, Ben Scheven, Richard Shelton and A. Damien Walmsley

Ultrasonic Industry Association, Annual Symposium 2024, Dublin, Ireland

Endothelial cell response to 45 kHz ultrasound

Lisa Shriane, Ben Scheven, Richard Shelton and A. Damien Walmsley

Ultrasonic Industry Association, Annual Symposium 2025, Halifax, Canada

7.6 Declaration of COVID-19 impact on research

Due to the restrictions in place during the COVID-19 pandemic, disruptions put upon the work planned for this study. Our School of Dentistry research laboratories were closed from March 2020 to August 2020. As a full-time member of technical staff upon reopening, the technical team had to work shift patterns including some days of extended hours from 8 – 6. Meaning my PhD research was unable to be completed in these shifts whilst the strict restrictions were in place until the start of 2021. There were also lab supply shortages and travel restrictions in place which delayed necessary collaborations with the Glasgow team for developing the tank configuration and further characterisations steps. Due to this, focus began on DuoSon device research. Once the tank had been characterised and established in Birmingham, work was then limited with time restraints of the PhD. The work that would have been carried out such as tube formation assay and other angiogenic assays has therefore been detailed in the future work section.